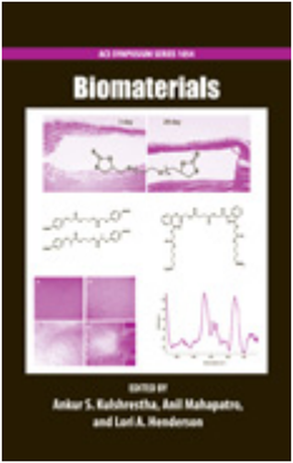

ACS SYMPOSIUM SERIES 1054

Biomaterials

EDITED BY

Ankur S. Kulshrestha, Anil Mahapatro,
and Lori A. Henderson

Downloaded by 89.163.34.136 on June 23, 2012 | http://pubs.acs.org
Publication Date (Web): November 18, 2010 | doi: 10.1021/bk-2010-1054.fw001

Biomaterials

In Biomaterials; Kulshrestha, A., et al.;
ACS Symposium Series; American Chemical Society: Washington, DC, 2010.

Downloaded by 89.163.34.136 on June 23, 2012 | http://pubs.acs.org
Publication Date (Web): November 18, 2010 | doi: 10.1021/bk-2010-1054.fw001

ACS SYMPOSIUM SERIES **1054**

Biomaterials

Ankur S. Kulshrestha, Editor
BD

Anil Mahapatro, Editor
Department of Chemistry
Norfolk State University

Lori A. Henderson, Editor
National Institute of Biomedical Imaging and Bioengineering
National Institutes of Health

Downloaded by 89.163.34.136 on June 23, 2012 | http://pubs.acs.org
Publication Date (Web): November 18, 2010 | doi: 10.1021/bk-2010-1054.fw001

Sponsored by the
ACS Division of Polymeric Materials: Science and Engineering

American Chemical Society, Washington, DC

Downloaded by 89.163.34.136 on June 23, 2012 | http://pubs.acs.org
Publication Date (Web): November 18, 2010 | doi: 10.1021/bk-2010-1054.fw001

Library of Congress Cataloging-in-Publication Data

Biomaterials / [edited by] Ankur S. Kulshrestha, Anil Mahapatro, Lori A. Henderson.
p. cm. -- (ACS symposium series; 1054)
Includes bibliographical references and index.
ISBN 978-0-8412-2567-1 (alk. paper)
1. Biomedical materials--Congresses. I. Kulshrestha, Ankur S. II. Mahapatro, Anil. III. Henderson, Lori A.
R857.M3B4766 2010
610.28--dc22
2010045031

The paper used in this publication meets the minimum requirements of American National Standard for Information Sciences—Permanence of Paper for Printed Library Materials, ANSI Z39.48n1984.

Copyright © 2010 American Chemical Society

Distributed by Oxford University Press

All Rights Reserved. Reprographic copying beyond that permitted by Sections 107 or 108 of the U.S. Copyright Act is allowed for internal use only, provided that a per-chapter fee of $40.25 plus $0.75 per page is paid to the Copyright Clearance Center, Inc., 222 Rosewood Drive, Danvers, MA 01923, USA. Republication or reproduction for sale of pages in this book is permitted only under license from ACS. Direct these and other permission requests to ACS Copyright Office, Publications Division, 1155 16th Street, N.W., Washington, DC 20036.

The citation of trade names and/or names of manufacturers in this publication is not to be construed as an endorsement or as approval by ACS of the commercial products or services referenced herein; nor should the mere reference herein to any drawing, specification, chemical process, or other data be regarded as a license or as a conveyance of any right or permission to the holder, reader, or any other person or corporation, to manufacture, reproduce, use, or sell any patented invention or copyrighted work that may in any way be related thereto. Registered names, trademarks, etc., used in this publication, even without specific indication thereof, are not to be considered unprotected by law.

PRINTED IN THE UNITED STATES OF AMERICA

Downloaded by 89.163.34.136 on June 23, 2012 | http://pubs.acs.org
Publication Date (Web): November 18, 2010 | doi: 10.1021/bk-2010-1054.fw001

Foreword

The ACS Symposium Series was first published in 1974 to provide a mechanism for publishing symposia quickly in book form. The purpose of the series is to publish timely, comprehensive books developed from the ACS sponsored symposia based on current scientific research. Occasionally, books are developed from symposia sponsored by other organizations when the topic is of keen interest to the chemistry audience.

Before agreeing to publish a book, the proposed table of contents is reviewed for appropriate and comprehensive coverage and for interest to the audience. Some papers may be excluded to better focus the book; others may be added to provide comprehensiveness. When appropriate, overview or introductory chapters are added. Drafts of chapters are peer-reviewed prior to final acceptance or rejection, and manuscripts are prepared in camera-ready format.

As a rule, only original research papers and original review papers are included in the volumes. Verbatim reproductions of previous published papers are not accepted.

ACS Books Department

Downloaded by 89.163.34.136 on June 23, 2012 | http://pubs.acs.org
Publication Date (Web): November 18, 2010 | doi: 10.1021/bk-2010-1054.pr001

Preface

The field of biomaterials has seen an exponential growth over the last few years leading to new strategies and frontiers in the biomedical arena. This growth has been catalyzed by the need to accelerate the discovery and translation of emerging technologies in a number of areas such as tissue engineering where the delivery of bioactive agents can help to treat, repair or restore function of damaged tissues. The emergence of these new biomaterial based technologies has resulted from the convergence of principles from various disciplines such as materials science, bioengineering, molecular biology, biochemistry and nanotechnology.

Motivations to improve health and lower long-term treatment costs to consumers and insurers has fueled continuous innovation towards developing novel polymeric compositions which can be used to manufacture medical devices with markedly lower risk of failure and adverse immune reactions. Polymers represent the most versatile class of biomaterials, being extensively applied in biomedical applications ranging from surgical and ocular devices, implants and supporting materials, drug delivery systems and drug device combinations, biosensors and other diagnostic assays, to tissue adhesives and tissue engineered constructs. This versatility results from the fact that polymers can be prepared in different compositions with a wide variety of structures and appropriate physicochemical, interfacial and biomimetic properties to meet specific end applications.

The purpose of this book is to publish, in one volume, the latest findings of the leading researchers in the field of polymeric biomaterials. It consists of 13 chapters which provide examples and reviews of recent developments in the synthesis, characterization, and applications of polymeric biomaterials

This book is based on a successful international symposium "Biomaterials and Bioengineering" held at the 239th National Meeting of the American Chemical Society (ACS) in Washington DC from August 16-20, 2009. The purpose of the symposium was to create a forum to foster dialogue and exchange of information between researchers, educators and developers of medical devices who are seeking to create new knowledge and technology by using polymeric biomaterials for various biomedical applications. Leaders in this field gathered to present their interesting and noteworthy findings. The participants represented many countries and included scientists from academics, industry, and government laboratories. Hopefully this book serves to transmit the latest information to the readers and also captures some of the excitement of the symposium in the process.

We thank the authors for their contributions and wish them success in their ongoing pursuit for novel biomaterials and advanced technologies that contribute to improvement in healthcare and quality of life. A special thanks to the ACS

In Biomaterials; Kulshrestha, A., et al.;
ACS Symposium Series; American Chemical Society: Washington, DC, 2010.

division of Polymeric Materials Science and Engineering for sponsoring the symposium and to the ACS books department for being patient through the compilation of this symposium series book.

Ankur S. Kulshrestha

BD
1 Becton Drive
Franklin Lakes, NJ 07417

Anil Mahapatro

Center for Biotechnology and Biomedical Sciences
Department of Chemistry
Norfolk State University
700 Park Avenue
Norfolk, VA 23504

Lori A. Henderson

National Institutes of Health
National Institute of Biomedical Imaging and Bioengineering
Division of Discovery Science and Technology
6707 Democracy Blvd. Suite 200
Bethesda, MD 20892

Downloaded by 89.163.34.136 on June 23, 2012 | http://pubs.acs.org
Publication Date (Web): November 18, 2010 | doi: 10.1021/bk-2010-1054.pr001

Downloaded by 89.163.34.136 on June 23, 2012 | http://pubs.acs.org
Publication Date (Web): November 18, 2010 | doi: 10.1021/bk-2010-1054.ch001

Chapter 1

Review: Polymeric Scaffold Materials for Two-Dimensional and Three-Dimensional *in Vitro* Culture of Hepatocytes

Amol V. Janorkar*

Department of Biomedical Materials Science, School of Dentistry, University of Mississippi Medical Center, 2500 North State Street, Jackson, MS 39216
***ajanorkar@sod.umsmed.edu**

In vitro culture of hepatocytes (liver cells) is a challenging culture system. Despite a volume of research, the effective biomaterials for hepatocyte culture that sustain a high level of biological function over an extended culture period and induce 3-dimensional (3-D) liver-like tissue structure remain elusive. In this article, a summary of the currently available polymeric biomaterials for long term hepatocyte culture is presented. This review particularly focuses on the synthetic and natural biomaterials proposed during the last decade (2000-2009) for *in vitro* liver cell culture in static condition. Specifically, the 2-D culture, 3-D encapsulation in hydrogels, culture on 3-D sponges, and culture on polymeric substrates that induce 3-D hepatocyte spheroid formation are discussed.

Introduction

Liver plays a central role in both endocrine and exocrine physiological functions including formation and secretion of bile, albumin, and urea, metabolism of cholesterol and fat, and detoxification. According to the annual report of the American Liver Foundation in 2000, hepatitis and other liver diseases affect 25 million Americans. Liver failure is the 8th most frequent cause of death in the United States, accounting for roughly 43,000 deaths each year. Liver transplantation is currently the only effective treatment for medically refractory liver failure. Liver transplantation has some shortfalls, however, including a shortage of donor organs, restrictions on potential recipients, and side effects of

In Biomaterials; Kulshrestha, A., et al.;
ACS Symposium Series; American Chemical Society: Washington, DC, 2010.

Downloaded by 89.163.34.136 on June 23, 2012 | http://pubs.acs.org
Publication Date (Web): November 18, 2010 | doi: 10.1021/bk-2010-1054.ch001

drugs used to prevent rejection after transplantation (*1*). The problem of organ scarcity is shown by the fact that nearly 2000 candidates for liver transplantation died on the waiting list in 2003. Over 500 of these patients were listed with a diagnosis of fulminant hepatic failure.

Poor diet and sedentary lifestyle, contributing factors of obesity, are responsible for more than 300,000 deaths per year, making it the second leading cause of preventable death after smoking (*2*). Obesity is now considered an epidemic as more than 65% of American adult population is classified as obese or overweight (*3*, *4*). Obesity predisposes individuals to an increased risk for many diseases (*5–14*) including cardiovascular disease (*5*), hypertension (*6*), type-2 diabetes (*7*) and non alcoholic fatty liver disease (NAFLD) (*9–14*). In particular, the prevalence of NAFLD ranges from 10% to 39% in various populations around the world, and is likely to increase due to the ever increasing number of obese individuals (*13*, *14*). The U.S. Preventive Services Task Force recommends clinicians to screen patients for obesity and offer a common mode of treatment that involves low-fat diet and exercise to control the patient's body weight and blood sugar levels (*15*, *16*). The optimal treatment for rapid cure must include intervention at the cellular level, but exact approaches still remain unclear.

In vitro culture of hepatocytes remains to be a fertile area of research as we look for hepatocytes that can be cultured at high cell densities and demonstrate high liver-specific functions (*17*). Such high-performing hepatocytes can then be used in an extracorporeal bioartificial liver device, which may provide the necessary support to a patient with an advanced liver disease until he receives a donated liver. The 2-dimensional (2-D) planar culture of hepatocytes is currently used to investigate new treatment approaches *in vitro*. Unfortunately, this over-simplified culture model does not represent the complex *in vivo* liver tissue. Creation of 3-D *in vitro* models of the liver tissue, therefore, will help understand the pathophysiology of liver diseases and discover new therapeutics. Polymer scaffolds that can support liver cell growth over a long-term culture period have great potential in finding the solutions to these problems.

Target *in Vitro* Liver Structures

Liver is organized into several hexagonal lobules (Fig. 1a) and within each lobule, hepatocytes are arranged into cords separated by adjacent sinusoids (Fig. 1b). An endothelium lies adjacent to the hepatic cord with a separation distance of about 500 nm called the space of Disse. Within the hepatic cords, hepatocytes appear to be closely packed cells (Fig. 1c) (*18*).

In vitro culture of hepatocytes (liver cells) is a challenging culture system. Over the last couple of decades, great strides have been made to determine the effective biomaterials for hepatocyte culture that sustain a high level of biological function over an extended culture period and induce a 3-dimensional (3-D) liver-like tissue structure. In this article, a summary of the currently available polymeric biomaterials for long term hepatocyte culture is presented. This review particularly focuses on the synthetic and natural biomaterials proposed during the last decade (2000-2009) for *in vitro* liver cell culture in static condition. Readers are referred to an excellent review of the design principles in biomaterials for tissue engineering

Downloaded by 89.163.34.136 on June 23, 2012 | http://pubs.acs.org
Publication Date (Web): November 18, 2010 | doi: 10.1021/bk-2010-1054.ch001

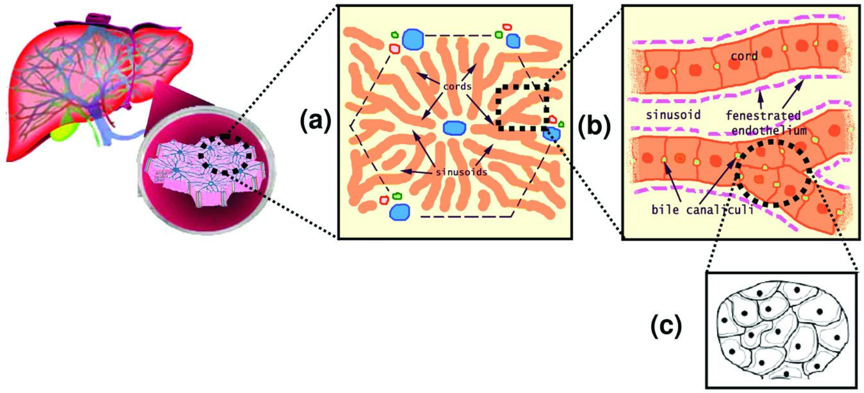

Figure 1. Schematic of the in vivo liver tissue structure consisting of (a) hepatic lobule and (b) hepatic cords and sinusoid. (c) target 3-D configuration that represents the cellular arrangements in the hepatic sinusoids. (Reproduced with permission from Ref. (18)).

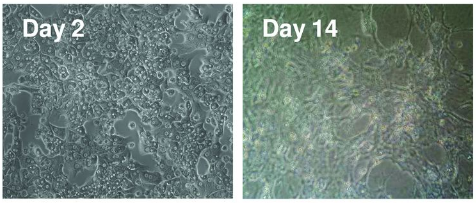

Figure 2. Representative phase images of hepatocytes cultured on tissue culture polystyrene surface

elsewhere (*19*). For comprehensive reviews of liver tissue engineering techniques that include discussions on cell sources, liver perfusion methods, culture of liver slices and tissue explants, co-culture of multiple cell types, microfluidic culture methods, and bioreactor designs, the readers are directed to ref. (*20–24*).

2-D Culture of Hepatocytes

For adherent cells, such as primary hepatocytes, the physicochemical nature of the substratum plays an important role in regulating cellular morphology, differentiation, and function. Several natural and synthetic polymers, including collagen, fibronectin, laminin, and RGD peptide-conjugates, have been evaluated for 2-D culture of primary hepatocytes (*25–29*). On these substrata, hepatocytes exhibit a spread, cuboidal morphology and differentiated phenotype, characterized by the secretion of albumin and urea. However, on most substrata, hepatocytes lose function over a culture period of 7 days, during which they undergo de-differentiation to a fibroblast-like phenotype (Fig. 2).

Methods to improve hepatocyte survival and differentiated function during long-term culture include the widely-used collagen gel sandwich configuration, which maintains hepatocyte viability and function over a period of 6-7 weeks (*30*,

Downloaded by 89.163.34.136 on June 23, 2012 | http://pubs.acs.org
Publication Date (Web): November 18, 2010 | doi: 10.1021/bk-2010-1054.ch001

31). An extensive summary of the work using cultured hepatocytes in the sandwich configuration has been presented elsewhere (*32*). Gomez-Lechon et al. used 3-D collagen gel matrix for encapsulation of hepatocytes; that resulted in a cell culture system similar to the collagen double gel configuration (*33*). Below are the two main directions in which research efforts have been focused in the past decade to achieve long-term 2-D hepatocyte culture.

Derivatives of Natural and Synthetic Polymers

Hyaluronic acid is a naturally occurring non-sulphated glycosaminoglycan consisting of a linear sequence of D-glucuronic and N-acetyl-D-glucosamine. It is present in the connective tissue, the synovial fluid of articular joints and the vitreous humor of the eye. A synthetic benzyl ester derivative of hyaluronic acid, HYAFF®, has been used for *in vitro* hepatocyte culture. HYAFF® can be processed into tubes, membranes, non-woven fabrics, gauzes, and sponges, making it an attractive material for tissue engineering and regenerative medicine. Catapano et al. reported a preliminary investigation on HYAFF® for hepatocyte culture and showed that the hepatocytes adherent to films of HYAFF® were as functional as those on collagen (*34*). Comprehensive review of HYAFF® as a scaffold for tissue engineering has been presented elsewhere (*35*).

Esaki et al. prepared lactose-modified cellulose films via an enzymatic reaction of regenerated cellulose films with lactose in lithium chloride/ dimethylacetamide solvent. The lactose-modified cellulose films showed better initial cell adhesion compared to the un-modified cellulose film (*36*).

Silk fibroin, a biocompatible protein produced by Bombyx mori silk worms, has been proposed as a possible alternative to collagen for *in vitro* hepatocyte culture. Cirrilo et al. prepared silk fibroin-collagen blend films with different silk fibroin content. Cells cultured on the blends performed comparably to those cultured on collagen (*37*). Gotoha et al. have synthesized the glycoconjugates of silk fibroin by the homogeneous chemical modification of solubilized silk fibroin with lactose using cyanuric chloride as a coupling spacer. The ^{1}H-NMR spectrum of the glycoconjugate showed new broad peaks attributed to methine and methylene protons of lactose with the estimated conjugation ratio of lactose to silk fibroin to be 0.20 (%w/w). The attached hepatocytes on the tissue culture polystyrene (TCPS) dishes coated with 0.1% (w/v) glycoconjugate showed a small and round morphology after 2.5 h, but migrated to form monolayer islands after 2 days and did not form a confluent monolayer (*38*).

Kidambi et al. demonstrated the successful attachment and spreading of primary hepatocytes on polyelectrolyte multilayer (PEM) films of synthetic polymers, namely, poly(diallyldimethyl ammonium chloride), poly(4-styrenesulfonic acid), poly(anetholesulfonic acid), and poly(vinylsulfonic acid), without the use of adhesive proteins such as collagen or fibronectin. The albumin and urea production on PEM surfaces was comparable to that of cells cultured on collagen-coated surface, however, reduced to zero by day 7 (*39*).

While more efforts in this direction are needed, the monolayer hepatocyte cultures on these newly synthesized materials still seem to suffer from similar issues faced with their culture on conventional collagen-based matrices.

In Biomaterials; Kulshrestha, A., et al.;
ACS Symposium Series; American Chemical Society: Washington, DC, 2010.

Downloaded by 89.163.34.136 on June 23, 2012 | http://pubs.acs.org
Publication Date (Web): November 18, 2010 | doi: 10.1021/bk-2010-1054.ch001

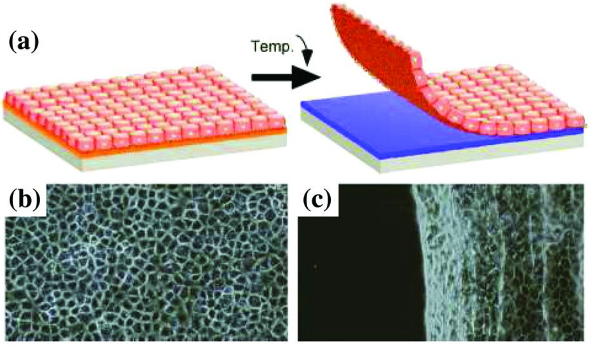

Figure 3. Cell sheet engineering using PIPAAm-grafted surfaces. (a) Schematic of temperature-induced recovery of intact monolayer cultures. (b) Confluent culture of endothelial cells on PIPAAm-grafted dishes at 37°C. (c) Detaching endothelial cell sheet by lowering culture temperature to 20°C. (Reproduced with permission from Ref. (73)).

Co-Culture of Hepatocytes with Other Cell Types

In vitro hepatocyte growth, migration, and/or differentiation can be modulated using the heterotypic cell-cell interactions, that is, the interaction of parenchymal cells (hepatocytes) with non-parenchymal cells (fibroblasts, endothelial cells, etc). Adult hepatocytes proliferate *in vivo*; however, the traditional *in vitro* monocultures of hepatocytes fail to replicate. The importance of the heterotypic cell–cell interactions has been demonstrated by a recent report by Cho et al., where, for the first time, a robust proliferative response of primary adult rat hepatocytes when co-cultured with mouse 3T3-J2 fibroblasts has been shown (*40*). A review of these techniques including the experimental approaches for co-culture of hepatocytes with non-parenchymal cells and proposed mechanisms of interaction can be found elsewhere (*41*, *42*).

Yang et al. argued that even with all the new materials and techniques discovered for tissue engineering in the past decades the overall progress of the field remained underachieved (*43*). Kushida et al. proposed that by avoiding a norm in the conventional cell culture techniques for cell harvest: the proteolytic treatment such as trypsinization, critical cell surface proteins such as ion channels, growth factor receptors, and cell-to-cell junction proteins can be preserved (*44*). Their efforts have resulted in a new class of temperature-responsive polymers based on poly(N-isopropylacrylamide) (PIPAAm) (*45–47*). The premise for use of PIPAAm is that it displays a lower critical solution temperature (LCST) around body temperature. Therefore, at 37°C, the PIPAAm is relatively hydrophobic and supports cell attachment and growth similarly to TCPS. However, upon temperature reduction below its LCST of 32°C, PIPAAm becomes hydrophilic and forces a spontaneous detachment of the attached cell layer without the need of trypsinization. A schematic is shown in Fig. 3. Using this “cell sheet engineering” approach, tissue-like structures of the skin (*48*), corneal epithelium (*49*), urothelium (*50*), periodontal ligament (*51*), cardiac muscle (*52*), kidney glomeruli, and liver lobules (*53*) have been attempted. Harimoto et al. achieved

Downloaded by 89.163.34.136 on June 23, 2012 | http://pubs.acs.org
Publication Date (Web): November 18, 2010 | doi: 10.1021/bk-2010-1054.ch001

double-layered co-culture of human aortic endothelial cells (HAECs) with rat hepatocytes by recovering a cell sheet of confluent HAECs cultured on PIPAAm surface and by placing the recovered HAEC sheet onto the rat hepatocyte layer directly. The rat hepatocytes in this structure maintained the albumin expression for over 41 days of culture (*53*).

Since its introduction by Decher (*54*), polyelectrolyte multilayer (PEM) assembly has shown great promise toward constructing complex 3-D tissue-like structures due to its nano-scale film structure and thickness. A typical PEM assembly is constructed by a sequential deposition positively and negatively charged polyelectrolyte (PE) solutions on a suitable substrate surface. A small amount of PE is adsorbed on the surface during each deposition leading to formation of a so-called ‘fuzzy’ structure initially and a more ordered layer structure as the deposition sequence is repeated several times. Previously Chan and co-workers have used PEM films to support hepatocyte attachment and function over 7 days (*39*). Rajagopalan et al. have reported the use of PEMs of DNA and chitosan as scaffolds to create layered hepatocyte-PEM-hepatocyte, hepatocyte-PEM-endothelial cell, and hepatocyte-PEM-fibroblast co-cultures (*55*).

Several novel techniques have been reported in the literature that use innovative micropatterning techniques for co-culture of hepatocytes with other cell types. For more information on these approaches the readers are directed to the works of Bhatia et al. (*56–59*), Griffith et al. (*60*, *61*), Khademhosseini et al. (*62–64*), Langer et al. (*65–68*), Okano et al. (*69–73*), and Yarmush et al (*74–77*).

While several new materials and culture techniques have been proposed for the 2-D hepatocyte culture recently, such a culture configuration always seems to suffer from hepatocyte de-differentiation and loss of liver-specific function over a short culture period. In addition, the 2-D culture configuration requires a large surface area to achieve high cell numbers for sufficient biological function. These issues may limit the development of this approach toward the next-generation bioartificial liver assist devices. A 2-D monolayer occupies almost 100% surface area. In contrast, the 3-D spheroid culture occupies only a fraction (20%) of the available surface area. Our results demonstrate that, on equivalent culture area, the primary rat hepatocytes cultured in the collagen gel sandwich secreted 85.2 ± 3.6 pg/cell/day albumin by day 7, which was sustained throughout the 3-week culture period. In comparison, the 3-D spheroid culture on the positively charged elastin-like polypeptide surface secreted 99.7 ± 4.0 pg/ cell/day albumin by day 7, which was sustained throughout the 3-week culture.

Due to its advantages over the 2-D monolayer hepatocyte culture, namely, the *in vivo* like morphology and sustained high levels of liver-specific function over a longer cultre period, the 3-D culture is being persued for the *in vitro* liver cell culture. Below are the three main research directions.

Hepatocytes Encapsulated in 3-D Hydrogels

Hydrogels have been a system of choice for hepatocyte culture because they allow diffusion of the cell culture medium constituents and harmful waste products, protect the shear-sensitive hepatocytes from the fluid motion when cultured in bioreactors or sample handing during static culture, and serve as a surface support for the attachment of the anchorage-dependent hepatocytes. Several biopolymer based hydrogels have been proposed for hepatocyte encapsulation as discussed below.

Alginate-Based Hydrogels

Alginate has been extensively used for encapsulation of hepatocytes. The alginate molecule consists of α-L-guluronic acid blocks, which cross-link in the presence of Ca^{2+} and help form the alginate hydrogel (*78*). Glicklis et al. examined the behavior of freshly isolated adult rat hepatocytes seeded within the alginate scaffolds. The scaffolds were prepared using the gelation–freeze technique, which involved crosslinking the alginate solution by calcium gluconate, followed by lyophilization. The resulting sponges had a highly porous structure with interconnecting pores with 100–150 μm diameter pores and 90% porosity. The hepatocytes in these hydrogels aggregated to form multicellular spheroids with diameters up to 100 μm, which is at the same magnitude of the sponge pore size. The maximal level of 60 pg albumin/cell/day was observed during the second week of the culture (*79*). This value falls within the range of that observed in the liver *in vivo* (*80*).

Miranda et al. used ultra-high viscosity alginate for the entrapment of hepatocyte aggregates and observed a 1.5-2 fold increase in albumin production rate and a 2 fold increase in urea production rate compared to non-encapsulated aggregates in bioreactor and spinner vessels (*81*). Ringel et al. encapsulated hepatocytes in the alginate gel by gently mixing equal volumes of hepatocyte suspension and sodium-alginate solution and subsequently collecting the mico-drops created by an air jet pellator in a polymerization buffer (glucose + HEPES-buffer + glutamine + insulin + BSA). The beads were then transferred into the cell culture medium. Approximately 3300 hepatocytes/mm^3 were encapsulated and the cells maintained their round shape (Fig. 4). Overall, the hepatocyte seeding density of 3.1×10^6 cells/mL was achieved. Application of this hydrogel system was demonstrated by determining the induction factors obtained with standard inducers, such as 3-methylcholanthrene or Phenobarbital. For example, activities of phenobarbital (0.75 mM) for induction of CYP2B and 3A isoenzymes (induction factors for testosterone hydroxylation in position 16β) were 2.5-fold higher for hepatocytes encapsulated in the alginate gel compared to the conventionally cultured hepatocytes on collagen-coated dishes (*82*). Dvir-Ginzberg et al. also used the porous alginate scaffold that enabled the efficient seeding of 10×10^6 cells/mL hepatocytes (*83*).

Several researchers have prepared 3-D hydrogel composite scaffolds involving alginate with other biopolymers. Seo et al. fabricated a highly porous hydrogel scaffold (pore size = 150-200 μm) through electrostatic interactions between alginate, galactosylated chitosan, and heparin (*84*). Alginate/xyloglucan composite hydrogels have also been reported in which hepatocytes aggregated to form multicellular spheroids with diameters up to 80 μm. On the other hand, most hepatocytes in the alginate hydrogels remained as single cells (*85*). Dvir-Ginzberg

Downloaded by 89.163.34.136 on June 23, 2012 | http://pubs.acs.org
Publication Date (Web): November 18, 2010 | doi: 10.1021/bk-2010-1054.ch001

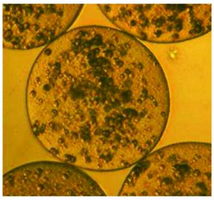

Figure 4. Hepatocytes embedded in alginate microspheres cultured for 4 days (200X). (Reproduced with permission from Ref. (82)).

et al. explored cultivation of newborn rat liver cell isolates, consisting of proliferating hepatocytes and progenitors, in macroporous alginate scaffolds (pore size = 50-100 µm; porosity = 90%) for 6 weeks as a way to reproduce hepatocyte terminal differentiation *in vitro*. Very high cell encapsulation density of 125 x 10^6/cm^3 was achieved; however, as is typical with fetal liver cells, a low albumin production rate of 3 pg/cell/day was observed. Histological and immunohistochemical examination for hepatic markers after 6 weeks of culture showed a spheroid structure consisting of a hepatocyte monolayer encasing an internal layer of dispersed cells (Fig. 5) (*86*).

Balakrishnan and Jayakrishnan created an injectable system using a periodate-oxidized sodium alginate that rapidly cross-linked with gelatin in the presence of sodium tetraborate (borax). The gelling time decreased with increase in concentration of the oxidized alginate, gelatin and borax and increase in the degree of oxidation of alginate. The hepatocytes enclosed in this hydrogel remained viable over a 2-week period (*87*).

Heparin-Based Hydrogels

Heparin is a component of the liver extracellular matrix (ECM) and binds a number of ECM proteins and growth factors via heparin binding domains. A heparin based hydrogel has been prepared via Michael addition reaction between the thiolated heparin and acrylated poly(ethylene glycol). Mixing of the primary rat hepatocytes with a pre-polymer solution during the Michael addition reaction resulted in the encapsulation of the cells into the heparin-based hydrogel (*88*). The encapsulated cells showed a moderate albumin production rate of 30-40 pg/cell/day on day 20. This enhanced liver-specific function of the encapsulated cells was attributed to the formation of large hepatic spheroids (diameter = 236 ± 14 µm) within the hydrogel. The albumin production rate was further improved to 70 pg/cell/day when hepatocyte growth factor (HGF) was incorporated into the hydrogel. Importantly, the elastic modulus for the 10 wt.% heparin gel was found to be 2300 ± 100 Pa in a fully hydrated state (*88*); similar to the one observed for the healthy liver (~1500 Pa) (*89*).

Fibrin-Based Hydrogels

Fibrin gel, formed by mixing fibrinogen with thrombin in the presence of Ca^{2+} was evaluated as a scaffold for hepatocyte transplantation in an athymic

Downloaded by 89.163.34.136 on June 23, 2012 | http://pubs.acs.org
Publication Date (Web): November 18, 2010 | doi: 10.1021/bk-2010-1054.ch001

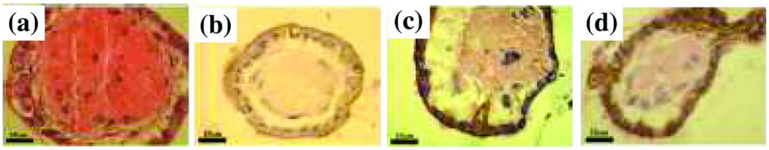

Figure 5. H&E staining of cross sections of cellular constructs revealed that in the alginate construct (a), the spheroid consists of a hepatocyte monolayer encasing an internal layer of dispersed cells. The hepatocytes were positively immunostained for CK18 (b), albumin (c), and the epithelial cell-to-cell adhesion marker, E-cadherin (d). (Reproduced with permission from Ref. (86)).

Downloaded by 89.163.34.136 on June 23, 2012 | http://pubs.acs.org
Publication Date (Web): November 18, 2010 | doi: 10.1021/bk-2010-1054.ch001

mouse model. One week after transplantation, opaque conglomerates of the transplanted hepatocytes and fibrin matrix were found on the intestinal mesentery and these conglomerates retained liver-specific functions (*90*). Bruns et al. evaluated a fibrin-based gel matrix as carrier for primary rat hepatocytes. A direct intrahepatic injection of these immobilized cells resulted in their integration into the host liver as evidenced by fluorescence microscopy and immunohistology (*91*). This approach is advantageous as less invasive transplanttation is possible compared to solid porous sponges and fiber-based scaffolds.

Poly(ethylene glycol)-Based Hydrogels

PEG based synthetic hydrogels, bearing cell-adhesive peptides, have been employed by Bhatia and co-workers for encapsulation and patterning of primary hepatocytes (*92*, *93*). Griffith et al. used galactose-conjugated poly(ethylene oxide) hydrogel to promote hepatocyte attachment and functional maintenance (*94*, *95*).

Temperature Sensitive Hydrogels

Park et al. prepared poly(organophosphazene) by a stepwise substitution reaction between poly(dichlorophosphazene) and L-isoleucine ethyl ester and α-amino-ω-methyl-poly(ethylene glycol). The polymer dissolved in cold water (< 20°C), but formed a gel at 39°C. Freshly isolated primary rat hepatocytes were cultured on positively charged Primeria dishes to induce spheroid formation. The spheroids were detached from the surface by gentle agitation, mixed with the polymer solution, and were encapsulated by gel formation. The encapsulated cells showed a moderate albumin production rate of 20 pg/cell/day on day 28 (*96*). Park et al. synthesized poly(N-isopropypacrylamide-co-acrylic acid) copolymer and conjugated it to RGD peptides via activation of the carboxylic acid groups on the acrylic acid subunit. The encapsulated cells showed a moderate albumin production rate of 18 pg/cell/day on day 28 (*97*, *98*).

A comparison of cells cultured in various 3-D hydrogels discussed above is shown in Table 1. It has been reported that 12 g albumin is synthesized and secreted per day in a 70 kg man, which is equivalent to 60 pg/cell/day, assuming an average of $2x10^{11}$ hepatocytes (*99*, *100*). Clearly, the cells secreted comparable albumin

Downloaded by 89.163.34.136 on June 23, 2012 | http://pubs.acs.org
Publication Date (Web): November 18, 2010 | doi: 10.1021/bk-2010-1054.ch001

Table 1. Comparison of cells cultured in various 3-D hydrogels

Hydrogel	*Cell Loading (10^6 x cells/cm^3)*	*Culture Period (days)*	*Albumin (pg/cell/ml)*	*Urea (pg/cell/ml)*	*Ref.*
Alginate	0.6	14	30	30	(*77*)
Alginate[1]	125	40	3	--	(*86*)
Heparin/PEG	2.0	20	30-40	50-80	(*87*)
Heparin/PEG + HGF	2.0	20	70	200	(*87*)
Poly(organophosphazene)	0.15	28	20	20	(*96*)
Poly(NiPAAm-co-AAc)/RGD	0.15	28	18	21	(*97*)

[1] Fetal liver cells; All others: rat hepatocytes

and urea during the culture period of up to 3 weeks. A cell encapsulation density of 1-2 x 10^6 cells/cm^3 seems to be optimal to achieve a higher albumin and urea secretion. The most notable exception is the cells cultured in presence of HGF, which demonstrated higher levels of liver-specific function. Additionally, the cell type cultured also has a definitive effect on the observed liver-specific function.

Unfortunately, the hydrogel environment often limits the oxygen and nutrient availability to the encapsulated hepatocytes leading to the loss of cell viability and biological function over time. This might potentially compromise the performance of future bioartificial liver assist devices. Therefore, a better understanding of the swelling and diffusion characteristics of the formed hydrogel is necessary. In addition, the mechanical properties of the hydrogel should match that of the native liver to provide an *in vivo* like microenvionment to the encapsulated hepatocytes.

Hepatocytes Cultured on 3-D Sponges

Three-dimensional porous sponges offer several advantages of the hydrogel systems and in addition provide a better mechanical stability compared to hydrogels. Several biopolymer based sponge architectures have been proposed for hepatocyte culture as discussed below.

PLGA-Based Scaffolds

Pioneering research on 3-D scaffolds for hepatocyte culture and transplantation has been performed using synthetic polymers such as poly(lactide-coglycolide) (PLGA) (*101*, *102*). Hepatocytes cultured within the PLGA foams showed high viability with a limited liver-specific gene expression (*103*). Hasirci et al. prepared foam disks from PLGA (lactic-to-glycolic mole ratio of 85:15) by lyophilization and coated them with either a type I collagen gel (0.1% w/v) or gelatin (5% w/v) to modify the surface chemistry and wettability. However, when these disks were used as scaffolds for rat hepatocyte culture, the DNA content as well as the urea synthesis of the seeded hepatocytes decreased significantly during the two weeks of culture (*104*).

Li et al. compared the interactions of cultured human hepatocytes with collagen-modified PLGA scaffolds to neat PLGA scaffolds. Porous PLGA scaffolds were prepared by freeze extraction that involved dissolving PLGA in dimethylsulfoxide (DMSO) and freezing the solution at –20°C. Subsequently, the DMSO was extracted and replaced with the ethanol-water solution, a non-solvent for PLGA. After extraction, the ethanol was removed by drying at room temperature resulting in the PLGA scaffold with pore size of 100–300 μm. On the other hand, collagen-PLGA composites were fabricated by freeze-drying that involved emulsification of type I collagen to a foam-like state by magnetic stirring and introducing it into the PLGA scaffolds with subsequent lyophilization. The primary human hepatocytes seeded on the PLGA scaffolds showed a moderate albumin production rate of 32 pg/cell/day on day 7, which was improved to 38 pg/cell/day for the collagen-modified PLGA scaffold (*105*).

To avoid the possible disadvantages (e.g., cytotoxicity) of scaffold preparation methods involving organic solvents, Zhu et al. prepared porous PLGA sponges by a solvent-free supercritical CO_2 gas-foaming method. The PLGA sponges showed desirable biodegradability, exhibited uniform pore size distribution with moderate interconnectivity, and provided a conductive environment for Hep3B cells as justified by better cell infiltration, higher proliferation and hepatic function (*106*).

Downloaded by 89.163.34.136 on June 23, 2012 | http://pubs.acs.org
Publication Date (Web): November 18, 2010 | doi: 10.1021/bk-2010-1054.ch001

Chitosan-Based Scaffolds

Chitosan is a partially deacetylated derivative of chitin. It has been a material of choice because it is a biocompatible and biodegradable polymer with structure similar to glycosaminoglycans (GAGs) present in the liver ECM. Li et al. prepared porous chitosan scaffolds with 90% porosity and mean pore sizes of 50-200 μm by lyophilization of chitosan solution. The scaffolds were further modified with water-soluble polyanionic species such as alginate and heparin. Hepatocytes cultured on these porous scaffolds exhibited a round cellular morphology with many microvilli evident on the cell surface (*107*). Later, the chitosan scaffold was modified with fructose via the reaction between the amine groups in chitosan with the aldehyde groups in fructose (*108*). Fructose was chosen as it is a specific ligand for asialoglycoprotein receptor (ASGPR) in hepatocytes and has been shown to protect hepatocytes under cold hypoxia before normothermic reoxygenation (*109*). The primary rat hepatocytes seeded on the chitosan scaffolds showed a moderate albumin production rate of 45 pg/cell/day on day 7, which improved to 55 pg/cell/day for the chitosan/fructose scaffold (*108*).

Fan et al. compared the liver-specific functions of hepatocytes cultured on 3-D sponges of chitosan and chitosan/galactosylated hyaluronic acid composite. The galactosylated hyaluronic acid was synthesized via covalent coupling of lactobionic acid with hyaluronic acid. The chitosan/galactosylated hyaluronic acid sponges were prepared via freeze-drying through the electrostatic interaction of carboxylic groups of galactosylated hyaluronic acid with amine groups of chitosan. An investigation into the effect of the freezing temperature during the freeze-drying process revealed that the porosity, pore size, and pore size

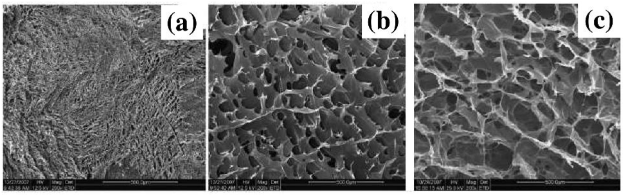

Figure 6. Scanning electron micrographs of chitosan/galactosylated hyaluronic acid scaffolds as a function of the freezing temperature (200 X). (a) liquid nitrogen; (b) -80°C; (c) -20°C. (Reproduced with permission from Ref. (110))

Downloaded by 89.163.34.136 on June 23, 2012 | http://pubs.acs.org
Publication Date (Web): November 18, 2010 | doi: 10.1021/bk-2010-1054.ch001

distribution were significantly affected by this chosen experimental parameter (Fig. 6). The primary rat hepatocyte seeded on the chitosan scaffold showed a low albumin production rate of 4 pg/cell/day on day 15, which was improved to 8 pg/cell/day for the chitosan/galactosylated hyaluronic acid composite scaffold. Moreover, the mechanical testing data showed that the Young's modulus of the chitosan/galactosylated hyaluronic acid composite scaffold (200 Pa) was lower than that for chitosan (400 Pa) scaffold (*110*); which was much lower than that of a healthy liver (~1500 Pa) (*89*).

As demonstrated above, chitosan lacks long-term mechanical stability. Therefore, Li et al. attempted to improve the mechanical properties of chitosan scaffolds by combining it with TiO_2. The TiO_2/chitosan composite scaffold containing 0.7% TiO_2 prepared by freeze-drying showed an irregular pore size structure (pore size = 180-420 µm) with the TiO_2 particles uniformly dispersed on the surface of the pore walls. The pure chitosan scaffold showed a regular pore structure (pore size = 80–200 µm). The compressive strength of the composite scaffolds (100-160 kPa) was significantly improved compared to that of pure chitosan scaffolds (65 kPa). The hepatic immortal HL-7702 cells attached on the pore walls of the chitosan scaffold showed a relatively high albumin production rate of 95 pg/cell/day on day 7, which was unaffected by the addition of the TiO_2 particles (*111*). Recently Jiankand et al. have reported the micro-fabrication of porous (>90% porosity) chitosan-gelatin hybrid scaffolds with the mean pore size of 100 µm that displayed microstructures similar to that of the portal vein, central vein, flow-channel network and hepatic chambers (*112*).

Hyaluronic Acid-Based Scaffolds

Hyaluronic acid is a non-sulfated glycosaminoglycan (GAG) in the matrix of embryonic and fetal tissues in the liver. Zavan et al. used HYAFF-11™ derived from the total esterification of hyaluronan with benzyl alcohol to prepare non-woven meshes of 50 µm-thick fibers. Hepatocytes adhered to these fibers within the scaffolds and formed aggregates and cords of several cells along the fibers. However, these cells showed a very low albumin production rate of 50 ng/10^6 cells/day on day 14. Enriching the HYAFF-11™ mesh with fibroblast-derived ECM improved the albumin production rate to 80 ng/10^6 cells/day on day 14 (*113*).

Downloaded by 89.163.34.136 on June 23, 2012 | http://pubs.acs.org
Publication Date (Web): November 18, 2010 | doi: 10.1021/bk-2010-1054.ch001

Synthetic Polymer-Based Scaffolds

Because of its favorable mechanical strength, thermal and chemical resistance, and excellent biocompatibility, polyethersulfone (PES) has been tried as a spongy scaffold for C3A cells. Spongy PES membranes were prepared using phase inversion process from mixture containing PES (based polymer), dimethylformamide (solvent), polyvinylpyrrolidone (small pore precursor), and cellulose (large pore precursor). Scanning electron microscopy analysis indicated that C3A cells attached to PES membranes forming microvilli characteristic for normal hepatocytes. These cells showed low albumin production rate of 2 pg/cell/day on day 10 (*114*). *In vivo* evaluation of these pre-seeded PES membranes transplanted to severe combined immunodeficiency (SCID/NOD) mice showed integration of the membrane after transplantation with recipient liver tissue (*115*).

Pahernik et al. used fiber extrusion to prepare 2-mm thick nonwoven polyurethane matrices with microfiber thickness of 20–60 µm, pore diameter of 10–200 µm, and 70% porosity. The primary porcine hepatocytes seeded on these scaffolds showed moderate albumin production rate of 53.7 ± 5.6 ng/h/µg DNA on day 7 (*116*).

Liver-Derived Biomatrix (LBM)-Based Scaffolds

Decellularized, biologically derived matrices represent an ideal way to capture the intricate in vivo microstructure of the liver tissue. Lin et al. demonstrated the use of decellularized, porcine LBM as a bioresorbable scaffold for primary adult rat hepatocytes. These hepatocytes maintained liver-specific functions such as albumin synthesis, urea production, and P-450 IA1 activity for up to 45 days (*117*). Linke et al. seeded porcine microvascular endothelial cells on a decellularized porcine jejunal segment with preserved vascular structures followed by a seeding of porcine hepatocytes onto the vascularized scaffold. This 2-stage seeding procedure resulted in a 3-D co-culture system with multiple hepatocyte layers lining the endothelial-cell generated capillary structures (*118*).

Microcarrier-Based Scaffolds

Cytodex-3, composed of a surface layer of denatured collagen covalently bound to a matrix of cross-linked dextran, exhibits high cellular affinity and hence, has been extensively adopted in the culture of anchorage-dependent animal cells (*119*). However, hepatocytes adhering to these microcarriers show irregular polygonal morphology and resemble that of monolayer growth on plain surfaces (*120*). Additionally, these microcarriers are expensive and often occupy a large part of the cost in the cultivation of anchorage-dependent cells (*121*). To encourage a multi-layer growth of the attached hepatocytes atop the microcarrier surface, Wu et al. prepared a macroporous chitosan microcarrier via mechanical stirring of a mixture of chitosan and liquid paraffin, followed by crosslinking with glutaraldehyde, removal of the liquid paraffin and unreacted glutaraldehyde, and finally, lyophilization of the crosslinked chitosan. The resulting microcareer of 300-500 μm size had an average pore size of 50 μm and 86% porosity. The microcareers were further modified with either lactose or maltose. Scanning electron micrographs of the porous chitosan microcarrier and hepatocytes cultured on lactose-modified chitosan microcarrier are shown in Fig. 7. The primary rat hepatocytes seeded on the lactose-modified microcarriers showed moderate albumin production rate of 25 pg/cell/day on day 13 (*122*). Keguo et al. prepared chitosan/gelatin composite microcarriers by a water-in-oil emulsion process with additional freezing and lyophilization. The resulting microcareer of 200–500 μm size had pore sizes ranging from 50–200 μm (*123*). Culture of hepatocytes on gelatin microcarriers has also been reported (*124*).

Zhu et al. used an oil-in-water emulsion solvent evaporation technique to prepare poly(3-hydroxybutyrate-co-3-hydroxyvalerate) (PHBV) microspheres. Results showed 2-times higher proliferation and 2-4 times more albumin secretion by the Hep3B cells seeded on the microspheres than that on 2-D surfaces (*125*). The proliferation of Hep3B cells was further improved when the microspheres were covalently conjugated with type I collagen, laminin, and fibronectin, using 1-ethyl-3-(3-dimethylaminopropyl) carbodiimide and N-hydroxysuccinimide (*126*). The preparation of PLGA/PHBV composite microcarriers with a core-shell structure has also been reported. These composite microcarriers exhibited a moderate degradation rate (55% mass loss over three months) and sustained delivery of the hepatocyte growth factor (HGF) with maintained bioactivity for at least 40 days. These results indicated that PLGA/PHBV composite microcarriers would be more suitable than the pure PHBV or PLGA microcarriers as a scaffold for hepatocyte culture (*127*).

Vegetable-Based Scaffolds

Chen et al. used a vegetable sponge prepared from a ripened dried fruit of Luffa cylindrica (*L. cylindrica*, loofa sponge) with porosity of 90% and an average pore size of 335 ± 65 μm. This material was used as a 3-D scaffold for the culture of rat hepatocytes. Rat hepatocytes formed spheroid aggregates and both urea synthesis and albumin secretion rates were maintained up to 7 days (*128*). The liver-specific functions were further improved by introducing a galactose moiety on the sponge surface using covalent bonding with lactobionic acid. In a packed bed reactor perfusion system, the primary rat hepatocytes showed high albumin production rate of 109 pg/cell/day over a 7-day culture period (*129*). Loofa sponge was also used as a 3-D scaffold for stationary and perfusion culture of human hepatoblastoma cell line C3A/HepG2. In static culture, C3A/HepG2 cells in loofa sponge showed higher alpha-fetoprotein and albumin secretion rates than those in polyurethane foam. In the perfusion culture, the immobilized C3A/HepG2 showed steady synthesis of albumin at 42 pg/cell/day over a 9-day culture period (*130*).

A comparison of cells cultured on various 3-D sponges discussed above is shown in Table 2. Clearly, the cells showed wide variation of albumin and urea secretion rates during the culture period of up to 2 weeks. The difference in the liver-specific functions can be attributed to several experimental factors. For example, the cell loading density plays an important role in the observed liver-specific function. This is demonstrated by the culture of primary rat hepatocytes

Downloaded by 89.163.34.136 on June 23, 2012 | http://pubs.acs.org
Publication Date (Web): November 18, 2010 | doi: 10.1021/bk-2010-1054.ch001

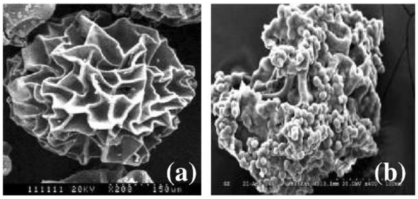

Figure 7. SEM images of (a) porous chitosan microcarrier (150X) and (b) hepatocytes cultured on lactose modified microcarrier (100X). (Reproduced with permission from Ref. (122)).

on the 3-D chitosan sponges, as culturing 0.2 x 10^6 cells/cm^3 yielded a low albumin production rate of 4 pg/cell/day on day 15, while culturing 1.7 x 10^6 cells/cm^3 yielded a moderate albumin production of 45 pg/cell/day on day 7. Additionally, the cell type cultured also has a definitive effect on the observed liver-specific function. It should be noted that, for most sponges summarized in Table 2, the average pore size was > 100 μm; this size has been shown to provide optimum viability and function, with no mass transfer limitations (*131*). In addition, the mechanical properties of the sponges need to be carefully considered as most of the currently available 3-D sponges demonstrate higher rigidity.

3-D Spheroid Culture of Hepatocytes in Static Conditions

It has been argued that spheroids exhibit excellent liver-specific function and show the closely packed morphology (Fig. 1c). Hepatocytes in a spheroid configuration have been shown to possess structural polarity and functional bile canaliculi. Hepatocytes cultured as spheroids generally exhibit excellent liver-specific differentiation and function. In the spheroid configuration, cohesive interactions between cells are greater than the adhesive interactions between the cells and substratum (*132*). Spheroid formation process involves cell translocation and changes in cell shape, indicative of the reorganization of the cytoskeletal elements (*133*). Tzanakakis et al. have demonstrated that an intact actin network was required to mediate these events and the enhanced differentiated function. However, microtubule integrity was not essential for an efficient hepatocyte spheroid self-assembly (*133*). Hasabe et al. have shown that induction of plasminogen activators and the subsequent plasmin generation on the hepatocyte surface play an important role in the spheroid formation process (*134*). Extensive investigation of the spheroid structure and morphology by Hu and co-workers using the time lapse microscopy and scanning and transmission electron microscopy revealed that cell movement and reorganization were involved in spheroid formation with a polarized cellular morphology and bile canalicular structures that surrounded each individual hepatocyte (*135*). Using real-time polymerase chain reaction (RT-PCR), Sakai et al. showed that the expression of genes involved in cell adhesion, metabolism, transcription, and intra-cellular transportation of primary rat hepatocytes were consistently higher in spheroid configuration than those in the monolayer culture for at least 10 days (*136*).

Downloaded by 89.163.34.136 on June 23, 2012 | http://pubs.acs.org
Publication Date (Web): November 18, 2010 | doi: 10.1021/bk-2010-1054.ch001

Downloaded by 89.163.34.136 on June 23, 2012 | http://pubs.acs.org
Publication Date (Web): November 18, 2010 | doi: 10.1021/bk-2010-1054.ch001

Table 2. Comparison of cells cultured on various 3-D sponges

Sponge	Avg. Pore Size	Porosity	Cell Loading	Culture Period	Albumin	Urea	Ref.
	(µm)	(%)	(10^6 x cells/cm^3)	(days)	(pg/cell/ml)		
PLGA[1]	100-300	--	0.03	13	32	2337	105
Collagen-PLGA[1]	100-300	90	0.03	13	38	3000	105
Chitosan[2]	112	90	0.2	15	4	2	110
Chitosan[2]	50-200	93	1.7	7	45	45	108
Chitosan[3]	80-200	90	1.0	14	95	25	111
Chitosan/galactose-hyaluronic acid [2]	140	90	0.2	15	8	4	110
Chitosan/fructose[2]	50-200	90	1.7	7	55	90	108
Chitosan/TiO_2[3]	80-420	--	1.0	14	95	25	111
HYAFF-11 [2]	–	–	2.0	14	0.05	--	113
ECM-Enriched HYAFF-11[2]	--	--	2.0	14	0.08	--	113
PES[4]	10-50	--	0.5	10	2	--	114

1: human hepatocytes; 2: primary rat hepatocytes; 3: HL-7702; 4: C3A cells

In general, positively charged surfaces or surfaces to which hepatocytes do not readily adhere have been shown to promote the spheroid formation (*137*). Surfaces such as agarose, Primeria, alginate, and Matrigel have been used in the past for this purpose (*37*, *133–136*, *138–140*). However, the spheroids formed on non-adherent surfaces are more prone to be dislodged from their surface anchorage point. Such non-attached spheroids lose their viability and biological-function at a much faster rate compared to the attached spheroids. Moreover, the spheroids formed on non-adherent surfaces (e.g., agarose) produce differentiated hepatocyte-specific functions to a lesser degree than those formed on positively charged surface (e.g., Primeria). Additionally, surface environments consisting of mainly positively charged polymers often prove cytotoxic to the anchorage-dependent hepatocytes and hence, low concentrations of such coating solutions are required to produce spheroids. Such low concentrations may provide non-uniform coatings. To overcome some of these disadvantages multiple new materials and culture configurations have been proposed for the long-term culture of hepatic spheroids. These attempts are summarized below.

Galactosylated Polymer Substrates

Surfaces presenting galactose moieties have been used to induce hepatocyte attachment and subsequent spheroid formation. Galactosylated surfaces interact with hepatocytes through the cell surface asialoglycoprotein receptor (ASGPR). Mammalian ASGPR is a hepatic lectin for receptor-mediated endocytosis, which binds galactose and N-acetylgalactosamine-terminated ligands in a calcium-dependent manner (*141*). Pioneering studies by Akaike and coworkers demonstrated the use of a galactose carrying polystyrene, poly(N-p-vinylbenzyl-4-*o*-β-D-galactopyranosyl-D-gluconamide) (PVLA) for the proliferation and differentiation of hepatocytes (*142*). A comprehensive review of the galactose-carrying polymers as ECM for liver tissue engineering has been presented by Akaike et al (*143*).

Park et al. showed that the rat hepatocyte adhesion to galactosylated chitosan-coated polystyrene dish (95% in 2 h) was significantly higher than that to the chitosan-coated dish (70% in 2 h). The cells attached to the galactosylated chitosan-coated surface subsequently formed spheroids through the interaction with galactose moieties and cationic groups of chitosan (*144*).

Lu et al. coated a poly(vinylidene difluoride) (PVDF) surface with galactose-tethered Pluronic polymer via hydrophobic–hydrophobic interaction between PVDF and the polypropylene oxide segment in Pluronic to achieve the galactose group grafting density of 15.4 nmol/cm^2. The cultured primary rat hepatocytes formed 100-200 μm-diameter spheroids and showed a moderate albumin production rate of 20 pg/cell/day on day 15 (*145*). Ying et al. immobilized galactose ligands on acrylic acid grafted poly(ethylene terephthalate) (PET) film and demonstrated its use for the hepatocyte spheroid culture (*146*). Unfortunately, the spheroids grown on galactose substrates detach easily from the substrata. Therefore, Du et al. developed a hybrid RGD/galactose carrying substratum by chemical grafting of both RGD peptide and galactose ligand to the PET film surface. Firstly, the PET film was activated by argon plasma

Downloaded by 89.163.34.136 on June 23, 2012 | http://pubs.acs.org
Publication Date (Web): November 18, 2010 | doi: 10.1021/bk-2010-1054.ch001

treatment and grafted with poly(acrylic acid) (PAA) via UV-induced graft polymerization. Subsequently, the PET-g-PAA surface was activated by a water-soluble carbodiimide and N-hydroxysulfosuccinimide and reacted with a mixture of 1-O-(6′-aminohexyl)-D-galactopyranoside and RGD peptide. In this dual functionality PET-hybrid substrate, the RGD peptide enhanced cell adhesion, while the galactose moiety induced spheroid formation synergistically. The primary rat hepatocytes cultured atop the PET-hybrid surface with 1:1 ratio of RGD:galactose formed a thick 3-D multilayers which was intermediate between the 3-D spheroids formed on the PET-galactose surface and the 2-D monolayer formed on the collagen dishes. Although this approach will be advantageous in asmuchas it could form stable 3-D hepatocyte architectures, the cultured cells showed a low albumin production rate of 16 pg/cell/day on day 7 (*147*).

Downloaded by 89.163.34.136 on June 23, 2012 | http://pubs.acs.org
Publication Date (Web): November 18, 2010 | doi: 10.1021/bk-2010-1054.ch001

Synthetic Polymer Substrates

Partially degradable composites of woven PET fabrics have been fabricated by coating a thin biodegradable PLGA film on one side and coating a PVLA film on the other side to improve cell attachment. Primary mouse hepatocytes cultured on this fabric surface aggregated to form spheroids (Fig. 8). The mesh size of the fabric influenced the hepatocyte aggregation behavior as 160-µm spheroids were formed on large meshes (720 µm) within 48 h, whereas the aggregation required 4 days on the smaller meshes (50 and 200 µm) (*148*, *149*). Risbud et al. prepared the PET fabric (fiber diameter = 40 µm and mesh size = 200 µm) coated with chitosan, collagen, or their blends. Textiles coated with collagen and all blends were incubated 37°C for 2 h for gelation. Both rat hepatocytes and HepG2 cells attached to all matrices and then formed spheroids. Average albumin secretion by HepG2 spheroids was 50–65 pg/cell/day (*150*).

Physical properties of the scaffold material such as surface wettability, hardness, and roughness play an important role in cell attachment, proliferation, and/or differentiation. Bartolo et al. compared the properties of membranes of polyetheretherketone (PEEK), polyurethane (PU), Nylon, PES, and PET. Surface energy of these membranes is shown in Fig. 9. The primary rat hepatocytes seeded on these membranes formed 3-D aggregates. The urea synthesis of these cells increased with the membrane surface free energy and was found to be maximum for the PEEK membranes with surface energy of 49–51 mJ/m^2 (Fig. 9). These results indicated that the moderate wettability of PEEK was responsible for improving the cell-surface interactions (*151*). Catapano et al. used microporous polypropylene membranes with varying surface wettabilities for rat hepatocyte adhesion and demonstrated that the hepatocyte viability and metabolic functions generally improved with the surface wettability (*152*).

Long-term maintenance and differentiation of human hepatocytes has been demonstrated using microporous membranes of 2:1 PEEK-PU blends. Human hepatocytes cultured on PEEK-PU membranes showed high albumin secretion of 100 pg/cell/day (*153*). Low-temperature ammonia-plasma modification of the PEEK-PU membranes grafted nitrogen-containing functional groups on their surface. The plasma treatment can modify the membrane surface properties without affecting the bulk properties. However, one disadvantage of the plasma

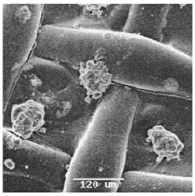

Figure 8. SEM image of hepatocyte aggregates on a 200-μm PET/PLGA/PVLA scaffold after 96 h. (Reproduced with permission from Ref. (148)).

modification process is the loss of the surface modification over time. For example, the water contact angle (WCA) results from Salerno et al. show that the WCA for the native PEEK- PU membrane was 80 ± 8°, which reduced to 41 ± 9° after the plasma modification. However, after 8 days of ageing in air, the WCA increased to 61 ± 3°. Human hepatocytes cultured on PEEK-PU membranes showed high albumin secretion rate of 84 pg/cell/day (*154*).

Inverse Colloidal Crystal (ICC) Substrates

Kotov et al. created of a 3-D scaffold with ICC geometry and a tight control over the scaffold porosity by infiltration of the hexagonal crystal lattice of polystyrene spheres with sol-gel formulation and subsequent annealing (*155*). Recently they reported Poly(acrylamide) hydrogel-based ICC geometry for the culture of HepG2 human hepatocellular carcinoma (HB-8065) cells. Their method involved creating the colloidal crystals via infiltration of poly(acrylamide) hydrogel precursor into the colloidal crystals formed by 50-200 μm diameter soda lime glass beads by centrifugation, free radical polymerization of the hydrogel precursor to create a transparent hydrogel matrix, and the subsequent dissolution of the glass beads using hydrogen fluoride. Using this method highly ordered 3-D ICC structures were formed with pore size that corresponded with the soda lime glass bead size. HepG2 cells seeded on these ICC scaffolds gradually self-assembled to form 3D spheroids over a period of 5 days. The spheroid size correlated well with the size of the ICC pores. For example, 46.5 ± 8.1 μm diameter spheroids were formed in scaffolds with 59.5 ± 1.9 μm pores, while 151.6 ± 20.0 μm diameter spheroids were formed in scaffolds with 218.6 ± 6.1 μm pores. These results indicated that uniform spheroids with a narrow size distribution could be obtained, which are important for the consistent evaluation of the relationships between cell cluster diameter and biological activity. The liver-specific function was demonstrated to be strongly dependent on the diameter of spheroid, however, the results failed to show improved liver-specific function for the HepG2 cells cultured on the 3-D ICC scaffolds compared to 2-D cell culture atop a TCPS plate (*156*).

Downloaded by 89.163.34.136 on June 23, 2012 | http://pubs.acs.org
Publication Date (Web): November 18, 2010 | doi: 10.1021/bk-2010-1054.ch001

Downloaded by 89.163.34.136 on June 23, 2012 | http://pubs.acs.org
Publication Date (Web): November 18, 2010 | doi: 10.1021/bk-2010-1054.ch001

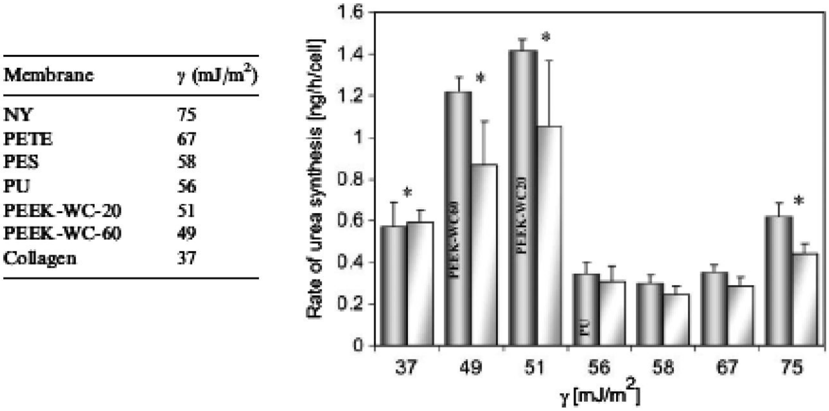

Membrane	γ (mJ/m²)
NY	75
PETE	67
PES	58
PU	56
PEEK-WC-20	51
PEEK-WC-60	49
Collagen	37

*Figure 9. Urea synthesis rate of liver cells cultured on membranes with different surface free energy (γ) after 24 h (full bar) and 48 h (shade bar) of culture reported as the mean of eight experiments ± standard deviation. * $p < 0.05$. (Reproduced with permission from Ref. (151)).*

Dendrimer Grafted Substrates

Kawase reported the use of starburst polyamidoamine (PAMAM) dendrimers for the rat hepatoma (H4-II-E-C3) cells. These dendrimers are highly branched spherical polymers with well-defined structures and a set number of terminal amine groups. A polystyrene surface was grafted with the PAMAM dendrimer by following a series of reaction steps: Firstly, 4-(3-trifluoromethylazirino) benzoyl-N-succinimide (TDBA-OSu) was photografted to the TCPS surface using UV light exposure. Then, TDBA-OSu was reacted with tris(2-aminoethyl)amine to create the first generation PAMAM dendrimer. These steps were repeated to create the PAMAM dendrimer. The PAMAM-dendrimer grafted polystyrene surface showed an improved ability for rat hepatoma cell attachment, proliferation, and albumin production (*157*). The PAMAM dendrimer was subsequently modified by conjugating the terminal amine groups with fructose, lecithin, and a tripeptide growth factor, Glycyl-L-Histidyl-L-Lysine. These modified dendrimers resulted in improved rat hepatoma cell attachment, proliferation, and albumin production compared to the non-modified PAMAM dendrimer (*158*). The fructose modified PAMAM dendrimers also resulted in reduced apoptosis of the attached hepatocytes compared to the non-modified PAMAM dendrimer (*159*). Further, it was demonstrated that simultaneous modification of the PAMAM dendrimers with fructose and galactose lead to higher urea synthesis and albumin gene expression, than did those cultured on single-ligand-modified dendrimers (*160*).

Growth Factor Presenting Substrates

In vitro cell culture frequently benefits from the use of growth factors that provide signals for cellular proliferation or differentiation. Hoshiba et al. investigated the effect of hepatocyte growth factor (HGF) on hepatocytes

Downloaded by 89.163.34.136 on June 23, 2012 | http://pubs.acs.org
Publication Date (Web): November 18, 2010 | doi: 10.1021/bk-2010-1054.ch001

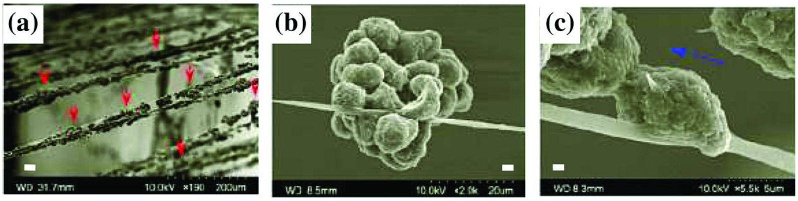
(a)
WD 31.7mm 10.0kV ×190 200um
(b)
WD 8.5mm 10.0kV ×2.5k 20um
(c)
WD 8.3mm 10.0kV ×5.5k 5um

Figure 10. SEM images of hepatocytes cultured on the aligned PLLA nanofibers (red arrows) on day 3. Blue arrows: direction of cell migration. Scale bars: (a) 200 µm;(b) 20µm; and (c) 5 µm. (Reproduced with permission from Ref. (163)).

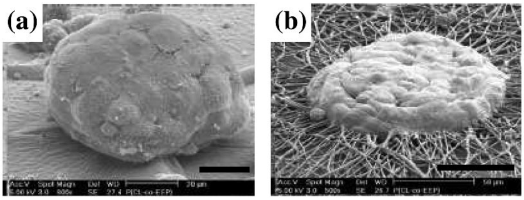

Figure 11. SEM images of the spheroid aggregates formed on PCLEEP (a) film and (b) nanofibrous scaffolds. Scale bars: (a) 20 µm and (b) 50µm. (Reproduced with permission from Ref. (164)).

cultured on natural ECMs (type I collagen, fibronectin, and laminin) and synthetic polymers: poly-L-lysine (PLL) and PVLA. Their results revealed that the hepatocytes underwent proliferation on type I collagen- and fibronectin-coated surfaces in the presence of HGF, whereas formed spheroids on laminin-, PVLA-, and PLL-coated surfaces in the presence of HGF (*161*).

Revzin et al. investigated solid-phase presentation of HGF on robotically printed microarrays of ECM proteins (collagen I, collagen IV, or laminin). Primary rat hepatocytes seeded onto HGF/ECM protein microarrays formed cellular clusters that corresponded in size to the dimensions of individual protein spots (500 µm diameter) and subsequently formed spheroids with a high albumin production rate of 60-120 pg/cell/day on day 6 (*162*).

Nanofibrous Substrates

By providing limited cell-substrate adhesion strength and restricting cell migration to uniaxial movement, Feng et al. induced spheroid formation in primary rat hepatocytes on aligned nanofibers of poly(L-lactic acid) coated with type-I collagen. The cell-substrate adhesion strength was limited by reducing the available contact area between individual cells and the substrate, that is, by using the nanofibers produced by electrospinning. The average diameter of nanofibers was 780 nm. Hepatocyte pseudopodes indicated directional migration of hepatocytes along the aligned nanofibers (Fig. 10), resulting in the formation of spherical or ellipsoid aggregates with average diameter of 61 µm and moderate albumin production (40 pg/cell/day on day 15) (*163*).

Downloaded by 89.163.34.136 on June 23, 2012 | http://pubs.acs.org
Publication Date (Web): November 18, 2010 | doi: 10.1021/bk-2010-1054.ch001

Table 3. Comarison of 3-D spheroids cultured on various substrates

Surface	Serum content in medium	Avg. Spheroid Size	Culture Period	Albumin	Urea	Ref.
	(%)	(μm)	(days)	(pg/cell/ml)		
PVDF/Gal-Pluronic	Serum-free	100-200	15	20	--	145
PEEK-PU	Serum-free	--	32	100	500	153
Plasma-modified PEEK-PU	Serum-free	--	19	84	96	154
PLLA nanofibers	5	61	15	40	20	163
PCLEEP film/Gal	5	50-300	5	15	15	164
PCLEEP nanofibers/Gal	5	20-100	5	15	15	164
PET-RGD/Gal	10	--	7	16	250	147
Chitosan film/Gal	10	50-100	7	40	30	165
Chitosan nanofibers/Gal	10	30-200	7	20	30	165
ELP-PEI	10	113	21	20	200	170

Downloaded by 89.163.34.136 on June 23, 2012 | http://pubs.acs.org
Publication Date (Web): November 18, 2010 | doi: 10.1021/bk-2010-1054.ch001

To determine the effect of nanofibrous scaffold morphology versus the surface chemistry on the hepatocyte attachment and function, Chua et al. compared the nanofibrous poly(ε-caprolactone-co-ethyl ethylene phosphate) (PCLEEP) scaffold with PCLEEP film. PCLEEP copolymer is a biodegradable polymer with ester and phosphate linkages in the backbone. Galactose ligands were introduced on the scaffold surfaces via covalent conjugation to a UV-grafted poly(acrylic acid) spacer. As shown in Fig. 11, the SEM images of the spheroid-like aggregates revealed that the aggregates formed on the PCLEEP nanofibrous scaffolds were flattened with well-integrated nanofibers. Hepatocytes cultured on both scaffolds exhibited similar functional profiles in terms of cell attachment, ammonia metabolism, albumin secretion, and cytochrome P450 enzymatic activity. These results indicate that the impact of the glycosylated surface chemistry is predominant over that of the nanofibrous morphology. Nevertheless, the hepatocyte aggregates integrated with the nanofibers would be better immobilized on the scaffold and would not detach from the substrate upon agitation, unlike those attached on the film surface (*164*).

Recently, preparation of galactosylated chitosan nanofibers (average diameter ~160 nm) by electrospinning was reported (*165*, *166*). Like those cultured on the PCLEEP nanofibers, the hepatocytes cultured on the galactosylated chitosan nanofibrous scaffold also formed immobilized flat aggregates, which did not detach during the cell culture period, while the spheroid aggregates cultured on the galactosylated chitosan film could be detached easily (*165*).

Chemo-Biologically Synthesized Substrates

Elstin-like polypeptides (ELPs) are a family of polypeptides derived from a portion of the primary sequence of mammalian elastin, VPGXG, where V = valine, P = proline, G = glycine, and X = any amino acid except proline (*167–169*). ELP exhibits a thermally-induced phase transition at a characteristic temperature called the inverse transition temperature (T_t). Above T_t, ELPs undergo a reversible intramolecular contraction and intermolecular coacervation leading to a coiled structure, resulting in an increased absorbance at 350 nm (*169*). Recombinant ELP, with the primary sequence of H_2N-MVSACRGPG[VGVPG]$_{40}$-WP-COOH, was produced in shaker flask using *E. coli* BLR(DE3) and purified by an inverse transition temperature (T_t) purification method. Poly(ethyleneimine), PEI, with a branched structure, was conjugated to the activated C-terminus acid group on the ELP using carbodiimide. This created a positively charged ELP. Primary rat hepatocytes plated on ELP-PEI formed cellular aggregates within 48 h and then formed spheroids with diameter of 113 ± 6 μm within 72 h. Hepatocyte spheroids on ELP-PEI surfaces exhibited a moderate rate of albumin production by day 7 (18-22 pg/cell/24h), which was sustained over a 21-day period (*170*).

A comparison of the 3-D spheroids of primary rat hepatocytes obtained on the various substrates discussed above is shown in Table 3. Clearly, the 3-D spheroids formed atop most surfaces secreted comparable albumin and urea during the culture period of up to 3 weeks. The most notable exceptions are the spheroids cultured atop the PEEK-PU blend surfaces which showed very high albumin and urea production and the spheroids cultured atop the PET-RGD/Gal and ELP-PEI

Downloaded by 89.163.34.136 on June 23, 2012 | http://pubs.acs.org
Publication Date (Web): November 18, 2010 | doi: 10.1021/bk-2010-1054.ch001

surfaces which secreted higher levels of urea. In general, several literature reports have found a serum-free or low serum (< 5%) environment to be favorable for the formation of hepatic spheroids (*145*, *153*, *154*, *163*, *164*). The high performance of the spheroids cultured on the PEEK-PU blend surfaces may therefore be attributed to the serum-free culture environment. The high performance of the PET-RGD/Gal and ELP-PEI surfaces can be attributed to the better attachment of hepatocytes.

Summary

Despite a volume of research, there still seems to be no consensus on the effective biomaterials to achieve an effective hepatocyte culture that will sustain a high level of biological function over an extended culture period. This is specifically because of the several limitations presented by the currently available culture systems. In 2-D culture, hepatocytes lose liver-specific function over a culture period of 1-2 weeks, during which they undergo de-differentiation to a fibroblast-like phenotype. The collagen gel sandwich culture is the current "gold standard" for 2-D hepatocyte culture. However, culturing hepatocytes in 2-D culture also has an important, innate limitation of requiring a large surface area to achieve high cell numbers for sufficient biological function, which will prove to be a major limiting factor for the development of this approach toward the next-generation bioartificial liver assist devices. Additionally and more importantly, the collagen gels are "bulky" with thickness of 100 μm (two orders of magnitude thicker than the Space of Disse, see Fig. 1b). Such gels are expected to hinder cell-cell culture communication vital in 3-D liver tissue structures.

Hydrogels have shown promise for hepatocyte culture. Unfortunately, the hepatocytes cultured in a hydrogel environment are often nutrient limited and lose their viability and biological function over time. This was mainly attributed to the impeded oxygen and nutrient transport through the hydrogel and might potentially compromise the performance of future bioartificial liver assist devices (*171*). Considerations for designing biodegradable hydrogels for cell encapsulation have been reviewed by Nicodemus and Bryant (*172*).

Three-dimensional porous sponges offer several advantages of the hydrogel systems and in addition provide a better mechanical stability compared to hydrogels. However, a critical control of the mechanical properties will be desired of the next generation sponges as a higher rigidity may comprise their use as potential implant materials. Considerations for designing 3-D scaffolds for cell culture have been reviewed by Kotov et al (*173*).

Hepatocytes in a spheroid configuration have been shown to possess structural polarity and functional bile canaliculi and have demonstrated higher levels of liver-specific function. However, the spheroids formed on non-adherent surfaces are more prone to be dislodged from their surface anchorage point. Such non-attached spheroids lose their viability and biological-function at a much faster rate compared to the attached spheroids. Additionally, most spheroids develop a necrotic center, with only a few viable cell layers on the outskirts, due to the limited nutrient supply to and removal of waste products from the cells at the spheroid core. The modeling studies by Glicklis et al. have shown 80% viability for 100-μm diameter spheroids (*174*). These issues may have limit the utility of spheroids in long-term applications. Recent advances in 3-D multicellular spheroid culture for biomedical research have been reviewed by Lin and Chang (*175*).

The new generation of hepatocyte culture systems is therefore needed through the successful partnership from researchers with cross-disciplinary expertise in synthetic chemistry, analytical methods for characterization of polymeric biomaterials, tissue engineering, and hepatocyte biology. Integration of these disciplines will have a significant impact in the liver tissue engineering research arena. Approaches such as the nanofibrous scaffolds which formed spheroids with well-integrated nanofibers and the chemo-biologically synthesized materials from genetically engineered biopolymers that combine the biocompatibility of ECM-based materials with the charged-functionality of the synthetic polymers may represent the new avenues for long-term liver cell culture. Scaffolds with controlled architecture can now be formed using computational topology design and solid free-form fabrication (*176*). These advances need to be incorporated in the future design of 3-D scaffold materials.

Downloaded by 89.163.34.136 on June 23, 2012 | http://pubs.acs.org
Publication Date (Web): November 18, 2010 | doi: 10.1021/bk-2010-1054.ch001

Acknowledgments

The new faculty start-up funding to AVJ from the School of Dentistry at the University of Mississippi Medical Center is gratefully acknowledged.

References

1. Seaberg, E.; Belle, S.; Beringer, K.; Schivins, J; Detre, K. *Clinical Transplants* **1998**, *12*, 17–37.
2. National Heart Lung and Blood Institute. *Obes. Res.* **1998**, *6*, 51S–209S.
3. Flegal, K. M.; Carroll, M. D.; Ogden, C. L.; Johnson, C. L. *JAMA, J. Am. Med. Assoc.* **2002**, *288*, 1723–1727.
4. Ogden, C. L.; Flegal, K. M.; Carroll, M. D.; Johnson, C. L. *JAMA, J. Am. Med. Assoc.* **2002**, *288*, 1728–1732.
5. Seidell, J. C.; Verschuren, W. M.; van Leer, E. M.Kromhout, D. *Arch. Intern. Med.* **1996**, *156*, 958–963.
6. Field, A. E.; Byers, T.; Hunter, D. J.; Laird, N. M.; Manson, J. E.; Williamson, D. F.; Willett, W. C.; Colditz, G. A. *Am. J. Epidemiol.* **1999**, *150*, 573–579.
7. Hu, F. B.; Manson, J. E.; Stampfer, M. J.; Colditz, G.; Liu, S.; Solomon, C. G.; Willett, W. C. *N. Engl. J. Med.* **2001**, *345*, 790–797.
8. Calle, E. E.; Rodriguez, C.; Walker-Thurmond, K.; Thun, M. J. *N. Engl. J. Med.* **2003**, *348*, 1625–1638.
9. Matteoni, C.; Younossi, Z. M.; Gramlich, T.; Boparai, N.; Liu, Y. C.; McCullough, A. *Gastroenterology* **1999**, *116*, 1413–1419.
10. Angulo, P. *N. Eng. J. Med.* **2002**, *346*, 1221–1231.
11. Festi, D.; Colecchia, A.; Sacco, T.; Bondi, M.; Roda, E.; Marchesini, G. Hepatic. *Obes. Rev.* **2004**, *5*, 27–42.

Downloaded by 89.163.34.136 on June 23, 2012 | http://pubs.acs.org
Publication Date (Web): November 18, 2010 | doi: 10.1021/bk-2010-1054.ch001

12. Wang, D.; Wei, Y.; Pagliassotti, M. J. *Endocrinology* **2006**, *147*, 943–951.
13. Yu, A. S.; Keeffe, E. B.; Mulhall, B. P.; Ong, J. P.; Younossi, Z. M. *Rev. Gastroenterol. Disord.* **2002**, *2*, 11–19.
14. Bellentani, S.; Saccocio, G.; Masutti, F.; Croce, L. S.; Brandi, G.; Sasso, F.; Cristanini, G.; Tiribelli, C. *Ann. Intern. Med.* **2000**, *132*, 112–117.
15. U.S. Preventive Services Task Force. *Ann. Intern. Med.* **2003**, *139*, 930–932.
16. Stein, C. J.; Colditz, G. A. *J. Clin. Endocrinol. Metab.* **2004**, *89*, 2522–2525.
17. Tilles, A. W.; Berthiaume, F.; Yarmush, M. L.; Tompkins, R. G.; Toner, M. *J. Hepatobiliary. Pancreat. Surg.* **2002**, *9*, 686–696.
18. http://www.siumed.edu/~dking2/erg/liver.htm (Last Accessed on 03/15/2010).
19. Griffith, L. G. *Ann. N.Y. Acad. Sci.* **2002**, *961*, 83–95.
20. Castell, J. V.; Gómez-Lechón, M. J. *Methods Mol. Biol.* **2009**, *481*, 35–46.
21. Nahmias, Y.; Berthiaume, F.; Yarmush, M. L. *Adv. Biochem. Eng. Biotechnol.* **2007**, *103*, 309–329.
22. Fiegel, H. C.; Kneser, U.; Kluth, D.; Metzger, R.; Till, H.; Rolle, U. *Pediatr. Surg. Int.* **2009**, *25*, 667–673.
23. Kulig, K. M.; Vacanti, J. P. *Transplant Immunol.* **2004**, *12*, 303–310.
24. Allen, J. W.; Bhatia, S. N. *Tissue Eng.* **2002**, *8*, 725–737.
25. Du, Y.; Chia, S.; Han, R.; Chang, S.; Tang, H.; Yu, H. *Biomaterials* **2006**, *27*, 5669–5680.
26. Horiuti, Y.; Nakamura, T.; Ichihara, A. J. *J. Biochem. (Tokyo)* **1982**, *92*, 1985–1994.
27. Tashiro, K.; Sephel, G. C.; Greatorex, D.; Sasaki, M.; Shirashi, N.; Martin, G. R.; Kleinman, H. K.; Yamada, Y. J. *J. Cell Physiol.* **1991**, *146*, 451–459.
28. Ijima, H.; Kawakami, K. J. *J. Biosci. Bioeng.* **2005**, *100*, 62–66.
29. Ying, L.; Yin, C.; Zhuo, R. X.; Leong, K. W.; Mao, H. Q.; Kang, E. T.; Neoh, K. G. *Biomacromolecules* **2003**, *4*, 157–65.
30. Dunn, J. C. Y.; Yarmush, M. L.; Koebe, H. C.; Tompkins, R. G. *FASEB J.* **1989**, *3*, 174–177.
31. Dunn, J. C. Y.; Tompkins, R. C.; Yamsush, M. L. *Biotechnol. Prog.* **1991**, *7*, 237–245.
32. Berthiaume, F.; Moghe, P. V.; Toner, M.; Yarmush, M. L. *FASEB J.* **1996**, *10*, 1471–1484.
33. Gomez-Lechon, M. J.; Jover, R.; Donato, T.; Ponsoda, X.; Rodriguez, C.; Stenzel, K. G.; Klocke, R.; Paul, D.; Guillen, I.; Bort, R.; Castel, J. V. *J. Cell. Physiol.* **1998**, *177*, 553–562.
34. Catapano, G.; De Bartolo, L.; Vico, V.; Ambrosio, L. *Biomaterials* **2001**, *22*, 659–665.
35. Vindigni, V.; Cortivo, R.; Iacobellis, L.; Abatangelo, G.; Zavan, B. *Int. J. Mol. Sci.* **2009**, *10*, 2972–2985.
36. Esaki, K.; Yokota, S.; Egusa, S.; Okutani, Y.; Ogawa, Y.; Kitaoka, T.; Goto, M.; Wariishi, H. *Biomacromolecules* **2009**, *10*, 1265–9.
37. Cirillo, B.; Morra, M.; Catapano, G. *Int. J. Artif. Organs* **2004**, *27*, 60–68.
38. Gotoha, Y.; Niimi, S.; Hayakawa, T.; Miyashita, T. *Biomaterials* **2004**, *25*, 1131–1140.

In Biomaterials; Kulshrestha, A., et al.;
ACS Symposium Series; American Chemical Society: Washington, DC, 2010.

39. Kidambi, S.; Lee, I.; Chan, C. *J. Am. Chem. Soc.* **2004**, *126*, 16286–16287.
40. Cho, C. H.; Berthiaume, F.; Tilles, A. W.; Yarmush, M. L. *Biotechnol. Bioeng.* **2008**, *101*, 345–356.
41. Bhatia, S. N.; Balis, U. J.; Yarmush, M. L. *FASEB J.* **1996**, *13*, 1883–1900.
42. Bhatia, S. N.; Balis, U. J.; Yarmush, M. L.; Toner, M. *Biotechnol. Prog.* **2008**, *14*, 378–387.
43. Yang, J.; Yamato, M.; Kohno, C.; Nishimoto, A.; Sekine, H.; Fukai, F.; Okano, T. *Biomaterials* **2005**, *26*, 6415–6422.
44. Kushida, A.; Yamato, M.; Konno, C.; Kikuchi, A.; Sakurai, Y.; Okano, T. *J. Biomed. Mater. Res.* **1999**, *45*, 355–362.
45. Yamada, N.; Okano, T.; Sakai, H.; Karikusa, F.; Sawasaki, Y.; Sakurai, Y. *Makromol. Chem. Rapid Commun.* **1990**, *11*, 571–576.
46. Okano, T.; Yamada, N.; Sakai, H.; Sakurai, Y. *J. Biomed. Mater. Res.* **1993**, *27*, 1243–1251.
47. Akiyama, Y.; Kikuchi, A.; Yamato, M.; Okano, T. *Langmuir* **2004**, *20*, 5506–5511.
48. Yamato, M.; Utsumi, M.; Kushida, A.; Konno, C.; Kikuchi, A.; Okano, T. *Tissue Eng* **2001**, *7*, 473–480.
49. Nishida, K.; Yamato, M.; Hayashida, Y.; Watanabe, K.; Maeda, N.; Watanabe, H.; et al. *Transplantation* **2004**, *77*, 379–385.
50. Shiroyanagi, Y.; Yamato, M.; Yamazaki, Y.; Toma, H.; Okano, T. *BJU Int.* **2004**, *93*, 1069–75.
51. Hasegawa, M.; Yamato, M.; Kikuchi, A.; Okano, T.; Ishikawa, I. *Tissue Eng.* **2005**, *11*, 469–478.
52. Shimizu, T.; Yamato, M.; Isoi, Y.; Akutsu, T.; Setomaru, T.; Abe, K.; et al. *Circ. Res.* **2002**, *90*, e40.
53. Harimoto, M.; Yamato, M.; Hirose, M.; Takahashi, C.; Isoi, Y.; Kikuchi, A.; et al. *J. Biomed. Mater. Res.* **2002**, *62*, 464–470.
54. Decher, G. Fuzzy Nanostructures. *Science* **1997**, *277*, 1232–1237.
55. Rajagopalan, P. R.; Shen, C. J.; Berthiaume, F.; Tilles, A. W.; Toner, M.; Yarmush, M. L. *Tissue Eng.* **2006**, *12*, 1553–1563.
56. Kim, S. S.; Utsunomiya, H.; Koski, J. A.; Wu, B. M.; Cima, M. J.; Albrecht, D. R.; Tsang, V. L.; Sah, R. L.; Bhatia, S. N. *Lab Chip* **2005**, *5*, 111–118.
57. Liu, V. L.; Bhatia, S. N. *Biomed. Microdevices* **2002**, *4*, 257–266.
58. Flaim, C. J.; Chien, S.; Bhatia, S. N. *Nat. Methods* **2005**, *2*, 119–125.
59. Albrecht, D. R.; Underhill, G. H.; Wassermann, T. B.; Sah, R. L.; Bhatia, S. N. *Nat. Methods* **2006**, *3*, 369–375.
60. Sohn, J.; Mukai, K.; Griffith, L. G.; Vacanti, J. P. *Ann. Surg.* **1998**, *228*, 8–13.
61. Powers, M. J.; Domansky, K.; Kaazempur-Mofrad, M. R.; Kalezi, A.; Capitano, A.; Upadhyaya, A.; Kurzawski, P.; Wack, K. E.; Stolz, D. B.; Kamm, R.; Griffith, L. G. *Biotechnol. Bioeng.* **2002**, *78*, 257–269.
62. Chang, T. Y.; Yadav, V. G.; De Leo, S.; Mohedas, A.; Rajalingam, B.; Chen, C. L.; Selvarasah, S.; Dokmeci, M. R.; Khademhosseini, A. *Langmuir* **2007**, *23*, 11718–11725.
63. Wright, D.; Rajalingam, B.; Selvarasah, S.; Dokmeci, M. R.; Khademhosseini, A. *Lab Chip* **2007**, *7*, 1272–1279.

Downloaded by 89.163.34.136 on June 23, 2012 | http://pubs.acs.org
Publication Date (Web): November 18, 2010 | doi: 10.1021/bk-2010-1054.ch001

64. Wright, D.; Rajalingam, B.; Karp, J. M.; Selvarasah, S.; Ling, Y.; Yeh, J.; Langer, R.; Dokmeci, M. R.; Khademhosseini, A. *J. Biomed. Mater. Res., Part A* **2008**, *85*, 530–538.
65. Fukuda, J.; Khademhosseini, A.; Yeo, Y.; Yang, X.; Yeh, J.; Eng, G.; Blumling, J.; Wang, C. F.; Kohane, D. S.; Langer, R. *Biomaterials* **2006**, *27*, 5259–5267.
66. Khademhosseini, A.; Yeh, J.; Eng, G.; Karp, J.; Kaji, H.; Borenstein, J.; Farokhzad, O. C.; Langer, R. *Lab Chip* **2005**, *5*, 1380–1386.
67. Fukuda, J.; Khademhosseini, A.; Yeh, J.; Eng, G.; Cheng, J.; Farokhzad, O. C.; Langer, R. *Biomaterials* **2006**, *27*, 1479–1486.
68. Khademhosseini, A.; Suh, K. Y.; Yang, J. M.; Eng, G.; Yeh, J.; Levenberg, S.; Langer, R. *Biomaterials* **2004**, *25*, 3583–3592.
69. Hirose, M.; Yamato, M.; Kwon, O. H.; Harimoto, M.; Kushida, A.; Shimizu, T.; Kikuchi, A.; Okano, T. *Yonsei Med. J.* **2000**, *41*, 803–813.
70. Yamato, M.; Kwon, O. H.; Hirose, M.; Kikuchi, A.; Okano, T. *J. Biomed. Mater. Res.* **2001**, *55*, 137–140.
71. Yamato, M.; Konno, C.; Kushida, A.; Hirose, M.; Utsumi, M.; Kikuchi, A.; Okano, T. *Biomaterials* **2000**, *2*, 981–986.
72. Tsudaa, Y.; Kikuchi, A.; Yamato, M.; Nakao, A.; Sakurai, Y.; Umezu, M.; Okano, T. *Biomaterials* **2005**, *26*, 1885–1893.
73. Kikuchi, A.; Okano, T. *J. Controlled Release* **2005**, *101*, 69–84.
74. Bhatia, S. N.; Balis, U. J.; Yarmush, M. L.; Toner, M. *J. Biomater. Sci., Polym. Ed.* **1998**, *9*, 1137–1160.
75. King, K. R.; Wang, S.; Irimia, D.; Jayaraman, A.; Toner, M.; Yarmush, M. L. *Lab Chip* **2007**, *7*, 77–85.
76. Cho, C. H.; Park, J.; Tilles, A. W.; Berthiaume, F.; Toner, M.; Yarmush, M. L. *BioTechniques* **2010**, *48*, 47–52.
77. Novik, E.; Maguire, T. J.; Chao, P.; Cheng, K. C.; Yarmush, M. L. *Biochem. Pharmacol.* **2010**, *79*, 1036–1044.
78. Draet, K. I.; Brae, G.S.; Smidsrød, O. *Carbohydr. Polym.* **1994**, *25*, 31–38.
79. Glicklis, R.; Shapiro, L.; Agbaria, R.; Merchuk, J. C.; Cohen, S. *Biotechnol. Bioeng.* **2000**, *67*, 344–353.
80. Peter, T. J.; Peter, J. C. *J. Biol. Chem.* **1972**, *247*, 3858–3864.
81. Miranda, J. P.; Rodrigues, A.; Tostoes, R. M.; Leite, S. B.; Zimmermann, H.; Carrondo, M. J.; Alves, P. M. *Tissue Eng., Part C* **2010** [Epub ahead of print].
82. Ringel, M.; von Mach, M. A.; Santos, R.; Feilen, P. J.; Brulport, M.; Hermes, M.; Bauer, A. W.; Schormann, W.; Tanner, B.; Schon, M. R.; Oesch, F.; Hengstle, J. G. *Toxicology* **2005**, *206*, 153–167.
83. Dvir-Ginzberg, M.; Gamlieli-Bonshtein, I.; Agbaria, R.; Cohen, S. *Tissue Eng.* **2003**, *9*, 757–766.
84. Seo, S. J.; Choi, Y. J.; Akaike, T.; Higuchi, A.; Cho, C. S. *Tissue Eng.* **2006**, *12*, 33–44.
85. Seo, S. J.; Akaike, T.; Choi, Y. J.; Shirakawa, M.; Kang, I. K.; Cho, C. S. *Biomaterials* **2005**, *26*, 3607–3615.
86. Dvir-Ginzberg, M.; Elkayam, T.; Cohen, S. *FASEB J.* **2008**, *22*, 1440–1449.
87. Balakrishnan, B.; Jayakrishnan, A. *Biomaterials* **2005**, *26*, 3941–3951.

Downloaded by 89.163.34.136 on June 23, 2012 | http://pubs.acs.org
Publication Date (Web): November 18, 2010 | doi: 10.1021/bk-2010-1054.ch001

88. Kim, M.; Lee, J. Y.; Jones, C. N.; Revzin, A.; Tae, G. *Biomaterials* **2010**, *31*, 3596–3603.
89. Li, L.; Sharma, N.; Chippada, U.; Jiang, X.; Schloss, R.; Yarmush, M. L. *Ann. Biomed. Eng.* **2008**, *36*, 865–876.
90. Gwak, S. J.; Choi, D.; Paik, S. S.; Lee, E. Y.; Lee, K. S.; Kim, B. S. *Biotechnol. Lett.* **2004**, *26*, 505–508.
91. Bruns, H.; Kneser, U.; Holzhüter, S.; Roth, B.; Kluth, J.; Kaufmann, P. M.; Kluth, D.; Fiegel, H. C. *Tissue Eng.* **2005**, *11*, 1718–1726.
92. Tsang, V. L.; Chen, A. A.; Cho, L. M.; Jadin, K. D.; Sah, R. L.; DeLong, S.; et al. *FASEB J.* **2007**, *21*, 790–801.
93. Underhill, G. H.; Chen, A. A.; Albrecht, D. R.; Bhatia, S. N. *Biomaterials* **2007**, *28*, 256–270.
94. Griffith, L. G.; Lopina, S. *Biomaterials* **1998**, *19*, 979–986.
95. Lopina, S. T.; Wu, G.; Merrill, E. W.; Griffith, L. G. *Biomaterials* **1996**, *17*, 559–569.
96. Park, H. K.; Song, S. C. J. *Biosci. Bioeng.* **2006**, *101*, 238–242.
97. Park, K.; Na, K.; Kim, S. W.; Jung, S. Y.; Park, K. H.; Chung, H. *Biotechnol. Lett.* **2005**, *27*, 1081–1086.
98. Park, K. H. *Biotechnol. Lett.* **2002**, *24*, 1131–1135.
99. Tavill, A. S.; McCullough, A. J. Protein metabolism and the liver. In *Wright's liver and biliary disease*; Millward-Sadler, G. H., Wright, R., Arthur, M. J. P., Eds.; 3rd ed.; W.B. Saunders Ltd: London, 1992; p 92.
100. Khalil, M.; Shariat-Panahi, A.; Tootle, R.; Ryder, T.; McCloskey, P.; Roberts, E.; Hodgson, H.; Selden, C. *J. Hepatol.* **2001**, *34*, 68–77.
101. Mikos, A. G.; Bao, Y.; Cima, L. G.; Ingber, D. E.; Vacanti, J. P.; Langer, R. *J. Biomed. Mater. Res.* **1993**, *27*, 183–189.
102. Mikos, A. G.; Thorsen, A. J.; Czerwonka, L. A.; Bao, Y.; Winslow, D. N.; Vacanti, J. P.; Langer, R. *Polymer* **1994**, *35*, 1068–1077.
103. Kaufmann, P. M.; Heimrath, S.; Kim, B. S.; Mooney, D. J. *Cell Transplant.* **1997**, *6*, 463–468.
104. Hasirci, V.; Berthiaume, F.; Bondre, S. P.; Gresser, J. D.; Trantolo, D. J.; Toner, M.; Wise, D. L. *Tissue Eng.* **2001**, *7*, 385–94.
105. Li, J.; Li, L.; Yu, H.; Cao, H.; Gao, C.; Gong, Y. *ASAIO J.* **2006**, *52*, 321–327.
106. Zhu, X. H.; Lee, L. Y.; Jackson, J. S.; Tong, Y. W.; Wang, C. H. *Biotechnol. Bioeng.* **2008**, *100*, 998–1009.
107. Li, J.; Pan, J.; Zhang, L.; Guo, X.; Yu, Y. *J. Biomed. Mater. Res., Part A* **2003**, *67*, 938–943.
108. Li, J.; Pan, J.; Zhang, L.; Yu, Y. *Biomaterials* **2003**, *24*, 2317–2322.
109. Evdokimova, E.; Martos, M.; Calderon, P. M. B. U. C. *Food Chem. Toxicol.* **1997**, *35*, 669–675.
110. Fan, J.; Shang, Y.; Yuan, Y.; Yang, J. *J. Mater. Sci.: Mater. Med.* **2010**, *21*, 319–327.
111. Zhao, L.; Chang, J.; Zhai, W. *J. Mater. Sci.: Mater. Med.* **2009**, *20*, 949–957.
112. Jiankang, H.; Dichen, L.; Yaxiong, L.; Bo, Y.; Hanxiang, Z.; Qin, L.; Bingheng, L.; Yi, L. *Acta Biomater.* **2009**, *5*, 453–61.

Downloaded by 89.163.34.136 on June 23, 2012 | http://pubs.acs.org
Publication Date (Web): November 18, 2010 | doi: 10.1021/bk-2010-1054.ch001

113. Zavan, B.; Brun, P.; Vindigni, V.; Amadori, A.; Habeler, W.; Pontisso, P.; Montemurro, D.; Abatangelo, G.; Cortivo, R. *Biomaterials* **2005**, *26*, 7038–7045.
114. Kinasiewicz, A.; Smietanka, A.; Dudzinski, K.; Chwojnowski, A.; Gajkowska, B.; Werynski, A. *Artif. Organs* **2008**, *32*, 747–752.
115. Kinasiewicz, A.; Dudzinski, K.; Chwojnowski, A.; Werynski, A.; Kawiak, J. *Transplant. Proc.* **2007**, *39*, 2914–2916.
116. Pahernik, S. A.; Thasler, W. E.; Doser, M.; Gomez-Lechon, M. J.; Castell, M. J.; Planck, H.; Koebe, H. G. *Cells Tissues Organs* **2001**, *168*, 170–177.
117. Lin, P.; Chan, W. C.; Badylak, S. F.; Bhatia, S. N. *Tissue Eng.* **2004**, *10*, 1046–53.
118. Linke, K.; Schanz, J.; Hansmann, J.; Walles, T.; Brunner, H.; Mertsching, H. *Tissue Eng.* **2007**, *13*, 2699–2707.
119. Wang, Y.; Ouyang, F. *Bioprocess Eng.* **1999**, *21*, 207–210.
120. Gao, Y.; Hu, H. Z.; Chen, K.; Yang, J. Z. *World J. Gastroenterol.* **2000**, *6*, 365–370.
121. Wang, Y.; Ouyang, F. *Bioprocess Eng.* **1999**, *21*, 207–210.
122. Wu, C.; Pan, J.; Bao, Z.; Yu, Y. *J. Mater. Sci: Mater. Med.* **2007**, *18*, 2211–2214.
123. Li, K.; Wang, Y.; Miao, Z.; Xu, D.; Tang, Y.; Feng, M. *Biotechnol. Lett.* **2004**, *26*, 879–883.
124. Xu, T.; Li, S.; Yu, Y. *J. Biomed. Mater. Res., Part A* **2003**, *65*, 306–310.
125. Zhu, X. H.; Wang, C. H.; Tong, Y. W. *J. Biomed. Mater. Res., Part B* **2007**, *82*, 7–16.
126. Zhu, X. H.; Gan, S. K.; Wang, C. H.; Tong, Y. W. *J. Biomed. Mater. Res., Part A* **2007**, *83*, 606–616.
127. Zhu, X. H.; Wang, C. H.; Tong, Y. W. *J. Biomed. Mater. Res., Part A* **2009**, *89*, 411–423.
128. Chen, J. P.; Lin, T. C. *Biotechnol. Prog.* **2005**, *21*, 315–319.
129. Chen, J. P.; Lin, T. C. *J. Biosci. Bioeng.* **2006**, *102*, 41–45.
130. Chen, J. P.; Yu, S. C.; Hsu, B. R.; Fu, S. H.; Liu, H. S. *Biotechnol. Prog.* **2003**, *19*, 522–527.
131. Kang, H.; Tabata, Y.; Ikada, Y. *Biomaterials* **1999**, *20*, 1339–1344.
132. Powers, M. J.; Griffith, L. G. *Microsc. Res. Tech.* **1998**, *43*, 379–384.
133. Tzanakakis, E. S.; Hansen, L. K.; Hu, W. S. *Cell Motility Cytoskeleton* **2001**, *48*, 175–189.
134. Hasebe, Y.; Akao, M.; Okumura, N.; Izumi, T.; Koh, T.; Seki, T.; Ariga, T. *Biochem. Biophys. Res. Commun.* **2003**, *308*, 852–857.
135. Peshwa, M. V.; Wu, F. J.; Sharp, H. L.; Cerra, F. B.; Hu, W. S. *In Vitro Cell Dev. Biol. Anim.* **1996**, *32*, 197–203.
136. Sakai, Y.; Yamagami, S.; Nakazawa, K. *Cells Tissues Organs* **2009** [Epub ahead of print].
137. Koide, N.; Sakaguchi, K.; Koide, Y. *Exp. Cell Res.* **1990**, *186*, 227–235.
138. Hasebe, Y.; Okumura, N.; Koh, T.; Kazama, H.; Watanabe, G.; Seki, T.; Ariga, T. *Hepatol. Res.* **2005**, *32*, 89–95.
139. Semler, E. J.; Ranucci, C. S.; Moghe, P. V. *Biotechnol. Bioeng.* **2000**, *69*, 359–369.

Downloaded by 89.163.34.136 on June 23, 2012 | http://pubs.acs.org
Publication Date (Web): November 18, 2010 | doi: 10.1021/bk-2010-1054.ch001

140. Lazar, A.; Madhusudan, P. V.; Wu, F. J.; Chi, C. M.; Cerra, F. B.; Hu, W.-S. *Cell Transplant.* **1995**, *4*, 259–268.
141. Wall, D. A.; Wilson, G.; Hubbard, A. L. *Cell* **1980**, *21*, 79–93.
142. Kobayashi, K.; Kobayashi, A.; Akaike, T. *Methods Enzymol.* **1994**, *247*, 409–418.
143. Cho, C. S.; Seo, S.J.; Park, I. K.; Kim, S. H.; Kim, T. H.; Hoshiba, T.; Harada, I.; Akaike, T. *Biomaterials* **2006**, *27*, 576–585.
144. Park, I. K.; Yang, J.; Jeong, H. J.; Bom, H. S.; Harada, I.; Akaike, T.; Kim, S. I.; Cho, C. S. *Biomaterials* **2003**, *24*, 2331–2337.
145. Lu, H. F.; Lim, W. S.; Wang, J.; Tang, Z. Q.; Zhang, P. C.; Kam, W.; Leong; Chia, S. M.; Yu, H.; Mao, H. Q. *Biomaterials* **2003**, *24*, 4893–4903.
146. Ying, L.; Yin, C.; Zhuo, R. X.; Leong, K. W.; Mao, H. Q.; Kang, E. T.; Neoh, K. G. *Biomacromolecules* **2003**, *4*, 157–165.
147. Du, Y.; Chia, S. M.; Han, R.; Chang, S.; Tang, H.; Yu, H. *Biomaterials* **2006**, *27*, 5669–5680.
148. Karamuk, E.; Mayer, J.; Wintermantel, E.; Akaike, T. *Artif. Organs* **1999**, *23*, 881–887.
149. Mayer, J.; Karamuk, E.; Akaike, T.; Wintermantel, E. *J. Controlled Release* **2000**, *64*, 81–90.
150. Risbud, M. V.; Karamuk, E.; Schlosser, V.; Mayer, J. *J. Biomater. Sci., Polym. Ed.* **2003**, *14*, 719–731.
151. De Bartolo, L.; Morelli, S.; Rende, M.; Gordano, A.; Drioli, E. *Biomaterials* **2004**, *25*, 3621–3629.
152. Catapano, G.; Di Lorenzo, M. C.; Della Volpe, C.; De Bartolo, L.; Migliaresi, C. *J. Biomater. Sci., Polym. Ed.* **1996**, *7*, 1017–1027.
153. De Bartolo, L.; Morelli, S.; Gallo, M. C.; Campana, C.; Statti, G.; Rende, M.; Salerno, S.; Drioli, E. *Biomaterials* **2005**, *26*, 6625–6634.
154. Salerno, S.; Piscioneri, A.; Laera, S.; Morelli, S.; Favia, P.; Bader, A.; Drioli, E.; De Bartolo, L. *Biomaterials* **2009**, *30*, 4348–4356.
155. Kotov, N. A; Liu, Y.; Wang, S.; Cumming, C.; Eghtedari, M.; Vargas, G.; Motamedi, M.; Nichols, J.; Cortiella, J. *Langmuir* **2004**, *20*, 7887–7892.
156. Lee, J.; Cuddihy, M. J.; Cater, G. M.; Kotov, N. A. *Biomaterials* **2009**, *30*, 4687–4694.
157. Kawase, M.; Kurikawa, N.; Miura, N.; Shiomi, T.; Ozawa, C.; Higashiyama, S.; Mizoguchi, T.; Yagi, K. *Artif. Organs* **1999**, *24*, 18–22.
158. Kawase, M.; Kurikawa, N.; Higashiyama, S.; Miura, N.; Shiomi, T.; Ozawa, C.; Mizoguchi, T.; Yagi, K. *J. Biosci. Bioeng.* **1999**, *88*, 433–437.
159. Kawase, M.; Shiomi, T.; Matsui, H.; Ouji, Y.; Higashiyama, S.; Tsutsui, T.; Yagi, K. *J. Biomed. Mater. Res.* **2001**, *54*, 519–524.
160. Higashiyama, S.; Noda, M.; Kawase, M.; Yagi, K. *J. Biomed. Mater. Res., Part A* **2003**, *64*, 475–482.
161. Hoshiba, T.; Wakejima, M.; Cho, C. S.; Shiota, G.; Akaike, T. *J. Biomed. Mater. Res., Part A* **2008**, *85*, 228–35.
162. Jones, C. N.; Tuleuova, N.; Lee, J. Y.; Ramanculov, E.; Reddi, H.; Zern, M. A.; Revzin, A. *Biomaterials* **2009**, *30*, 3733–3741.
163. Feng, Z. Q.; Chu, X. H.; Huang, N. P.; Leach, M. K.; Wang, G.; Wang, Y. C.; Ding, Y. T.; Gu, Z. Z. *Biomaterials* **2010**, *31*, 3604–3612.

Downloaded by 89.163.34.136 on June 23, 2012 | http://pubs.acs.org
Publication Date (Web): November 18, 2010 | doi: 10.1021/bk-2010-1054.ch001

164. Chua, K. N.; Lim, W. S.; Zhang, P.; Lu, H.; Wen, J.; Ramakrishn, S.; Leong, K. W.; Mao, H. Q. *Biomaterials* **2005**, *26*, 2537–2547.
165. Feng, Z. Q.; Chu, X.; Huang, N. P.; Wang, T.; Wang, Y.; Shi, X.; Ding, Y.; Gu, Z. Z. *Biomaterials* **2009**, *30*, 2753–2763.
166. Chu, X. H.; Shi, X. L.; Feng, Z. Q.; Gu, Z. Z.; Ding, Y. T. *Biotechnol. Lett.* **2009**, *31*, 347–352.
167. Urry, D. W. *J. Protein Chem.* **1988**, *7*, 1–34.
168. Urry, D. W. *Prog. Biophys. Mol. Biol.* **1992**, *57*, 23–57.
169. Urry, D. W. *J. Phys. Chem.* **1997**, *101*, 11007–11028.
170. Janorkar, A. V.; Rajagopalan, P.; Yarmush, M. L.; Megeed, Z. *Biomaterials* **2008**, *29*, 625–632.
171. Nyberg, S. L.; Shatford, R. A.; Peshwa, M. V.; White, J. G.; Cerra, F. B.; Hu, W. S. *Biotechnol. Bioeng.* **1993**, *41*, 194–203.
172. Nicodemus, G. D.; Bryant, S. J. *Tissue Eng., Part B* **2008**, *14*, 149–165.
173. Lee, J.; Cuddihy, M. J.; Kotov, N. A. *Tissue Eng., Part B* **2008**, *14*, 61–86.
174. Glicklis, R.; Merchuk, J. C.; Cohen, S. *Biotechnol. Bioeng.* **2004**, *86*, 672–680.
175. Lin, R. Z.; Chang, H. Y. *Biotechnol. J.* **2008**, *3*, 1172–1184.
176. Hollister, S. J. *Nat. Mater.* **2005**, *4*, 518–524.

Downloaded by 89.163.34.136 on June 23, 2012 | http://pubs.acs.org
Publication Date (Web): November 18, 2010 | doi: 10.1021/bk-2010-1054.ch001

Downloaded by STANFORD UNIV GREEN LIBR on June 23, 2012 | http://pubs.acs.org
Publication Date (Web): November 18, 2010 | doi: 10.1021/bk-2010-1054.ch002

Chapter 2

Fabrication and Degradation of Nanofibers Based on Luminescent Boron Dye-PLGA Blends

**Richard A. Murray,[1,2] Guoqing Zhang,[1] Drew Harmata,[2]
Rebekah A. Neal,[2] Edward A. Botchwey,[2] and Cassandra L. Fraser[1,2,*]**

**[1]Department of Chemistry, University of Virginia, Charlottesville, VA 22904
[2]Department of Biomedical Engineering, University of Virginia,
Charlottesville, VA 22904
*fraser@virginia.edu**

Light emitting, oxygen sensing boron biomaterials fabricated as nanofibers could play useful roles in tissue engineering. As has been demonstrated with boron polylactide nanoparticles in tumor models, these dual emissive biomaterials can serve as ratiometric oxygen sensors with excellent spatial and temporal resolution. Imaging oxygenation is also important in tissue engineering contexts to assess nutrient flow, cell and tissue viability, and to correlate this important physiological parameter with other variables important to successful transplantation, regeneration, and healing. As a first step toward these ends, here we report the fabrication of boron dye/polylactide blends as nanofibers via electrospinning. Optical characterization of nanofibers and preliminary degradation studies are presented.

Introduction

Tissue engineering and transplantation are important strategies for treating injury and disease. For example, Type I diabetes can be treated with beta-islet transplantation (*1*). Damaged tissues may be repaired by the creation of effective scaffolding materials that mimic the composition and architecture of regenerate tissues, thus providing the necessary chemical and mechanical cues that drive cellular differentiation (*2*). In both of these approaches it is critical that tissue be kept viable before transfer to a host, and accurate measures of cell and tissue

In Biomaterials; Kulshrestha, A., et al.;
ACS Symposium Series; American Chemical Society: Washington, DC, 2010.

viability are required in the the clinic to monitor viability over time. Previously, oxygen consumption rates have proven a useful method to assess islet quality for correlation with transplant success and desired clinical outcome after surgery, namely diabetes reversal (*3*). Declining oxygen partial pressures (pO_2) of tissue samples in specially designed chambers were determined using phosphorescence quenching and a fiber optic sensor. However, currently lacking is the ability to measure oxygen levels in tissues or three-dimensional biomaterials and scaffolds in a more convenient and distributed manner. It is ideal to generate pO_2 maps of tissues with good spatial and temporal resolution to identify hypoxic regions and ways that they change over time. Recent successes in using nanosensors for tumor hypoxia imaging (*4*), however, inspire our efforts to use oxygen responsive biomaterials in tissue engineering contexts as well.

Recently we reported a new class of light emitting boron biomaterials that exhibit both fluorescence (F) and unusual room temperature phosphorescence (RTP) (*5*). The former serves as a molecular probe and oxygen invariant internal standard whereas the latter can be utilized as a sensitive optical sensor for oxygen. Difluoroboron dibenzoylmethane-poly(lactic acid) derivatives, BF_2dbmPLA, including iodide heavy atom substituted systems, have been formulated as powders, films, and nanoparticles (Figure 1) (*6*). Nanoparticles ~70 nm in size are readily taken up by cells, their emission is bright, and materials are quite photostable relative to other commonly used dyes in biology (*7*). Boron polylactide nanoparticles have also been used in combination with a mouse dorsal window chamber tumor model to generate maps of tissue oxygenation (*4*). Directed toward the goal of utilizing boron biomaterials with built-in optical oxygen sensing capability as responsive scaffolds for tissue engineering, here we explore the fabrication, optical characterization, and degradation of boron dye-poly(lactic-co-glycolic acid) (PLGA) blends as nanofibers.

Downloaded by STANFORD UNIV GREEN LIBR on June 23, 2012 | http://pubs.acs.org
Publication Date (Web): November 18, 2010 | doi: 10.1021/bk-2010-1054.ch002

Experimental Section

Materials

The boron dyes BF_2dbm(I)OH (**1**) (*4*) and difluoroboron 4-methoxy-dibenzoylmethane), BF_2dbmOMe (**2**) (*8*), were prepared as previously reported. PLGA (50:50) (M_w = 65 kDa, M_n = 40, PDI = 1.6) and PLGA (85:15) (M_w = 109 kDa, PDI = 1.5) were obtained from Lakeshore Biomaterials. Solvents, CH_2Cl_2 and THF, were dried and purified by passage through alumina columns. Boron trifluoride diethyl etherate (Aldrich, purified, redistilled) and all other reagents and solvents were used as received without further purification.

Optical Measurements

UV-vis spectra were recorded on a Hewlett-Packard 8452A diode-array spectrophotometer in CH_2Cl_2. Steady-state fluorescence emission spectra were recorded on a Horiba Fluorolog-3 Model FL3-22 spectrofluorometer (double-grating excitation and double-grating emission monochromators). Room-temperature phosphorescence spectra were recorded with the same

Downloaded by STANFORD UNIV GREEN LIBR on June 23, 2012 | http://pubs.acs.org
Publication Date (Web): November 18, 2010 | doi: 10.1021/bk-2010-1054.ch002

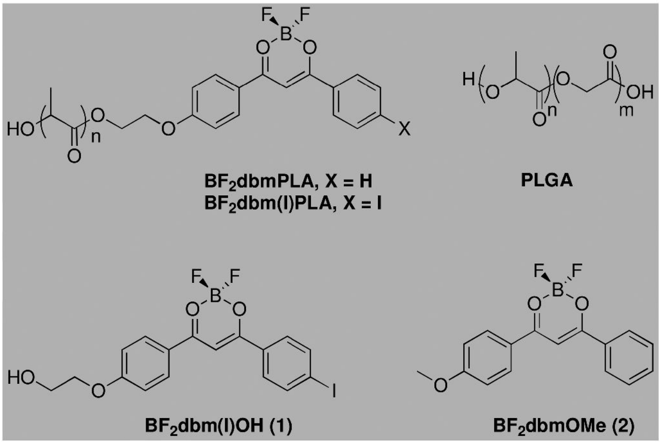

*Figure 1. Chemical structures of difluoroboron dibenzoylmethane polylactides, poly(lactic-co-glycolic acid) (PLGA), and iodide- (**1**) and methoxy-substituted (**2**) dyes.*

instrument except that a pulsed xenon lamp (λ_{ex} = 369 nm; duration < 1 ms) was used and spectra were collected with a 1 ms delay after excitation. Time-correlated single-photon counting (TCSPC) fluorescence lifetime measurements were performed with a NanoLED-370 (369 nm) excitation source and DataStation Hub as the SPC controller. Phosphorescence lifetimes were measured with a 500 ns multi-channel scalar (MCS) excited with a pulsed xenon lamp (λ_{ex} = 369 nm; duration < 1 ms). Lifetime data were analyzed with DataStation v2.4 software from Horiba Jobin Yvon.

Nanofiber Fabrication

For nanofiber fabrication, the polymer or dye/polymer blend was dissolved in DMF:THF (1:1) at varying concentrations (10-20%). An Aladdin-1000 Syringe pump was used to dispense the dye/polymer solution from a syringe though an 18 gauge needle at a specified flow rate (0-5 mL/h). A Gamma High Voltage power supply was used to generate a voltage difference between the syringe and the collecting plate (10-25 kV). Nanofibers were collected on grounded aluminum substrates situated a given distance (10-25 cm) from the needle tip. An aluminum plate was used as the collector for electron microscopy and plasma treated glass coverslips were used as collectors to determine luminescence. Specifically 50:50 PLGA samples loaded and unloaded with dye were electrospun at 30% (w/v) 50:50 PLGA in THF:DMF with an 18 kV driving voltage, 15 cm collecting distance, and a 1 mL/h flow rate. BF$_2$dbm(I)OH (**1**) was added at 5% (w/w) to loaded samples. An additional 5% (w/w) 50:50: PLGA was added to unloaded samples. For 85:15% PLGA samples, parameters were adjusted to 20% (w/v) PLGA in 1:1 DMF:THF, 3 mL/h flow rate, and 1% (w/w) BF$_2$dbmOMe (**2**). Driving voltage and collecting distance are as above for 50:50 PLGA.

Downloaded by STANFORD UNIV GREEN LIBR on June 23, 2012 | http://pubs.acs.org
Publication Date (Web): November 18, 2010 | doi: 10.1021/bk-2010-1054.ch002

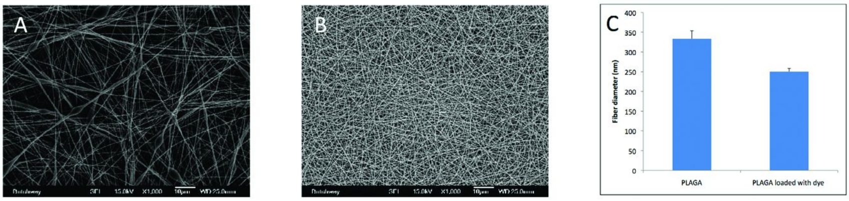

*Figure 2. Scanning electron micrographs of electrospun 50:50 PLGA nanofibers unloaded (A) and with iodide dye (**1**) (B), demonstrating fiber diameters in the nanoscale range (C). Error bars represent standard error.*

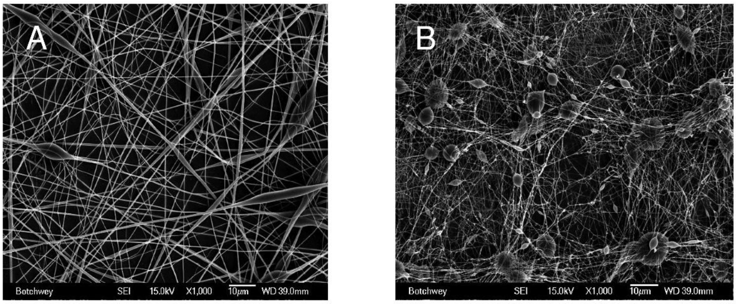
A
Botchwey SEI 15.0kV X1,000 10μm WD 39.0mm
B
Botchwey SEI 15.0kV X1,000 10μm WD 39.0mm

*Figure 3. Scanning electron micrographs of electrospun 85:15 PLGA nanofibers blended (A) and not blended with BF_2dbmOMe dye (**2**) showing beaded morphology (B).*

Imaging

The luminescence of the nanofiber scaffolds were captured with a Zeiss Axioskop 40 microscope with HBO arc lamp. Fluorescence was captured using a DAPI filter. Phosphorescence was captured using a FITC filter. PLGA fibers were imaged on 6400 JEOL scanning electron microscope (SEM) with Orion Image Processing. Samples were placed on SEM mounts, then sputter coated with gold for 200 seconds at 60 milliamps. All scanning electron micrographs were imaged at a 25-39 cm working distance and 15 kV accelerating voltage.

Degradation Studies

To analyze degradation rates of the nanofibers with and without dye present, samples of both the polymer alone and the polymer/dye blend were cut from electrospun mats and immersed in phosphate buffered saline (PBS) at 37 °C on a rocker to simulate physiological conditions. Samples were removed every seven days and dried in vacuo to remove residual solvent before dissolving in THF for analysis of molecular weights were by GPC (THF, 25 °C, 1.0 mL/min) against polystyrene standards using an autosampler (molecular weights multiplied by 0.58 correction factor (*9*)). A Polymer Labs 5µm mixed-C guard column and two GPC columns along with Agilent Technologies instrumentation (series 1100 HPLC) were used in GPC analysis.

Downloaded by STANFORD UNIV GREEN LIBR on June 23, 2012 | http://pubs.acs.org
Publication Date (Web): November 18, 2010 | doi: 10.1021/bk-2010-1054.ch002

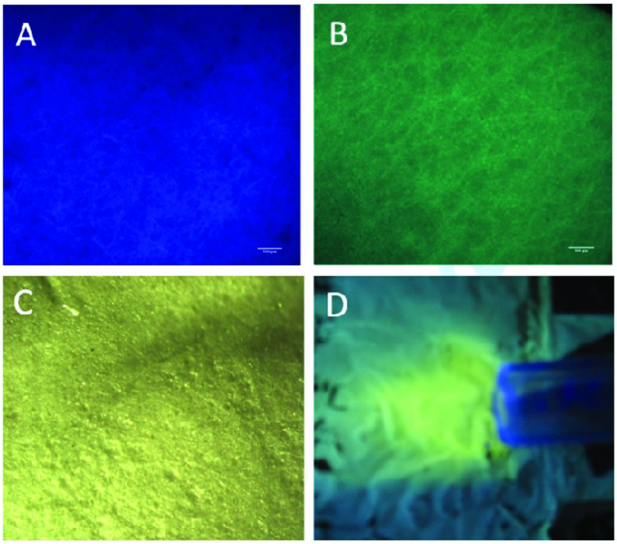

*Figure 4. Nanofiber scaffolds of 50:50 PLGA loaded with BF_2dbm(I)OH dye (**1**) imaged with a fluorescence microscope (A-B). In the presence of oxygen, blended nanofiber scaffolds showed strong fluorescence (λ = 459 nm, blue) (A). Under a hypoxic conditions, strong phosphorescence intensity was observed (λ= 531 nm, green) (B). The blended nanofibers appear chartreuse under a halogen lamp in both air and hypoxic environments (C). Figure D shows a photographic image of a 85:15 PLGA:BF_2dbm(I)OH (**1**) (5% w/w) loaded fiber mat on a grounded aluminum collector under a stream of oxygen-free natural gas with UV black light excitation (λ = 365 nm). Yellow-green phosphorescence "turn on" is evident under the gas stream, whereas surrounding regions show darker darker green-blue color characteristic of solid-state fluorescence. (see color insert)*

Nanofiber Fabrication

Readily processable boron dye polymer blends were fabricated as nanofibers. The iodide dye (**1**) was selected for these studies, given the enhanced phosphorescence triplet emission observed with heavy atom substitution (*4*). PLGA was chosen over PLA for this initial nanofiber study, given its faster degradation and common use in tissue engineering. The electrospinning technique allows for the manipulation of process parameters to adjust fiber diameter and morphology. Specifically, the boron dye BF_2dbm(I)OH (**1**) was blended with 50:50 poly(lactic-*co*-glycolic acid) (PLGA) (**2**) in 1:1 THF:DMF solution. PLGA solutions with (loaded) and without the dye (unloaded) were subjected to the same electrospinning processing parameters for comparison. Fiber morphologies are depicted in SEM micrographs in Figure 2. Mean fiber diameter was 330 nm +/- 144 nm for unloaded nanofibers and decreased to ~251 +/-65 nm for loaded fibers (Figure 2C). The presence of the highly polar difluoroboron dye affects the spinning process, resulting in smaller diameter fibers and a denser mesh are obtained for dye-containing solutions. This size range and below is ideal for cell attachment and growth, as it closely mimics the nanoscale dimensions of the

Downloaded by STANFORD UNIV GREEN LIBR on June 23, 2012 | http://pubs.acs.org
Publication Date (Web): November 18, 2010 | doi: 10.1021/bk-2010-1054.ch002

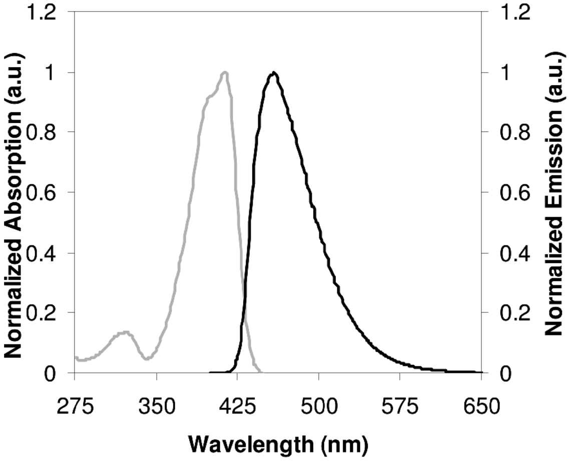

Figure 5. Normalized absorption (grey line) and emission (black line) spectra of 50:50 PLGA dye blends after the electrospinning process in THF:DMF (1:1). Absorption maxima: 413 nm. Emission maximum: 459 nm. (Note: Spectra of dye:PLGA samples before and after electrospinning were identical.)

extracellular matrix. In addition, under these conditions the loaded nanofibers display none of the beaded defects which can occur within electrospun fiber meshes. This uniform fiber geometry suggests that the loaded scaffolds could be ideal materials for drug delivery with a consistent release profile and no burst release common for beaded defects. An example of beaded defects is shown in Figure 3 for dye-free 85:15 PLGA but not for fibers of the same polymer when doped with BF_2dbmOMe (**2**).

Optical Characterization

When exposed to UV light, nanofiber meshes of blended PLGA-dye displayed dual emissive properties, verifying that the dye maintains its phosphorescent and fluorescent properties after electrospinning processing. Blue and yellow-green emission colors are clearly evident visually and with wavelength detection (Figure 4 A and B). Phosphorescence “turn on” is shown in a photographic image under oxygen-free gas stream. (Note that in addition to inert gases like nitrogen or argon, triplet emission turns on under other oxygen-free atmospheres such as natural gas or carbon dioxide as well.) Dye polymer blends were also analyzed by luminescence spectroscopy, before and after electrospinning. Identical excitation and emission spectra are noted for dye-polymer blends in before spinning and for fibers redissolved after spinning in 1:1 DMF:THF (Figure 5). These findings too, indicate that dye and its characteristic emissive properties are still present after the spinning process.

Table I. GPC Data[a] for Nanofiber Scaffolds Versus Time in Phosphate Buffered Saline Solution

	PLGA Scaffold		*PLGA Scaffold + Dye*	
Day	M_n	*PDI*	M_n	*PDI*
0	25,000	1.83	25,000	1.8
7	21,400	1.96	23,900	1.83
14	14,900	2.29	16,300	2.1
21	13,700	1.85	15,100	1.77

[a] Determined in THF with RI detection vs polystyrene standards.

Downloaded by STANFORD UNIV GREEN LIBR on June 23, 2012 | http://pubs.acs.org
Publication Date (Web): November 18, 2010 | doi: 10.1021/bk-2010-1054.ch002

Degradation Studies

PLGA (50:50) fibers were subjected to degradation studies in phosphate buffered saline (PBS) media, with and without the dye as a control. Scaffold samples were analyzed every seven days for 21 days. Samples were dried in vacuo before dissolving in THF for molecular weight analysis by GPC versus polystyrene standards. As shown in Table I, samples degrade gradually over time, as evidenced by decreasing molecular weights. Degradation rates for dye-free and loaded fibers are comparable, with the dye-containing material showing slightly slower degradation. For example, the molecular weight of polymers comprising PLGA unloaded fibers decreased 45% versus a 40% decrease for loaded fibers after 21 days.

Optical properties of PLGA/dye scaffold materials were monitored for samples versus time in PBS solution. Steady state emission spectra, provided in Figure 6, reveal the expected singlet and triplet emissions. Fluorescence maxima are evident at 468 nm, and phosphorescence, at 531 nm. The lower energy phosphorescence band drops rapidly in intensity initially, and then intensity decreases more slowly over time. It is known that phosphorescence intensity and F/P ratios are sensitive to dye concentration in solid state PLA materials (*4*). Dye leaching from the matrix, hydrolysis of the difluoroboron center, fiber swelling in PBS solution, or a combination of these processes together, serve to decrease the concentration of dye per volume, that is, the dye-dye distances and fluorophore-fluorophore interactions in the material. Dye leaching from surface sites or initial fiber swelling seem the most likely causes of the initial rapid drop in triplet intensity, with more gradual hydrolysis of the boron center over time, similar to what is typically seen in PLA nanoparticles in aqueous solution (*6*). A slight shift in fluorescence emission maxima over time is consistent with previous observations of blue shifted emission (468 to 459 nm) with decreasing dye concentration in the material (*10*).

Room-temperature phosphoprescence lifetime data are collected in Table II. Along the degradation process, the lifetimes exhibit a consistently increasing trend (4.68 ms, 0 d to 5.17 ms, 21 d), presumably due to decreased contribution from delayed fluorescence. As has been discussed previously, in addition to the major RTP peaks, high energy shoulders that closely match the emission

Downloaded by STANFORD UNIV GREEN LIBR on June 23, 2012 | http://pubs.acs.org
Publication Date (Web): November 18, 2010 | doi: 10.1021/bk-2010-1054.ch002

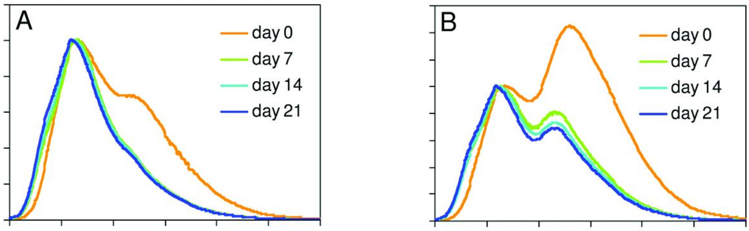

Figure 6. Steady state emission spectra of 50:50 PLGA:dye nanofiber scaffolds in the solid state versus time in phosphate buffered saline solution under air (A) and nitrogen (B) atmospheres.

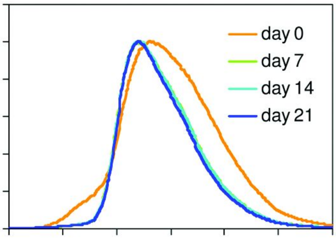

Figure 7. Room temperature phosphorescence (RTP) emission under nitrogen for nanofiber scaffolds after 0, 7, 14, and 21 days in PBS solution. The phosphorescence spectrum was recorded with a pulsed Xe lamp (λ=369 nm; duration <1 ms) and the data was collected with a 1 ms delay after excitation.

maxima of fluorescence are constantly observed for the boron-polymer system in the solid state (*10*). The high energy shoulder, or delayed fluorescence (~ 470 nm, shown in Figure 7 for day 0) is attributed to thermally repopulated singlet excited state. When F-F interactions are weaker due to dye leaching or polymer matrix degradation, the singlet-triplet energy gap increases and thus, the delayed fluorescence probable. Since delayed fluorescence has a much faster decay rate (ns vs ms for RTP), the lifetimes of the degraded samples are, as a result longer. Furthermore, as the dye molecules become more isolated, the decay tends to reach a more linear fit as well.

Conclusion

Nanofiber scaffolds are currently under investigation as skin bandages and patches, peripheral nerve conduits, in addition to islet delivery scaffolds and other tissue engineering applications. As such, an oxygen-sensing nanofiber scaffold would show immediate applicability in many areas of tissue engineering and regenerative medicine. Results from these preliminary studies are very promising for the use of boron dyes as dual emissive oxygen sensors in biodegradable polymer blends or dye-polymer conjugates. The material retains its emissive properties after nanofiber processing and like PLA nanoparticles in aqueous suspension, even upon swelling and during more rapid PLGA polymer

Table II. Room Temperature Phosphorescence Emission Data for Nanofiber Scaffolds Versus Time in Phosphate Buffered Saline

Day	*λ_P[a] (nm)*	*τ_{RTP}[b] /κ^2 (ms)*	*Decay*[c]
0	531	4.68/1.32	triple
7	522	5.12/1.08	double
14	520	5.13/1.10	double
21	521	5.17/1.02	pseudo single

[a] Phosphorescence emission maxima. [b] Room temperature phosphorescence lifetime. [c] Lifetime data fit to indicated exponential decay.

Downloaded by STANFORD UNIV GREEN LIBR on June 23, 2012 | http://pubs.acs.org
Publication Date (Web): November 18, 2010 | doi: 10.1021/bk-2010-1054.ch002

degradation in aqueous buffer conditions. An advantage of dual emissive boron biomaterials, is that they can serve as concentration independent ratiometric sensors and imaging agents. Oxygen sensitive phosphorescence and a built in oxygen insensitive fluorescence standard arise from the same dye, so both are affected at once in a predictable way by dye leaching, degradation or given other reasons for variable amounts of dye in a given sample region. Investigation of nanofiber processing of other dye containing biomaterials and their nanofiber processing, optical properties, degradation and ultimately, tissue engineering applications serve as the subject of future reports.

Acknowledgments

We thank the National Science Foundation (CLF: CHE 0718879; EAB: EFRI 0736002) and the National Institutes of Health (RAN: University of Virginia Biotechnology Training Program 5T32GM008715-08) for support for this research.

References

1. Shapiro, A. M. J.; Lakey, J. R. T.; Ryan, E. A.; Korbutt, G. S.; Toth, E.; Warnock, G. L.; Kneteman, N. M.; Rajotte, R. V. *New Eng. J. Med.* **2000**, *343*, 230.
2. Wieghaus, K. A.; Gianchandani, E. P.; Brown, M. L.; Papin, J. A.; Botchwey, E. A. *Tissue Eng.* **007**, *13*, 2561.
3. Papas, K. K.; Pisania, A.; Wu, H.; Weir, G. C.; Colton, C. K. *Biotechnol. Bioeng.* **2007**, *98*, 1071.
4. Zhang, G.; Palmer, G. M.; Dewhirst, M. W.; Fraser, C. L. *Nat. Mater.* **2009**, *8*, 747.
5. Zhang, G.; Chen, J.; Payne, S. J.; Kooi, S. E.; Demas, J. N.; Fraser, C. L. *J. Am. Chem. Soc.* **2007**, *129*, 8942.
6. Pfister, A.; Zhang, G.; Zareno, J.; Horwitz, A. F.; Fraser, C. L. *ACS Nano* **2008**, *2*, 1252.
7. Contraras, J.; Xie, J.; Chen, Y. J.; Pei, H.; Zhang, G.; Fraser, C. L; Hamm-Alvarez, S. Submitted.

8. Cogné-Laage, E.; Allemand, J.-F.; Ruel, O.; Baudin, J.-B.; Croquette, V.; Blanchard-Desce, M.; Jullien, L. *Chem.-Eur. J.* **2004**, *10*, 1445.
9. (a) Baran, J.; Duda, A.; Kowalski, A.; Szymanski, R.; Penczek, S. *Macromol. Rapid Commun.* **1997**, *18*, 325−333. (b) Save, M.; Schappacher, M.; Soum, A. *Macromol. Chem. Phys.* **2002**, *203*, 889−899.
10. Zhang, G.; Kooi, S. E.; Demas, J. N.; Fraser, C. L. *Adv. Mater.* **2008**, *20*, 2099–2104.

Downloaded by STANFORD UNIV GREEN LIBR on June 23, 2012 | http://pubs.acs.org
Publication Date (Web): November 18, 2010 | doi: 10.1021/bk-2010-1054.ch002

Chapter 3

Polymer Gel Systems for Nerve Repair and Regeneration

Shanfeng Wang* **and Lei Cai**

Departments of Materials Science and Engineering, The University of Tennessee, Knoxville, TN 37996, USA
***swang16@utk.edu**

Downloaded by CORNELL UNIV on June 23, 2012 | http://pubs.acs.org
Publication Date (Web): November 18, 2010 | doi: 10.1021/bk-2010-1054.ch003

Material design is crucial in overcoming numerous barriers for peripheral nerve, spinal cord and brain injuries. Injectable polymers play an important role in providing permissive microenvironments by incorporating ECM proteins, neurotrophic factors, and neural stem cells to achieve enhanced regenerated functions, though big challenges still remain. Many biodegradable polymeric networks have been developed by using chemical crosslinking or/and physical gelation to facilitate axonal ingrowth and investigate their roles in interacting with biological cues. In this review, we will focus on recent progress in polymeric gel systems developed for nerve tissue engineering applications and how their physical properties can be tailored to regulate nerve cell functions and satisfy the clinical needs, together with other chemical and biological factors for nerve repair.

1. Introduction

As the medical background of this review, peripheral nerve and spinal cord injuries (SCI) that occur with accidental trauma or during the course of surgery and chronic neurodegenerative diseases (e.g. Parkinson's disease and Alzheimer's desease) have been a challenging clinical problem for surgeons (*1–25*). For example, each year in the U.S., several million people suffer from serious traumatic, iatrogenic or non-traumatic peripheral nerve injuries (*1–25*). Failure to restore these damaged nerves can lead to the loss of muscle function, impaired sensation, and painful neuropathies (*1–25*). The gold standard in surgery, autologous nerve graft, has disadvantages such as limited source, additional surgery, and mismatch between injured nerve and donor nerve (*1–25*). Therefore, synthetic nerve conduits have been fabricated to bridge the long gap between injured peripheral nerve stumps. Suitable nerve conduit materials should satisfy requirements including capability of resisting tear, suturability, and easiness of being incorporated with support cells and nerve growth factor (NGF) (*1–25*). Although numerous polymeric biomaterials have been applied to fabricate nerve conduits (*1–25*), there only exist limited number of crosslinkable and biodegradable polymeric systems for this purpose. Considering the wide range of applicable fabrication methods using injectable polymers such as stereolithography, we focus on the recent progress in polymer gels for nerve tissue engineering applications in this review.

Polymeric gelation systems are promising in nerve regeneration and brain repair applications because of their unique properties of injectability, biocompatibility, and controllable mechanical properties and degradability (*21–23*). Site-specific delivery can be easily achieved by direct injection (*21–23*). Great efforts have been made on material design strategies to meet different requirements for treatment of damaged peripheral nerve, spinal cord, and brain tissue (*1–25*). Hydrogels are polymer networks that are able to retain aqueous solutions encapsulated with drugs, growth factors and cells for desired functioning *in vivo*. Hydrophobic gels generally have more stable networks in aqueous condition and better mechanical properties. Besides serving as nerve scaffold materials and filler materials, polymer gels can also deliver extracellular cell-matrix (ECM) proteins, neurotrophic factors and stem cells enhance their biological performance in functional recovery (*1–25*).

Because of the significance of nerve-related issues, there exist numerous review articles on the scaffold and filler materials and strategies for nerve repair and regeneration (*1–25*); however, there are only a few specific reviews focused on polymer gel systems for this purpose and they are about hydrogels and luminal fillers (*21–23*). Neurotrophic factors play a key role in inducing nerve regeneration and there are approaches to use polymeric biomaterials as drug delivery carriers for these neutrophic factors (*24*, *25*). In this review, we focus on the recent progress in using polymer gels for fabricating nerve scaffolds, investigating the interactions between nerve cells and polymer substrates, and building controlled release systems for nerve repair.

2. Gelation Systems for Nerve Repair

Polymeric network systems can be majorly classified into two categories according to the mechanisms of gelation. Polymer networks crosslinked by covalent bonds are chemical gels, including both hydrogels and hydrophobic gels (or organogels), while the formation of a physical gel occurs via physical association such as hydrogen bonding, electrostatic interaction, difference in hydrophobicity, and crystallization (*26–30*). From their sources, polymeric biomaterials can be also categorized into natural and synthetic polymers. Most natural polymers used in biomedical applications are hydrophilic and many of

Downloaded by CORNELL UNIV on June 23, 2012 | http://pubs.acs.org
Publication Date (Web): November 18, 2010 | doi: 10.1021/bk-2010-1054.ch003

them have been modified into chemically crosslinkable systems for preparing hydrogels (*21*). Natural polymers that are constituents in body tissues can also form physical gels by varying their concentration in aqueous solutions, temperature, pH value, or charge characteristics and density (*29–34*). In this section, we focus on the preparation of these polymer gel systems and will discuss their applications in Sections 3 and 4.

2.1. Chemically Crosslinkable Systems

Many polymer species can form covalently crosslinked gel systems via free radical polymerization initiated either by heat or light, but not all of them have been explored for applications in nerve regeneration because of inappropriate mechanical properties and biocompatibility concerns. For preparation of chemically crosslinked hydrogels hydrogels, four primary methods are used i.e. (1) photo-crosslinking of unsaturated carbon-carbon double bonds such as acrylates, fumarates, and methacrylates; (2) Michael addition reaction; (3) click chemistry, and (4) enzyme-catalyzed reaction (*28*).

Majority of currently investigated gelation systems are based on numerous natural polymers and a few synthetic polymers. Examples of synthetic polymers include polyethylene glycol (PEG), poly(2-hydroxyethyl methacrylate) (pHEMA), polyacrylamide (PAM), polydimethylsiloxane (PDMS), and polycaprolactone (PCL) because of their ease of processing and biocompatibility. These polymers are injectable and can be photo-crosslinked to achieve good networks. In addition, they can be further modified by copolymerization with polylactic acid (PLA) or polyglycolic acid (PGA) groups to facilitate biodegradation.

Non-degradable polymers were initially applied in fabricating nerve conduits, for example, polyethylene (PE), expanded polytetrafluoroethyelene (ePTFE or Gore-Tex), polyvinyl chloride (PVC), and PDMS (*1*, *2*, *7*). The first biomaterial used in clinical trials was silicone tube because of its availability with mature fabrication methods, excellent biocompatibility, and favorable elastomeric properties for implantation (*1–14*). It is still the most frequently used material for fabricating artificial nerve grafts (*1–14*). As a widely used material for micro-fabrication techniques, PDMS can be easily fabricated into various patterns to control cell migration and proliferation. However, PDMS is not degradable and consequently they remain in situ as a foreign body and cause a chronic foreign body reaction with excessive scar tissue formation that ultimately limits recovery of nerve function (*10*). These non-degradable polymeric systems are not the focus of this review. PDMS substrates with modulated stiffness were used to investigate the role of surface stiffness in modulating neuronal cell behavior, which will be discussed in Section 3.1.

First, hydrogels based on natural polymers such as agarose, alginate, chitin/chitosan, collagen, gelatin, and hyaluronan/hyaluronic acid have been prepared for nerve repair. An agarose hydrogel modified with a cysteine compound containing a sulfhydryl protecting group provides a photolabile substrate that can be patterned with biochemical cues by immobilizing the adhesive fibronectin peptide fragment, glycine–arginine–glycine–aspartic acid–serine (GRGDS) for

Downloaded by CORNELL UNIV on June 23, 2012 | http://pubs.acs.org
Publication Date (Web): November 18, 2010 | doi: 10.1021/bk-2010-1054.ch003

Downloaded by CORNELL UNIV on June 23, 2012 | http://pubs.acs.org
Publication Date (Web): November 18, 2010 | doi: 10.1021/bk-2010-1054.ch003

3D cell migration and neurite outgrowth (*35*). Agarose hydrogels can also be used for fabricating anisotropic scaffolds for peripheral nerve regeneration (*36*). Alginate gel crosslinked with ethylenediamine and water-soluble carbodiimide has been used to overcome high cytotoxicity and large foreign-body reaction from calcium ions used excessively to form physical gels with negatively-charged alginate (*37*, *38*). Sodium alginate can also be oxidized into alginate dialdehyde (ADA) with different degree of oxidation and consequently ADA can react with gelatin to form hydrogels (*39*).

Chitin hydrogel tubes with suitable tube permeability and mechanical properties can be prepared in a cylindrical mold containing a cylindrical core after *N*-acetylation of chitosan using a two-fold excess of acetic anhydride (*40*). Photo-polymerizable methacrylamide chitosan (MAC) can be crosslinked in the presence of photoinitiator 2,2-dimethoxy-2-phenylacetophenone (DMP) dissolved in 1-vinyl-2-pyrrolidone (NVP) (*41*). Native collagen solution can be neutralized with NaOH and then mixed with microbial transglutaminase (mTGase) to form crosslinked collagen scaffold with a laminin peptide gradient (*42*). Collagen hydrogel can be also formed by mixing neutralized collagen solution with *N*-1[3-(trimethoxysilyl)propyl] diethylenetriamine (DETA) coated glass cover-slips (*43*). Brownish nerve conduits can be also made from a 1-ethyl-3-(3-dimethylaminopropyl)carbodiimide (EDC)/*N*-hydroxysuccinimide (NHS) cross-linked gelatin (*44*). Multiply styrenated gelatin dissolved in PBS can be photo-polymerized into fibers, rods, and nerve conduits (*45*).

Hyaluronan (hyaluronic acid or HA, hyalunronate) is a high-molecular-weight negatively-charged glycosaminoglycan found in the ECM of humans (*21*). Photocrosslinable cinnamoyl hyaluronan derivative has been synthesized by conjugating cinnamic acid in to the carboxyl of hyaluronan using aminopropanol as a spacer (*46*, *47*). Nerve conduits can be fabricated using this photocrosslinkable HA in a PDMS mold and filled with collagen gel and Schwann cells and neurosphere (*46*, *47*). Methacrylated-HA (MeHA) has been prepared by adding methacrylic anhydride to HA or sodium hyaluronate and photo-crosslinked in the presence of Irgacure 2959 from Ciba Specialty Chemicals (*48*–*50*). HA/polylysine hydrogel with a weight ratio of 5:1 (HA:polylysine) has been prepared using EDC as the crosslinking agent and the hydrogel coated with polylysine can be used as a transfer system for transplantation of neural stem cells (*51*). Three-dimensional gelatin/hyaluronan hydrogel structures used for traumatic brain injury can be prepared by mixing sodium hyaluronate solution in phosphate buffered saline (PBS) with gelatin solution and crosslinked with glutaraldehyde (*52*). HA-collagen (type I or II) sponge with an open porous structure and mechanical properties similar to brain tissue can be developed by a freeze-drying technique and crosslinked with water-soluble carbodiimide (*53*).

Synthetic hydrogels are mostly based on PEG and poly(2-hydroxylethyl methacrylate) (pHEMA) (*21*). Hydrogels based on PEG diacrylate that is photo-crosslinked with peptides conjugated to monoacrylated PEG has been found to support neurite extension of pheochromocytoma (PC12) cells (*54*). Hydrogels based on oligomeric PEG fumarate (oPF) or PEG fumarate (PEGF) can be synthesized by incorporating fumarate groups into PEG chain. They have been further photo-crosslinked with a positively charged monomer,

Downloaded by CORNELL UNIV on June 23, 2012 | http://pubs.acs.org
Publication Date (Web): November 18, 2010 | doi: 10.1021/bk-2010-1054.ch003

[2-(methacryloyloxy) ethyl]-trimethylamoonium chloride, to supply better support on cell attachment and neurite extension of dorsal root ganglion (DRG) neurons (*55*). In one approach, neural cells can be photo-encapsulated into the PEG methacrylate hydrogels with grafted PLA and PGA to build their own micro-environment to survive, proliferate, and differentiate into neurons and glia tuned by controlled degradation rate of the polymer network within 1-3 weeks (*56*). By end-capping triblock copolymer PLA-PEG-PLA with methacrylate or acrylate functionalities, PLA-PEG-PLA-dimethacrylate (PLA-PEG-PLA-DMA) and PLA-PEG-PLA-diacrylate (PLA-PEG-PLA-DA) have been synthesized (*57–59*). An injectable liquid polymer solution of acrylated PLA-PEG-PLA macromer has been photo-crosslinked into biodegradable hydrogel with neurotrophin-3 (NT-3) embedded (*57*). NT-3 is released sustainably from the hydrogel for over two weeks and the treated animals show greater axon growth and rewiring that demonstrated the improved functional outcome to promote regeneration after spinal cord injury (*57*).

Hydrogels based on three synthetic methacrylate polymers are used for nerve repair: pHEMA (*60*), pHEMA-MMA (*61–63*), and poly(hydroxypropyl methacrylate) (pHPMA) (*64*). Nerve conduits fabricated using pHEMA and pHEMA-MMA suffer from partial collapse after implantation (*21*). In order to overcome this shortcoming, Katayama *et al.* has invented a nerve guidance hydrogel tube using PCL coil-reinforced pHEMA-MMA through injection molding (*63*). It demonstrates equivalence to autografts after both 8 and 16 weeks of implantation in terms of nerve and muscle action potential velocity and axon density (*63*). pHPMA hydrogels can be prepared by polymerizing hydroxypropyl methacrylate (HPMA) in the presence of a crosslinker, methylene bisacrylamide, and a initiator, azobisisobutironitrile (AIBN) and the hydrogels can be incorporated with RGD peptides to support better axonal ingrowth in nerve repair (*64*).

PCL fumarates (PCLFs) have been developed in Yaszemski's laboratory by incorporating unsaturated fumarate segments into PCL blocks to make it crosslinkable (*65*). A novel proton scavenger, potassium carbonate (K_2CO_3) has been employed in the esterification of PCL diol or PEG precursors with hydroxyl end groups instead of traditionally-used triethylamine (TEA) to avoid coloration and potential toxic byproducts resulting from complexation between TEA and unsaturated acyl chlorides (*66*). PCLF can be injected and photo-crosslinked using a molding technique into porous scaffolds and single-lumen or multi-channel nerve conduits with excellent biocompatibility and controllable physical properties to support rat Schwann cell precursor line (SpL201) cell attachment and proliferation as well as guiding axon ingrowth for peripheral nerve regeneration (*67*, *68*). Mechanical properties can be well tailored by crystallinity and crosslink density through monomers of different molecular weights (*65–70*). A series of multi-block PPF-*co*-PCL copolymers has been developed using crosslinkable poly(propylene fumarate) (PPF) and PCL to achieve a wide range of mechanical properties for hard and soft tissue replacements such as bone and nerve repair (*71*, *72*). PCL diacrylates (PCLDAs) and triacrylates (PCLTAs) have recently been developed in our lab by end-capping PCL diols or triols with more reactive acrylate groups to improve the crosslinking efficiency and then produce defect-free nerve conduits (*73*, *74*). Roles of crosslinking density and crystallinity are illustrated in modulated mechanical properties and controlled nerve cell responses (*68–74*).

2.2. Physical Gels

A soft agar matrix and a firm agar substratum have been used to evaluate the cell locomotion of neurons and glial cells (*75*). As one linear polysaccharide derived from red algae, agarose is soluble in water at temperature above 65°C and gels at a temperature between 17 and 40°C, depending on the degree of hydroxylethyl substitutions on its side chains (*76*). Agarose has been used as an *in situ* gelling hydrogel for investigating the rate of DRG neurite extension (*76*) and conformal repair of spinal cord defects and local deliveryafter sinal cord injury when combined with lipid microtubules loaded with brain derived neurotrophic factor (BDNF) (*77*). Neural stem cells can be encapsulated in the hydrogels formed by sodium alginate upon adding calcium chloride ($CaCl_2$) (*78*).

Downloaded by CORNELL UNIV on June 23, 2012 | http://pubs.acs.org
Publication Date (Web): November 18, 2010 | doi: 10.1021/bk-2010-1054.ch003

Chitin or chitosan are promising natural polymers for a wide range of biomedical applications. Permeable chitin tubes have been fabricated from chitosan solution at different degree of deacetylation using mold casting with controlled mechanical properties. Biocompatibility of these tubes has been evaluated by good support for DRG cell adhesion and neurite outgrowth (*40*). Chitosan gel sponge scaffolds were also developed for peripheral nerve regeneration by transplanting Schwann cells derived from bone marrow stromal cells (BMSCs) (*79*). A thermo-responsive chitosan porous gel scaffold has been fabricated at body temperature by adding a polyol salt to a pH-neutral chitosan solution and further immobilized with poly(D-lysine) to improve cell adhesion and neuron survival (*80*). Chitosan have also been modified by conjugation of hydroxybutyl groups to be a thermo-reversible gel with controlled water contents and a gelation temperature of lower than 37°C (*81*). Minimal cytotoxicity and good proliferation of human mesenchymal stem cells (hMSCs) encapsulated in the gel indicate its potential as injectable cell carriers for reconstruction of a degenerated intervertebral disk (*81*).

Collagen, viscous fibronectin, fibrin, and fibrin + fibronectin (FB/FN) have been tested as filler materials in an experimental knife-cut cavity in the rat spinal cord (*82*). Collagen gel can be also used as injectable delivery system (*83*, *84*). Fibrin gel derived from isogenic rat plasma with $CaCl_2$ in a triblock copolymer of L-lactide, glycolide, and caprolactone can be used as luminal fillers in bioabsorbable polymer conduits for enhancing peripheral nerve regeneration (*85*). Hyaluronic acid can also form a physical hydrogel for loading BDNF by crosslinking it with the peptide carrying oligohistidine segments at both termini (*86*). Extracted from human hair, hard a-keratin can be used to form a reconstructed keratin hydrogel to promote integrin-mediated adhesion of neural progenitor cells (*87*).

Methylcellulose (MC) has been used as thermo-responsive, injectable scaffold which can dissolve in water at room temperature and then form a soft gel at 37 °C (*21*). MC has been microinjected into brains of rats after cortical impact injury to demonstrate its excellent biocompatibility for repair of defects in

Downloaded by CORNELL UNIV on June 23, 2012 | http://pubs.acs.org
Publication Date (Web): November 18, 2010 | doi: 10.1021/bk-2010-1054.ch003

the brain (*88*). Fast-gelling injectable blends of hyaluronan and methylcellulose (HAMC) can be used for intrathecal, localized delivery to the injured spinal cord (*89*, *90*). As a structural polysaccharide, xyloglucan can form hydrogels as the result of hydrophobic associations of the glucan backbone (*21*). Xyloglucan has been modified with poly(D-lysine) to form a thermoresponsive hydrogel for enhancing neurite outgrowth from primary neurons and neural stem cells (*91*).

Amphiphilic diblock copolypeptide hydrogels composed of lysine, homoarginine or glutamate with leucine boasted tailored density, mechanical properties and porosity by tuning copolymer chain length, composition and concentration have achieved desired *in vivo* deposits. They are injected as liquids to form gels with a storage modulus of 100-400 Pa in the brain of mice, in which no toxicity is detected and they integrate well with host cells and nerve fibers (*92*). Self-assembling peptide scaffolds have been developed for investigating neurite outgrowth and active synapse formation (*93*). As one thermoresponsive polymer that can form a hydrogel at temperatures above its lower critical solution temperature (LCST) of 29-32°C, poly(N-isopropylacrylamide)-*co*-poly(ethylene glycol) (PNIPAAm-PEG) has been used to form an injectable scaffold for spinal cord repair (*94*).

For numerous uncrosslinked polymers used in nerve repair, gelation also exists because of crystallization or chain entanglement. These polymers can be injected as a less viscous melt at the processing temperature higher than their T_m and later solidify upon cooling. Poly(α-hydroxy acid)s including PLA, PGA and poly(lactic-co-glycolic acid) (PLGA) have been used extensively as biocompatible polymers for preparing nerve conduits for axon regeneration (*1–25*, *95–98*). Sundback *et al.* developed a novel injection method for PLGA using thermally induced phase transition technique to fabricate porous nerve conduits with semi-permeable skins (*95*). Hadlock *et al.* (*96*, *97*) and Moore *et al.* (*98*) used PLGA to fabricate multi-channel scaffolds by rapid solvent evaporation after injection. These scaffolds containing Schwann cells have been found to promote axon regeneration *in vivo* with 3D reconstructions of histological sections (*97*, *98*). PCL networks discussed earlier combine both chemical networks linked by crosslinks and physical networks associated by crystalline domains to render appropriate mechanical properties such as flexibility and tear resistance (*66–74*).

3. Nerve Cell-Material Interactions

Cell-material interactions are essential to the tissue engineering applications of biomaterials. In the past several decades, pioneer scientists have achieved great understanding on the roles of biomaterials' surface physicochemical characteristics in determining cell responses (*99–101*). These factors can be divided into three major categories: surface chemistry such as hydrophilicity, charge characteristics and density, surface morphology, and surface mechanical properties. Surface physicochemical characteristics are correlated together to influence cell behavior. Surface topography tends to influence cell spreading because of an effect called "contact cue guidance" (*99–101*). Also, rough surface can increase surface area for cells to attach and proliferate (*99–101*). It is of crucial importance to understand how polymer gels support, interact with, and regulate nerve cells in their attachment, morphology, migration, proliferation, and differentiation. ECM proteins and neurotropic factors can be readily incorporated with polymer gels to enhance nerve cell performance and/or encapsulate neural stem cells for targeted regeneration.

3.1. Mechanical Cues

Since Pelham and Wang reported that surface stiffness of polymer substrate could play a critical role in determining cell phenotype and proliferation (*102*, *103*), investigations have been performed on numerous polymeric biomaterials with varying mechanical properties, particularly hydrogels coated with adhesive proteins (*104–107*). Less attention was paid to hydrophobic polymeric systems in the role of surface stiffness in regulating cell behavior (*65*, *67*, *69*, *71*, *72*, *74*). Extensive studies have been performed on the role of hydrogel stiffness in determining cell spreading, proliferation, and differentiation (*41*, *48*, *54*, *75*, *76*, *78*, *104–114*). A few hydrophobic polymer networks based on PDMS, PCLF, PCLDA, and their blends with PPF have also been studied in terms of surface stiffness's role in regulating nerve cells (*68–70*, *72–74*, *115*). Mechanical properties of substrates have recently demonstrated important cues to control neural cells and particularly neural stem cells' fate. Researchers have attempted to independently control substrate stiffness over the range of interests of brain and neural tissue while minimizing possible effects from other material parameters. Gelation systems are good models for modulating substrate rigidity by precise control of crosslink density via varying crosslinking time, crosslinker concentration, and molecular weight of precursor.

As mentioned in Section 2.1, sequentially photo-crosslinked MeHA hydrogels developed by Marklein and Burdick have elastic moduli range from 3 kPa to 100 kPa and hMSCs are found to favor stiffer gels in terms of spreading and proliferation (*49*). PAM crosslinked with bisacrylamide at different concentrations are able to vary crosslinking density to achieve shear modulus from ~10 Pa to 10 kPa. Similarly PC12 neurites display a threshold response to substrate stiffness of ~100 kPa, stiffer than substrates showing good neurites branching with no significant difference, but softer substrates cannot support neurites (*111*). PC12 cells are also found to exhibit longest neurite extension on more flexible PEGDA hydrogels with modulus from 40-400 kPa via varying the monomer concentration (*54*, *107*).

Engineered protein and DNA crosslinked hydrogels have been developed for their ease of independently tuning multiple properties including stimuli-response, degradation or erosion rate, reversible gelation, mechanics and neural cell behavior (*34*, *112*). Mechanical cues have been investigated for PC12 cell differentiation using a DNA crosslinked hydrogel with stiffness from ~100 Pa to 30 kPa (*112*). Spinal cord neurons are found to extend more primary dendrites but shorter axons on stiffer gels (*112*). Photo-polymerizable methacrylamide chitosan has been developed to study substrate stiffness effect to neural stem cells (NSCs). It is found that stiffness is an important factor that optimized at 3.5 kPa for proliferation and < 1 kPa for differentiation to neurons (*41*). Saha *et al.* also

Downloaded by CORNELL UNIV on June 23, 2012 | http://pubs.acs.org
Publication Date (Web): November 18, 2010 | doi: 10.1021/bk-2010-1054.ch003

found different preference of neurons and astrocytes towards substrate moduli using interpenetrating networks based on PAM and PEG (*114*). The neurons favors softer gels (~100-500 Pa) while astrocytes prefer stiffer substrate (~1-10 kPa) (*114*), consistent with the findings using DNA hydrogels (*112*). Mechanical properties of natural gels such as alginate can be controlled as well by varying concentrations of calcium ions in solution (*78*). The rate of proliferation of NSCs decreases with the increase in the modulus ranging from ~100 Pa to 10 kPa (*78*).

In contrast, it is demonstrated that SpL201 cells favor stiffer substrate of ~100 MPa than ~1 MPa on hydrophobic surfaces of photo-crosslinked PCLF or PCLA networks and hybrid polymer networks consisting of PPF and PCL (*68*, *70*, *72–74*). As a conditionally immortalized Schwann cell precursor line that generates myelin, SpL201 cells used in this study are different from neurons in both cell type and functions as they can differentiate into early Schwann cell-like cells, which belong to glial cells, and also can upregulate Oct-6 and myelin gene expression upon forskolin treatment (*116*). In addition, Schwann cell precursor is a favorable cell type for myelin repair in the central nervous system because it can circumvent some of the major problems associated with the use of Schwann cells (*117*). As discovered earlier, soft substrates can stimulate neurite extension and branching while inhibit glial cell spreading and proliferation, although mechanism of regulation is still under investigation (*75*, *107–110*, *114*, *115*). It should be noted that the surface stiffnesses of hydrophobic networks consisting of PCL and/or PPF were greatly higher than those of hydrogels (normally less than 1 MPa), which have to be incorporated with polycations such as poly(L-lysine), matrigel, and adhesive proteins to allow cells to attach and proliferate (*102*, *103*, *108*).

Downloaded by CORNELL UNIV on June 23, 2012 | http://pubs.acs.org
Publication Date (Web): November 18, 2010 | doi: 10.1021/bk-2010-1054.ch003

3.2. ECM Proteins and Neurotrophic Factors

Both ECM proteins and neurotrophic factors incorporated in polymer gels serve as important cues to promote regeneration behavior *in vivo* (*24*, *25*). ECM proteins like laminin, collagen and fibronectin play important roles in axonal development and nerve repair. Collagen type I is the main component of ECM. Its mechanical strength and degradation properties have been improved by crosslinking with mTGase, as discussed in Section 2.1. Incorporation of laminin in collagen scaffolds helps more neurites differentiated from PC12 cells at higher concentration of laminin (*42*). Crosslinked proteins exhibit tunable degradation from less than a week to a longer term via cleavage of a neurites secreted protease-urokinase plasminogen activator (uPA) (*34*). The gels support PC12 cell adhesion and differentiation that increased with the density of RGD peptides incorporated (*34*).

The neurotrophic factors that have been investigated include NGF, NT-3, BDNF, fibroblast growth factor (FGF), and ciliary-neurotrophic factor (CNTF) (*24*, *25*, *118*). Prepared using double-emulsion technique, PLGA microspheres have been widely employed as carriers to deliver these neurotrophic factors such as the glial cell line derived neurotrophic factor (GDNF) (*119*, *120*), NGF (*121*), and carbidopa (CD)/levodopa (LD) (*122*). Microspheres injected in the brain or nerve tissue can have controlled release profiles of these factors for various diseases in nervous system. Injectable and biodegradable PEG hydrogels have also been combined with basic fibroblast growth factor (bFGF-2) and collagen to support survival and growth of neural cells while these two factors act differently than either applied individually (*58*). The release rate of neurotrophins in PEG hydrogels are controlled by the crosslinking density of the network. CNTF incorporated and released in the degradable acrylated PLA-PEG-PLA macromer have significantly stimulated outgrowth of neurites in numbers and lengths (*59*).

3.3. Neural Stem Cell Encapsulation

Gelation systems offer microenvironment with good biocompatibility, tunable mechanical properties and controlled release of neurotrophins to be used as potential cell carriers for transplantation of NSCs (*28*). Stem cells boasted pluripotency to be differentiated into functional cells to replace neurons and secrete neurotrophic factors in the damaged neural tissue (*18*). HA hydrogels discussed in Section 2.1 are widely used as cell carriers. HA hydrogels can provide a unique microenvironment with tunable physical properties for human embryonic stem cells (hEMCs) to internalize while maintaining their undifferentiated state and genetic integrity until being directed to differentiate (*50*). HA hydrogels incorporated with polylysine can achieve better neural stem cell differentiation (*51*). NSCs growth and differentiation are well-supported by the HA-collagen sponge-like scaffolds (*53*). HA hydrogels are loaded with BDNF to demonstrated improved survival of transplanted neural cells (*86*).

3D collagen hydrogels have been used to entrap embryonic hippocampal neurons that could maintain their neuronal phenotype as they are at traditional 2D cultures (*43*). Chitosan gel spongy scaffolds has been used to transplant BMSC-derived Schwann cells *in vivo*. A suitable microenvironment is provided for regenerating axons that were found 7 days after surgery and extended into the host distal nerve segment at 14 days (*79*). PLGA is crosslinked with chitosan to fabricate scaffolds with appropriate mechanical properties for BMSCs to differentiate into neurons in the presence of NGF (*123*). PLGA microspheres can also be good microcarriers for pluripotent stem cells. By incorporating retinoic acid, P19 cell are supported and induced to differentiate into neurons on the surface of PLGA microspheres (*124*).

4. Applications in Nerve Repair

Injectable gelation systems including hydrogels, scaffolds and microspheres can be used to give mechanical support and deliver drugs and cells *in situ* to help nerve regeneration. Unique challenges are rendered when we design gelation systems to create guiding conduits for axon ingrowth and a permissive microenvironment for promoting nerve regeneration in a controlled, localized manner (*1–25*).

Downloaded by CORNELL UNIV on June 23, 2012 | http://pubs.acs.org
Publication Date (Web): November 18, 2010 | doi: 10.1021/bk-2010-1054.ch003

Downloaded by CORNELL UNIV on June 23, 2012 | http://pubs.acs.org
Publication Date (Web): November 18, 2010 | doi: 10.1021/bk-2010-1054.ch003

4.1. Central Nerve Regeneration

Diseases relating to central nerves are traumatic brain injury (TBI), chronic disorders like Parkinson's disease, and Alzheimer's disease, and SCI (*1*, *19*). Injectable systems can replace damaged tissue or cavity of irregular shapes and delivery therapeutics to help functional recovery. As described in Section 2.2, PNIPAAm-PEG injectable scaffold platform for treatment of SCI have been fabricated with desired mechanical properties to achieve sustained release of BDNF and NT-3 and the survival of BMSCs up to 4 weeks (*94*).

A growth permissive, *in situ* gelling agarose scaffold has been fabricated and embedded with BDNF releasing mircrotubules (*77*). These scaffolds are able to fill the irregular cavities in the spinal cord (*77*). BDNF enhances neurites growth into the scaffolds and reduces inflammatory response of the agarose *in vivo* 6 weeks after implantation (*77*). Thermo-responsive xyloglucan hydrogel scaffolds with similar mechanical properties to native spinal cord have been investigated for applications in neural tissue engineering of SC. Immobilized with poly(D-lysine), the scaffolds well support differentiation of primary cortical neurons, neural stem cells and axonal extensions under both 2D and 3D conditions (*91*). Collagen in a highly concentrated solution has been developed as localized drug delivery system. Epidermal growth factor (EGF) and bFGF-2 were injected together with collagen solution intrathecally at the site of injury. It has been proved to significantly enhance ependymal cell proliferation 14 days post injection to demonstrate successful delivery of growth factors for injured spinal cord (*83*). Keratin-based hydrogels containing polypeptide can promote neural progenitor cell adhesion and proliferation while preventing infiltration of inflammatory cells to create suitable microenvironment for treatment of Parkinson's disease (*86*).

4.2. Peripheral Nerve Regeneration

The major challenge facing peripheral nerve regeneration (PNS) is to use artificial nerve conduits capable of bridging long gaps at the site of injury (*1–14*). The "gold standard" for peripheral nerve repair is to use autologous nerve grafts, which however, do not result in complete functional regeneration. Therefore, synthetic nerve guidance channels have been explored to achieve potentially better control of desired properties and regenerative ability compared with autograft (*1–14*). Luminal fillers such as factors or cells carried in the gelation systems serve as important enhancement in nerve regeneration (*22*).

As described in Section 2.2, anisotropic scaffolds of agarose hydrogels containing laminin and NGF has been prepared and compared with isotropic scaffolds and autografts to regenerate 20 mm nerve gap in rats (*36*). Regenerating axons are only observed four months post implantation in both laminin and NGF anisotropic scaffolds, which are comparable with autografts, but not found in isotropic scaffolds (*36*).

Synthetic crosslinked PCLF and PPF-*co*-PCL nerve conduits prepared via photo-crosslinking and a molding technique are biocompatible with the rat tissue with minimal inflammatory response or existence of macrophages (*68*, *72*). These nerve conduits made from hydrophobic polymer networks remain connected and intact after the implantation without being deformed or swollen by body fluids (*68*, *72*). Nerve cables with myelinated axons have been found in crosslinked PCLF nerve conduits after 6 and 17 weeks of implantation (*68*).

4.3. Drug Delivery for Nerve Repair

Polymeric gelation systems for drug delivery are becoming increasingly attractive and controllable for nerve regeneration in both short-term and long-term uses (*118*). HAMC hydrogels described earlier in Section 2.2 have promising characteristics such as fast-gelling, non-cell adhesive, degradability and biocompatibility within the intrathecal space for one month (*89*). Drug-loaded hydrogels remain at the site of injection and deliver drugs to the spinal cord over the life of the material (*89*). This system has been examined to achieve broader release profiles by loading PLGA micro-particles in the gel (*90*). Six molecules have been tested at satisfactory diffusivity with a controlled release from 1 to 28 days (*90*). PLGA microspheres encapsulating proteins have also been entrapped between a chitosan inner tube and a chitin outer tube to achieve local delivery of bovine serum albumin (BSA) for over two months under a degradation-controlled release following an initial burst release. EGF has been co-encapsulated with BSA to be released for 56 days and sustain bioactivity for at least 14 days (*125*). Injectable polymer scaffolds derived from oxidized alginate crosslinked with gelatin in the presence of sodium tetraborate have been developed with controlled gelling time and crosslinking parameters in-situ. These scaffolds have been evaluated to be biocompatible and a model drug has been used to demonstrate their potentials as drug delivery vehicle (*39*).

Collagen gels loaded with NGF have been used to reduce the amount of NGF required for PC12 cell culture to 1/30th of the amount used in daily addition method. Collagen gels achieve economized controlled release of NGF without influencing cell viability, apoptosis and differentiation for potential large-scale culture of neuronal or stem cell (*85*). pHEMA with conjugated lysine segment have been assessed as hydrogel-coated devices for release rate of NGF to induce DRG neurons. FDA-approved pHEMA hydrogels are as soft as brain tissue. It is demonstrated that NGF combined in the pHEMA hydrogel has similar effect as bath-applied NGF at the same concentration (*60*). Targeted delivery has been achieved by tetanus toxin C fragment conjugated to PLGA-PEG nanoparticles using a biotin-binding protein neutravidin to selectively target neuroblastoma cells *in vitro*, whereas not targeting liver or endothelial cells (*126*).

5. Conclusions and Future Directions

In summary, injectable polymer systems have been used as biomaterials for nerve repair and regeneration. The applications include scaffold structural materials, fillers, substrates for supporting nerve cell proliferation and differentiation, and drug delivery systems to release neurotrophic factors such as NGF and other anti-cancer drugs. More advanced injectable polymeric

Downloaded by CORNELL UNIV on June 23, 2012 | http://pubs.acs.org
Publication Date (Web): November 18, 2010 | doi: 10.1021/bk-2010-1054.ch003

systems with better functionalities are expected to be developed for nerve tissue engineering applications.

Acknowledgments

This work was supported by the start-up fund from the University of Tennessee, Knoxville.

References

1. Schmidt, C. E.; Leach, J. B. Neural tissue engineering: strategies for repair and regeneration. *Annu. Rev. Biomed. Eng.* **2003**, *5*, 293–347.
2. Fields, R. D.; Le Beau, J. M.; Longo, F. M.; Ellisman, M. H. Nerve regeneration through artificial tubular implants. *Prog. Neurobiol.* **1989**, *33*, 87–134.
3. Bellamkonda, R.; Aebischer, P. Tissue engineering in the nervous system. *Biotechnol. Bioeng.* **1994**, *43*, 543–554.
4. Heath, C. A.; Rutkowski, G. E. The development of bioartificial nerve grafts for peripheral-nerve regeneration. *Trends Biotechnol.* **1998**, *16* (4), 163–168.
5. Evans, G. R. D. Challenges to nerve regeneration. *Seminars in Surgical Oncology* **2000**, *19*, 312–318.
6. Belkas, J. S.; Shoichet, M. S.; Midha, R. Peripheral nerve regeneration through guidance tubes. *Neurol. Res.* **2004**, *26*, 151–60.
7. Kannan, R. Y.; Salacinski, H. J.; Butler, P. E. M.; Seifalian, A. M. Artificial nerve conduits in peripheral-nerve repair. *Biotechnol. Appl. Biochem.* **2005**, *41*, 193–200.
8. Ciardelli, G.; Chiono, V. Materials for peripheral nerve regeneration. *Macromol. Biosci.* **2006**, *6*, 13–26.
9. Meek, M. F.; Coert, J. H. US Food and Drug Administration/Conformit Europe-approved absorbable nerve conduits for clinical repair of peripheral and cranial nerves. *Ann. Plast. Surg.* **2008**, *60* (4), 466–72.
10. Ichihara, S.; Inada, Y.; Nakamura, T. Artificial nerve tubes and their application for repair of peripheral nerve injury: an update of current concepts. *Injury, International Journal of the Care of the Injured* **2008**, *39s4*, S29–S39.
11. Johnson, E. O.; Soucacos, P. N. Nerve repair: experimental and clinical evaluation of biodegradable artificial nerve guides. *Injury, International Journal of the Care of the Injured* **2008**, *39s*, S30–S36.
12. de Ruiter, G. C. W.; Malessy, M. J. A.; Yaszemski, M. J.; Windebank, A. J.; Spinner, R. J. Designing ideal conduits for peripheral nerve repair. *Neurosurgical Focus* **2009**, *26* (2), E5-1–9.
13. Chiono, V.; Tonda-Turo, C.; Ciardelli, G. Artificial scaffolds for peripheral nerve reconstruction. *Essays on Peripheral Nerve Repair and Regeneration* **2009**, *87*, 173–198.
14. Huang, Y.-C.; Huang, Y.-Y. Biomaterials and strategies for nerve regeneration. *Artif. Organs* **2006**, *30* (7), 514–22.

Downloaded by CORNELL UNIV on June 23, 2012 | http://pubs.acs.org
Publication Date (Web): November 18, 2010 | doi: 10.1021/bk-2010-1054.ch003

15. Geller, H. M.; Fawcett, J. W. Building a bridge: engineering spinal cord repair. *Experimental Neurology* **2002**, *174*, 125–136.
16. Novikova, L. N.; Novikov, L. N.; Kellerth, J.-O. Biopolymers and biodegradable smart implants for tissue regeneration after spinal cord injury. *Curr. Opin. Neurol.* **2003**, *16*, 711–715.
17. Zhang, N.; Yan, H.; Wen, X. Tissue-engineering approaches for axonal guidance. *Brain Res. Rev.* **2005**, *49*, 48–64.
18. Zhong, Y.; Bellamkonda, R. V. Biomaterials for the central nervous system. *J. R. Soc., Interface* **2008**, *5*, 957–975.
19. Norman, L. L.; Stroka, K.; Espinoza, H. A. Guiding axons in the central nervous system: a tissue engineering approach. *Tissue Eng., Part B* **2009**, *15*, 291–305.
20. Madigan, N. N.; McMahon, S.; O'Brien, T.; Yaszemski, M. J.; Windebank, A. J. Current tissue engineering and novel therapeutic approaches to axonal regeneration following spinal cord injury using polymer scaffolds. *Respir. Physiol. Neurobiol.* **2009**, *169*, 183–199.
21. Nisbet, D. R.; Crompton, K. E.; Horne, M. K.; Finkelstein, D. I.; Forsythe, J. S. Neural tissue engineering of the CNS using hydrogels. *J. Biomed. Mater. Res.* **2008**, *87B*, 251–263.
22. Chen, M. B.; Zhang, F.; Lineaweaver, W. C. Luminal fillers in nerve conduits for peripheral nerve repair. *Ann. Plast. Surg.* **2006**, *57*, 462–471.
23. Yan, H.; Zhang, F.; Chen, M. B.; Lineaweaver, W. C. Conduit luminal additives for peripheral nerve repair. *Int. Rev. Neurobiol.* **2009**, *87*, 199–225.
24. Terenghi, G. Peripheral nerve regeneration and neurotrophic factors. *J. Anat.* **1999**, *194*, 1–14.
25. Willerth, S. M.; Sakiyama-Elbert, S. E. Approaches to neural tissue engineering using scaffolds for drug delivery. *Adv. Drug Delivery Rev.* **2007**, *59*, 325–338.
26. Hoffman, A. S. Hydrogels for biomedical applications. *Ann. N. Y. Acad. Sci.* **2001**, *944*, 62–73.
27. Yu, L.; Ding, J. Injectable hydrogels as unique biomedical materials. *Chem. Soc. Rev.* **2008**, *37*, 1473–1481.
28. Liu, S. Q.; Tay, R.; Khan, M.; Ee, P. L. R.; Hedrick, J. L.; Yang, Y. Y. Synthetic hydrogels for controlled stem cell differentiation. *Soft Matter* **2010**, *6*, 67–81.
29. Jeong, B.; Gutowska, A. Lessons from nature: stimulate-responsive polymers and their biomedical applications. *Trends Biotechnol.* **2002**, *20* (7), 305–311.
30. Zhang, S. Emerging biological materials through molecular self-assembly. *Biotechnol. Adv.* **2002**, *20*, 321–339.
31. Jeong, B.; Bae, Y. H.; Lee, D. S.; Kim, S. W. Biodegradable block copolymers as injectable drug-delivery system. *Nature* **1997**, *388*, 860–862.
32. Wang, C.; Stewart, R. J.; Kopecek, J. Hybrid hydrogels assembled from synthetic polymers and coiled-coil protein domains. *Nature* **1999**, *397*, 417–420.

Downloaded by CORNELL UNIV on June 23, 2012 | http://pubs.acs.org
Publication Date (Web): November 18, 2010 | doi: 10.1021/bk-2010-1054.ch003

Downloaded by CORNELL UNIV on June 23, 2012 | http://pubs.acs.org
Publication Date (Web): November 18, 2010 | doi: 10.1021/bk-2010-1054.ch003

33. Shen, W.; Zhang, K.; Kornfield, J. A.; Tirrell, D. A. Tuning the erosion rate of artificial protein hydrogels through control of network topology. *Nat. Mater.* **2006**, *5*, 153–158.
34. Straley, K. S.; Heilshorn, S. C. Independent tuning of multiple biomaterial properties using protein engineering. *Soft Matter* **2008**, *5*, 114–124.
35. Luo, Y.; Shoichet, M. S. A photolabile hydrogel for guided three dimensional cell growth and migration. *Nat. Mater.* **2004**, *3*, 249–253.
36. Dodla, M. C.; Bellamkonda, R. V. Differences between the effect of anisotropic and isotropic laminin and nerve growth factor presenting scaffolds on nerve regeneration across long peripheral nerve gaps. *Biomaterials* **2009**, *29*, 33–46.
37. Hashimoto, T.; Suzuki, Y.; Suzuki, K.; Nakashima, T; Tanihara, M.; Ide, C. Peripheral nerve regeneration using non-tubular alginate gel crosslinked with covalent bonds. *J. Mater. Sci.: Mater. Med.* **2005**, *16*, 503–509.
38. Kataoka, K.; Suzuki, Y.; Kitada, M.; Ohnishi, K.; Suzuki, K.; Tanihara, M.; Ide, C.; Endo, K.; Nishimura, Y. Alginate, a bioresorbable material derived from brown seaweed, enhances elongation of amputated axons of spinal cord in infant rats. *J. Biomed. Mater. Res.* **2001**, *54*, 373–384.
39. Balakrishnan, B; Jayakrishnan, A. Self-cross-linking biopolymers as injectable in situ forming biodegradable scaffolds. *Biomaterials* **2009**, *26*, 3941–3951.
40. Freier, T.; Montenegro, R.; Koh, H. S.; Shoichet, M. S. Chitin-based tubes for tissue engineering in the nervous system. *Biomaterials* **2005**, *26*, 4624–4632.
41. Leipzig, N. D.; Shoichet, M. S. The effect of substrate stiffness on adult neural stem cell behavior. *Biomaterials* **2009**, *30*, 6867–6878.
42. Yao, L.; Damodaran, G.; Nkolskaya, N.; Gorman, A. M.; Windebank, A.; Pandit, A. The effect of laminin peptide gradient in enzymatically cross-linked collagen scaffolds on neurite growth. *J. Biomed. Mater. Res.* **2010**, *92A*, 484–492.
43. Xu, T.; Molnar, P.; Gregory, C.; Das, M.; Boland, T.; Hickman, J. J. Electrophysiological characterization of embryonic hippocampal neurons cultured in a 3D collagen hydrogel. *Biomaterials* **2009**, *30*, 4377–4383.
44. Chang, J.-Y.; Lin, J.-H.; Yao, C.-H.; Chen, J.-H.; Lai, T.-Y.; Chen, Y.-S. *In vivo* evaluation of a biodegradable EDC/NHS-cross-linked gelatin peripheral nerve guide conduit material. *Macromol. Biosci.* **2007**, *7*, 500–507.
45. Gamez, E.; Goto, Y.; Nagata, K.; Iwaki, T.; Sasaki, T.; Matsuda, T. Photofabricated gelatin-based nerve conduits: nerve tissue regeneration potentials. *Cell Transplant.* **2004**, *13*, 549–564.
46. Sakai, Y.; Matsuyama, Y.; Takahashi, K.; Sato, T.; Hattori, T.; Nakashima, S.; Ishiguro, N. New artificial nerve conduits made with photocrosslinked hyaluronic acid for peripheral nerve regeneration. *Bio-Med. Mater. Eng.* **2007**, *17*, 191–197.
47. Miyamoto, K.; Sasaki, M.; Minamisawa, Y.; Kurahashi, Y.; Kano, H.; Ishikawa, S. Evaluation of *in vivo* biocompatibility and biodegradation of photocrosslinked hyaluronate hydrogels (HAD gels). *J. Biomed. Mater. Res.* **2004**, *70A*, 550–559.

48. Seidlits, S. K.; Khaing, Z. Z.; Petersen, R. R.; Nickels, J. D.; Vanscoy, J. F.; Shear, J. B.; Schmidt, C. E. The effects of hyaluronic acid hydrogels with tunable mechanical properties on neural progenitor cell differentiation. *Biomaterials* **2010**, *31* (14), 3930–3940.
49. Marklein, R. A.; Burdick, J. A. Spatially controlled hydrogel mechanics to modulate stem cell interactions. *Soft Matter* **2010**, *6*, 136–143.
50. Gerecht, S.; Burdick, J. A.; Gerreira, L. S.; Townsend, S. A.; Langer, R.; Novakovic, G. V. Hyaluronic acid hydrogel for controlled self-renewal and differentiation of human embryonic stem cells. *Proc. Natl. Acad. Sci., U.S.A.* **2007**, *104*, 11298–11303.
51. Ren, Y. J.; Zhou, Z. Y.; Cui, F. Z. Hyaluronic acid/polylysine hydrogel as a transfer system for transplantation of neural stem cells. *J. Bioact. Compat. Polym.* **2009**, *24*, 56–61.
52. Zhang, T.; Yan, Y.; Wang, X.; Xiong, Z.; Lin, F.; Wu, R.; Zhang, R. Three-dimensional gelatin and gelatin/hyaluronan hydrogel structures for traumatic brain injury. *J. Bioact. Compat. Polym.* **2007**, *22*, 19–29.
53. Wang, T. W.; Spector, M. Development of hyaluronic acid-based scaffolds for brain tissue engineering. *Acta Biomater.* **2009**, *5*, 2371–2384.
54. Gunn, J. W.; Turner, S. D.; Mann, B. K. Adhesive and mechanical properties of hydrogels influence neurite extension. *J. Biomed. Mater. Res.* **2005**, *72A*, 91–97.
55. Dadsetan, M.; Knight, A. M.; Lu, L.; Winderbank, A. J.; Yaszemski, M. J. Stimulation of neurite outgrowth using positively charged hydrogels. *Biomaterials* **2009**, *30*, 3874–3881.
56. Mahoney, M. J.; Anseth, K. S. Three-dimensional growth and function of neural tissue in degradable polyethylene glycol hydrogels. *Biomaterials* **2006**, *12*, 2265–2274.
57. Piantino, J.; Burdick, J. A.; Goldberg, D.; Langer, R.; Benowitz, L. I. An injectable, biodegradable hydrogel for trophic factor delivery enhances axonal rewiring and improves performance after spinal cord injury. *Exp. Neurol.* **2006**, *201*, 359–367.
58. Mahoney, M. J.; Anseth, K. S. Contrasting effects of collagen and bFGF-2 on neural cell function in degradable synthetic PEG hydrogels. *J. Biomed. Res.* **2007**, *81A*, 269–278.
59. Burdick, J. A.; Ward, M.; Liang, E.; Young, M. J.; Langer, R. Stimulation of neurite outgrowth by neurotrophins delivered from degradable hydrogels. *Biomaterials* **2007**, *27*, 452–469.
60. Jhaveri, S. J.; Hynd, M. R.; Mesfin, N. D.; Turner, J. N.; Shain, W.; Ober, C. K. Release of nerve growth factor from HEMA hydrogel-coated substrates and its effect on the differentiation of neural cells. *Biomacromolecules* **2009**, *10*, 174–183.
61. Midha, R.; Munro, C. A.; Dalton, P. D.; Tator, C. H.; Shoichet, M. S. Growth factor enhancement of peripheral nerve regeneration through a novel synthetic hydrogel tube. *J. Neurosurg.* **2003**, *99*, 555–565.
62. Tsai, E. C.; Dalton, P. D.; Shoichet, M. S.; Tator, C. H. Synthetic hydrogel guidance channels facilitate regeneration of adult rat brainstem motor

Downloaded by CORNELL UNIV on June 23, 2012 | http://pubs.acs.org
Publication Date (Web): November 18, 2010 | doi: 10.1021/bk-2010-1054.ch003

axons after complete spinal cord transaction. *J. Neurotrauma* **2004**, *21* (6), 789–804.

63. Katayama, Y.; Montenegro, R.; Freier, T.; Midha, R.; Belkas, J. S.; Shoichet, M. S. Coil-reinforced hydrogel tubes promote nerve regeneration equivalent to that of nerve autografts. *Biomaterials* **2006**, *27*, 505–518.
64. Woerly, S.; Pinet, E.; de Robertis, L.; van Diep, D.; Bousmina, M. Spinal cord repair with PHPMA hydrogel containing RGD peptides (NeuroGel). *Biomaterials* **2001**, *22*, 1095–1111.
65. Wang, S.; Lu, L.; Gruetzmacher, J. A.; Currier, B. L.; Yaszemski, M. J. Synthesis and characterizations of biodegradable and crosslinkable poly(ε-caprolactone fumarate), poly(ethylene glycol fumarate), and their amphiphilic copolymer. *Biomaterials* **2006**, *27* (6), 832–412.
66. Cai, L.; Wang, S. Elucidating colorization in the functionalization of hydroxyl-containing polymers using unsaturated anhydrides/acyl chlorides in the presence of triethylamine. *Biomacromolecules* **2010**, *11*, 304–307.
67. Wang, S.; Yaszemski, M. J.; Gruetzmacher, J. A.; Lu, L. Photo-crosslinked poly(ε-caprolactone fumarate) networks: roles of crystallinity and crosslinking density in determining mechanical properties. *Polymer* **2008**, *49*, 5692–5699.
68. Wang, S.; Yaszemski, M. J.; Knight, A. M.; Gruetzmacher, J. A.; Windebank, A. J.; Lu, L. Photo-crosslinked poly(ε-caprolactone fumarate) networks for guided peripheral nerve regeneration: material properties and preliminary biological evaluations. *Acta Biomater.* **2009**, *5*, 1531–1542.
69. Wang, S.; Kempen, D. H.; Yaszemski, M. J.; Lu, L. The roles of matrix polymer crystallinity and hydroxyapatite nanoparticles in modulating material properties of photo-crosslinked composites and bone marrow stromal cell responses. *Biomaterials* **2009**, *30*, 3359–3370.
70. Wang, S.; Kempen, D. H.; Simha, N. K.; Lewis, J. L.; Windebank, A. J.; Yaszemski, M. J.; Lu, L. Photo-cross-linked hybrid polymer networks consisting of poly(propylene fumarate) and poly(caprolactone fumarate): controlled physical properties and regulated bone and nerve cell responses. *Biomacromolecules* **2008**, *9*, 1229–1241.
71. Wang, S.; Lu, L.; Gruetzmacher, J. A.; Currier, B. L.; Yaszemski, M. J. A biodegradable and cross-linkable multiblock copolymer consisting of poly(propylene fumarate) and poly(ε-caprolactone): Synthesis, characterization, and physical properties. *Macromolecules* **2005**, *38*, 7358–7370.
72. Wang, S.; Kempen, D. H.; de Ruiter, G. C. W.; Spinner, R. J.; Windebank, A. J.; Lu, L.; Yaszemski, M. J. Molecularly engineered photo-crosslinkable polymers with controlled physical properties for bone and nerve regeneration. **2010**, submitted.
73. Cai, L.; Wang, S. Poly(ε-caprolactone) acrylates synthesized using a facile method for fabricating networks to achieve controllable physicochemical properties and tunable cell responses. *Polymer* **2010**, *51*, 164–177.
74. Cai, L.; Wang, S. Parabolic dependence of cell responses on the composition of polymer networks with controllable crosslinking density and crystallinity. **2010**, submitted.

Downloaded by CORNELL UNIV on June 23, 2012 | http://pubs.acs.org
Publication Date (Web): November 18, 2010 | doi: 10.1021/bk-2010-1054.ch003

75. Strassman, R. J.; Letourneau, P. C.; Wessells, N. K. Elongation of axons in an agar matrix that does not support cell locomotion. *Exp. Cell Res.* **1973**, *81*, 482–487.
76. Balgude, A. P.; Yu, X.; Szymanski, A.; Bellamkonda, R. V. Agarose gel stiffness determines rate of DRG neurite extension in 3D cultures. *Biomaterials* **2001**, *22*, 1077–1084.
77. Jain, A.; Kim, Y. T.; McKeon, R. J.; Bellamkonda, R. V. In situ gelling hydrogels for conformal repair of spinal cord defects, and local delivery of BDNF after spinal cord injury. *Biomaterials* **2009**, *27*, 497–504.
78. Banerjee, A.; Arha, M.; Choudhary, S.; Ashton, R. S.; Bhatia, S. R.; Schaffer, D. V.; Kane, R. S. The influence of hydrogel modulus on the proliferation and differentiation of encapsulated neural stem cells. *Biomaterials* **2009**, *20*, 4695–4699.
79. Ishikawa, N.; Suzuki, Y.; Dezawa, M.; Kataoka, K.; Ohta, M.; Cho, H.; Ide, C. Peripheral nerve regeneration by transplantation of BMSC-derived Schwann cells as chitosan gel sponge scaffolds. *J. Biomed. Res.* **2009**, *89A*, 118–1124.
80. Crompton, K. E.; Goud, J. D.; Bellamkonda, R. V.; Gengenbach, T. R.; Finkelstein, D. I.; Horne, M. K.; Forsythe, J. S. Polylysine-functionalised thermoresponsive chitosan hydrogel for neural tissue engineering. *Biomaterials* **2007**, *28*, 441–449.
81. Dang, J. M.; Sun, D. D. N.; Ya, Y. S.; Sieber, A. N.; Kostuik, J. P.; Leong, K. W. Temperature-responsive hydroxybutyl chitosan for the culture of mesenchymal stem cells and intervertebral disk cells. *Biomaterials* **2006**, *27*, 406–428.
82. King, V. R.; Alovskaya, A.; Wei, D. Y. T.; Brown, R. A.; Pristley, J. V. The use of injectable forms of fibrin and fibronectin to support axonal ingrowth after spinal cord injury. *Biomaterials* **2010**, *31*, 4447–4456.
83. Hamann, M. C. J.; Tator, C. H.; Shoichet, M. S. Injectable intrathecal delivery system for localized administration of EGF and FGF-2 to the injured rat spinal cord. *Exp. Neurol.* **2005**, *194*, 106–119.
84. Bhang, S. H.; Lee, T. J.; Lim, J. M.; Lim, J. S.; Han, A. M.; Choi, C. Y.; Kwon, Y. H. K.; Kim, B.-S. The effect of controlled release of nerve growth factor from collagen gel on the efficiency of neural cell culture. *Biomaterials* **2009**, *20*, 126–132.
85. Nakayama, K.; Takakuda, K.; Koyama, Y.; Itoh, S.; Wang, W.; Mukai, T.; Shirahama, N. Enhancement of peripheral nerve regeneration using bioabsorbable polymer tubes packed with fibrin gel. *Artif. Organs* **2007**, *31* (7), 500–508.
86. Nakaji-Hirabayashi, T.; Kato, K.; Iwata, H. Hyaluronic acid hydrogel loaded with genetically-engineered brain-derived neurotrophic factor as a neural cell carrier. *Biomaterials* **2009**, *30*, 4581–4589.
87. Nakaji-Hirabayashi, T.; Kato, K.; Iwata, H. Self-assembling chimeric protein for biodegradable hydrogels interacting with integrins expressed on neural stem progenitor cells. *Biomacromolecules* **2008**, *9*, 1411–1416.
88. Tate, M. C.; Shear, D. A.; Hoffman, S. W.; Stein, D. G.; LaPlaca, M. C. Biocompatibility of methylcellulose-based constructs designed for

Downloaded by CORNELL UNIV on June 23, 2012 | http://pubs.acs.org
Publication Date (Web): November 18, 2010 | doi: 10.1021/bk-2010-1054.ch003

Downloaded by CORNELL UNIV on June 23, 2012 | http://pubs.acs.org
Publication Date (Web): November 18, 2010 | doi: 10.1021/bk-2010-1054.ch003

intracerebral gelation following experimental traumatic brain injury. *Biomaterials* **2001**, *22*, 1113–1123.

89. Gupta, D.; Tator, C. H.; Shoichet, M. S. Fast-gelling injectable blend of hyaluronan and methylcellulose for intrathecal, localized delivery to the injured spinal cord. *Biomaterials* **2006**, *27*, 2370–2379.
90. Baumann, M. D.; Kang, C. E.; Stanwick, J. C.; Wang, Y.; Kim, H.; Lapitsky, Y.; Shoichet, M. S. An injectable drug delivery platform for sustained combination therapy. *J. Controlled Release* **2009**, *138*, 205–213.
91. Nisbet, D. R.; Moses, D.; Gengenbach, T. R.; Forsythe, J. S.; Finkelstein, D. I.; Horne, M. K. Enhancing neurite outgrowth from primary neurons and neural stem cells using thermoresponsive hydrogel scaffolds for the repair of spinal cord injury. *J. Biomed. Res.* **2009**, *89A*, 24–35.
92. Yang, C. Y.; Song, B. B.; Ao, Y.; Nowak, A. P.; Abelowitz, R. B.; Korsak, R. A.; Havton, L. A.; Deming, T. J.; Sofroniew, M. V. Biocompatibility of amphiphilic diblock copolypeptide hydrogels in the central nervous system. *Biomaterials* **2009**, *30*, 2881–2898.
93. Holmes, T. C.; de Lacalle, S.; Su, X.; Liu, G.; Rich, A.; Zhang, S. Extensive neurite outgrowth and active synapse formation on self-assembling peptide scaffolds. *Proc. Natl. Acad. Sci., U.S.A.* **2000**, *97* (12), 6728–6733.
94. Comolli, N.; Neuhuber, B.; Fischer, I.; Lowman, A. In vitro analysis of PNIPAAm-PEG, a novel, injectable scaffold for spinal cord repair. *Acta Biomater.* **2009**, *5*, 1046–1055.
95. Sundback, C.; Hadlock, T.; Cheney, M.; Vacanti, J. Manufacture of porous polymer nerve conduits by a novel low-pressure injection molding process. *Biomaterials* **2003**, *24*, 819–830.
96. Hadlock, T.; Elisseeff, J.; Langer, R.; Vacanti, J.; Cheney, M. A tissue-engineered conduit for peripheral nerve repair. *Arch. Otolaryngol., Head Neck Surg.* **1998**, *124*, 1081–1086.
97. Hadlock, T.; Sundback, C.; Hunter, D.; Cheney, M.; Vacanti, J. P. A polymer foam conduit seeded with Schwann cells promotes guided peripheral nerve regeneration. *Tissue Eng.* **2000**, *6* (2), 119–127.
98. Moore, M. J.; Friedman, J. A.; Lewellyn, E. B.; Mantila, S. M.; Krych, A. J.; Ameenuddin, S.; Knight, A. M.; Lu, L.; Currier, B. L.; Spinner, R. J.; Marsh, R. W.; Windebank, A. J.; Yaszemski, M. J. Multiple-channel scaffolds to promote spinal cord axon regeneration. *Biomaterials* **2006**, *27*, 419–429.
99. Harbers, G. M.; Grainger, D. W. Cell-material interactions: fundamental design issues for tissue engineering and clinical considerations. In *Introduction to Biomaterials*; Guelcher, S. A.; Hollinger, J. O., Eds.; Boca Raton: CRC Press, 2005; pp 15−45.
100. Wong, J. Y.; Leach, J. B.; Brown, X. Q. Balance of chemistry, topography, and mechanics at the cell-biomaterial interface: issues and challenges for assessing the role of substrate mechanics on cell response. *Surf. Sci.* **2004**, *570*, 119–33.
101. Saltzman, W. M.; Kyriakides, T. R.. Cell interactions with polymers. In *Principles of Tissue Engineering*, 3rd ed.; Lanza, R.; Langer, R.; Vacanti, J., Eds.; San Diego: Elsevier Academic Press, 2007; pp 279−96

In Biomaterials; Kulshrestha, A., et al.;
ACS Symposium Series; American Chemical Society: Washington, DC, 2010.

102. Pelham, R. J.; Wang, Y.-L. Cell locomotion and focal adhesions are regulated by substrate flexibility. *Proc. Natl. Acad. Sci., U.S.A.* **1997**, *94*, 13661–5.
103. Pelham, R. J.; Wang, Y.-L. Cell locomotion and focal adhesions are regulated by the mechanical properties of the substrate. *Biol. Bull.* **1998**, *194*, 348–349.
104. Discher, D. E.; Janmey, P.; Wang, Y.-L. Tissue cells feel and respond to the stiffness of their substrate. *Science* **2005**, *310*, 1139–1143.
105. Georges, P. C.; Janmey, P. A. Cell type-specific response to growth on soft materials. *J. Appl. Physiol.* **2005**, *98*, 1547–1553.
106. Levental, I.; Georges, P. C.; Janmey, P. A. Soft biological materials and their impact on cell function. *Soft Matter* **2007**, *3*, 299–306.
107. Nemir, S.; West, J. L. Synthetic materials in the study of cell response to substrate rigidity. *Ann. Biomed. Eng.* **2010**, *38*, 2–20.
108. Flanagan, L. A.; Ju, Y.-E.; Marg, B.; Osterfield, M.; Janmey, P. A. Neurite branching on deformable substrates. *NeuroReport* **2002**, *13*, 2411–2415.
109. Georges, P. C.; Miller, W. J.; Meaney, D. F.; Sawyer, E. S.; Janmey, P. A. Matrices with compliance comparable to that of brain tissue select neuronal over glial growth in mixed cortical cultures. *Biophys. J.* **2006**, *90*, 3012–18.
110. Kostic, A.; Sap, J.; Sheetz, M. P. RPTP alpha is required for rigidity-dependent inhibition of extension and differentiation of hippocampal neurons. *J. Cell Sci.* **2007**, *120*, 3895–3904.
111. Leach, J. B.; Brown, X. Q.; Jacot, J. G.; DiMilla, P. A.; Wong, J. Y. Neurite outgrowth and branching of PC12 cells on very soft substrates sharply decreases below a threshold of substrate rigidity. *J. Neural Eng.* **2007**, *4*, 26–34.
112. Jiang, F. X.; Yurke, B.; Firestein, B. L.; Langrana, N. A. Neurite outgrowth on a DNA crosslinked hydrogel with tunable stiffnesses. *Ann. Biomed. Eng.* **2008**, *36*, 1565–1579.
113. Stroka, K. M.; Aranda-Espinoza, H. Neutrophils display biphasic relationship between migration and substrate stiffness. *Cell Motil. Cytoskeleton* **2009**, *66*, 328–41.
114. Saha, K.; Keung, A. J.; Irwin, E. F.; Li, Y.; Little, L.; Schaffer, D. V.; Healy, K. E. Substrate modulus directs neural stem cell behavior. *Biophys. J.* **2009**, *95*, 4426–4438.
115. Teixeira, A. I.; Ilkhanizadeh, S.; Wigenius, J. A.; Duckworth, J. K.; Inganäs, O.; Hermanson, O. The promotion of neuronal maturation on soft substrates. *Biomaterials* **2009**, *30*, 4567–72.
116. Lobsiger, C. S.; Smith, P. M.; Buchstaller, J.; Schweitzer, B.; Franklin, R. J. M.; Suter, U.; Taylor, V. SpL201: a conditionally immortalized Schwann cell precursor line that generates myelin. *Glia* **2001**, *36*, 31–47.
117. Woodhoo, A.; Sahni, V.; Gilson, J.; Setzu, A.; Franklin, R. J. M.; Blakemore, W. F.; Mirsky, R.; Jessen, K. R. Schwann cell precursors: a favorable cell for myelin repair in the Central Nervous System. *Brain* **2007**, *130*, 2175–85.
118. Halliday, A. J.; Cook, M. J. Polymer-based drug delivery devices for neurological disorders. *CNS & Neurological Disorders - Drug Targets* **2009**, *8*, 205–221.

Downloaded by CORNELL UNIV on June 23, 2012 | http://pubs.acs.org
Publication Date (Web): November 18, 2010 | doi: 10.1021/bk-2010-1054.ch003

119. Jollivet, G.; Aubert-Pouessel, A.; Clavreul, A.; Venier-Julienne, M.-C.; Remy, S.; Montero-Menei, C. N.; Benoit, J.-P.; Menei, P. Striatal implantation of GDNF releasing biodegradable microspheres promotes recovery of motor function in a partial model of Parkinson's disease. *Biomaterials* **2004**, *25*, 933–942.
120. Jiang, C.; Moore, M. J.; Zhang, X.; Klassen, H.; Langer, R.; Young, M. Intravitreal injections of GDNF-loaded biodegradable microspheres are neuroprotective in a rat model of glaucoma. *Mol. Vision* **2007**, *13*, 1783–1792.
121. Pean, J. M.; Menei, P.; Morel, O.; Menei, C. N. M.; Benoit, J. P. Intraseptal implantation of NGF-releasing microspheres promote the survival of axotomized cholinergic neurons. *Biomaterials* **2000**, *12*, 2097–2101.
122. Arica, B.; Kas, H. S.; Moghdam, A.; Akalan, N.; Hincal, A. A. Carbidopa/levodopa-loaded biodegradable microspheres in vivo evaluation on experimental Parkinsonism in rats. *J. Controlled Release* **2005**, *102*, 689–697.
123. Kuo, Y. C.; Yeh, C. F.; Yang, J. T. Differentiation of bone marrow stromal cells in poly(lactide-*co*-glycolide)/chitosan scaffolds. *Biomaterials* **2009**, *30*, 6604–6613.
124. Newman, K. D.; McBurney, M. W. Poly(D,L lactic-co-glycolic acid) microspheres as biodegradable microcarriers for pluripotent stem cells. *Biomaterials* **2004**, *25*, 5763–5771.
125. Goraltchouk, A.; Scanga, V.; Morshead, C. M.; Shoichet, M. S. Incorporation of protein-eluting microspheres into biodegradable nerve guidance channels for controlled release. *J. Controlled Release* **2006**, *110*, 400–407.
126. Townsend, S. A.; Evrony, G. D.; Gu, F. X.; Schulz, M. P.; Brown, R. H., Jr; Langer, R. Tetanus toxin C fragment-conjugated nanoparticles for targeted drug delivery to neurons. *Biomaterials* **2007**, *28*, 5176–5184.

Downloaded by CORNELL UNIV on June 23, 2012 | http://pubs.acs.org
Publication Date (Web): November 18, 2010 | doi: 10.1021/bk-2010-1054.ch003

Chapter 4

Surface Patterning Using Self Assembled Monolayers (SAMs)

Rahul Bhure and Anil Mahapatro[*]

Center for Materials Research (CMR), Center for Biotechnology and Biomedical Sciences (CBBS), Department of Chemistry, Norfolk State University (NSU), Norfolk, VA 23504
[*]amahapatro@nsu.edu

Self Assembled Monolayers (SAMs) are nanostructures and are a fundamental component of nanoscience and nanotechnology. SAMs are a preferred tool for carrying out surface modification of a variety of materials and are a subject of widespread scientific attention across many disciplines. The ability to tailor the physical, mechanical as well as the chemical properties of the final substrate has placed SAMs in a unique position in materials science and surface chemistry in particular. Patterning of a SAM is an important step as secondary modification which further enhances the feasibility of SAMs for specific solutions to many problems in nanoscience. Here we present a brief introduction to the subject of SAM patterning by providing an introduction to the concept of a Self Assembled Monolayer (SAM) followed by a brief review of mixed SAMs. After this, the various strategies and techniques available for patterning SAMs are presented and some of their potential biomedical applications discussed.

1. Introduction

Nanoscience is termed as the science of objects and structures in the range of 1-100 nm (*1*, *2*). The complementary fields of nanoscience and nanotechnology are one of the most interesting and fascinating areas of science for researchers as well as for the public imagination. Newer tools and techniques for understanding and analyzing atomic, molecular and colloidal scale objects, such as scanning probe and electron microscopes have been a critical factor in the emergence of nanoscience. This area has got a lot of attention in recent times and is an exciting subject because of the range of possibilities as well as the products coming out of this field in the near future. However, we have started seeing concrete evidence of this in many areas like organic electronics, electronic devices, etc. Chemistry has played an important part in development of nanofabrication as materials and structures on the nanoscale are byproducts of the chemical reactions which involve the formation and breaking of chemical bonds between atoms. Biology has also given a greater understanding of nanoscience. The cell is considered to be one of the more sophisticated nanomachines with critical components in the nanometer scale dimensions. Some of these are catalysts, enzymes, ribosomes, proteins and protein RNA aggregates, lipid bilayers, ion channels, cytoskeletal elements, DNA, RNA, motor proteins, vacuoles and mitochondria (*3*). These systems interact with each other to carry out various functions through complicated chemical pathways. These bionanostuctures enable functions like motility, replication, metabolism and apoptosis, in the body and give us new strategies for constructing artificial nanosystems (*1*, *3*, *4*).

Controlling the surface and the interfacial properties become crticical at this scale. Almost 90 % of all the biological reactions happen at the surface (*5*). There is a tremendous increase in the surface area for nanostructured materials as compared to macroscopic materials. They have a high percentage of their constituent atoms at the surface. The volume of an object decreases rapidly than the surface area with a relation of the order of $S/V \alpha l^{-1}$, where l has atomic or molecular dimensions. Hence the scaling behavior indicates that at the nanoscale we have an extremely large surface area (*1*). The structure and chemical characteristics within many nanostructures and nanoassemblies will have a bearing on the larger macroscopic objects altering their physical properties.We take a look at these aspects via the concept of self assembly of nanostructures on surfaces which can alter the physical and chemical properties of the surface. We will first focus on the topic of self assembled monolayers and later at the nanotechnology aspect of patterning these self assembled monlayers along with a review of current methodologies.

2. Self Assembly

The general definition for self assembly is the spontaneous formation of complex hierarchical structures from pre-designed building blocks, typically involving multiple energy scales and multiple degrees of freedom (*6*). Self-assembly is also a very widely observed phenomenon in nature, as in the formation of for e.g., membranes from lipid molecules, or inside the living cell. Molecular self assembly can also be defined as the spontaneous association of molecules under equilibrium conditions into stable, structurally well defined aggregates joined by non covalent bonds. To acquire a basic understanding, the process can be looked from a biological as well as a chemical perpective. The basic idea for self assembly is inspired from biology which has examples like folding of polypeptide chains into functional proteins and chains of RNA into functional t-RNA (*7*), the formation of the double helix (*8*) and the formation of the cell membranes from phospholipids (*9*). The information that guides the assembly process is in the characteristics (for example, topographies, shapes, surface functionalities, and electrical potentials) of the subunits. The final structure is reached by equilibrating to the form of the lowest free energy. As the final self-assembled structures are close to or at thermodynamic equilibrium, they tend to reject defects (*2*, *10*, *11*). Self-assembly is the route followed in biological systems for the formation of the cell and its components. These structures are enormously complex and very small, and their formation in biological systems suggests that self-assembly may provide a route for certain types of patterned nanostructures.

Different approaches for the demonstration of self assembly have been tried out. These include two dimensional and three dimensional structures with dimensions ranging from molecular, mesocopic and macroscopic sizes (*12*). Some of the examples for these kinds of structures are self assembled monolayers (*13*, *14*), structures (micelles and liposomes) derived from aggregated surfactant molecules (*15*), phase-separated block copolymers (*16*, *17*), crystallized proteins (*18*) or colloidal particles (*19*) and aggregated mesoscale objects. Although self assembly originated in the study of molecules, it is a strategy which in principle can be applied to all scales. Self assembly provides one solution to the fabrication of ordered aggregates from components with sizes from micrometers to nanometers. These sizes fall awkwardly between those that can be manipulated by chemistry and those that can be manipulated using conventional manufacturing. It gives an opportunity for builing systems with new kinds of functionality in biology.

2.1. Organic Thin Films

The subject of organic thin films is quite an old field. About 200 years ago, Franklin observed the behavior of oil on the surface of water (*20*). This was followed by the preparation of monolayers at the air-water interface by Pockels (*21*). This was followed by works of Rayleigh (*22*), Hardy (*23*), Devaux (*24*) and others. As a mark of respect to Langmuir, the monolayers of amphiphilic molecules on the surface of water were named after him (*25*). The first study about the deposition of organic films on solid substrates was carried out by Blodgett with the deposition of carboxylic acids (*26*). A detailed study on a system of self assembled monolayers was carried out by Zisman by the adsorption of a surfactant molecule on clean metal surface (*27*). This work created limted interest at the time as its importance was not understood. In 1983, Allara and Nuzzo formed SAMs of alkyldisulphides on Au by depositing in dilute surfactant solutions (*28*). This important discovery led to a renewed interest in the field and since then many systems having different surfactants and substrates have been studied. In these systems, the particular case of alkanethiols on Au is the most widely studied and is considered to be a model for all related developments in the field (*29*).

Organic thin films exhibit optical, electrical, mechanical, optoelectronical and chemical properties which are not present in inorganic materials. Another reason for greater interest in organic thin films is because of the possibility of the

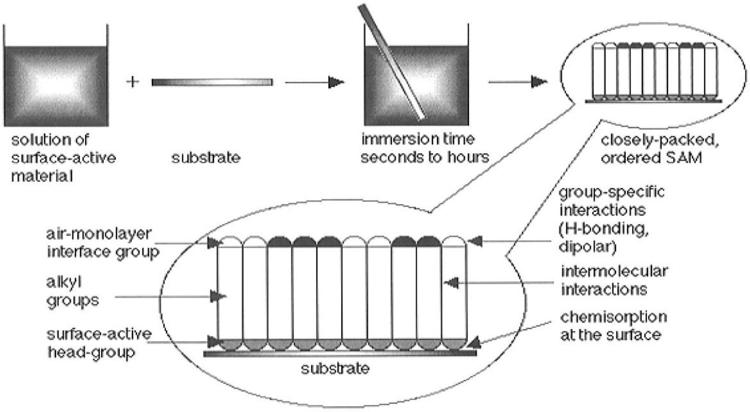
solution of
surface-active
material
+
substrate
immersion time
seconds to hours
closely-packed,
ordered SAM
group-specific
interactions
(H-bonding,
dipolar)
air-monolayer
interface group
alkyl
groups
intermolecular
interactions
surface-active
head-group
chemisorption
at the surface
substrate

Figure 1. Formation of Self Assembled Monolayers (SAMs) by the solution deposition technique. Chemical bond formed by the head group with the substrate and the intermolecular interactions of the molecule (29). Adapted from Ref (29). Copyright 1996 American Chemical Society.

tunability of the surface properties by chemically modifying only the terminal or the end functional group while leaving the rest of the molecule relatively unchanged. There are different methods of growing organic thin films. Langmuir films consist of amphiphilic molecules having an affinity to a liquid surface like water with a hydrophilic group attracted to the solution and the hydrophobic group sticking out of the solution (*30*). Langmuir films deposited on solid substrates are called as Langmuir-Blodgett films. Self Assembled Monolayers (SAMs) can be grown on top of the substrates by either solution depositions or by vapour deposition of the surfactant molecule. Other techniques for growing thin films are Organic Molecular Beam Epitaxy (OMBE) or Organic Molecular Beam Deposition(OMBD) which is similar to the ultrahigh vacuum evaporation techniques used for depositing inorganic films.

3. Self Assembled Monolayers (SAMs)

Self Assembled Monolayers are themselves nanostructures which form a component of nanoscience and nanotechnology. Self assembled monolayers (SAMs) can be defined as ordered molecular self assemblies that are formed spontaneously by the adsorption of a surfactant with a special affinity of its headgroup to the surfactant. Figure 1 shows the self assembly process for the solution deposition technique. In this method, the solution contains millimolar concentration of the surfactant molecule and the substrate is brought into contact by dipping it in the solution. After a specific period of time, we get a well ordered monolayer of SAMs having a good two dimensional symmetry. The surfactant molecules are made up of a surface - active headgroup which will react with the substrate by chemical reaction, a long alkyl chain which forms the “backbone” of the assembly and a terminal end group which determines the surface functionality and properties for the entire SAM.

The formation of monolayers of the surfactant molecules by spontaneous adsorption is the demonstration of the general phenomenon of self assembly. The study of SAMs gives us a basic idea about the structure - property relationship, self organization and interfacial phenomenon. We have the opportunity to tailor both the headgroup as well as the tail group. Beacause of this, SAMs are well suited to study competing intermolecular, molecular substrate and molecule solvent interactions like ordering, growth, wetting, adhesion, lubrication and corrosion (*29*).

The reason why SAMs are so attractive and are driving a lot of research can be summarized as: 1. The relative ease of preparation of SAMs, i.e. they do not require UltraHigh Vaccum (for ex. Molecular Beam Epitaxy [MBE]) and specialized equipment (for ex. Langmuir Blodgett Films); 2. Ability to tune the properties of the surface by modifying the structure; 3. Ability of SAMs to be used as building blocks in forming other complex structures. They are crtitical compents for stabilizing and functionalizing preformed nanometer scale objects such as thin films, nanowires, colloids, and other nanostructures; 4. Coupling of the external environment to the electronic (i.e. current-voltage responses, electrochemistry) and optical (local refractive index, surface plasmon frequency) properties of metallic structures; 5. They bridge the gap between molecular level nanostructures and macroscopic properties like wetting, adhesion and friction (*1*, *6*).

3.1. SAMs of Alkanethiolate on Au

The adsorption of alkanethiols on Au(111) is the most studied system for the formation of SAMs. Since the discovery by Allara and Nuzzo (*28*) regarding the formation of disulphides on gold, the area has been gaining a lot of attention and is the focus of an ever expanding body of work. Whitesides and Nuzzo are the pioneers in this field and have laid the foundation for the basic understanding of the self assembly process (*31*). Sulphur compounds have been found to have a special affinity to transistion metal surfaces (*13*). This is thought to be the case because of its ability to form multiple bonds with surface metal clusters (*32*). Among the several different groups that can bind to gold include n-alkyl sulphide (*33*), di n-alkyl disulphides (*28*), thiophenols (*34*), mercaptopyridines (*35*), mercaptoanilines (*36*), thiophenes (*37*), cysteines (*38*), xanthates (*39*), thio-carbaminates (*40*), thiocarbamates (*41*), thioureas (*42*), mercaptoimidazoles (*43*) and alkaneselenols (*44*). Love et al. have done an excellent review of all the different surfactant molecules that have been formed and studied on the gold surface (*1*). The system is used as model system for studying the self assembly process across a wide range of areas in nanoscience and nanotechnology. One of the main reasons for the success of using this system is that the gold surface is relatively chemically inert and an oxide surface is not readily formed on the surface which is often the case with many metals. Freshly formed gold surface does get contaminated easily with adventitious materials. Even under UHV conditions, Au surface shows carbon contamination (easily detected with XPS). However, SAMs are good at displacing this contamination and forming a well ordered surface. This phemonenon is fairly established in literature (*1*).

SAMs can make a conductive metal surface to be relatively insulating, yet the movement of electrons is made possible by the application of potentials when it is integrated in electrochemical cells. The fundamental studies carried out on thiol-Au system give us opportunites to develop many of the applied systems. The structures formed by the adsorption of n-alkanethiols are well ordered and crystalline. When a gold substrate is exposed to the thiol solution or to the vapor phase thiols, a bond is formed between the sulphur and the gold atoms. This bond has an energy of ~ 44 kcal/mol and it forms rapidly within seconds to minutes (*45*). After this, the hydrocarbon chains provide a significant amount of order to the assembly. A uniform coverage of the monolayer takes place laterally over the exposed substrate with a threshold concentration requirement of about $\sim 10^{15}$ molecules/cm^2. Studies have been carried out detailing the orientation of the monolayer on the surface and the effect of the headgroup and the tailgroups affecting their packing and the macroscopic interfacial properties. The physical structure and the chemical properties of the monolayers have been studied by many characterization techniques in order to determine the macroscopic characteristics of the film. These techniques have helped researchers form a comprehensive image of the arrangement of the monolayer. SAMs formed at standard conditions are affected by a complex mixture of thermodynamics and kinetics. Some of the defects that are formed in the monolayer lattice include domain boundaries of the SAM, vacancies within the crystalline lattice of the molecules and large grain boundaries (*46*). With the presence of a multicomponent system, having multiple thiol molecules, the adsorption process is found to be highly dynamic and thiol molecules exchange with other thiols in the solution or the vapour phase with a majority of these events happening at structural defect sites. This is followed by a second step of slower exchange which is presumed to occur within the domain itself (*13*). Substrate vacany islands, adsorbate vacancies in the molecular lattice and domain boundaries are critical sites in the monolayer that affect the post adsorption processing of the film (*47*). The body of knowledge which is formed on the model system of alkanethiol-gold, allows researchers to control the types, densities and distribution of defects of the final monolayer. The quality of the film coupled with various other advantages of self assembly, allows for further downstream processing like patterning, manipulation, post-adsorption processing, thermal annealing and backfilling of defects with new adsorbates.

3.2. Other Systems for Formation of SAMs

SAMs have been formed with a varierty of other surfactant molecules on many different kinds of substrates. Although the alkanethiol-gold system is very well studied, it may not be the right choice for every application. Depending on the application and the binding characteristics of the surfactant headgroup to the surface of the substrate, several prominent class of surfactants have found roles in self assembly. SAMs of organosilanes assembled on silicon dioxide surfaces have played an important role in the creation of patterned nanostructures (*29*). The silicon dioxide surface is hydrolyzed by moisture and is present in the form of hydroxyl groups. These groups then condense with the silane headgroup of the surfactant forming a thin layer of a polysiloxane. This layer gives greater stability compared to the thiol-Au system and provides a robust system. Organosilane SAMs on SiO_2 have been very useful in the photoresist industry. Alkytrichlorosilanes are the most studied group among the organosilanes and within this group, Octadecyltrichlorosilane (OTS) has been used extensively for SAM formation. OTS forms well ordered SAMs on hydroxylated surfaces. Other surfactant molecules that have been investigated include trimethoxysilanes (*48*), dimethyl chlorosilanes (*48*), organosilicon hydrides (*49*), phosphonic acids (*50*, *51*), phosphates (*52*), hydroxamic acid (*53*) and carboxylic acids (*54*). The formation and stability of SAMs on engineering metals such as steel, stainless steel, aluminum, copper, and brass has been discussed by Van Alsten (*55*). SAMs are finding applications on an increasingly diverse range of substrates like metals, alloys, polymers, etc. and self assembly is becoming more application oriented. Several excellent reviews have looked at the range of different headgroups and tailgroups for SAM formation along with a variety of substrates (*1*, *6*, *29*, *46*).

4. Applications of SAMs

4.1. Applications in Thin Metal Films

SAMs are an important tool for nanoscience and nanotechnology as they have been useful in studying several properties at the macroscopic level by influencing their chemical properties and structure. Interfacial phenomenon studied using SAMs are wetting (*56*, *57*), corrosion (*58*), adhesion (*59*, *60*), tribology (*61*, *62*), charge transfer through molecules (*63*, *64*), nucleation and growth of crystals on surfaces (*65*) and model surfaces for biochemistry and cell biology (*1*, *66*, *67*). SAMs can be used as etch resists where hydrophobic terminated SAMs can form a layer over metal films and protect it from wet chemical etchants (*68*). SAMs are used in electrochemistry where they form a barrier over the electrodes to protect them from the electroactive species of the solution (*69*). One method uses hydrophobic SAMs to block a redox species (from the electrolyte solution) from diffusing into the electrode itself (*70*). In a different approach mixed SAMs are coated on the surface of the electrode where one molecular component terminates with the electroactive species (for example Ferrocene). The immobilization of the redox species on the SAM minimizes the effect of diffusion in the current responses (*71*). SAMs have been widely used in the area of organic/molecular electronics. It is an evolving field and is getting a lot of attention. SAMs are used in electrical contacts wherein they would have molecules sandwiched between two metal contacts. In one type of junction, SAM coated on a metal film is used as one contact and a second contact is formed on top of the organic surface by either : (1) depositing a metal film by thermal evaporation or electrodeposition (*72*); (2) transferring a metal film by floatation or nanocontact printing (*73*); (3) positioning a conducting probe (STM (*74*), conducting AFM (*75*), crossing wire (*76*)) or (4) making a contact with a liquid metal contact (mercury) (*77*). There are excellent reviews available which have summarized in detail the role of SAMs in organic electronics for a variety of applications (*78*, *79*).

SAMs are also useful as substrates for crystallization. Parameters influencing the nucleation of crystalline solid and liquid phases can be tested by using a system of SAMs grown on metal substrates (*1*). SAMs are used for controlling the orientation of ionic crystals nucleated on surfaces. The influence of the structure of SAMs and the surface topography on liquid crystals are subjects of increasing interest. Crystals of many different types of materials have been grown on SAMs and they include proteins (*80*), enantiomerically pure amino acids (*81*), semiconductors (*82*), iron minerals (*83*), calcium phosphate (*84*) and carbonate minerals (*65*). Another application of SAMs is its use as a useful component in the alignment of liquid crystals. Orientation of the liquid crystals depends on the topography of the surface that is supporting the crystal. SAM- liquid crystal systems are useful in detecting binding of proteins, such as antibodies, to the ligands displayed by the SAM surfaces (*85*).

4.2. SAMs in Biology and Biochemistry

Biological membranes that define the boundaries of cells are naturally occurring examples of nanostructured organic materials. There are many different types of the membrane bound assemblies which make up the membrane. These assemblies control many different processes in living organisms (from bacteria to complex, multicelluar organisms) (*86*). SAMs in general serve as model systems for studying biological and biochemical processes. They mimic the biological surfaces and are nanostructures formed by self assembly just like them. SAMs serve as model biological surfaces and serve as protein resistant surfaces. Alkanethiol SAMs with tri-hexa(ethylene glycol) termination are used as standard SAMs to study biology and biochemistry (*87*). SAMs with L-lysine-D-alanine groups are found to mimic part of cell wall of Gram-positive bacteria recognized by the antibiotic vancomycin and they have enabled the development of bifunctional polymers capable of binding bacterial surfaces and recruiting antibodies to the surface (*88*). SAMs are important components for arrays of biomolecules. Some of these biomolecules are DNA (*89*), proteins (*90*), carbohydrates (*91*) and antibodies (*92*, *93*). Figure 2 shows immobilization of the protein streptavidin on mixed alkanethiolate SAMs. Research is also active for the use of SAMs in cell biology. SAMs provide a method for generating model organic surfaces with ligands to which cells can attach or with which they can interact. One of the examples for a cell-surface interaction is the mechanism of immobilization of cells on surfaces. This has been studied using SAMs that present peptide sequences that bind to transmembrane receptors (*94*).

4.3. SAMS in Nanostructures

Electrodeposited rods are very useful and have a lot of applications. They are used as circuit components (*95*), have applications in biology (*96*) and used as barcode tags (*97*). An increasing number of these applications involve the rods being orthogonally functionalized on the various metallic sections using different kinds of SAMs (*98*). SAMs on metallic barcodes have been used to perform DNA hybridization essays and immuno-assays (*99*). The same kind of membranes available which are used to make the nanorods are also used in the manufacture of gold nanotubes using electroless deposition methods (*100*).

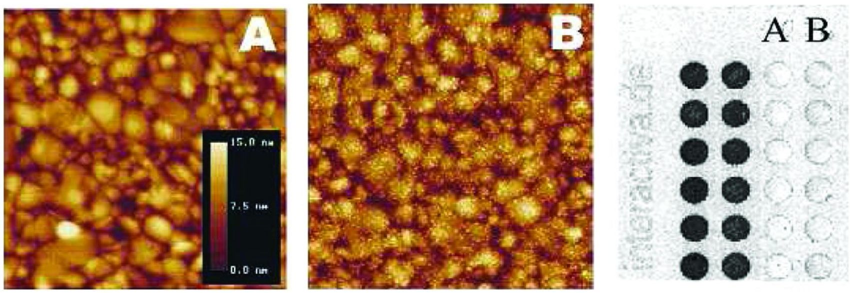

(i) (ii) (iii)

Figure 2. Immobilization of biomolecules : AFM images of before (i) and after (ii) immobilization of Streptavidin on mixed alkanethiolate SAMs on Au substrate. Streptavidin coated gold chips can be used as DNA biosensors. Fig(iii) shows section of a fluorescence scan of hybridization interactions between a Cy5-labeled 89-mer target DNA and a complementary immobilized 24-mer capturing probe(dark spots) on a streptavidin coated XNA on Gold biochip. Spot row A : negative control with an immobilized 24-mer mismatch oligonucleotide. Spot row B : Background signal showing unspecific interaction between target DNA and a streptavidin surface without a capturing probe24-mer oligonucleotide (89). Adapted from Ref (89). Copyright 2002 American Chemical Society.

These nanopores then serve as channels for the passive transport of small organic molecules across membranes (*101*). The length of the alkanethiols also affects the transport properties of the pore (*102*). Charged SAMs that are formed from cysteine (Cys) are useful for controlling the flow of ions through nanopores (*103*). Spatz and coworkers have used metallic nanostructures in the form of gold dots with varying lateral spacing functionalized with SAMs of a cyclic derivative of the Arg-Gly-Asp(cRGD) peptide (linked to mercaptopropionic acid) to study cell adhesion (*104*). Van Duyne and coworkers have shown that the shape of nanoparticles, the solvent in which the measurement is performed, the supporting surface, and the alkanethiols used to form the SAM on the surface all affect the frequency and the line shape of the Localized Surface Plasmon Resonance (LSPR) of these particles (*105*, *106*). E beam deposition of thin layers of metal onto arrays of colloidal spheres forms metallic half shells. SAMs are used to consolidate the shape and convert the hard shell surface into hydrophobic surfaces (*107*). Bao et al. have functionalized asymmetric gold spheres with SAMs of thiolated single stranded DNA (*108*). SAMs also play a crtical role in functionalizing nanoparticles and have applications in the fields of biocompatible surfaces on quantum dots, functionalized magnetic nanoparticles and nanoparticles with polyvalent display of ligands (*1*). Cadmium selenide nanoparticles coated with a less reactive and less toxic layer of zinc sulphide (*109*) can be functionalized with a SAM of thiolated DNA molecules or proteins either directly or via ligand exchange (*110*). In the field of magnetic nanoparticles, Xu et al. have reported using thiol chemistry to functionalize FePt nanoparticles which are useful for carrying out separations (*111*).

5. Multicomponent / Mixed (SAMs)

Once the mechanism for the formation of self assembled monolayers has been studied, the next step would be to look into the kind of mechanisms happening when two or more surfactant molecules are present in the system. The dynamics played between the competing molecules along with processes and conditions affecting the formation of the resulting SAM has been reviewed in this section. Patterning of SAMs involves placing molecules in a defined manner with specific spatial arrangements. Different SAMs are phase separated into domains once they are organized either by spontaneous assembly or if they are deliberately placed in a specific pattern.

5.1. Spontaneous Phase Separation

When two different SAMs are mixed in a solution and exposed to the substrate, both species will adsorb onto the substrate at varying degrees. If these molecules have different molecular composition, they will aggregate into homogeneous domains to maximize self interactions through van der Waals bonding or hydrogen bonding. Factors affecting the competition for the available surface include relative solvation of the adsorbates by the solution, sticking probability of each molecule and the degree of interaction between the adsorbates. Systems that have been studied in detail include coadsorption of short chain and long chain alkanethiols (*112*), molecules that are different in both chain length and functional group (ex. 3-mercaptopropanol and n-tetradecanethiol) (*113*), molecules of similar length but differing terminal groups (ex. N-hexadecanethiol and its methyl ester analog (*114*), n-undecanethiol and 11-mercaptoundecanoic acid) (*115*) and molecules of similar length but differing, buried functional groups (ex. 3-mercapto-N-nonylpropionamide and n-decanethiol) (*47*). However it is found that if the surfactants are relatively similar to each other, then there is difficulty in phase separation and that even it might not been possible (*47*). The likelihood of exchange is decreased due to similar energies of solvation. Whitesides et al. have concluded that ratio of adsorbates in solution does not mirror that of the surface bound adsorbate composition (*116–118*). When the terminal groups of two surfactants are vastly different in polarity, homogenous phase separation has been observed. STM data have concluded that molecules which are vastly different in their chain length along with end group functionality, will also phase separate (*119*). Phase separation has also been reported for molecules having different functional groups buried near the film metal interace. An example of this is a mixture of n-alkanethiolate and an adsorbate containing an amide group buried near the sulfur headgroup (*120*). Figure 3 shows a typical STM image of mixed SAMs on a graphite substrate.

5.2. Post Adsorption Phase Separation

It is possible to direct the assembly and consequent separation of adsorbates by thermally processing the homogeneous, single component SAMs followed by exposure to a second molecule which will eventually form binary component

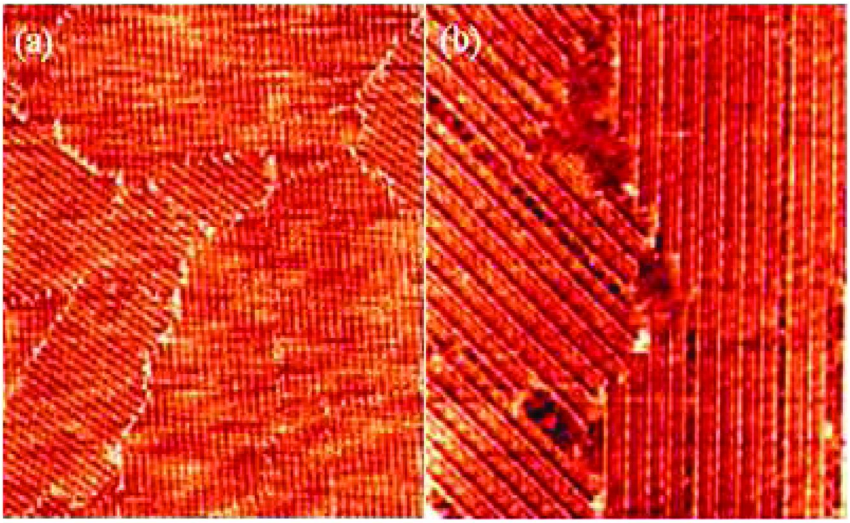

Figure 3. Typical STM images of mixed ordered monolayer of Tetrathiafulvalene (TTF) and n-$C_{14}H_{30}$ molecules on highly oriented pyrolytic graphite (HOPG) substrate at various scales a) 300 x 300 nm^2 and b) 120 x 120 nm^2 (121). Adapted from Ref (121) Copyright 2010 American Chemical Society

SAMs (*47*). Domains of adsorbate are found to coalesce with a decrease in the number of vacancy islands by heating the SAM in ethanol.

5.3. Host-Guest Self Assembled Monolayers

This method is useful in better understanding of the intermolecular dynamics of the adsorbates on surfaces, mechanisms of adsorption and exchange of adsorbates. Molecules are placed on a surface having low fractional surface coverage within a pre-existing matrix of a SAM. Incoming (guest) molecules will insert into a (host) SAM at its local defect sites (*46*). When defect density of SAM is high, molecules will insert at higher fractional surface coverage (*122*). If guest adsorbates are placed into the SAM and then the SAM is backfilled with another adsorbate from the gas phase, then the fractional coverage decreases (*123*).

5.4. Electrochemical Modification of Adsorbates

Electrochemistry can be used to manipulate the adsorbates themselves by electrolytically cleaving the Au-SR bond at the interface, resulting in a free thiolate and Au^o (*124*). Thiols are displaced from metal electrodes by applying reductive potentials and also it is possible to remove them from surfaces using oxidative potentials (*124*, *125*). It can also be used for phase separation of binary component SAMs (*126*). There are several applications of this method. It is used in creating ultra-sensitive, sequence specific detectors of nucleic acid hybridization (*127*), and fabricating patterned arrays of enzymes (*128*). Patterned arrays of enzymes have been made by reductively desorbing particular segments of alkanethiolate SAMs with scanning electrochemical microscope (SECM). Reductive desorption in predetermined areas by the SECM tip leads to the formation of a bare gold surface.

6. Methods for SAM Characterization

While it is not possible to mention all the different types of techniques used for SAMs, a representative list is shown for the major types of techniques. Several other reviews are available where the different types can be looked into (*129–131*). Microscopy based techniques like Scanning Tunneling Microscope (STM) (*132*) and Atomic Force Microscope (AFM) (*130*) are used to obtain a direct image of the surface including minute surface defects and for distinguishing between multicomponent systems. Low Energy Electron Diffraction (LEED) (*131*), Grazing Incidence X-Ray Diffraction (GIXD) (*133*) and low energy atom diffraction (LEAD) (*134*) have been used for diffraction from 2D structure of SAMs. X-ray reflectivity (*135*) provides information on the electron density profile along the surface normal viz. surface roughness, film thickness and electron densities. The growth and structure can also be studied using spectroscopic techniques such as Infrared Spectroscopies (IR) (*129*), Second harmonic generation (SHG) (*136*), Sum frequency generation(SFG) (*137*), Surface enhanced Raman Scattering (SERS) (*129*), High resolution electron energy loss spectroscopy (HREELS) (*131*), Near Edge X-ray Absorption fine structure spectroscopy (NEXAFS) (*138*), and X-ray photoelectron spectroscopy(XPS) (*129*). IR employs transition dipoles associated with the vibtrational modes to determine the structure of the molecule. For ex. organization of the alkyl chain. In the case of XPS, deeper energy levels are exploited to determine the binding state of the headgroup (ex.S-Au) or simply the mass coverage. Figure 4 shows SAM characterized using a Scanning Tunneling Microscope (STM).

Contact Angle Measurements are used to determine the wetting behavior i.e. to determine the hydrophobicity or hydrophilicity (*129*). Various other techniques are used to determine the surface coverage or the thickness such as ellipsometry (*140*), surface plasmon spectroscopy (*141*), quartz crystal microbalance (*130*), metastable induced electron spectroscopy(MIES) (*142*), nuclear magnetic resonance (*130*), electron spin resonance (*143*), and x-ray standing waves (*144*). Along with these techniques, a lot of other techniques are being increasingly applied as more work is gradually carried out in this subject.

7. Patterning

Patterning process is critical in many areas of modern science and technology such as production of integrated circuits, information storage devices and display units. It is also an important step in the fabrication of microelectromechanical systems (MEMS), miniaturized sensors, microfluidic devices, biochips, photonic bandgap crystals, micro-optical components and diffractive optical components (*145*). The process of patterning is also known as lithography and it involves

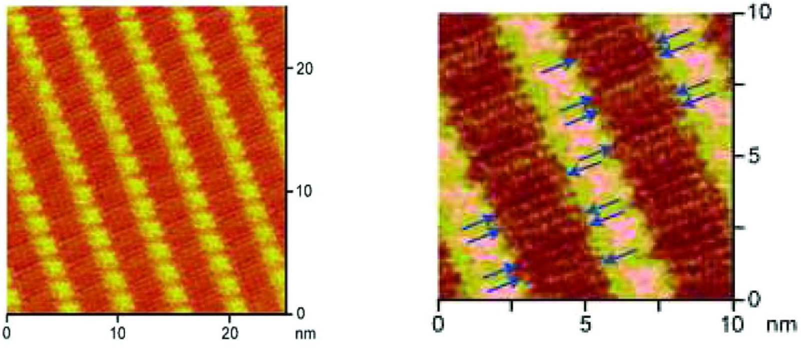

(a) (b)

Figure 4. SAM Characterization: (a)STM image of a C_{24}OPP SAM at the solid-liquid interface (25 nm x 25 nm). Tunneling conditions : I = 30 pA; V= -600mV. (b)High-magnification STM image of a C_{24}OPP SAM. The blue arrows indicate the alkyl chains. The contrast of the image is enhanced to see the alkyl chains (139). Adapted from Ref (139) Copyright 2008 American Chemical Society.

flow of information that typically begins with the design of a pattern in the form of a dataset and ends at a patterned array of features on the surface of a substrate. In a generalized manner, a lithographic process is made up of the following key steps: 1. A predesigned set of patterns in the form of a master or a mask; 2. Means to mediate the transfer or replication of patterns; 3. A responsive material which is generally a functional material capable to be used as a resist for further steps and 4. Appropriate metrology tools. The number of transistors on a chip doubles every 18 months and with this trend, densities with about 1 billion transistors/cm^2 could be achieved in the foreseeable future (*146*). Similar trends of complexity and integration may also be found in other devices such as MEMS, sensors, microfluidic devices and biochips (*147*, *148*). As of today the patterning of most of the functional materials is achieved by using photolithography where the minimum feature size scales with the wavelength of light exposure. However there are many inherent energy and size limitations that accompany with this method and researchers are finding out new methods to overcome these limitations. With this in mind, there are many unconventional patterning techniques which can overcome these limitations as they do not solely rely on focused energetic beams. These techniques include soft lithography and scanning probe lithography (SPL) and they can be applied to a variety of different substrates including those which cannot be patterned using traditional techniques. These techniques are simple, can be used in a laboratory and do not require expensive equipment. These techniques are still under active research and are not available to be commercialized as of now. However, they can serve as a complementary tool for the existing technologies for patterning systems which cannot be patterned using traditional techniques, such as curved surfaces, biologically compatible environments and for the fabrication of chemical patterns (*5*, *149*, *150*).

7.1. Conventional Techniques of Patterning

7.1.1. Photolithography

Over the past decades photolithography has been the main method for semiconductor device fabrication due to its simplicity and high throughput. In this method, the photons transfer the geometric pattern from a photomask to a photosensitive film called as the photoresist. The solubility of the photoresist is altered on exposure to photons which leads to the patterning of the surface when portions of the resist are dissolved in a developer. If the photoresist has a positive tone, the regions exposed to light become soluble in the developer while the regions not exposed remain insoluble. In a negative tone, the process is reversed. Exposure is achieved via one of the 3 methods : contact, proximity or projection.

7.1.2. Electron Beam and Ion beam Lithography

Electron beam (*151*) and ion beam lithographies (*152*) are are maskless direct write techniques which employ the use of a focused electron beam or an ion beam respectively to etch the substrate as the beam is scanned across the surface. These methods provide a route which is resource intensive but definitely provides an effective means of achieving features with low resolutions in the order of a few nanometers. Ion beam lithography is different than other conventional lithographic techniques because it allows for deposition of material and thus gives the ability to repair substrates such as masks or interconnects (*153*, *154*). However, both electron beam and ion beam lithographies are slow, taking hours to write one pattern which can be written in minutes using photolithography. Hence these methods are currently not suited for large scale manufacturing and their prime purpose is fabrication of photomasks for research applications (*155*).

7.1.3. X-ray and Extreme Ultraviolet Lithography

X-Ray Lithography (XRL) is a technique which is quite similar to photolithography as it uses short wavelengths for light exposure (0.4-100nm), targeting sub 10nm resolution patterning (*156*). When XRL was first introduced, although it was technically superior it was found to be a difficult technique and it failed in providing circuits and surfaces more economically than photolithography (*157*). A variant of this technique called as soft XRL made mask fabrication more convenient by using reduction optics and thick masks. This technique operates at 13 nm wavelength and it was later renamed to extreme ultraviolet lithography (EUVL) (*158*). The limitations with these technique are the intensity of the source at 13 nm and short noise limitations (*159*). Resists with higher sensitivity are expected to improve the performance for this technique.

The techniques mentioned here are basic and the ones which have been reported extensively. However there are many other techniques and the list of these techniques is growing every year as researchers are renewing their focus on these areas. It is not possible to summarize all the techniques which are used for patterning in general and is beyond the scope of this review. However there are other reviews available which have summed up a majority of these techniques (*2*, *148*, *160–162*).

8. Patterning of Self Assembled Monolayers (SAMs)

SAMs are prepared both in single and multiple components in predetermined spatial distributitions or simply put, SAMs are patterned. The patterning process can be carried out in different ways viz. 1. Selective removal of particular adsorbates, 2. Selective placement of particular adsorbates, 3. Selective reactions of adsorbates, 4. By the destruction of adsorbates by energetic beams, or 5. Delibrate removal with techniques like scanning probe microscopes. Once the adsorbates have been placed on the surface in a predetermined fashion, the remaining surface which is bare or exposed can be "backfilled" using a new adsorbate, giving us a multi- functional surface. SAM patterning is important in order to understand the fundamental organizations and interactions of mixed monolayers on surfaces. Functional nanostructures can be created completely or in part from the "bottom up" using SAMs. The development of patterned SAMs is critical as they can be used as sacrificial structures (a means to an end), as well as final structures or supports as the patterning of adsorbates gives a predisposed reactivity to the surface (*46*). Patterned SAMs are also important in nanotechnology applications. One of the requirements for the development of nanoelectronic devices is the ability to position and pattern molecular components selectively on surfaces which provide regularity to the overall structure.

8.1. Soft Lithography

Although a lot of improvements have been observed in the traditional patterning techniques of photolithography, electron beam lithography,etc., we face certain challenges which cannot be addressed using these traditional approaches. Some of the challenges are adapting these systems to emerging applications and areas of research that require unusual systems and materials (ex. Bioelectronics, plastic electronics, etc.), structures with nanometer dimensions (i.e. below 50-100 nm), large patterned areas (areas larger than few square centimeters) or non planar (rough or curved surfaces). These can be addressed using soft lithography (*163*). Soft Lithography describes how materials such as flexible, elastomeric polymers are used as the basic means of transferring and fabricating structures on various substrates. The chemical systems or nanostructures that are created by using soft lithography are not damaged by the tools that are used to create them and hence can be easily integrated into systems where other techniques might prove to be damaging (ex.electron beam lithography). These techniques have achieved widespread applications in academic and industrial laboratories throughout the world for applications ranging from photonics and biotechnology to microfluidics and electronics. There is a lot of literature available for the description of the various soft lithographic techniques that are available such as Microcontact Printing (μCP), micromolding in capillaries (MIMIC), solvent assisted micromolding (SAMIM), replica molding, microtransfer molding, etc. (*161*). In this review, we will focus on the techniques which can be applied for patterning of SAMs.

8.1.1. Microcontact Printing

This is a technique for patterning of SAMs on a substrate which is analogous to printing ink with a rubber stamp. Figure 5 shows a schematic summary of the printing process. This method is quite popular because of the ease of fabricating printing tools, relatively high spatial resolution of the features that are produced and a large printing capacity (*46*). In the first step of the process, a flexible, elastic, polymeric stamp is created from relief patterns and typically the elastomer that is used is Polydimethylsiloxane (PDMS). This stamp is then dipped in a solution of "Ink", which is typically the surfactant SAM solution. Once the stamp has been inked and dried, the stamp is brought into contact with the substrate to be patterned (ex. Au). The stamp is briefly pressed against the substrate and the SAM molecules transfer from the polymer surface to the substrate where they self assemble into patterns predetermined by the relief patterns of the stamp (*161*).

After the formation of the monolayers of SAM, the quality and fidelity of the features of the pattern vary with several parameters like stamp deformation, adsorbate concentration, stamping time and applied "backpressure" (*165*). Taking into account the resolution of μCP, which is limited to the dimensions and the structural rigidity of the elastomeric stamp, simple sub-50 micron resolution has been achieved by using specific inks and stamp geometries (*166*). Microcontact printing using the alkanethiol-gold system has been extensively studied and the various modifications to this basic system are widely reported. The mechanisms for the mass transport of the thiols during the process include the following steps: (1) diffusion from the bulk of the stamp to the interface between the stamp and the surface of the gold contacted by the stamp; (2) diffusion away from the edges of the stamp and across the gold surface and (3) vapor transport through the gas phase. The relative contributions of each of these effects on the overall mechanism of pattern formation is not clearly understood (*165*). The composition and mass coverage of the SAMs formed by μCP have been studied by contact angle goniometry, STM, AFM, XPS, RAIRS, ellipsomtery, electrochemistry, time of flight secondary ion mass spectroscopy (TOF-SIMS), GIXD, NEXAFS and Sum Frequency Generation (SFG) spectroscopy (*1*). The studies conducted using the above experimental techniques show that the SAMs formed by microcontact printing are usually a complex mixture of phases and can reach a state of organization that is spectroscopically indistinguishable from the SAMs formed from adsorption from solution.

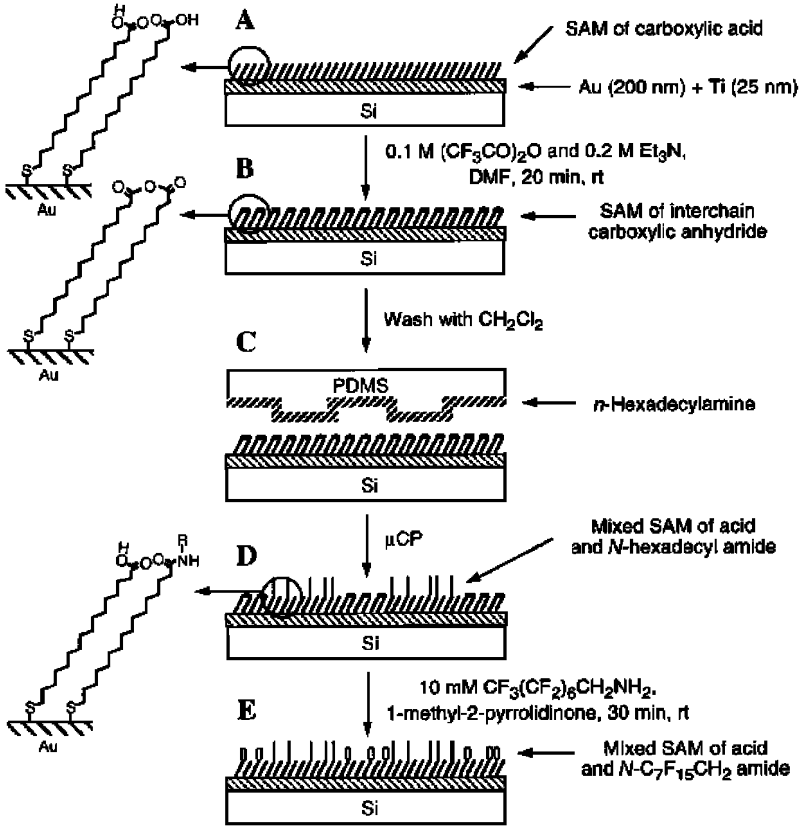
A
SAM of carboxylic acid
Au (200 nm) + Ti (25 nm)
Si
Au
0.1 M $(CF_3CO)_2O$ and 0.2 M Et_3N, DMF, 20 min, rt
B
SAM of interchain carboxylic anhydride
Si
Au
Wash with CH_2Cl_2
C
PDMS
n-Hexadecylamine
Si
µCP
D
Mixed SAM of acid and N-hexadecyl amide
Si
Au
10 mM $CF_3(CF_2)_6CH_2NH_2$, 1-methyl-2-pyrrolidinone, 30 min, rt
E
Mixed SAM of acid and N-$C_7F_{15}CH_2$ amide
Si

Figure 5. Schematic representation of the procedure for patterning a SAM that presents two different N-alkyl amides using µCP and chemical reaction. The diagram represents the composition of the SAM, but not the conformation of the groups in it (164). Adapted from Ref (164). Copyright 1998 American Chemical Society

8.1.2. Nanotransfer Printing

The process of nanotransfer printing (nTP) is an improvement over the existing system of microcontact printing by involving the patterning of thin solid films. Figure 6 gives a schematic representation of the process along with a SEM image of a pattern generated. In this method, metal features are printed on top of the SAM functionalized substrate, where the role of the SAM is that of an adhesion layer between the substrate and the patterned metal film. Nanotransfer printing has been carried out for a variety of materials for substrates and stamps and it has been found that a well defined chemistry is required for building up complex patterned features. The edge resolution obtained using this process for the patterned features is between 5 and 15 nm, which is comparable to the edge resolution of the PDMS stamp as well as the grain size of the evaporated metal.

The solid ink (patterned metal) has a greater affinity to the substrate than the stamp in order for large areas to be transferred (*167*, *168*).

8.1.3. Microfluidic Patterning

Microfluidic patterning is a simple, flexible and inexpensive method to create patterned SAMs on gold using microfluidics. With the use of a microfluidic cassette, alkanethiols are rapidly patterned on a gold surface to generate monolayers and mixed monolayers. The schematic representation of the process is as shown in Figure 7. By controlling the reaction parameters, permeation of alkanethiols in the surrounding PDMS microcassette can be used to create different patterned feature sizes and to generate well defined SAM surface gradients with a single microfluidic chip. By employing centrifugation for allowing spatial and temporal control of patterned cells in conjunction with PDMS surface masking, these substrates can be used for dynamic, cell migration assays and contiguous cocultures (*169*).

8.1.4. Area Selective Atomic Layer Deposition (ALD)

By combining the processes of microcontact printing and atomic layer deposition(ALD), 3D nanoscale structures can be created by using selective ALD. In this case the sequential self limiting steps of ALD enable precise control over film thickness, composition and uniformity. Jiang et al. (*170*), have shown a demonstration of this technique where, PDMS stamps with octadecyltrichlorosilane (OTS) monolayers on it were brought in contact with the substrate. After the creation of patterned SAMs, the remaining areas were deposited with the ALD films.

8.1.5. Microdisplacement Printing

In this technique the surface is first coated with a labile monolayer such as 1-adamantanethiolate (AD), which is susceptible to molecular exchange. The stamp is then dipped in an ink such as alkanethiol which can displace the labile SAM via competitive adsorption in the areas of the stamp (*172*). The labile SAM in this technique prevents lateral diffusion of patterned molecules. Also, backfilling is not required as the labile monolayer remains in uncontacted regions, preventing pattern degradation and dissolution. Due to hindered molecular diffusion, multiple sample steps can be employed to pattern proximal structures without pattern degradation between patterning steps (*165*, *173*).

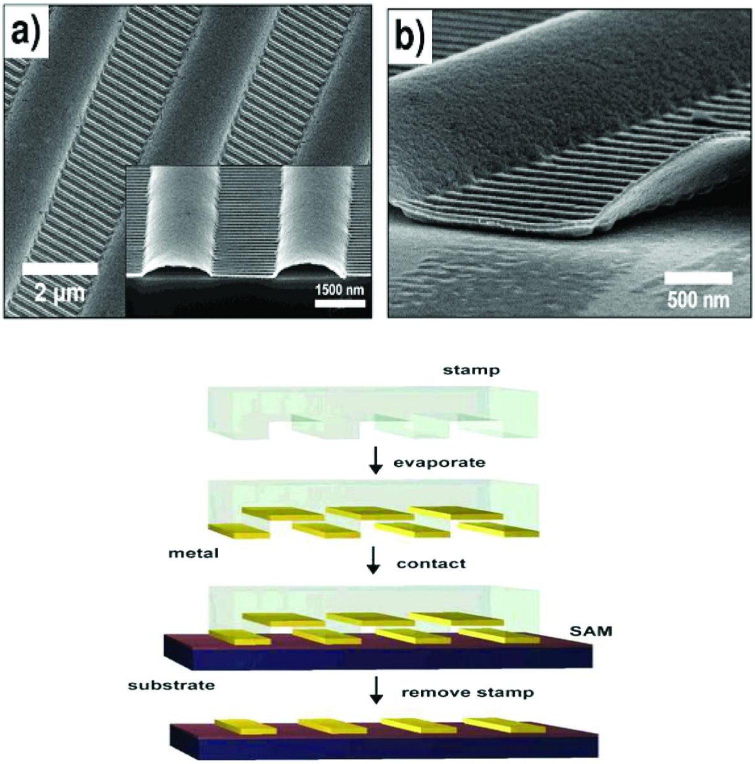

Figure 6. TOP a) SEM images of continuously curved Au (20nm thick) microchannels connected by arrays of orthogonally aligned nano channels. (a)Top and cross-sectional (inset) views; (b) angled view that illustrates the connection of the microchannels to the nano-channels. Bottom: Schematic of the nanotransfer printing process (167, 168). Adapted from Ref (167) and (168).Copyright 2004 and 2003 American Chemical Society.

8.1.6. Microcontact Insertion Printing

In this technique a PDMS stamp dipped in molecular ink is brought in contact with a surface coated with a SAM which is not easily displaced (*174*). Hence, the molecules on the stamp are deposited only in the areas which are not completely covered by the pre-existing SAM such as defect sites including domain boundaries and substrate vacancy islands. By adjusting the degree of molecular insertion and exchange between patterned molecules and the pre-existing SAM, the resulting molecular composition in the chemical pattern can be controlled (from isolated single molecules to bundles of molecules). The pre-existing monolayer presents a limitation on the lateral diffusion of the patterned molecules (*175*).

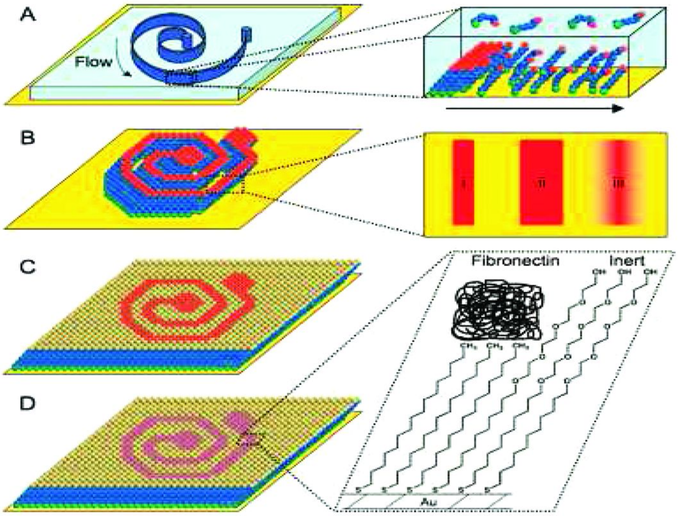

Figure 7. Patterning SAMs on gold via microfluidic lithography (μFL). (A) A PDMS microfluidic cassette is placed in direct contact with a bare gold substrate and a solution of alkanethiol is flowed through the channel. Inset: a representation of SAM formation in microfluidic channels.(B) After rinsing with ethanol and removal of the microfluidic cassette, a patterned SAM resulted. Inset: By adjusting alkanethiol concentration and solvent conditions, SAMs can be formed that (i) replicate PDMS features, (ii) have broadened dimensions, or (iii) create surface gradients. (C) The gold substrate was then backfilled with a solution of a second alkanethiol, resulting in a highly ordered SAM. (D) For cell attachment, hexadecanethiol is patterned within a background of tetra(ethylene glycol)-terminated undecanethiol. Fibronectin is then adsorbed only to the hydrophobic pattern. Inset: a molecular view of the cell-compatibile SAM after adsorption of fibronectin (171). Adapted from Ref (171) Copyright American Chemical Society.

8.1.7. Multilayer Transfer Printing

Instead of prepatterning a surface, Hammond et al. have employed layer by layer growth to self assemble multilayer films of molecular inks on PDMS stamps before stamping by a process of multilayer transfer printing (MTP) (*176*). Polyelectrolyte multilayers are assembled on PDMS by alternating adsorption of polyanion and polycation pairs. Once the required layer of multilayer thickness is achieved, the stamp is brought in contact with the substrate wherein the multilayers are transferred in the areas of contact. The charge on the substrate must be complementary to the charge on the topmost layer on PDMS for pattern transfer to occur.

8.2. SPM / AFM Based Patterning Techniques

8.2.1. Dip Pen Nanolithography

Dip pen Nanolithography (DPN) is one of the most widely used patterning techniques in which the materials on the tip are transferred to the surface while scanning either in the static mode or dynamic mode. It adapts the concept of writing with a pen to the nanoscale (*177*). Here, the AFM tip acts as the source of ink which is for ex. the SAM molecule. The mechanism of the tip - substrate molecular transport is still under debate and is likely to be affected by a number of parameters like composition of both the ink and the surface, nature of contact, distribution and mobility of the ink on the tip, water solubility of the ink and temperature and humidity at which the experiment is carried out. To improve the capacity and storage of ink on the tip some attempts are been made to integrate an ink storage and transfer system into the instrumentation. In line with the general trend seen in scanning probe techniques, DPN is also a serial technique which has a drawback of slow scanning speed while fabricating large patterns. With an aim of increasing the throughput and the accessible area, parallel probe cantilever arrays have been developed to realize multi-pen writing (*178*). Figure 8 shows a Lateral Force Microscopy (LFM) image of 16-Mercaptohexadecanoic acid (MHA) SAM patterned using DPN.

8.2.2. Nanografting

It is a technique developed by Liu et al. which is based on AFM and it combines adsorbate displacement with self assembly process (*180*). It can be used on the creation of both positive as well as the negative patterns (*181*). In this technique the AFM tip is dipped in an alkanethiol solution and is used to distrupt alkanethiol molecules of a different surfactant already formed on the gold surface. Spatial resolutions of the order of 1 nm have been achieved with various shapes and compositions (*180*). The major advantage of this technique is the low force (~2 nN) required to displace SAMs which minimizes probe wear. In this case the exchange prevents diffusion of patterned molecules at the same time adding new chemical functionality to the surface. This technique can be utilized in fabricating multi dimensional metallic structures, nanoscale metal junctions and connections (*182*). This technique can also be used to remove proteins tethered to SAM functionalized surfaces (*183*). Mirkin and coworkers have developed a "molecular eraser" based on this technique, in which pre-existing patterns can be selectively modified and / or removed with nanometer precision (*184*). By disrupting the SAM within pre-fabricated features while scanning with an ink-coated probe, features can be modified or erased, depending on the type of ink.

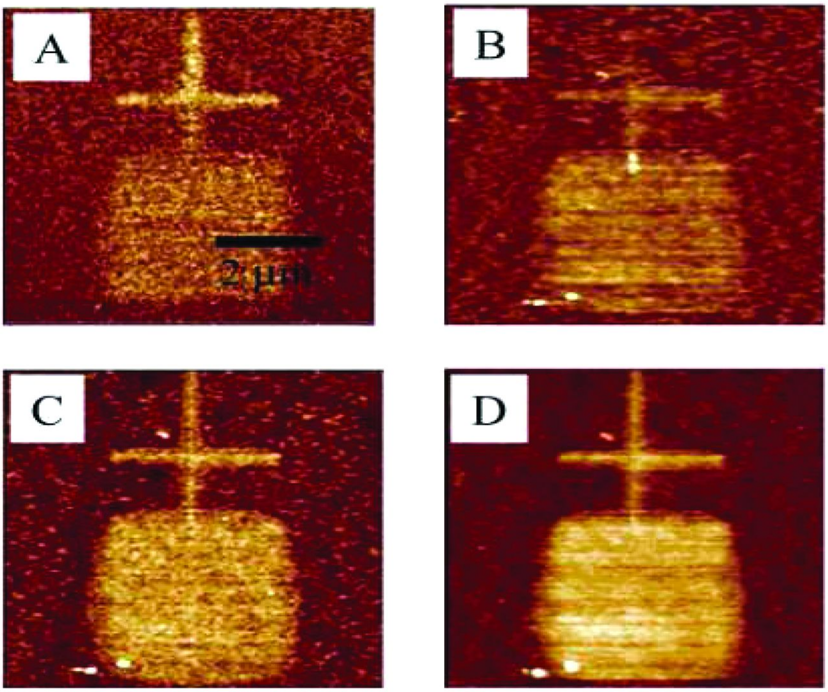

Figure 8. (A) Lateral force image of an MHA SAM on gold patterned by DPN. (B) Height image of biotin amine coupled to the MHA SAM after back filling the background in (A) with an EG3 SHSAM and activation of the terminal COOH groups of the MHA SAM. (C) Height image of the same surface after incubation of the biotin pattern in (B) with streptavidin.(D) Height image of the surface after incubation of the streptavidin pattern in (C) with biotinylated BSA (179). Adapted from Ref (179) Copyright 2002 American Chemical Society

8.2.3. Nanoshaving

The process of mechanical scratching, shaving or nanoshaving can be considered to be one of the simpler routes for carrying out patterning using an AFM. Here, the tip is employed to displace materials from the sample surface which creates pits or trenches surrounded by walls consisting of the initial substrate material. The tip has to be durable in order to withstand deformation and contamination after repeated scanning. Selected protions of the nanometer scaled SAM molecules are displaced with a carefully selected force (*185*). The desorbed molecules are discarded from the tip surface contact region as the solubility of the material in a polar solvent is high. The use of nanoshaving for selective mechanical bond breaking of a particular adsorbate has several requirements, the molecular headgroup of the SAM layer should be well anchored to the substrate and a rigid molecular backbone with at least one relatively weak bond where the AFM tip can shear off part of the molecule is needed (*178*).

8.2.4. Tapping Mode AFM Nanolithography of Alkanethiols

Tapping mode atomic force microscopy operates by the use of a vibrating cantilever near its vibrating frequency (~100 KHz) which comes in contact with the surface at the bottom of each oscillating cycle, offering a less damaging imaging method. Tapping mode AFM is commonly used as a method for imaging surfaces made up of soft materials, including proteins, DNA, polymers, etc. The technique has also been successfully demonstrated in manipulating nanoparticles, dissecting biomolecules, etching polymer thin layers and performing nanolithography, such as nano-oxidation of silicon surface and dip pen lithography (*178*). Ling et al. (*186*) have demonstrated the use of tapping mode AFM in patterning 1-octadecanethiol and 1-decanethiol using tapping mode AFM in solution and dip-pen techniques.

8.3. Other Techniques for Patterning of SAMs

8.3.1. SAM Patterning by Photolithography

Irradiation of SAMs of alkanethiolates on exposure to UV light radiation through a pattern of apertures leads to the photo-oxidation of SAMs (*187*, *188*). The oxidized materials can be removed by dissolving them into a polar solvent like water, ethanol, etc. In this case, the optical elements of the system determine the minimum resolution of the features produced. In the case of a projection microscope using a mercury lamp as a UV light source, the resolution limit is ~0.3 µm (*189*). Exposure times of 15-20 mins are required for power densities of ~ 5 W/cm^2 at the sample surface (*1*, *187*).

8.3.2. Electron - Beam Lithography

Electron beams have the ability to generate patterns on the substrates coated with SAMs (*190*). Low energy beams of electrons (10-100 eV) are capable of inducing a number of chemical changes in SAMs of thiolates. Some of the reactions that happen because of the electron beam are cleavage of bonds (C-S and C-H), formation of C=C, cross linking of adjacent molecules, fragmentation of molecules and conformational disorder (*191*). On exposure to low energy electrons, alkanethiolates become more disordered and hence are more susceptible to desorption (*192*).

8.3.3. X-Ray Lithography

X-rays provide us with an alternate form of high energy radiation in order to carry out patterning of SAMs (*193*). This technique is analogous to electron beam lithography in the sense that the nature of the chemical damage caused by these techniques is similar. The photoelectrons and secondary electrons that are generated because of the X-rays degrade the SAM patterns and to some extent the resolution of the SAM pattern (*194*). Grunze et. al. have done detailed studies for this method of pattern formation (*191*).

8.3.4. Atomic Beam Lithography

The neutral atoms of rare gases, when excited to metastable states (~8-20 eV above the ground state) have the ability to damage the SAMs formed from alkanethiolates (*195*). The energy released upon the collision of the metastable atom with the SAM and upon its return to the ground state is believed to be the reason for the ionization of the organic material in the SAM (*196*, *197*). It is also believed to be the reason for causing conformational disorder in the alkyl chain in the SAM (*198*). Another contribution to the damage of SAMs is provided by the generation of secondary electrons (*199*). The exposure times required are of the order of 15 min and feature size of about 50 nm are achievable.

8.3.5. Formation of Gradients

The different methods of forming chemical gradients on top of a surface using SAMs can be summarized as : 1. Competitive adsorption between two different thiols deposited on the substrate (*200*), 2. Formation of two different thiols from the opposite ends of the substrate supporting a polysaccharide matrix (*201*), 3. Electrochemical desorption of thiols from static or dynamic potential gradients (*202*), 4. Gray scale photolithography on photosensitive SAMs (*203*). The applications include research in studying fundamental properties of wetting and adhesion (*204*), research in cell biology related to cell adhesion (*205*), chemotaxies (*206*) and neuron growth (*207*).

8.3.6. Ink-Jet Printing

Ink-Jet printing is a commercial technique for depositing nanolitre volumes of organic dyes on paper or plastic. This technique can be adapted for depositing SAM molecules on top of the surface (*208*). Although this technique might have some limitations like disorder of the SAMs, the ability to pattern large areas sometimes might supercede the need for high quality SAMs (*209*).

8.3.7. Topographically Directed Assembly

The surface topography including minor features and surface defects will cause a significant level of disorder of the SAMs compared to the ones formed on flat surfaces (*210*). The width of the deformations are dependent on the cross sectional topography of the substrate. Thiolates in the disordered regions can be exchanged with other thiols and a SAM containing a second functional group can be formed.

8.3.8. Orthogonal Self Assembly

This method involves fabrication of substrates composed of two or more different materials having specific affinity towards one of the SAM molecules being deposited for patterning. Some of the systems that have been tried out include carboxylic acids on Al and thiols on gold (*211*), isonitriles on platinium and thiols on gold (*212*) and silanes on silicon oxide and thiols on gold (*213*).

8.3.9. Patterning with Scanning Tunneling Microscope (STM)

Scanning tunneling microscope has been used for creating patterns on SAMs on certain systems. Here, the energies used are low (~10 eV) which will result in low emission of secondary electrons. The energies of the tunneling electrons that are injected into the features are of sufficient energies to break the chemical bond. Lines having widths of 15 nm have been produced using STM (*214*). Gorman et al. have carried out studies on patterning SAMs using STM under a fluid media (*215*). Kleineberg et al. have carried out studies for the use of STM on a variety of systems such as alkanethiolates and arylthiolates on gold, and OTS on silicon dioxide under Ultra High Vacuum (UHV) conditions (*216*). The effect of various parameters like bias voltage, tunneling current, scan speed and orientation on the mechanism of patterning with STM were analyzed. The patterns were transferred to the substrate using wet chemical etching techniques. The limitation of the process is the slow speed of patterning and to overcome this parallel processing methods, like with for ex. having an array of tips, are been proposed. Some groups have used techniques like having a computer assisted design (CAD) software in combination with the scanning tunneling microscope, to enhance the efficiency of the rastering of the probe tips in a predetermined manner (*217*).

8.3.10. Nanoimprint Lithography

Nanoimprint Lithography (NIL) technique was invented by Chao et al. (*218*), and has turned out to be a very good alternative to optical lithography for applications in general. Here, the fabrication of nanostructures is done by embossing a resist coated substrate with a 3-D mold. Some of the types of nanoimprint embossing technologies are thermal embossing, laser assisted (LADI) and step and flash imprint lithography (SFIL) (*219–221*). One of the challenges in NIL is resist adhesion to the mold. Jung et al. (*222*) have successfully used organosilane SAMs to form a coating on the surface of the mold and have compared the effect of solution based and vapor based formation techniques. Falconnett et al. have combined NIL and SAMs to develop a novel method for the patterning of proteins with nanoscale resolution (*223*). Byeon et al. (*224*) have demonstrated the use of creating nano patterns using thiol SAM treated nickel template. Si is the conventional material used for fabrication of templates used in NIL and its properties were compared by using a Ni template in NIL. A hydrophobic SAM was formed on Au deposited on the Ni substrate. The disadvantage here is that the repeated contact between the mask and the substrate makes NIL more suscept to defects. However, it remains as a future contender for nanomanufacturing as patterning is not dependent on radiation and hence not limited by diffraction, interference and backscattering.

8.3.11. Block Copolymers

Block copolymers are a type of macromolecules which are made up of different covalently linked homopolymer blocks (*225*). Chemical guiding patterns can serve as a substrate for the guiding of the self assembly process involving block copolymers. Nealy et al. have used chemically patterned surfaces to direct the self assembly of the block copolymers into macroscopically ordered domains with nanoscale precision and substrate registration (*226*). In a typical example, Kim et al. have prepared a scheme of diblock copolymer epitaxial assembly on various patterned surfaces. First, a SAM is spin cast on a Si substrate and is then patterned using lithography. The chemical composition of the exposed areas is then modified using photon irradiation for SAMs. This is followed by removal of the resist which yields different functionalities. Diblock copolymers are then spin cast on the chemically patterend surface, which then self assemble into different domains that register to substrate patterns (*227*).

8.3.12. Molecular Ruler Method

The molecular ruler method can be considered to be a hybrid technique which combines the technique of conventional photolithography and self assembly to create nanometer scale features in a parallel manner (*228*). Multilayered self assembled monoloayers are used to determine the gap between two pre fabricated lithographically defined patterns (*229*). The dimension of the resulting feature is controlled by using different length of the organic molecule/surfactant and by assembling the desired number of stacked layers. Kind et al. (*229*) have carried out studies on the molecular ruler method by using the alkanethiol on gold system. Initially a basic pattern having a Au structure is fabricated using lithography. This is then functionalized using alternating layers of α-ω mercaptoalkanoic acid bound by coordinated copper ions. A subsequent metal evaporation leads to precisely defined gaps. The position and thickness of the final structure is determined by the locations of the parent structures and the thickness of the surfactant taken. The robustness and stability of the molecular ruler method make it very compatible with other patterning techniques which can be utilized in the fabrication of complex structures (*230*).

8.3.13. Lithography Assisted Chemical Patterning

This is a technique which combines molecular self assembly and photolithography to generate multifunctional surfaces avoiding cross contamination and edge problems encountered in other chemical patterning techniques like mircocontact printing (*231*). Initially a SAM is coated on a substrate followed by coating of the SAM by a bi-resist layer composed of a lift-off resist (LOR) and photoresist (PR). By combining the solvability in ethanol and photolithography, the bilayer resist is patterned and is subsequently exposed to UV/Ozone for removing the unprotected areas. When this system is exposed to thiol solution, we get a chemically functionalized /patterned surface.

8.3.14. Electron Beam Chemical Nanolithography

Electron beam chemical nanolithography was first developed by Grunze et al. and it is a technique which uses a focused electron beam to induce chemical reactions with the terminal functionalities in the monolayer (*232*, *233*). Eck et al. have showed that the terminal functionalities in biphenyl monolayers are converted into amino groups when exposed to low energy electrons (50 eV) (*234*). Features that are smaller than 10 nm can be obtained using field electron scanning electron microscope (FESEM), as it eliminates the need of a photomask which is required in normal electron beam, due to its ability to tightly focus the higher electron energies. Patterning a molecular layer than a bulk material limits backscattering which helps in getting a ultrahigh resolution patterning. Many other SAM molecules have been used as a positive and negative tone electron beam resists to generate high resolution structures (*235–237*).

9. Laser Patterning of Self Assembled Monolayers

9.1. Direct Laser Patterning (DLP)

Vaidya et al. (*238*) had first mentioned about using lasers for patterning of SAMs. They has used a computerized laser ablation system to form patterns on SAMs by laser induced desorption of SAMs. The system used was that of alkanethiols of Oligo(ethylene glycol) terminated SAM on Au film which was deposited on a glass slide. However the studies carried out by them were at a very elementary level and left a gap in knowledge. Shadnam et al., had reported the first complete work for carrying out direct laser patterning on SAMs (*239*). The feasibility for carrying out laser patterning of monoalyers was studied for the first time. A laser beam is considered to be an excellent tool for carrying out precise localized heating of the substrate. It can result in activation or acceleration of endothermic chemical reactions (*240*). In this case, the approach of “direct patterning” eliminates the requirement of photolithography, directly or indirectly. The desired pattern is formed by the relative motion of the laser beam. The method is non contact and flexible viz. several terminal groups can be used at the same time. The technique can be applied to a wide variety of substrates and it has the potential to form complex patterns. Last minute changes to the design pattern can be introduced. It is a fast and simple procedure for SAM patterning. Ar ion laser at 488 nm was used to produce patterns of different wettabilities in the shape of a straight line with widths in the micrometer range. 1-hexadecanethiol monolayer was desorbed by laser irradiation from the gold substrate. Then the susbtrate was dipped in a solution containing 16-mercaptohexadecanoic acid which then self assembled on the surfaces which were available by irradiation. They also carried out thermodynamic and kinetic studies on the chemical reactions involved in the patterning process. Hartmann et al. carried out direct laser patterning process on SAMs of octadecylsiloxane formed on oxidized silicon (*241*). Their experiments also strongly support a photothermal excitation mechanism.

9.2. Chemically Specific Laser Patterning of SAMs

The process of localized heating which results in pattern formation by the ablation of both the solid substrate and SAM molecules is called as chemically non specific patterning. Figure 9 gives a schematic representation of the process. The selective breaking of the SAM molecule and the substrate by the application of heat is termed as chemically specific patterning. When talking in terms of laser usage, the process is termed chemically specific laser patterning. Iverson et al. (*242*) have used this technique in order to carry out patterning of alkanethiolate SAMs on gold by using a Ar ion laser at 488 nm. A common limitation for the application of laser beams for patterning of SAMs is avoiding surface damage caused by the thermal ablation of Au. The changes in the topographic patterns introduced by Au ablation affects the adsorption of biomolecules (*243*) and cells (*244*) which are not desirable in chemical patterning of SAMs. By tuning the parameters like laser power and irradiation time, specific SAM desorption was achieved without any gold ablation. SAM films were exposed to a focused laser using a confocal microscope. The use of a high numerical aperature (NA) lens tightly focused the beam, which allowed for the generation of patterns in the micrometer and sub micrometer length scale.

9.3. Surface Gradient Formation Using Self Assembled Monolayers

Meyyappan et al. (*245*), have demonstrated the formation of surface energy gradients using the direct laser patterning on alkanethiolates on gold system. First a 1-hexadecanethiol (HDT) SAM on Au was selectively desorbed using a focused laser beam. By continous variation in the incident laser intensity along a straight line, a desorption gradient was produced on the surface. This gradient was then backfilled using a second SAM of 16-mercaptohexadecanoic acid to introduce a wettability gradient. This method can be used to make different types of gradients using contrasting SAMs. Gradients of different shapes, lengths, sizes, steepnesses and widths can be produced using the technique. SIMS showed that the desorption of HDT was found to be most sensitive for incident laser intensity ranging between 29.15 and 6.5 kW/cm^2.

9.4. SAM Patterning Using Single Pulse Laser Interference Lithography (SPLIL)

Single pulse laser interference lithography is a new technique of parallel patterning of SAMs which is dependent on the fast thermal desorption of the SAM on the nanosecond scale. This leads to formation of sharp structures due

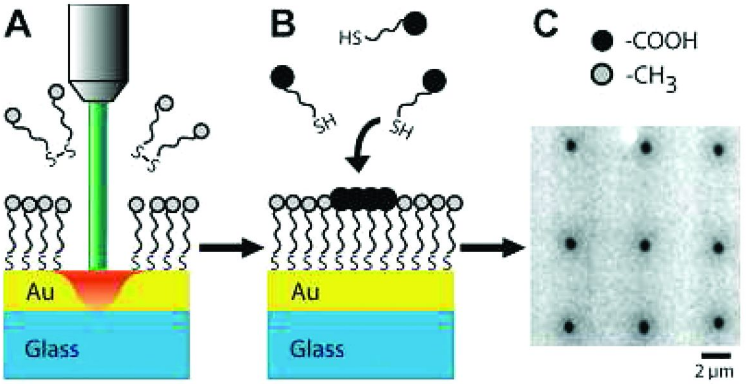

Figure 9. Alkanethiol SAM Laser Patterning: A. Irradiation with laser causes local heating of the Au substrate and leads to the desorption of the 1-undecanethiol (UDT) (gray moelcules). B. The bare Au areas are then exposed to 11-mercaptodecanoic(MDA) (black molecules). C. SEM image of the resultant substrate (242). Adapted from Ref (242) Copyright 2009 American Chemical Society.

to the short thermal desorption length. The removal of the SAM molecule by the laser exposure is then monitored using surface plasomn resonance (SPR) measurements. On comparison with direct laser patterning technique, this is a parallel method which allows for the formation of patterns in square millimeters at a single shot. Because of the nanosecond pulse length it is not necessary to stabilize the experiments against lateral drifts. Standard laser optics can be used in the patterning process due to the coherent laser beam in the UV-Vis region. The period can be varied over a long range by varying the angle of incidence of the laser beams. For creating more complicated structures, holographic techniques can also be applied. The patterning of the SAM in the presence of the UV-Vis light can take place either by a photothermal or a photochemical process (*246*). Either a chemical modification or thermal desorption of the thiol molecules or both could result from the interaction of the sample with the intense nanosecond pulse. Structures down to 800 nm to 300 nm width were fabricated using this technique.

10. Applications of Patterned SAMs

10.1. Patterned SAMs in Nanoscience

Research is being carried out in the area of quantum dots which has shown to have a great potential for solar power collection (*247*, *248*). For large scale utilization of solar power the efficiencies need to be increased. But arrangement of quantum dots into assemblies to get those levels of efficiencies are yet to be realised. Self assembled monolayers can be a possible solution for this. In thermoelectric applications, low dimensional materials are preferred as they allow for creation of efficient systems (*249*). Nanowires, nanotubes and quantum dots are used in microelectronic circuits which are important components in high performance transistors (*250*, *251*), single electron devices (*252*) and nonvolatile memory (*253*). Surface chemical patterning can achieve the controlled deposition of the above mentioned nanoparticles for device fabrication (*254–256*). Fast and accurate sensors have been in demand for a long time in industries like medical, defense and manufacturing. The basic function of a sensor is to transform changes in the chemical environment to a corresponding change in the detection system. In order to get the sensor signals such that they are specific to a particular analyte or a set of analytes, the surface chemistry should be tuned while keeping the bulk properties of the semiconductor intact. Multiplexed arrays of nanowire sensors can be functionalized with different sensing affinities using microspotting methods used in biomolecular arrays, or by Dip Pen Nanolithography for other higher density systems. Nanosensors have already been made for rapid detection of metal ions (*257*), gases (*258*), biomolecules (*259*), temperature (*260*, *261*) and mechanical strain (*262*).

10.2. Patterned SAMs in Biology and Biomedicine

Microcontact printing and electrochemistry are two patterning techniques that are well suited for patterning SAMs and are especially well suited for biological processes. Patterning reactive SAMs have applications in biological and biochemical studies. Microcontact printing has been used in the manufacture of microfluidic channels that deliver chemotactic agents reproducibly to neutrophil cells in order to understand their physical response to gradients of chemoattractants. It has also been used in patterning cells on substrates. The molecules can be printed in specific locations which results in adherence to predetermined regions followed by their selective release (*263*). Mrksich el al. have done detailed studies that control specific interactions between adherent cells and electroactive, self assembled monolayers substrates. They have combined soft lithography, organic synthesis and electrochemical techniques to present a detailed study of the adhesion and release of cells and biomolecules to self assembled systems. The interactions of cells and proteins with the surface can be promoted by attaching ligands to the SAM. With this purpose, Mrksich et al. have immobilized ligands at the surface of SAMs by Diels-Alder chemistry. Synthesis of SAMs has been carried out which can represent a tripeptide recognition factor (arginine-glycine-asparagine, RGD) which has been shown to regulate adhesion in between cells and extracellular matrices to which they attach (*264*). Also an interesting feature of this system is that it is reversible. Once the attachment of ligands, biomolecules, or cells has been done to the film, they can be removed by reduction using an applied potential from the gold electrode upon which the SAM has been adsorbed. Researchers at IBM-Zurich have shown that a protein solution can be directly inked to a PDMS stamp, and that a monolayer of protein transfers to the substrate beneath (*265*). In the case of delicate proteins, it might be possible to functionalize them with the use of biotin handles and then transfer them to an avidin coated substrate using self assembly route as compared to generic placement of molecules. Redox active enzymes have been immobilized on the surface of patterned SAMs with an aim to create functional SAMs. Example is immobilization of cytochrome *c* on a binary component SAM of

3-mercaptopropionic acid and n-hexadecanethiol (*266*). Arnold et al. have carried out immobilization of cytochrome *c* on binary component, phase separated SAMs, with mixtures of n-decanethiolate and 11-mercaptoundecanoic acid (*267*). Figure 10 shows a carbohydrate conjugate immobilized on a SAM using microcontact printing. Capadona et al. have examined the effects of fibronectin and cell adhesion on mixed SAMs involving methyl and OEG terminated alkanethiolates (*268*).

Proteins can be directly printed by functionalzing the surface of the substrate by using microcontact printing (*269*) or DPN (*270*). Surface arrays of immobilized biomolecules which selectively capture proteins, can be used in basic research to discover and define interactions that make up biological processes (*271*), for detection of disease specific markers for diagnostic purposes (*272*), or for purification. Surface arrays composing different proteins can be can be created without time consuming separation or purification processes. The biologically active regions of a nanoarray are decreasing in size. Hence, the number of proteins available to react on each spot decreases proportionally. The attachment of these proteins to the surface must be carefully controlled to ensure that active sites are presented to the surroundings and are not passivated by the surface or other attached structures. Patterned SAMs have also been used for "Lab on Chip" applications where microspotted arrays of surface immobilized oligonucleotides and peptides have produced significant data by allowing a large number of experiments to be conducted simultaneously. There is interest in expanding this principle to non biological chemical reactions. A majority of work done on this area involves enclosed microfluidic channels and other 3-dimensional structures (*274*, *275*).

The recent development of technologies to analyze numerous biomolecules and cells has led to a lot of development in the areas of microarrays for microelectromechanical systems fro biological applications (BioMEMS). BioMEMs involve the use of several different types of probes composed of DNA (*276*, *277*) proteins/peptides (*278*, *279*), or cells (*280*) that are usually arrayed on the chip. The technique for arraying probes on the substrate is one of the most important factors necessary for achieving high sensitivity and high reproducibility of the microarray analyses. SAMs of organosilane have attracted considerable attention as a base material for patterning the probes (*281*).

Other applications include a biologically inspired method to harvest water using patterns with extreme wetting contrast (*282*), and surface guided surface assembly of capsules for drug delivery (*283*). Guided self assembly shows great potential for integrating highly functional nano materials into well defined architectures that can be used for a variety of applications.

11. Conclusion

Self Assembled Monolayers (SAMs) are the most elementary form of nanometer scale organic thin film material. SAMs demonstrate that microscopic molecular level phenomenon and processes of design, synthesis and organization have a direct influence on the macroscopic properties of systems. SAMs have

In Biomaterials; Kulshrestha, A., et al.;
ACS Symposium Series; American Chemical Society: Washington, DC, 2010.

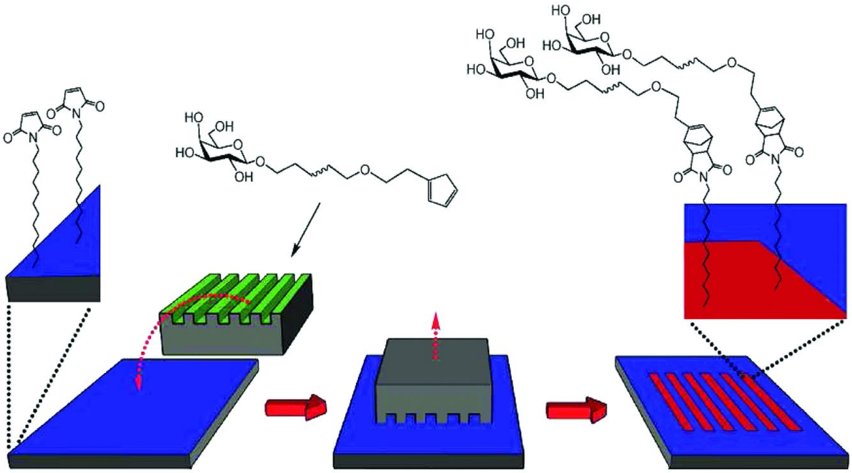

Figure 10. Schematic overview of the immobilization of a carbohydrate -cyclopentadiene conjugate on a maleimide terminated SAM by microcontact printing. The aim here is to form complex carbohydrate arrays of different types (273). Adapted from Ref (273) Copyright 2009 American Chemical Society.

the capacity to assemble on to surfaces of any size and geometry and they provide a highly flexible method to tailor the interfaces between nanometer scale structures and their environments with molecular precision. SAMs are fundamental components for many other forms of nanotechnology. SAMs are used as a basic foundation for the design and development of nanostructures on top of surfaces. Patterning SAMs involves increasing the complexity of the surface by providing multiple functionality, development of complex architectures and providing a specific spatial distribution for the various nanostructures including SAMs themselves. It allows for defining regions in order to provide further functionality. Patterned and multicomponent SAMs have been used in microfabrication, nanofabrication, lithographic selective etching in electronics industry, bionanotechnology, immobilization of biomolecules, etc. For these applications newer techniques are coming up very fast for creating patterns on SAMs while some of the existing techniques are being modified and combined with other techniques to form many hybrid techniques. This field is expanding at a rapid rate and due to its interdisciplinary nature is ripe for future investigation by researchers.

Acknowledgments

We thank the Center for Materials Research (CMR), Center for Biotechnology and Biomedical Sciences (CBBS), Department of Chemistry, Norfolk State University for contribution towards this work.

References

1. Love, J. C.; Estroff, L. A.; Kriebel, J. K.; Nuzzo, R. G.; Whitesides, G. M. *Chem. Rev.* **2005**, *105* (4), 1103–1170.
2. Xia, Y.; Rogers, J. A.; Paul, K. E.; Whitesides, G. M. *Chem. Rev.* **1999**, *99* (7), 1823–1848.
3. Alberts, B.; Johnson, A.; Lewis, J.; Raff, M.; Roberts, L.; Walter, P. *Molecular Biology of the Cell*; 4th ed.; Garland Science: London, 2002.
4. Weibel, D. B.; DiLuzio, W. R.; Whitesides, G. M. *Nat. Rev. Microbiol.* **2007**, *5* (3), 209–218.
5. Castner, D. G.; Ratner, B. D. *Surf. Sci.* **2002**, *500* (1−3), 28–60.
6. Schreiber, F. *Prog. Surf. Sci.* **2000**, *65* (5−8), 151–257.
7. Creigton, T. E. *Proteins: Structures and Molecular Properties*; Freeman: New York, 1983.
8. Sanger, W. *Principles of Nucleic Acid Structures*; Springer-Verlag: New York, 1986.
9. Ringsdorf, H.; Schlarb, B.; Venzmer, J. *Angew. Chem., Int. Ed. Engl.* **1988** (27), 113–158.
10. Whitesides, G. M.; Mathias, J. P.; Seto, C. T. *Science* **1991**, *254* (5036), 1312–1319.
11. Whitesides, G. M. *Sci. Am.* **1995**, *273* (3), 146.
12. Isaacs, L.; Chin, D. N.; Bowden, N.; Xia, Y.; Whitesides, G. M. *Perspectives in Supermolecular Chemistry*; John & Wiley: New York, 1999; p 1−46.
13. Dubois, L. H.; Nuzzo, R. G. *Annu. Rev. Phys. Chem.* **1992**, *43* (1), 437–463.
14. Emmanuel, D.; Heinz, S.; Bruno, M.; Hans, B. *Adv. Mater.* **1997**, *9* (9), 741–746.
15. Lasic, D. D. *Angew. Chem., Int. Ed. Engl.* **1994**, *33*, 1685–1698.
16. Bates, F. S. *Science* **1991**, *251* (4996), 898–905.
17. Samson, A. J.; Chen, X. L. *Science* **1999**, *283* (5400), 372–375.
18. Douglas, K.; Clark, N. A.; Rothschild, K. J. *Appl. Phys. Lett.* **1990**, *56* (7), 692–694.
19. Pileni, M. P. *Langmuir* **1997**, *13* (13), 3266–3276.
20. Franklin, B. *Philos. Trans. R. Soc., London* **1774**, *64*, 445.
21. Pockels, A. *Nature* **1891**, *43*, 437.
22. Rayleigh, L. *Philos. Mag.* **1899**, *48*, 321.
23. Hardy, W. B. *Proc. R. Soc. London, Ser. A* **1912**, *86*, 610.
24. Devaux, H. *Smithson. Inst., Annu. Rep.* **1913**, 261.
25. Langmuir, I. *J. Am. Chem. Soc.* **1917**, *39*, 1848.
26. Blodgett, K. *J. Am. Chem. Soc.* **1935**, *57*, 1007.
27. Bigelow, W. C.; Pickett, D. L.; Zisman, W. A. *J. Colloid Interface Sci.* **1946**, *1*, 513.
28. Nuzzo, R. G.; Allara, D. L. *J. Am. Chem. Soc.* **1983**, *105* (13), 4481–4483.
29. Ulman, A. *Chem. Rev.* **1996**, *96* (4), 1533–1554.
30. Gaines, G. L., Jr. *Insoluble Monolayers at Liquid - Gas Interfaces*; Interscience: NewYork, 1966.
31. Bain, C. D.; Troughton, E. B.; Tao, Y. T.; Evall, J.; Whitesides, G. M.; Nuzzo, R. G. *J. Am. Chem. Soc.* **1989**, *111* (1), 321–335.

32. Sellers, H.; Ulman, A.; Shnidman, Y.; Eilers, J. E. *J. Am. Chem. Soc.* **1993**, *115*, 9389.
33. Troughton, E. B.; Bain, C. D.; Whitesides, G. M.; Allara, D. L.; Porter, M. D. *Langmuir* **1988**, *4*, 365.
34. Sabatani, E.; Cohen-Boulakia, J.; Bruening, M.; Rubinstein, I. *Langmuir* **1993**, *9*, 2974.
35. Bryant, M. A.; Joa, S. L.; Pemberton, J. E. *Langmuir* **1992**, *9*, 753.
36. Hill, W.; Wehling, B. *J. Phys. Chem.* **1993**, *97*, 9451.
37. Li, T. T. T.; Liu, H. Y.; Weaver, M. J. *J. Am. Chem. Soc.* **1984**, *106* (5), 1233–1239.
38. Cooper, J. M.; Greenough, K. R.; McNeil, C. J. *J. Electroanal. Chem.* **1993**, *347*, 267.
39. Ihs, A.; Uvdal, K.; Liedberg, B. *Langmuir* **1993**, *9*, 733.
40. Arndt, T.; Schupp, H.; Schepp, W. *Thin Solid Films* **1989**, *178*, 319.
41. Mielczarski, J. A.; Yoon, R. H. *Langmuir* **1991**, *7*, 101.
42. Edwards, T. R. G.; Cunnane, V. J.; Parsons, R.; Gani, D. *J. Chem. Soc., Chem .Commun.* **1989**, 1041–1043.
43. Arduengo, A. J.; Moran, J. R.; Rodriguez-Paradu, J.; Ward, M. D. *J. Am. Chem. Soc.* **1990**, *112*, 6153.
44. Samanat, M. G.; Broen, C. A.; Gordon, J. G. *Langmuir* **1992**, *8*, 1615.
45. Nuzzo, R. G.; Dubois, L. H.; Allara, D. L. *J. Am. Chem. Soc.* **1990**, *112* (2), 558–569.
46. Smith, R. K.; Lewis, P. A.; Weiss, P. S. *Prog. Surf. Sci.* **2004**, *75* (1−2), 1–68.
47. Bumm, L. A.; Arnold, J. J.; Charles, L. F.; Dunbar, T. D.; Allara, D. L.; Weiss, P. S. *J. Am. Chem. Soc.* **1999**, *121*, 8017.
48. Helmy, R.; Fadeev, A. Y. *Langmuir* **2002**, *18* (23), 8924–8928.
49. Fadeev, A. Y.; Helmy, R.; Marcinko, S. *Langmuir* **2002**, *18* (20), 7521–7529.
50. Gawalt, E. S.; Avaltroni, M. J.; Koch, N.; Schwartz, J. *Langmuir* **2001**, *17* (19), 5736–5738.
51. Raman, A.; Dubey, M.; Gouzman, I.; Gawalt, E. S. *Langmuir* **2006**, *22* (15), 6469–6472.
52. Hofer, R.; Textor, M.; Spencer, N. D. *Langmuir* **2001**, *17* (13), 4014–4020.
53. Folkers, J. P.; Gorman, C. B.; Laibinis, P. E.; Buchholz, S.; Whitesides, G. M.; Nuzzo, R. G. *Langmuir* **1995**, *11* (3), 813–824.
54. Raman, A.; Gawalt, E. S. *Langmuir* **2007**, *23* (5), 2284–2288.
55. VanAlsten, J. G. *Langmuir* **1999**, *15*, 7605.
56. Whitesides, G. M.; Laibinis, P. E. *Langmuir* **1990**, *6*, 87.
57. Nishi, N.; Hobara, D.; Yamamoto, M.; Kakiuchi, T. *J. Chem. Phys.* **2003**, *118*, 1904.
58. Burleigh, T. D.; Gu, Y.; Donahey, G.; Vida, M.; Waldeck, D. H. *Corrosion* **2001**, *57*, 1066.
59. Houston, J. E.; Kim, H. I. *Acc. Chem. Res.* **2002**, *35*, 547.
60. Petrenko, V. F.; Peng, S. *Can. J. Phys.* **2003**, *81*, 387.
61. Leggett, G. J. *Anal. Chim. Acta* **2003**, *479*, 17.
62. Ahn, H. S.; Cuong, P. D.; Park, S.; Kim, Y. W.; Lim, J. C. *Wear* **2003**, *255*, 819.

63. Adams, D. M.; Brus, L.; Chidsey, C. E. D.; Creager, S.; Creutz, C.; Kagan, C. R.; Kamat, P. V.; Lieberman, M.; Lindsay, S.; Marcus, R. A.; Metzger, R. M.; Michel-Beyerle, M. E.; Miller, J. R.; Newton, M. D.; Rolison, D. R.; Sankey, O.; Schanze, K. S.; Yardley, J.; Zhu, X. *J. Phys. Chem. B* **2003**, *107*, 6668.
64. Salomon, A.; Cahen, D.; Lindsay, S.; Tomfohr, J.; Engelkes, V. B.; Frisbie, C. D. *Adv. Mater.* **2003**, *15*, 1881.
65. Aizenberg, J. *J. Chem. Soc., Dalton Trans.* **2000**, 3963.
66. Ostuni, E.; Yan, L.; Whitesides, G. M. *Colloids Surf., B* **1999**, *15*, 3.
67. Mrksich, M. *Curr. Opin. Chem. Biol.* **2002**, *6*, 794.
68. Xia, Y.; Zhao, X.-M.; Whitesides, G. M. *Microelectron. Eng.* **1996**, *32*, 255.
69. Chidsey, C. E. D.; Murray, R. W. *Science (Washington, D.C.)* **1986**, *231*, 25.
70. Porter, M. D.; Bright, T. B.; Allara, D. L.; Chidsey, C. E. D. *J. Am. Chem. Soc.* **1987**, *109* (12), 3559–3568.
71. Chidsey, C. E. D. *Science (Washington, D.C.)* **1991**, *251*, 919.
72. Wang, W.; Lee, T.; Reed, M. A. *Phys. Rev. B: Condens. Matter* **2003**, *68*, 035416/1.
73. Vilan, A.; Cahen, D. *Adv. Funct. Mater.* **2002**, *12*, 795.
74. Dunbar, T. D.; Cygan, M. T.; Bumm, L. A.; McCarty, G. S.; Burgin, T. P.; Reinerth, W. A.; Jones, L.; Jackiw, J. J.; Tour, J. M.; Weiss, P. S.; Allara, D. L. *J. Phys. Chem. B* **2000**, *104* (20), 4880–4893.
75. Beebe, J. M.; Engelkes, V. B.; Miller, L. L.; Frisbie, C. D. *J. Am. Chem. Soc.* **2002**, *124*, 11268.
76. Kushmerick, J. G.; Pollack, S. K.; Yang, J. C.; Naciri, J.; Holt, D. B.; Ratner, M. A.; Shashidhar, R. *Ann. N.Y. Acad. Sci.* **2003**, *1006*, 277.
77. Chabinyc, M. L.; Holmlin, R. E.; Haag, R.; Chen, X.; Ismagilov, R. F.; Rampi, M. A.; Whitesides, G. M. *ACS Symp. Ser.* **2003**, *844*, 16.
78. Lee, T.; Wang, W.; Klemic, J. F.; Zhang, J. J.; Su, J.; Reed, M. A. *J. Phys. Chem. B* **2004**, *108*, 8742.
79. Salomon, A.; Cahen, D.; Lindsay, S.; Tomfohr, J.; Engelkes, V. B.; Frisbie, C. D. *Adv. Mater.* **2003**, *15*, 1881.
80. Pham, T.; Lai, D.; Ji, D.; Tuntiwechapikul, W.; Friedman, J. M.; Lee, T. R. *Colloids Surf., B* **2004**, *34*, 191.
81. Lee, A. Y.; Ulman, A.; Myerson, A. S. *Langmuir* **2002**, *18*, 5886.
82. Jiang, P.; Liu, Z.-F.; Cai, S.-M. *Langmuir* **2002**, *18*, 4495.
83. Nagtegaal, M.; Stroeve, P.; Tremel, W. *Thin Solid Films* **1998**, *571*, 327–329.
84. Tarasevich, B. J.; Chusuei, C. C.; Allara, D. L. *J. Phys. Chem. B* **2003**, *107*, 10367.
85. Espinoza, L. A. T.; Schumann, K. R.; Luk, Y. Y.; Israel, B. A.; Abbott, N. L. *Langmuir* **2004**, *20*, 2375.
86. Mammen, M.; Chio, S.-K.; Whitesides, G. M. *Angew. Chem., Int. Ed.* **1998**, *37*, 2755.
87. Pale-Grosdemange, C.; Simon, E. S.; Prime, K. L.; Whitesides, G. M. *J. Am. Chem. Soc.* **1991**, *113* (1), 12–20.
88. Metallo, S. J.; Kane, R. S.; Holmlin, R. E.; Whitesides, G. M. *J. Am. Chem. Soc.* **2003**, *125*, 4534.

89. Riepl, M.; Enander, K.; Liedberg, B.; Schaferling, M.; Kruschina, M.; Ortigao, F. *Langmuir* **2002**, *18* (18), 7016–7023.

90. Lee, Y.-S.; Mrksich, M. *Trends Biotechnol.* **2002**, *20*, S14.

91. Love, K. R.; Seeberger, P. H. *Angew. Chem., Int. Ed.* **2002**, *41*, 3583.

92. Herrwerth, S.; Rosendahl, T.; Feng, C.; Fick, J.; Eck, W.; Himmelhaus, M.; Dahint, R.; Grunze, M. *Langmuir* **2003**, *19*, 1880.

93. Huck, W. T. S.; Stroock, A. D.; Whitesides, G. M. *Angew. Chem., Int. Ed.* **2000**, *39* (6), 1058–1061.

94. Roberts, C.; Chen, C. S.; Mrksich, M.; Martichonok, V.; Ingber, D. E.; Whitesides, G. M. *J. Am. Chem. Soc.* **1998**, *120*, 6548.

95. Kovtyukhova, N. I.; Mallouk, T. E. *Chem. Eur. J.* **2002**, *8*, 4355.

96. Reich, D. H.; Tanase, M.; Hultgren, A.; Bauer, L. A.; Chen, C. S.; Meyer, G. J. *J. Appl. Phys.* **2003**, *93*, 7275.

97. Keating, C. D.; Natan, M. J. *Adv. Mater.* **2003**, *15*, 451.

98. Martin, B. R.; Dermody, D. J.; Reiss, B. D.; Fang, M. M.; Lyon, L. A.; Natan, M. J.; Mallouk, T. E. *Adv. Mater.* **1999**, *11*, 1021.

99. Nicewarner-Pena, S. R.; Freeman, R. G.; Reiss, B. D.; He, L.; Pena, D. J.; Walton, I. D.; Cromer, R.; Keating, C. D.; Natan, M. J. *Science (Washington, D.C.)* **2001**, *294*, 137.

100. Martin, C. R.; Kohli, P. *Nat. Rev. Drug Discovery* **2003**, *2*, 29.

101. Jirage, K. B.; Hulteen, J. C.; Martin, C. R. *Science (Washington, D.C.)* **1997**, *278*, 655.

102. Jirage, K. B.; Hulteen, J. C.; Martin, C. R. *Anal. Chem.* **1999**, *71*, 4913.

103. Kang, M. S.; Martin, C. R. *Langmuir* **2001**, *17*, 2753.

104. Arnold, M.; Cavalcanti-Adam, E. A.; Glass, R.; Blummel, J.; Eck, W.; Kantlehner, M.; Kessler, H.; Spatz, J. P. *ChemPhysChem* **2004**, *5*, 383.

105. Haynes, C. L.; VanDuyne, R. P. *J. Phys. Chem. B* **2001**, *105*, 5599.

106. Jensen, T. R.; Malinsky, M. D.; Haynes, C. L.; VanDuyne, R. P. *J. Phys. Chem. B* **2000**, *104*, 10549.

107. Love, J. C.; Gates, B. D.; Wolfe, D. B.; Paul, K. E.; Whitesides, G. M. *Nano Lett.* **2002**, *2*, 891.

108. Bao, Z.; Chen, L.; Weldon, M.; Chandross, E.; Cherniavskaya, O.; Dai, Y.; Tok, J. B. H. *Chem. Mater.* **2002**, *14*, 24.

109. Chan, W. C. W.; Maxwell, D. J.; Gao, X. H.; Bailey, R. E.; Han, M. Y.; Nie, S. M. *Curr. Opin. Biotechnol.* **2002**, *13*, 40.

110. Chan, W. C. W.; Nie, S. M. *Science (Washington, D.C.)* **1998**, *281*, 2016.

111. Gu, H.; Ho, P.-L.; Tsang, K. W. T.; Wang, L.; Xu, B. *J. Am. Chem. Soc.* **2003**, *125* (51), 15702–15703.

112. Folkers, J. P.; Laibinis, P. E.; Whitesides, G. M. *Langmuir* **1992**, *8*, 1330.

113. Hobara, D.; Kakiuchi, T. *Electrochem. Commun.* **2001**, *3*, 154.

114. Stranick, S. J.; Parikh, A. N.; Tao, Y. T.; Allara, D. L.; Weiss, P. S. *J. Phys. Chem.* **1994**, *98*, 7636.

115. Bain, C. D.; Whitesides, G. M. *Langmuir* **1989**, *5*, 1370.

116. Laibinis, P. E.; Fox, M. A.; Folkers, J. P.; Whitesides, G. M. *Langmuir* **1991**, *7*, 3167.

117. Laibinis, P. E.; Nuzzo, R. G.; Whitesides, G. M. *J. Phys. Chem.* **1992**, *96*, 5097.

118. Folkers, J. P.; Laibinis, P. E.; Whitesides, G. M. *J. Adhes. Sci. Technol.* **1992**, *6*, 1397.
119. Sawaguchi, T.; Sato, Y.; Mizutani, F. *J. Electroanal. Chem.* **2001**, *496*, 50.
120. Smith, R. K.; Reed, S. M.; Lewis, P. A.; Monnell, J. D.; Clegg, R. S.; Kelly, K. F.; Bumm, L. A.; Hutchison, J. E.; Weiss, P. S. *J. Phys. Chem. B* **2001**, *105* (6), 1119–1122.
121. Zhao, M.; Deng, K.; Jiang, P.; Xie, S.-S.; Fichou, D.; Jiang, C. *J. Phys. Chem. C* **2009**, *114* (3), 1646–1650.
122. Donhauser, Z. J.; Mantooth, B. A.; Kelly, K. F.; Bumm, L. A.; Monnell, J. D.; Stapleton, J. J.; Price, D. W., Jr.; Rawlett, A. M.; Allara, D. L.; Tour, J. M.; Weiss, P. S. *Science* **2001**, *292* (5525), 2303–2307.
123. Donhauser, Z. J.; Mantooth, B. A.; Pearl, T. P.; Kelly, K. F.; Nanayakkara, S. U.; Weiss, P. S. *Jpn. J. Appl. Phys.* **2002**, *41*, 4871–4877.
124. Widrig, C. A.; Chung, C.; Porter, M. D. *J. Electroanal. Chem.* **1991**, *310*, 335.
125. Mirsky, V. M. *Trends Anal. Chem.* **2002**, *21*, 439.
126. Munakata, H.; Kuwabata, S.; Ohko, Y.; Yoneyama, H. *J. Electroanal. Chem.* **2001**, *496*, 29.
127. Satjapipat, M.; Sanedrin, R.; Zhou, F. M. *Langmuir* **2001**, *17*, 7637.
128. Wilhelm, T.; Wittstock, G. *Electrochim. Acta* **2001**, *47*, 275.
129. Ulman, A. *An Introduction to Ultra thin Organic Films : From Langmuir-Blodgett to Self-Assembly*; Academic Press: Boston, 1991.
130. Ulman, A., Ed. *Self-assembled monolayers of thiols, Thin Films*; Academic Press: San Diego, 1998; Vol. 24.
131. Luth, H. *Surfaces and Interfaces of Solids*; Springer: Berlin, 1993.
132. Poirier, G. E. *Chem. Rev.* **1997**, *97*, 1117.
133. Feidenhans'l, R. *Surf. Sci. Rep.* **1989**, *10*, 105.
134. Scoles, G., Ed. *Atomic and Molecular Beam Methods Oxford*; Oxford University Press: Oxford, 1992; Vol. 1−2.
135. Tolan, M. *X-ray Scattering from Soft-Matter Thin Films, Springer Tracts in Modern Physics*; Springer: Heidelberg, 1999; Vol. 148.
136. Dannenberger, O.; Buck, M.; Grunze, M. *J. Phys. Chem. B* **1999**, *103*, 2202.
137. Yeganeh, M. S.; Dougal, S. M.; Polizzotti, R. S.; Rabinowitz, P. *Phys. Rev. Lett.* **1995**, *74*, 1811.
138. Stohr, J. *NEXAFS Spectroscopy*; Springer: New York, 1992.
139. Ikeda, T.; Asakawa, M.; Miyake, K.; Goto, M.; Shimizu, T. *Langmuir* **2008**, *24* (22), 12877–12882.
140. Wasserman, S. R.; Whitesides, G. M.; Tidswell, I. M.; Ocko, B. M.; Pershan, P. S.; Axe, J. D. *J. Am. Chem. Soc.* **1989**, *111* (15), 5852–5861.
141. Aust, E. F.; Sawodny, M.; Ito, S.; Knoll, W. *Scanning* **1994**, *16*, 533.
142. Heinz, B.; Morgner, H. *Surf. Sci.* **1997**, *372*, 100.
143. Risse, T.; Hill, T.; Beckendorf, M.; Katter, U. J.; Schlienz, H.; Hamann, H.; Freund, H. J. *Langmuir* **1996**, *12*, 5512.
144. Zegenhagen, J. *Surf. Sci. Rep.* **1993**, *18*, 199.
145. Madou, M. J. *Fundamentals of Microfabrication : The Science of Miniaturization*, 2nd ed.; CRC Press: Boca Raton, FL, 2001.

146. In The International Technology Roadmap For Semiconductors, Semiconductor Industry Association, San Jose, CA, 2003
147. M.Gad-El-Hak, E. *The MEMS Handbook*; CRC Press: Boca Raton, FL, 2001.
148. Geissler, M.; Xia, Y. *Adv. Mater.* **2004**, *16* (15), 1249–1269.
149. Chen, C. S.; Mrksich, M.; Huang, S.; Whitesides, G. M.; Ingber, D. E. *Biotechnol. Prog.* **1998**, *14*, 356–63.
150. Bernard, A.; Renault, J. P.; Michel, B.; Bosshard, H. R.; Delamarche, E. *Adv. Mater.* **2000**, *12*, 1067–70.
151. Nakayama, Y.; Okazaki, S.; Saitou, N.; Wakabayashi, H. *J. Vac. Sci. Technol., B* **1990**, *8*, 1836–40.
152. Ximen, H.; Defreez, R. K.; Orloff, J.; Elliott, R. A.; Evans, G. A.; Carlson, N. W.; Lurie, M.; Bour, D. P. *J. Vac. Sci. Technol., B* **1990**, *8*, 1361–5.
153. Kohlmannvonplaten, K. T.; Buchmann, L. M.; Petzold, H. C.; Brunger, W. H. *J. Vac. Sci. Technol., B* **1992**, *10*, 2690–4.
154. Hosono, K.; Nagamura, Y.; Kusunose, H.; Yoshioka, N.; Watakabe, Y.; Akasaka, Y. *Jpn. J. Appl. Phys., Part 1* **1992**, *31*, 4468–73.
155. Hahmann, P.; Bettin, L.; Boettcher, M.; Denker, U.; Elster, T.; Jahr, S.; Kirschstein, U. C.; Kliem, K. H.; Schnabel, B. *Microelectron. Eng.* **2007**, *84*, 774–8.
156. Khan, M.; Han, G.; Tsvid, G.; Kitayama, T.; Maldonado, J.; Cerrina, F. *J. Vac. Sci. Technol., B* **2001**, *19*, 2423–7.
157. Warlaumont, J. *J. Vac. Sci. Technol., B* **1989**, *7*, 1634–41.
158. Wurm, S.; Jeon, C.; Lercel, M. J. *Proc. SPIE* **2007**, *6517*, 651705.
159. Anderson, C. N.; Naulleau, P. P. *J. Vac. Sci. Technol., B* **2009**, *27*, 665–70.
160. Xia, Y.; Tien, J.; Qin, D.; Whitesides, G. M. *Langmuir* **1996**, *12* (16), 4033–4038.
161. Xia, Y.; Whitesides, G. M. *Angew. Chem., Int. Ed.* **1998**, *37*, 550–575.
162. Menard, E.; Meitl, M. A.; Sun, Y.; Park, J.-U.; Shir, D. J.-L.; Nam, Y.-S.; Jeon, S.; Rogers, J. A. *Chem. Rev.* **2007**, *107* (4), 1117–1160.
163. Rogers, J. A.; Nuzzo, R. G. *Mater. Today* **2005**, *8* (2), 50–56.
164. Yan, L.; Zhao, X.-M.; Whitesides, G. M. *J. Am. Chem. Soc.* **1998**, *120* (24), 6179–6180.
165. Delamarche, E.; Schmid, H.; Bietsch, A.; Larsen, N. B.; Rothuizen, H.; Michel, B.; Biebuyck, H. *J. Phys. Chem. B* **1998**, *102*, 3324–34.
166. Jang, S. G.; Choi, D. G.; Kim, S.; Jeong, J. H.; Lee, E. S.; Yang, S. M. *Langmuir* **2006**, *22*, 3326–31.
167. Zaumseil, J.; Meitl, M. A.; Hsu, J. W. P.; Acharya, B. R.; Baldwin, K. W.; Loo, Y.-L.; Rogers, J. A. *Nano Lett.* **2003**, *3* (9), 1223–1227.
168. Menard, E.; Bilhaut, L.; Zaumseil, J.; Rogers, J. A. *Langmuir* **2004**, *20* (16), 6871–6878.
169. Brian, M. L.; Nathan, P. W.; Muhammad, N. Y. *ChemBioChem* **2008**, *9* (16), 2628–2632.
170. Jiang, X. R.; Chen, R.; Bent, S. F. *Surf. Coat. Technol.* **2007**, *201*, 8799–807.
171. Lamb, B. M.; Barrett, D. G.; Westcott, N. P.; Yousaf, M. N. *Langmuir* **2008**, *24* (16), 8885–8889.

172. Dameron, A.; Hampton, J. R.; Gillmor, S. D.; Hohman, J. N.; Weiss, P. S. *J. Vac. Sci. Technol., B* **2005**, *23*, 2929–32.
173. Dameron, A. A.; Hampton, J. R.; Smith, R. K.; Mullen, T. J.; Gillmor, S. D.; Weiss, P. S. *Nano Lett.* **2005**, *5*, 1834–7.
174. Srinivasan, C.; Mullen, T. J.; Hohman, J. N.; Anderson, M. E.; Dameron, A. A.; Andrews, A. M.; Dickey, E. C.; Horn, M. W.; Weiss, P. S. *ACS Nano* **2007**, *1*, 191–201.
175. Lewis, P. A.; Donhauser, Z. J.; Mantooth, B. A.; Smith, R. K.; Bumm, L. A.; Kelly, K. F.; Weiss, P. S. *Nanotechnology* **2001**, *12*, 231–7.
176. Bennett, R. D.; Hart, A. J.; Miller, A. C.; Hammond, P. T.; Irvine, D. J.; Cohen, R. E. *Langmuir* **2006**, *22*, 8273–6.
177. Baba, A.; Sato, F.; Fukuda, N.; Ushijima, H.; Yase, K. *Nanotechnology* **2009**, *20*, 1085301.
178. Rosa, L. G.; Liang, J. *J. Phys.: Condens. Matter* **2009**, *21* (48), 483001.
179. Hyun, J.; Ahn, S. J.; Lee, W. K.; Chilkoti, A.; Zauscher, S. *Nano Lett.* **2002**, *2* (11), 1203–1207.
180. Xu, S.; Miller, S.; Laibinis, P. E.; Liu, G. Y. *Langmuir* **1999**, *15*, 7244–51.
181. Liu, G. Y.; Xu, S.; Qian, Y. L. *Acc. Chem. Res.* **2000**, *33*, 457.
182. Joachim, C.; Gimzewski, J. K.; Aviram, A. *Nature* **2000**, *408*, 541–8.
183. Tinazli, A.; Piehler, J.; Beuttler, M.; Guckenberger, R.; Tampe, R. *Nat. Nanotechnol.* **2007**, *2*, 220–5.
184. Jang, J. W.; Maspoch, D.; Fujigaya, T.; Mirkin, C. A. *Small* **2007**, *3*, 600–5.
185. Hu, Y.; Das, A.; Hecht, M. H.; Scoles, G. *Langmuir* **2005**, *21*, 9103.
186. Liang, J.; Rosa, L. G.; Scoles, G. *J. Phys. Chem. C* **2007**, *111*, 17275–84.
187. Behm, J. M.; Lykke, K. R.; Pellin, M. J.; Hemminger, J. C. *Langmuir* **1996**, *12*, 2121.
188. Ando, M.; Kawasaki, M.; Imazeki, S.; Sasaki, H.; Kamata, T. *Appl. Phys. Lett.* **2004**, *85*, 1849.
189. Love, J. C.; Wolfe, D. B.; Jacobs, H. O.; Whitesides, G. M. *Langmuir* **2001**, *17*, 6005.
190. Sondag-Huethorst, J. A. M.; van Helleputte, H. R. J.; Fokkink, L. G. J. *Appl. Phys. Lett.* **1994**, *64*, 285.
191. Zharnikov, M.; Grunze, M. *J. Vac. Sci. Technol., B* **2002**, *20*, 1793.
192. Golzhauser, A.; Geyer, W.; Stadler, V.; Eck, W.; Grunze, M.; Edinger, K.; Weimann, T.; Hinze, P. *J. Vac. Sci. Technol., B* **2000**, *18*, 3414.
193. Klauser, R.; Hong, I. H.; Wang, S. C.; Zharnikov, M.; Paul, A.; Goelzhaeuser, A.; Terfort, A.; Chuang, T. J. *J. Phys. Chem. B* **2003**, *107*, 13133.
194. Heister, K.; Zharnikov, M.; Grunze, M.; Johansson, L. S. O.; Ulman, A. *Langmuir* **2001**, *17*, 8.
195. Berggren, K. K.; Bard, A.; Wilbur, J. L.; Gillaspy, J. D.; Helg, A. G.; McClelland, J. J.; Rolston, S. L.; Phillips, W. D.; Prentiss, M.; Whitesides, G. M. *Science (Washington, D.C.)* **1995**, *269*, 1255.
196. Heinz, B.; Morgner, H. *Surf. Sci.* **1997**, *372* (1−3), 100–116.
197. Harada, Y.; Masuda, S.; Ozaki, H. *Chem. Rev.* **1997**, *97* (6), 1897–1952.
198. Chabinyc, M. L.; Love, J. C.; Thywissen, J. H.; Cervelli, F.; Prentiss, M. G.; Whitesides, G. M. *Langmuir* **2003**, *19*, 2201.

199. Bard, A.; Berggren, K. K.; Wilbur, J. L.; Gillaspy, J. D.; Rolston, S. L.; McClelland, J. J.; Phillips, W. D.; Prentiss, M.; Whitesides, G. M. *J. Vac. Sci. Technol., B* **1997**, *15*, 1805.
200. Morgenthaler, S.; Lee, S.; Zuercher, S.; Spencer, N. D. *Langmuir* **2003**, *19*, 10459.
201. Liedberg, B.; Wirde, M.; Tao, Y.-T.; Tengvall, P.; Gelius, U. *Langmuir* **1997**, *13*, 5329.
202. Plummer, S. T.; Bohn, P. W. *Langmuir* **2002**, *18*, 4142.
203. Herbert, C. B.; McLernon, T. L.; Hypolite, C. L.; Adams, D. N.; Pikus, L.; Huang, C. C.; Fields, G. B.; Letourneau, P. C.; Distefano, M. D.; Hu, W.-S. *Chem. Biol.* **1997**, *4*, 731.
204. Chaudhury, M. K.; Whitesides, G. M. *Science (Washington, D.C.)* **1992**, *256*, 1539.
205. Plummer, S. T.; Wang, Q.; Bohn, P. W.; Stockton, R.; Schwartz, M. A. *Langmuir* **2003**, *19*, 7528.
206. Jeon, N. L.; Baskaran, H.; Dertinger, S. K. W.; Whitesides, G. M.; Van De Water, L.; Toner, M. *Nat. Biotechnol.* **2002**, *20*, 826.
207. Dertinger, S. K. W.; Jiang, X.; Li, Z.; Murthy, V. N.; Whitesides, G. M. *Proc. Natl. Acad. Sci. U.S.A.* **2002**, *99*, 12542.
208. Bietsch, A.; Hegner, M.; Lang, H. P.; Gerber, C. *Langmuir* **2004**, *20*, 5119.
209. Pardo, L.; Wilson, W. C., Jr.; Boland, T. *Langmuir* **2003**, *19*, 1462.
210. Black, A. J.; Paul, K. E.; Aizenberg, J.; Whitesides, G. M. *J. Am. Chem. Soc.* **1999**, *121*, 8356.
211. Laibinis, P. E.; Hickman, J. J.; Wrighton, M. S.; Whitesides, G. M. *Science (Washington, D.C.)* **1989**, *245*, 845.
212. Hickman, J. J.; Laibinis, P. E.; Auerbach, D. I.; Zou, C.; Gardner, T. J.; Whitesides, G. M.; Wrighton, M. S. *Langmuir* **1992**, *8*, 357.
213. Shabtai, K.; Cohen, S. R.; Cohen, H.; Rubinstein, I. *J. Phys. Chem. B* **2003**, *107*, 5540.
214. Lercel, M. J.; Redinbo, G. F.; Pardo, F. D.; Rooks, M.; Tiberio, R. C.; Simpson, P.; Craighead, H. G.; Sheen, C. W.; Parikh, A. N.; Allara, D. L. *J. Vac. Sci. Technol., B* **1994**, *12*, 3363.
215. Gorman, C. B.; Carroll, R. L.; He, Y. F.; Tian, F.; Fuierer, R. *Langmuir* **2000**, *16*, 6312.
216. Kleineberg, U.; Brechling, A.; Sundermann, M.; Heinzmann, U. *Adv. Funct. Mater.* **2001**, *11*, 208.
217. Cruchon-Dupeyrat, S.; Porthun, S.; Liu, G.-Y. *Appl. Surf. Sci.* **2001**, *175*, 636.
218. Chou, S. Y.; Krauss, R.; Renstrom, P. J. *Science* **1996**, *272*, 85–7.
219. Guo, L. J. *Adv. Mater.* **2007**, *19*, 495–513.
220. Bogdanski, N.; Wissen, M.; Mollenbeck, S.; Scheer, H. C. *Microelectron. Eng.* **2008**, *85*, 825–9.
221. Schift, H. *J. Vac. Sci. Technol., B* **2008**, *26*, 458–80.
222. Jung, G.-Y.; Li, Z.; Wu, W.; Chen, Y.; Olynick, D. L.; Wang, S.-Y.; Tong, W. M.; Williams, R. S. *Langmuir* **2005**, *21* (4), 1158–1161.
223. Falconnet, D.; Pasqui, D.; Park, S.; Eckert, R.; Schift, H.; Gobrecht, J.; Barbucci, R.; Textor, M. *Nano Lett.* **2004**, *4* (10), 1909–1914.

224. Byeon, K. J.; Hwang, S. Y.; Yang, K. Y.; Lee, H. *J. Nanosci. Nanotechnol.* **2009**, *9* (7), 4103–7.
225. Black, C. T. *ACS Nano* **2007**, *1*, 147–50.
226. La, Y. H.; Edwards, E. W.; Park, S. M.; Nealey, P. F. *Nano Lett.* **2005**, *5*, 1379–84.
227. Kim, S. O.; Solak, H. H.; Stoykovich, M. P.; Ferrier, N. J.; De Pablo, J. J.; Nealey, P. F. *Nature* **2003**, *424*, 411–4.
228. Anderson, M. E.; Mihok, M.; Tanaka, H.; Tan, L. P.; Horn, M. W.; McCarty, G. S.; Weiss, P. S. *Adv. Mater.* **2006**, *18*, 1020–2.
229. Kind, M.; Woll, C. *Prog. Surf. Sci.* **2009**, *84*, 230–78.
230. Tanaka, H.; Anderson, M. E.; Horn, M. W.; Weiss, P. S. *Jpn. J. Appl. Phys., Part 2* **2004**, *43*, L950–3.
231. Anderson, M. E.; Srinivasan, C.; Hohman, J. N.; Carter, E. M.; Horn, M. W.; Weiss, P. S. *Adv. Mater.* **2006**, *18*, 3258–60.
232. Golzhauser, A.; Eck, W.; Geyer, W.; Stadler, V.; Weimann, T.; Hinze, P.; Grunze, M. *Adv. Mater.* **2001**, *13*, 806–9.
233. Geyer, W.; Stadler, V.; Eck, W.; Golzhauser, A.; Grunze, M.; Sauer, M.; Weimann, T.; Hinze, P. *J. Vac. Sci. Technol., B* **2001**, *19*, 2732–5.
234. Eck, W.; Stadler, V.; Geyer, W.; Zharnikov, M.; Golzhauser, A.; Grunze, M. *Adv. Mater.* **2000**, *12*, 805–8.
235. Maeng, I. S.; Park, J. W. *Langmuir* **2003**, *19*, 4519–22.
236. Golzhauser, A; Geyer, W; Stadler, V; Eck, W; Grunze, M; Edinger, K; T, W.; P, H. *J. Vac. Sci. Technol., B* **2000**, *18*, 3414–8.
237. Zharnikov, M.; Grunze, M. *J. Vac. Sci. Technol., B* **2002**, *20*, 1793–807.
238. Vaidya, R.; Tender, L. M.; Bradley, G.; O'Brien, M. J., II; Cone, M.; López, G. P. *Biotechnol. Prog.* **1998**, *14* (3), 371–377.
239. Shadnam, M. R.; Kirkwood, S. E.; Fedosejevs, R.; Amirfazli, A. *Langmuir* **2004**, *20* (7), 2667–2676.
240. Friebel, S.; Aizenberg, J.; Abad, S.; Wiltzius, P. *Appl. Phys. Lett.* **2000**, *77* (15), 2406–2408.
241. Hartmann, N.; Balgar, T.; Bautista, R.; Franzka, S. *Surf. Sci.* **2006**, *600* (18), 4034–4038.
242. Iversen, L.; Younes-Metzler, O.; Martinez, K. L.; Stamou, D. *Langmuir* **2009**, *25* (21), 12819–12824.
243. Martele, Y.; Naessens, K.; VanDaele, P.; Baets, R.; Callewaert, K.; Schacht, E. *Polym. Int.* **2003**, *52*, 1641.
244. Li, P.; Bakowsky, U.; Yu, F. Y.; Loehbach, C.; Muecklich, F.; Lehr, C. M. *IEEE Trans. Nanobiosci.* **2003**, *2*, 138.
245. Meyyappan, S.; Shadnam, M. R.; Amirfazli, A. *Langmuir* **2008**, *24* (6), 2892–2899.
246. Baeuerle, D. *Laser Processing and Chemistry*; Springer: New York, 2000.
247. Nozik, A. J. *Physica E* **2002**, *14*, 115–120.
248. McDonald, S. A.; Konstantatos, G.; Zhang, S. G.; Cyr, P. W.; Klem, E. J. D.; Levina, L.; Sargent, E. H. *Nat. Mater.* **2005**, *4*, 138–U114.
249. Heremans, J. P. *Acta Phys. Pol., A* **2005**, *108*, 609–634.
250. Javey, A.; Guo, J.; Wang, Q.; Lundstrom, M.; Dai, H. *Nature* **2003**, *424*, 654–657.

251. Zheng, G.; Lu, W.; Jin, S.; Lieber, C. M. *Adv. Mater.* **2004**, *16*, 1890–1893.

252. Matsuoka, K.; Kataura, H.; Shiraishi, M. *Chem. Phys. Lett.* **2006**, *417*, 540–544.

253. Wang, S. G.; Sellin, P. J.; Zhang, Q.; Yang, D. J. J. *Curr. Nanosci.* **2005**, *1*, 43–46.

254. Klinke, C.; Hannon, J. B.; Afzali, A.; Avouris, P. *Nano Lett.* **2006**, *6*, 906–910.

255. Chung, S. W.; Ginger, D. S.; Morales, M. W.; Zhang, Z. F.; Chandrasekhar, V.; Ratner, M. A.; Mirkin, C. A. *Small* **2005**, *1*, 64–69.

256. Myung, S.; Lee, M.; Kim, G. T.; Ha, J. S.; Hong, S. *Adv. Mater.* **2005**, *17*, 2361.

257. Aguilar, A. D.; Forzani, E. S.; Li, X.; Tao, N.; Nagahara, L. A.; Amlani, I.; Tsui, R. *Appl. Phys. Lett.* **2005**, *87*, 193108–193103.

258. Comini, E. *Anal. Chim. Acta* **2006**, *568*, 28–40.

259. Wanekaya, A. K.; Chen, W.; Myung, N. V.; Mulchandani, A. *Electroanalysis* **2006**, *18*, 533–550.

260. Saraiya, A.; Porwal, D.; Bajpai, A. N.; Tripathi, N. K.; Ram, K. *Synth. React. Inorg. Met.-Org. Chem.* **2006**, *36*, 163–164.

261. Dorozhkin, P. S.; Tovstonog, S. V.; Golberg, D.; Zhan, J.; Ishikawa, Y.; Shiozawa, M.; Nakanishi, H.; Nakata, K.; Bando, Y. *Small* **2005**, *1*, 1088–1093.

262. Li, Z.; Dharap, P.; Nagarajaiah, S.; Barrera, E. V.; Kim, J. D. *Adv. Mater.* **2004**, *16*, 640–643.

263. Jiang, X.; Ferrigno, R.; Mrksich, M.; Whitesides, G. M. *J. Am. Chem. Soc.* **2003**, *125*, 2366.

264. Yousaf, M. N.; Mrksich, M. *J. Am. Chem. Soc.* **1999**, *121*, 4286.

265. Michel, B.; Bernard, A.; Bietsch, A.; Delamarche, E.; Geissler, M.; Juncker, D.; Kind, H.; Renault, J. P.; Rothuizen, H.; Schmid, H.; Schmidt-Winkel, P.; Stutz, R.; Wolf, H. *IBM J. Res. Dev.* **2001**, *45*, 697.

266. Hobara, D.; Imabayashi, S.; Kakiuchi, T. *Nano Lett.* **2002**, *2*, 1021.

267. Arnold, S.; Feng, Z. Q.; Kakiuchi, T.; Knoll, W.; Niki, K. *J. Electroanal. Chem.* **1997**, *438*, 91.

268. Capadona, J. R.; Collard, D. M.; Garcia, A. J. *Langmuir* **2002**, *19*, 1847.

269. Kane, R. S.; Takayama, S.; Ostuni, E.; Ingber, D. E.; Whitesides, G. M. *Biomaterials* **1999**, *20* (23−24), 2363–2376.

270. Lee, K. B.; Park, S. J.; Mirkin, C. A.; Smith, J. C.; Mrksich, M. *Science* **2002**, *295*, 1702–1705.

271. Zhu, H.; Bilgin, M.; Bangham, R.; Hall, D.; Casamayor, A.; Bertone, P.; Lan, N.; Jansen, R.; Bidlingmaier, S.; Houfek, T.; Mitchell, T.; Miller, P.; Dean, R. A.; Gerstein, M.; Snyder, M. *Science* **2001**, *293*, 2101–2105.

272. Hamelinck, D.; Zhou, H.; Li, L.; Verweij, C.; Dillon, D.; Feng, Z.; Costa, J.; Haab, B. B. *Mol. Cell. Proteomics* **2005**, *4*, 773–784.

273. Wendeln, C.; Heile, A.; Arlinghaus, H. F.; Ravoo, B. J. *Langmuir*.

274. Qin, D.; Xia, Y.; Xu, B.; Yang, H.; Zhu, C.; Whitesides, G. M. *Adv. Mater.* **1999**, *11*, 1433–1437.

275. Besson, E.; Gue, A. M.; Sudor, J.; Korri-Youssoufi, H.; Jaffrezic, N.; Tardy, J. *Langmuir* **2006**, *22*, 8346–8352.

276. Lockhart, D. J.; Dong, H.; Byrne, M. C.; Follettie, M. T.; Gallo, M. V.; Chee, M. S.; Mittmann, M.; Wang, C.; Kobayashi, M.; Norton, H.; Brown, E. L. *Nat. Biotechnol.* **1996**, *14*, 1675.
277. Schena, M.; Shalon, D.; Davis, R. W.; Brown, P. O. *Science* **1995**, *270*, 467.
278. Mooney, J. F.; Hunt, A. J.; McIntosh, J. R.; Liberko, C. A.; Walba, D. M.; Rogers, C. T. *Proc. Natl. Acad. Sci. U.S.A.* **1996**, *93*, 12287.
279. Schutkowski, M.; Reimer, U.; Panse, S.; Dong, L.; Lizcano, J. M.; Alessi, D. R.; Mergener, J. S. *Angew. Chem., Int. Ed.* **2004**, *43*, 2671.
280. Suzuki, I.; Sugio, Y.; Moriguchi, H.; Jimbo, Y.; Yasuda, K. *J. Nanobiol.* **2004**, *2*, 7.
281. Kira, A.; Okano, K.; Hosokawa, Y.; Naito, A.; Fuwa, K.; Yuyama, J.; Masuhara, H. *Appl. Surf. Sci.* **2009**, *255* (17), 7647–7651.
282. Zhai, L.; Berg, M. C.; Cebeci, F. C.; Kim, Y.; Milwid, J. M.; Rubner, M. F.; Cohen, R. E. *Nano Lett.* **2006**, *6*, 1213–1217.
283. Hillebrenner, H.; Buyukserin, F.; Kang, M.; Mota, M. O.; Stewart, J. D.; Martin, C. R. *J. Am. Chem. Soc.* **2006**, *128* (13), 4236–4237.

Chapter 5

Advancing SPRi Measurements with Novel Biosensors for Studying Surface-Biomolecule Interactions

Michael C. Weiger,[1],* Khaled Aamer,[1] Joachim Kohn,[2] and Matthew L. Becker[3]

[1]Polymers Division, National Institute of Standards and Technology, Gaithersburg, MD 20899
[2]New Jersey Center for Biomaterials, Rutgers University, Piscataway, NJ 08854
[3]Department of Polymer Science, University of Akron, Akron, OH 44325
***michael.weiger@nist.gov**

Through years of scientific research and development, surface plasmon resonance (SPR) has become a sensitive, quantitative and rapid measurement method with abundant applications in the fields of biology and biomaterials. The present contribution provides a brief overview of SPR history, development of SPR imaging and expanding sensor platforms while also briefly reviewing their many applications. We supplement these discussions with the introduction of new biosensor platforms for SPR imaging 1) composed of the primary mineral component in bone, hydroxyapatite (HA) and 2) tyrosine-derived polycarbonates which are utilized in many biomedical applications. These biosensors are completed with microfluidic flow channels to facilitate kinetic measurements. We describe the fabrication of the multilayer sensor surfaces and also demonstrate surface plasmon generation. We also highlight the utility and potential of these sensor platforms to characterize the binding kinetics of small peptides, engineered to bind specifically to these materials in order to facilitate development of new probes and modifiers for biomaterials.

Introduction

Before attempting to explore the vast, and often confounding, complexities of biological interactions using surface plasmon resonance (SPR) techniques, it is important to learn some history and gain a basic understanding of the method. First, what is a surface plasmon? Surface plasmons (SP)s are collective oscillations of surface charge density or electromagnetic waves. These waves are excited and propagate parallel to a metal/dielectric interface upon excitation by an external electric field, such as light (*1*, *2*). They are essentially coupled with the evanescent wave trapped on the surface because of their interaction with the free electrons of the metal. The excitation of surface plasmons was first recorded back in 1902 by R.W. Woods at Johns Hopkins University when he reported 'anomalies' in the spectrum of light diffracting on a metallic grating (*3*). Later theoretical work by Zenneck in 1907 and Fano in 1941 framed Wood's observations in the context of the excitation of electromagnetic surface waves (*4*, *5*). Ultimately in 1968, Otto demonstrated that the 'anomalies' or decline in reflectivity (intensity of reflected light) seen during attenuated total reflection upon illumination of a thin metal film through a prism was due to surface plasmons (Fig. 1a) (*6*). That same year, Kretschmann and Raether also reported surface plasmon excitation using an analogous prism configuration of the attenuated total reflection method (Fig. 1b) (*7*).

Most SPR systems used today utilize the 'Kretschmann' configuration in which a prism serves to couple an incident light beam to a metal/dielectric interface via the phenomenon of total internal reflection (Fig. 1b). Although several metals including silver, gold, copper, and aluminum support SP generation, thin films (~ 50 nm) of silver and gold are most commonly used in SPR sensor systems (*8*, *9*). Excitation of surface plasmons typically involves guiding p-polarized, monochromatic light to the face of a prism, which is optically coupled to the substrate containing the metal film, at multiple angles of incident greater than the critical angle for total internal reflection (TIF). The evanescent wave generated from the total internal reflection of the incident light source is able to couple with the free, oscillating electrons in the metal film at multiple angles of incidence.

There is however an incident angle at which surface plasmons are maximally excited. This unique angle is often referred to as the resonance angle (θ_R) (*10*). If the intensity of the reflected light (the reflectivity) is monitored, the angle at which it reaches a minimum corresponds to the θ_R and the surface plasmon is said to be resonantly excited (Fig. 2). Depending on the type of metal film, dielectric medium and wavelength of the incident light (λ), the resonant SPs will propagate 1 μm to 200 μm in the longitudinal direction along the metal film before decaying (*2*). Similarly, the SP's evanescent field probes the medium normal to the metal film, typically between 100 nm to 500 nm from the metal surface when using a visible light source (*11*). Any changes in the refractive index near the metal/dielectric interface will alter the characteristic of the incident light wave coupled to the surface plasmon. This leads to changes in, but not limited to, the resonance angle and intensity of the reflected light source (*12*). This sensitivity to changes in refractive index allows for the label–free detection of analytes and small molecules that adsorb onto the metal/dielectric interface. Under certain conditions, a linear

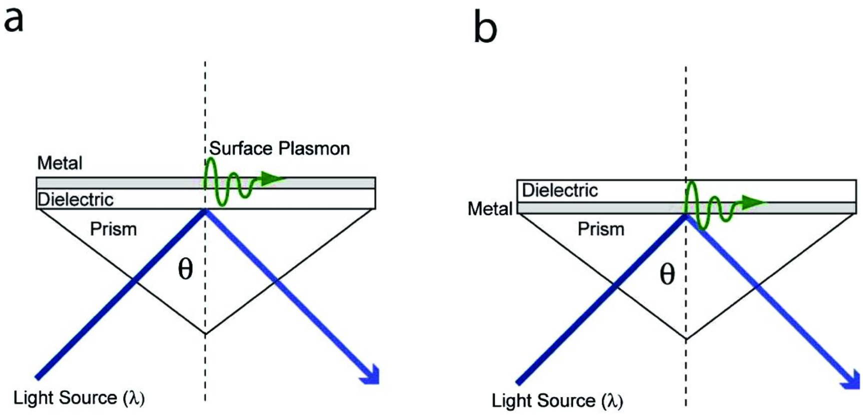

Figure 1. (a) Otto and (b) Kretschmann configurations for SPR (see color insert)

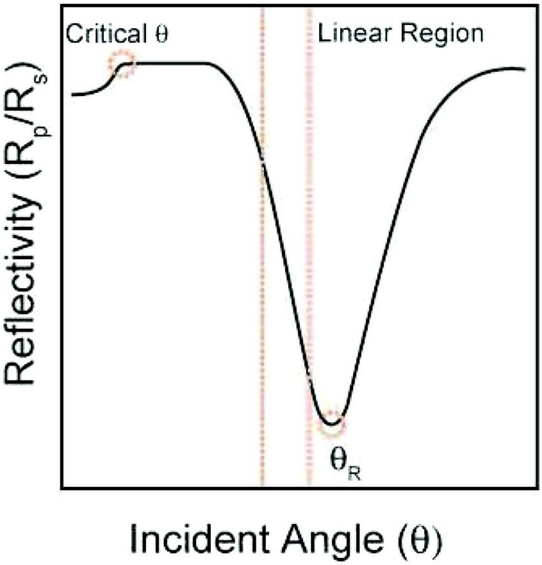

Figure 2. Surface plasmon resonance curve with characteristic critical angle θ, resonance angle θ_R and linear region where $\Delta\theta_R$ is proportional to $\Delta(R_p/R_s)$. (see color insert)

relationship exists between the amount of mass adsorbed and the relative change in resonance angle ($\Delta\theta_R$), which is directly proportional to the local change in the refractive index (*13*, *14*). From these principles, SPR technology has grown into an evolving analytical technique typically used to characterize and quantify molecular interactions at an interface. It has gained particular application as a sensor system used to study biomolecular binding events and their kinetics (*15*). A further extension of the SPR technique emerged with a microscopy based system which made high through-put measurements possible. Additional extensions of the SPR technique, which are beyond the scope of this text, have also been and continue to be made.

Surface Plasmon Resonance Imaging

In 1988, Rothenhausler and Knoll introduced a new microscope technique they coined surface plasmon microscopy (SPM). Using the Kretschmann configuration, they imaged a 3 mm area patterned with alternating Ag and Ag/cadmium arachidate (CH_3-$(CH_2)_{18}COO$-$)_2Cd^{2+}$) layers and observed that intensity contrast could be achieved between areas of different thickness. Not surprisingly, when they compared the reflectivity curve for both regions, the minimums occurred at different θ_R angles. They concluded that any difference in optical properties, like changes in refractive index or layer thickness, would yield measureable differences in the reflectivity and θ_R, and ultimately change the contrast or intensity of those regions. Rothenhausler and Knoll further reasoned that SPM was capable of high spatial resolution imaging ($\leq$ 1 μm), but that the level of resolution did dependent upon the wavelength of the excitation source (*16*). With the advent of the two dimensional array photodiodes and charge coupled detector (CCD) cameras, the intensity of the reflected light over larger and larger areas of the metal/dielectric surface can be monitored simultaneously, facilitating high through-put analysis of biomolecular binding events. Current SPM or SPR imaging setups typically consist of a beam of expanded and collimated, p-polarized monochromatic light (laser or LED) passing through a prism such that it totally internally reflects onto a senor surface containing a thin metal film. The reflected light intensity from the illuminated area of the surface is monitored at a fixed incident angle by a CCD camera (*17*). By imaging the sensor surface at a fixed incident angle within the linear response region of the reflectivity curve (Fig. 2), changes in light intensity due to analytes or biomolecules adsorbing to the sensor surface, altering the refractive index at the surface, remains proportional to the change in θ_R, which is a read-out of the amount of analyte adsorbed to the sensor surface. SPR imaging (SPRi) can monitor adsorption of an analyte to the sensor surface in real time with a temporal resolution of ~ 1 s and a spatial resolution on the order of 5 μm (*18*). Most SPRi setups incorporate some type of flow cell which allows the introduction and removal of the analyte to and from the biosensor surface. The pioneering work by the research groups of Wolfgang Knoll and Robert Corn established SPRi as an excellent tool for determining the extent of adsorption, the rates of association and dissociation, and equilibrium binding constants describing interactions between proteins, DNA, RNA, and a variety of other biomolecules or ligands (*19–22*). At the heart of every SPRi system is the sensor surface which directly impacts the performance characteristics as well as the experimental systems that can be studied.

Surface Sensor Platforms

In general, a SPR biosensors consists of an optically clear, rigid substrate (glass slide or prism surface) upon which a thin layer of metal (Cu, Al, Au, and Ag) is deposited. While there are several metals that support SP generation, the most commonly used are Au and Ag. Due to its stability, Au is the metal most often used in SPR biosensors. Ag on the other hand is chemically unstable and prone to oxidation in both air and aqueous environments. However, Ag provides the sharpest SPR signal, enhanced penetration length and has greater sensitivity to thickness and refractive index variations (*8*, *23–25*). Ultimately, the metal selected will depend on the experimental application. Atop the metal film, a surface recognition element is incorporated giving the biosensor its probing functionalities. Au and Ag films are an attractive base because they are amendable to the chemisorption of self-assemble monolayers (SAMs), a common building block for the surface recognition element. SAMs of alkanethiols or disulfides with varying end groups (aliphatic, amines, thiols, aldehydes, or carboxylic groups) have been extensively utilized to activate the metal surfaces and provide platforms for immobilizing polymers, proteins, DNA, RNA, peptides, and many other biomolecules that make up the surface recognition element (*18*, *26–28*). An additional technique makes use of biotinylated SAMs and biomolecules conjugated with its binding partner streptavidin, or vice versa, in order to immobilize them on the biosensor surface (*29*). Another general method for immobilizing proteins and antibodies to the biosensor surface uses a carboxymethyldextran matrix typically bound to a gold film (*30*). There are even reports of polymers being used as the surface recognition element (*31*). Custom built and commercial SPR and SPRi systems employing these surface recognition elements have become instrumental in measuring binding kinetics between DNA-DNA, RNA-DNA, protein-DNA, antigen-antibody, and numerous other biological and even biomaterial interactions (*32*).

SPR is becoming an increasingly powerful tool for biomaterial characterization. Most biomaterials are made of metallic materials (stainless steel, titanium, gold, etc.), polymers and/or composites of polymers and biomolecules. How these materials interact with peptides, proteins, and even the membranes of cells within the body is vital to their performance and favorable integration into the body. Along this front, SPRi has been successfully used to characterize the degradation and hydration of polymeric interfaces in addition to the extent of proteins adsorption onto polymeric surfaces, both events expected to be encountered within the body (*33*, *34*). More recently, SPR has been used to determine the binding affinity of small peptides identified through phage display toward inorganic surfaces. Using this information, these peptides have the potential to modify and even template biomaterial surfaces made of gold and TiO_2 (*35–37*).

Novel Hydroxyapatite Sensor and SPRi System

In the field of orthopedic implants and bone replacement as well as restorative dental materials, the mineral hydroxyapatite (HA) has been used as a surface coating since 1980 (*38*). Hydroxyapatite (HA) [$Ca_5(PO_4)_3(OH)$] is one of several forms of calcium phosphate (CP) including: amorphous calcium phosphate ACP [$Ca_3(PO_4)_2{\bullet}xH_2O$], monocalcium phosphate [Ca (H_2PO_4)], dicalcium phosphates DCPs [$Ca_2(HPO_4)_2{\bullet}xH_2O$], tricalcium phosphate TCP[$Ca_3(PO_4)_2$], and octacalcium phosphate OCP [$Ca_8H_2(PO_4)_6{\bullet}xH_2O$]. Among these, HA is the most stable and is the prominent inorganic component in both teeth and bone. Because of the excellent biocompatibility and low cytotoxicity of HA, it has become a promising material for clinical use. Due to its poor mechanical properties however, HA is usually used as an implant coating or incorporated into a biomaterial to enhance bonding to bone or promote cellular in-growth respectively (*39*). Many orthopedic implants are often coated with HA using plasma spraying or sputtering techniques (*38*, *40*). In an effort to advance SPRi measurement capabilities and further explore biological interactions at an HA interface, our lab fabricated a novel 4-layer, HA SPR biosensor by employing plasma sputtering. By making use of this method's ability to deposit nanometer layers of materials, we successfully crafted a new SPR senor surface and integrated it into custom SPRi setup (*41*).

Our SPR imaging system represents a hybrid SPR instrument that can make full angle resonance scans and single angle image scans for multiple parallel flow channels simultaneously. We use the angle resonance scans for characterization of biosensor platforms and single angle imaging which we report as the change in reflectivity, $\Delta(R_p/R_s)$, as a function of time for monitoring the binding kinetics of adsorbing biomolecules to the senor surface. We built our HA biosensor atop a simple glass ($n = 1.522$) substrate. Four thin films were then sequentially sputtered on the glass substrate in a rectangular pattern (Fig. 3a). The number, thickness and composition of each thin film affect the intensity and shape of the measured SPR signal, the reflectivity (R_p/R_s) and ultimately the sensors ability to detect adsorbing species. Our HA sensor consisted of a very thin layer of Cr (0.44 nm to 0.6 nm) to provide a robust adhesive layer for the second metal layer, Ag (50.7 nm to 53.6 nm). To mitigate any degradation of the Ag layer, a thin layer of TiO_2 (1.1 nm to 2.8 nm) was deposited which also provides an adhesive layer for the final HA (10 nm to 20 nm) layer.

To complete the SPR sensor, a microfluidic device with 6 parallel flow channels was fabricated using standard soft lithographic techniques (*42*, *43*) and attached to the SPR sensor (Fig. 3b). The whole device was optically coupled to the prism in our SPRi system with refractive index-matching immersion oil (Fig. 3c). For a more detailed description of this set-up, we refer the reader to our most recent publication (*41*).

Every SPR sensor has a unique reflectivity curve with characteristic features that are dependent on the thickness and refractive index of each layer. These reflectivity characteristics, while complex, can be described by Fresnel theory. Due to the sensitivity of this technique to minute changes in the surface composition and or thickness, it is essential that the reflectivity curve describing the system be measured. Following these guidelines, we confirmed that our HA biosensor indeed supports surface plasmon generation by successfully measuring a reflectivity curve (Fig. 4a) (*41*). Next we used a multilayer Fresnel model, implemented using a custom MATLAB code, to estimate the reflectivity (R_p/R_s)

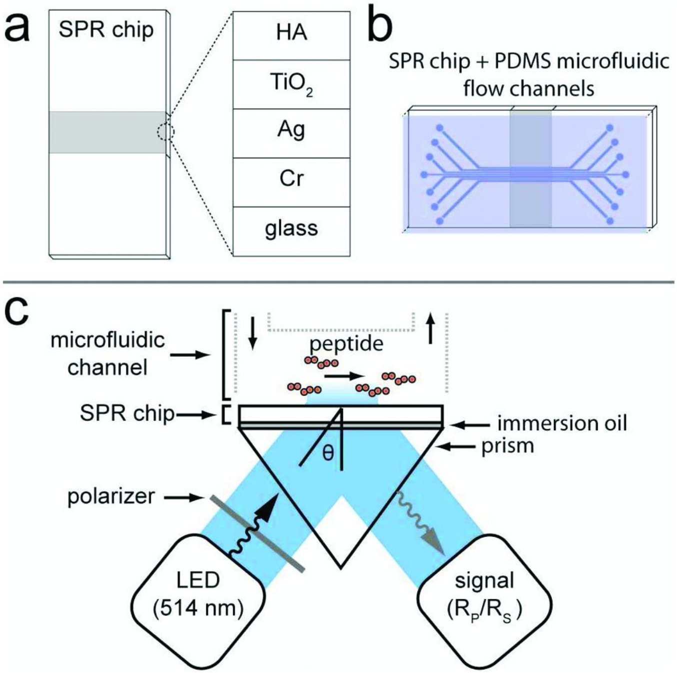

Figure 3. (a) Hydroxyapatite biosensor coupled with (b) a microfluidic device and (c) the complete SPR imaging system. (Reprinted from Biomaterials, ***2010,*** *31 (11), 2955-2963. Weiger et. al. "Quantification of the binding affinity of a specific hydroxyapatite binding peptide" with permission from Elsevier) (see color insert)*

as a function of incident angle (θ) for our 4-layer sensor. After applying a least-square parameter fit, the Fresnel description showed good agreement with our experimental data (Fig. 6a) and gave thickness estimates for each layer [Cr (0.44 nm), Ag (53.6 nm), TiO2 (1.1 nm) and HA (22 nm)] similar to those measured by layer-deposition rate [Cr (0.6 nm), Ag (50.7 nm), TiO2 (2.8 nm)], AFM and SEM [HA (10-25 nm)] (*41*). According to theory, the measured $\Delta(R_p/R_s)$ at a fixed θ is proportional to $\Delta\theta_R$ (i.e. density of surface absorbed molecules); however, for our SPRi system this relationship holds only for $\Delta(R_p/R_s) < 0.06$ (Fig. 4b) (*41*). It is critical to identify measurement limitations of every SPR senor to insure proper interpretation of results. Further, our SPRi system is theoretically capable of detecting changes in refractive index of $\approx 5 \times 10^{-5}$ refractive index units (RIU) which is comparable to many SPR systems in use today (*17*, *29*).

To further demonstrate the capabilities of our HA biosensor and SPRi system, we recently employed them to determine the binding affinity of a peptide sequence (SVSVGMKPSPRPGGGK) that binds preferentially to HA over its precursor, amorphous calcium phosphate (*41*, *44*). Subsequent peptides that bind to calcium phosphate substrates have also been identified, but the methods utilized to assess binding did not yield quantitative measures of the peptides' affinity toward their

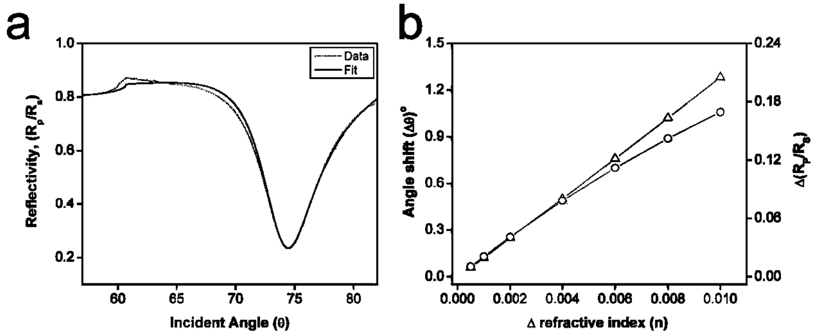

Figure 4. HA coated biosensor support surface plasmon generation (a) and (b) has a range where $\Delta(R_p/R_s)$ is proportional to $\Delta\theta_R$. (Reprinted from Biomaterials, ***2010,*** *31 (11), 2955-2963. Weiger et. al. "Quantification of the binding affinity of a specific hydroxyapatite binding peptide" with permission from Elsevier)*

substrates (*45*). We believe that SPRi, with the appropriate biosensor platform, is a likely successor and compliment to measurement techniques such as enzyme-linked immunosorbent assay (ELISA) and quartz crystal microbalance (QCM) which have fallen short in providing sufficient quantitative measures of peptide affinities toward calcium based minerals. Further, SPRi allows kinetic information to be collected which will aid in identifying the mechanisms of surface binding.

In our most recent study, we delivered the above mentioned HA-specific peptide via our microfluidic device to our HA biosensor surface at several concentrations and then monitored the binding kinetics in real time with our SPRi system (Fig. 5). The experiments were conducted under equilibrium conditions and the change in reflectivity $\Delta(R_p/R_s)$ was measured for each peptide concentration.

Fig. 5 shows the average reflectivity measurements (n = 3) as a function of time for three different concentrations of the HA-specific peptide. After the introduction of the peptide, surface binding was detected as seen by the increase in the reflectivity, $\Delta(R_p/R_s)$. The reflectivity approached equilibrium after 20 min to 30 min and stabilized at $\Delta(R_p/R_s)$ values that fall within the range where $\Delta(R_p/R_s)$ is proportional $\Delta\theta_R$ (Fig. 4b) and thus, corresponds to amount of surface-bound HA-specific peptide. From this data we constructed an equilibrium binding curve and employed a simple mathematical model to extract the binding affinity, quantified by the equilibrium dissociation constant (K_D). We were able to determine that the HA-specific peptide binds with a $K_D = 14.1\ \mu M \pm 3.8\ \mu M$, a relatively high affinity considering the small size of the peptide and unique nature of HA. In subsequent studies, we used our SPRi system to investigate which amino acid segments in the HA-specific peptide significantly impact the affinity to HA (*41*).

We have also sought to further investigate the presentation and stability of HA on the surface of our SPRi biosensor. Previously, we concluded that both HA and tricalcium phosphate (TCP) were present on the surface of our HA biosensor (*41*). Under an aqueous environment, the less stable polymorph TCP would likely dissolve leaving the more stable HA on the surface. Indeed, during equilibration of the sensor surface with buffer before the introduction of the HA-specific peptide,

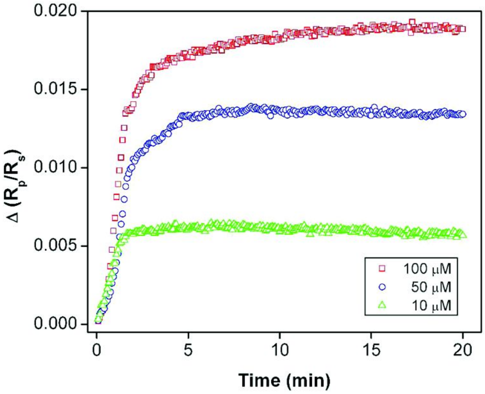

Figure 5. The HA coated SPR biosensor allows real-time monitoring of peptide binding kinetics, facilitating equilibrium binding studies. (see color insert)

a slight decrease in the reflectivity was sometimes observed. In an effort to further characterize the biosensor surface, we conducted a simple experiment to verify this observation as well as identify where the HA-peptide was likely binding on the surface. Using AFM, we first imaged the HA biosensor surface under dry conditions (Fig. 6a) and found a heterogeneous population of sub-micron domains, presumably the HA and TCP. The surface density of mineral domains greater than 5 nm in height was ≈ 14.9 particles/μm^2 (n =1) and had a domain size (average major axis) of 405 ± 286 nm. We further found that the surface had a characteristic roughness of $R_{rms} \approx 10.2 \pm 5.9$ nm.

Next, we incubated the surface with a buffered solution of the HA-specific peptide (200 μM) for 1 hr and imaged the surface with fluid AFM (Fig. 6b). Under these conditions, the surface density of domains greater than 5 nm in height increased to ≈ 25.4 particles/μm^2 and the domain size (average major axis) decreased to 141 ± 208 nm. The surface roughness under fluid was also reduced, $R_{rms} \approx 9.8 \pm 2.2$ nm. We believe this data provide more evidence that TCP dissolves from the surface while the more the stable HA domains remain for the peptide to bind to. We are conducting further computational and experimental studies to determine the precise mechanism by which the peptide interacts with HA and how its presentation on this SPR sensor might impact binding measurements.

We believe this mineral-based SPR sensor will support future studies involving HA coated materials and provided insights into biomolecular interactions and potentially cellular responses occurring at the tissue/biomaterial interface. While HA is an important coating for bone and other implants, the application of polymeric materials as biomaterials for tissue engineering continues to be an exciting area of study.

Polymeric SPRi Sensors

Polymers have long been and continue to be applied in the biomaterials, biomedical and biomedicine fields as tissue engineering scaffolds, implants,

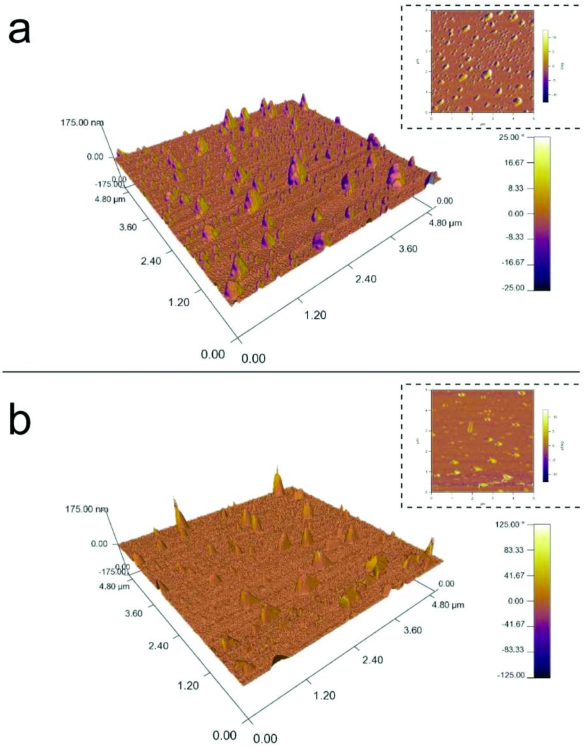

Figure 6. AFM height and phase images of HA biosensor surface under (a) dry and (b) fluid conditions (insets - 2D phase images). (see color insert)

vehicles for drug delivery and more. The ability to interrogate how biological molecules of the body interact with as well as identify which molecules preferentially decorate the surface of such polymeric devices is invaluable information for both clinical application and fundamental science. Such information will allow for improved design and engineering of biomaterials as well as insuring proper application of new materials.

One class of polymers of particular note for its recent FDA approval for implantable devices, are degradable tyrosine-derived polycarbonates (*46*). These materials are finding numerous applications in, but not limited to, orthopedic implants, tissue scaffolds, and deployable cardiovascular stents (*47–49*). Recently, thin films of poly(desaminotyrosyl tyrosine ethyl ester carbonate), poly(DTE carbonate) and an iodinated analogue poly(I_2-DTE carbonate), as seen in Fig. 7a, were used to assess the impact of the iodine functionalization on protein (fibronectin) adsorption and osteoblast cell morphology (*50*). As a next step to advance the study of biomolecule/polymer interactions, our lab set out to develop SPR sensor platforms that incorporate each of these polymers.

Building from our HA biosensor, we use plasma sputtering to deposit thin layers of Cr and Ag. Next, we deposited a self-assembled monolayer of 3-mercaptopropionic acid (3-MPA) atop the Ag layer to provide a hydrophilic surface that the polymer solutions can wet. Thin films (20-50 nm) of the

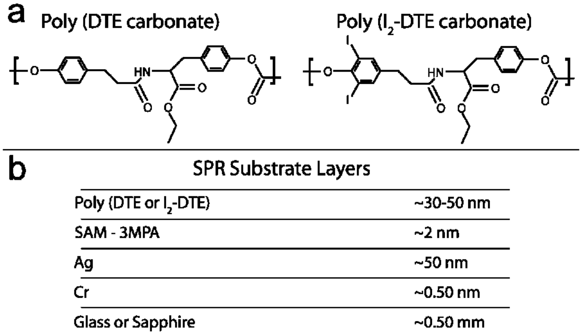

Poly (DTE or I$_2$-DTE)	~30-50 nm
SAM - 3MPA	~2 nm
Ag	~50 nm
Cr	~0.50 nm
Glass or Sapphire	~0.50 mm

Figure 7. (a) Polycarbonates and (b) layer composition of polymer coated SPRi biosensors.

poly(DTE) or poly(I_2-DTE) were then spun-cast using 2 % (by mass in 1,4-dioxane) solutions of the respective polymers (Fig. 7b).

Using our SPRi system described earlier, we were able to generate reflectivity curves for our poly(DTE) and poly(I_2-DTE) SPR sensors when they were exposed to air (Fig. 8). The two polymer sensors exhibited different resonance angles, θ_R, which we attribute to thickness differences in the polymer films. Currently, we are optimizing our coating process and adapting the sensor to a fluid environment. We intend to utilize these SPRi sensor platforms to measure the binding affinities of peptides our lab has identified that bind selectively to poly(DTE) and poly(I_2-DTE). Our hope is that this polymeric SPR sensor platform will spur the development of others allowing more interactions between biomolecules and polymers/biomaterials to be investigated.

Conclusions

For decades, SPR sensing has been used to investigate the extent and kinetics of numerous molecular and biomolecular binding events. It is a powerful technique suited for interrogating biology and biomaterials at the interface. The ability of this technique to detect small changes in refractive index with high sensitivity ($<10^{-6}$ RIU), temporal (~ 1 s) and spatial (~ 4 μm) resolution makes it an ideal, label free measurement tool. With the advent of microfluidics and now nanofluidics, current studies in the literature have reported measuring > 1000 interactions simultaneously while utilizing only small amounts of expensive biomolecules, helping to making them very cost effective techniques. SPR continues to evolve with the contributions by many research groups whose energy and drive have made advances in system designs, optics, light sources and what we have focused on in this chapter, the biosensor platforms. We have briefly described novel biosensor platforms developed by in our lab to further advance SPRi measurements. We reported the successful fabrication and implementation of a biocompatible mineral-based sensor to measure the binding affinity of a unique peptide probe while also presenting our most recent polymer-based sensor platforms. Through creativity and innovation, both commercial and custom SPR

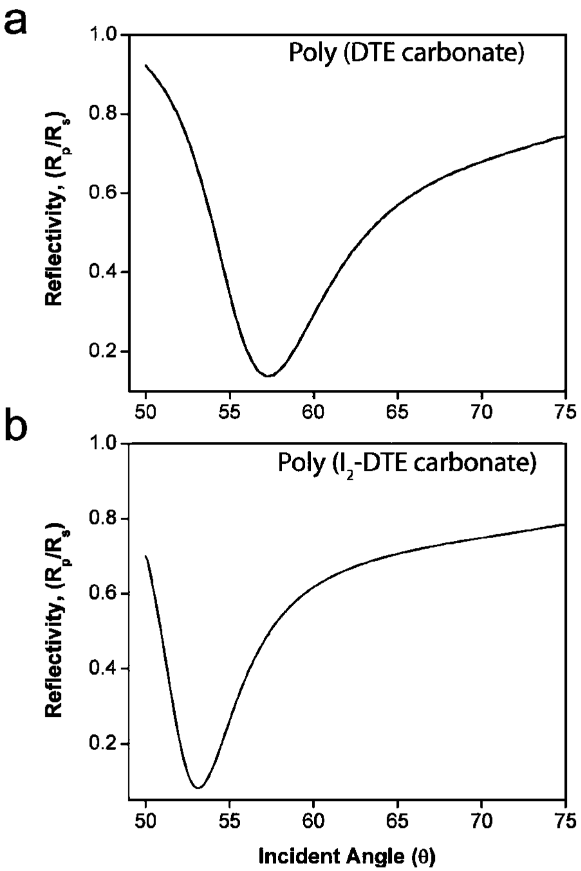

Figure 8. Surface plasmon resonance curve for (a) tyrosine-derived polycarbonate and (b) an iodinated analogue sensor platform.

and SPRi systems are continually being improved upon and applied in the field of biomaterials and beyond.

Acknowledgments

The authors gratefully acknowledge support from a National Institute of Standards and Technology (NIST) Innovation in Measurement Science Award in Cellular Biometrology and National Research Council/ NIST postdoctoral fellowships to Marc D. Roy and MCW. The authors would also like to thank Alexander Peterson, Nicole Moore and the NIST Center for Nanoscale Science and Technology for their valuable contributions to this work. Certain commercial equipment, instruments, or materials are identified in this paper in order to specify the experimental procedure adequately. Such identification is not intended to imply recommendation or endorsement by the National Institute of Standards and Technology, nor is it intended to imply that the materials or equipment identified are necessarily the best available for the purpose.

References

1. *Handbook of Surface Plasmon Resonance*; RSC Publishing: 2008.
2. Barnes, W.; Dereux, A.; Ebbesen, T. Surface plasmon subwavelength optics. *Nature* **2003**, *424* (6950), 824–830.
3. Wood, R. A suspected case of the electrical resonance of minute metal particles for light-waves. A new type of absorption. *Philos. Mag.* **1902**, *3* (13−18), 396–410.
4. Zenneck, J. Breeding of even electromagnetic waves along an even conducting surface and its relation to radiotelegraphy. *Ann. Phys.* **1907**, *23* (10), 846–866.
5. Fano, U. The theory of anomalous diffraction gratings and of quasi-stationary waves on metallic surfaces (Sommerfeld's waves). *J. Opt. Soc. Am.* **1941**, *31* (3), 213–222.
6. Otto, A. Excitation of nonradiative surface plasma waves in silver by method of frustrated total reflection. *Z. Phys.* **1968**, *216* (4), 398–&.
7. Kretschm, E; Raether, H. Radiative decay of non radiative surface plasmons excited by light. *Z. Naturforsch., A: Astrophys., Phys. Phys. Chem.* **1968**, *A23* (12), 2135–&.
8. Debruijn, H.; Kooyman, R.; Greve, J. Choice of metal and wavelength for surface-plasmon resonance sensors - some considerations. *Appl. Opt.* **1992**, *31* (4), 440–442.
9. Homola, J. *Surface Plasmon Resonance Based Sensors*; Springer-Verlag Berlin Heidelberg: New York, 2006; Vol. 4.
10. Matsubara, K.; Kawata, S.; Minami, S. A compact surface-plasmon resonance sensor for measurement of water in process. *Appl. Spectrosc.* **1988**, *42* (8), 1375–1379.
11. Homola, J. Present and future of surface plasmon resonance biosensors. *Anal. Bioanal. Chem.* **2003**, *377* (3), 528–539.
12. Nylander, C.; Liedberg, B.; Lind, T. Gas-detection by means of surface-plasmon resonance. *Sens. Actuators* **1982**, *3* (1), 79–88.
13. Jung, L.; Campbell, C.; Chinowsky, T.; Mar, M.; Yee, S. Quantitative interpretation of the response of surface plasmon resonance sensors to adsorbed films. *Langmuir* **1998**, *14* (19), 5636–5648.
14. Tumolo, T.; Angnes, L.; Baptista, M. S. Determination of the refractive index increment (dn/dc) of molecule and macromolecule solutions by surface plasmon resonance. *Anal. Biochem.* **2004**, *333* (2), 273–279.
15. Green, R.; Frazier, R.; Shakesheff, K.; Davies, M.; Roberts, C.; Tendler, S. Surface plasmon resonance analysis of dynamic biological interactions with biomaterials. *Biomater.* **2000**, *21* (18), 1823–1835.
16. Rothenhausler, B.; Knoll, W. Surface-plasmon microscopy. *Nature* **1988**, *332* (6165), 615–617.
17. Campbell, C.; Kim, G. SPR microscopy and its applications to high-throughput analyses of biomolecular binding events and their kinetics. *Biomaterials* **2007**, *28* (15), 2380–2392.

18. Haussling, L.; Ringsdorf, H.; Schmitt, F.; Knoll, W. Biotin-functionalized self-assembled monolayers on gold - surface-plasmon optical studies of specific recognition reactions. *Langmuir* **1991**, *7* (9), 1837–1840.
19. Aust, E. F.; Sawodny, M.; Ito, S.; Knoll, W. Surface-plasmon and guided optical-wave microscopies. *Scanning* **1994**, *16* (6), 353–361.
20. Zizlsperger, M.; Knoll, W. Multispot parallel on-line monitoring of interfacial binding reactions by surface plasmon microscopy. *Horizons 2000 - Aspects of Colloid and Interface Science at the Turn of the Millenium* **1998**, *109*, 244–253.
21. Thiel, A.; Frutos, A.; Jordan, C.; Corn, R.; Smith, L. In situ surface plasmon resonance imaging detection of DNA hybridization to oligonucleotide arrays on gold surfaces. *Anal. Chem.* **1997**, *69* (24), 4948–4956.
22. Jordan, C.; Frutos, A.; Thiel, A.; Corn, R. Surface plasmon resonance imaging measurements of DNA hybridization adsorption and streptavidin/DNA multilayer formation at chemically modified gold surfaces. *Anal. Chem.* **1997**, *69* (24), 4939–4947.
23. Kooyman, R.; Kolkman, H.; Vangent, J.; Greve, J. Surface-plasmon resonance immunosensors - sensitivity considerations. *Anal. Chim. Acta* **1988**, *213* (1−2), 35–45.
24. Giebel, K. F.; Bechinger, C.; Herminghaus, S.; Riedel, M.; Leiderer, P.; Weiland, U.; Bastmeyer, M. Imaging of cell/substrate contacts of living cells with surface plasmon resonance microscopy. *Biophys. J.* **1999**, *76* (1), 509–516.
25. Lecaruyer, P.; Canva, M.; Rolland, J. Metallic film optimization in a surface plasmon resonance biosensor by the extended Rouard method. *Appl. Opt.* **2007**, *46* (12), 2361–2369.
26. Mrksich, M.; Sigal, G. B.; Whitesides, G. M. Surface-Plasmon Resonance Permits In-Situ Measurement Of Protein Adsorption On Self-Assembled Monolayers Of Alkanethiolates On Gold. *Langmuir* **1995**, *11* (11), 4383–4385.
27. Silin, V.; Weetall, H.; Vanderah, D. J. SPR studies of the nonspecific adsorption kinetics of human IgG and BSA on gold surfaces modified by self-assembled monolayers (SAMs). *J. Colloid Interface Sci.* **1997**, *185* (1), 94–103.
28. Sigal, G. B.; Mrksich, M.; Whitesides, G. M. Using surface plasmon resonance spectroscopy to measure the association of detergents with self-assembled monolayers of hexadecanethiolate on gold. *Langmuir* **1997**, *13* (10), 2749–2755.
29. Homola, J. Surface plasmon resonance sensors for detection of chemical and biological species. *Chem. Rev.* **2008**, *108* (2), 462–493.
30. Liedberg, B.; Lundstrom, I.; Stenberg, E. Principles of biosensing with an extended coupling matrix and surface-plasmon resonance. *Sens. Actuators, B* **1993**, *11* (1−3), 63–72.
31. Green, R. J.; Davies, J.; Davies, M. C.; Roberts, C. J.; Tendler, S. J. B. Surface plasmon resonance for real time in situ analysis of protein adsorption to polymer surfaces. *Biomaterials* **1997**, *18* (5), 405–413.

32. Smith, E. A.; Corn, R. M. Surface plasmon resonance imaging as a tool to monitor biomolecular interactions in an array based format. *Appl. Spectrosc.* **2003**, *57* (11), 320A–332A.
33. Chen, X. Y.; Davies, M. C.; Roberts, C. J.; Shakesheff, K. M.; Tendler, S. J. B.; Williams, P. M. Dynamic surface events measured by simultaneous probe microscopy and surface plasmon detection. *Anal. Chem.* **1996**, *68* (8), 1451–1455.
34. Green, R. J.; Davies, M. C.; Roberts, C. J.; Tendler, S. J. B. Competitive protein adsorption as observed by surface plasmon resonance. *Biomaterials* **1999**, *20* (4), 385–391.
35. Seker, U. O.; Wilson, B.; Sahin, D.; Tamerler, C.; Sarikaya, M. Quantitative affinity of genetically engineered repeating polypeptides to inorganic surfaces. *Biomacromolecules* **2009**, *10* (2), 250–7.
36. Tamerler, C.; Oren, E. E.; Duman, M.; Venkatasubramanian, E.; Sarikaya, M. Adsorption kinetics of an engineered gold binding Peptide by surface plasmon resonance spectroscopy and a quartz crystal microbalance. *Langmuir* **2006**, *22* (18), 7712–8.
37. Sano, K.; Sasaki, H.; Shiba, K. Utilization of the pleiotropy of a peptidic aptamer to fabricate heterogeneous nanodot-containing multilayer nanostructures. *J. Am. Chem. Soc.* **2006**, *128* (5), 1717–1722.
38. Sun, L. M.; Berndt, C. C.; Gross, K. A.; Kucuk, A. Material fundamentals and clinical performance of plasma-sprayed hydroxyapatite coatings: A review. *J. Biomed. Mater. Res.* **2001**, *58* (5), 570–592.
39. Itiravivong, P.; Promasa, A.; Laiprasert, T.; Techapongworachai, T.; Kuptniratsaikul, S.; Thanakit, V.; Heimann, R. Comparison of tissue reaction and osteointegration of metal implants between hydroxyapatite/Ti alloy coat: an animal experimental study. *J. Med. Assoc. Thailand* **2003**, *86* (2), S422–31.
40. Yang, Y. Z.; Kim, K. H.; Ong, J. L. Review on calcium phosphate coatings produced using a sputtering process - an alternative to plasma spraying. *Biomaterials* **2005**, *26* (3), 327–337.
41. Weiger, M. C.; Park, J. J.; Roy, M. D.; Stafford, C. M.; Karim, A.; Becker, M. L. Quantification of the binding affinity of a specific hydroxyapatite binding peptide. *Biomaterials* **2010**, *31* (11), 2955–2963.
42. McDonald, J. C.; Duffy, D. C.; Anderson, J. R.; Chiu, D. T.; Wu, H. K.; Schueller, O. J. A.; Whitesides, G. M. Fabrication of microfluidic systems in poly(dimethylsiloxane). *Electrophoresis* **2000**, *21* (1), 27–40.
43. Sia, S. K.; Whitesides, G. M. Microfluidic devices fabricated in poly(dimethylsiloxane) for biological studies. *Electrophoresis* **2003**, *24* (21), 3563–3576.
44. Roy, M. D.; Stanley, S. K.; Amis, E. J.; Becker, M. L. Identification of a highly specific hydroxyapatite-binding peptide using phage display. *Adv. Mater.* **2008**, *20* (10), 1830–+.
45. Segvich, S. J.; Smith, H. C.; Kohn, D. H. The adsorption of preferential binding peptides to apatite-based materials. *Biomaterials* **2009**, *30* (7), 1287–1298.

46. Food and Drug Adminstration. TyRx AIGIS(RX) Cardiac Rhythum Medical Device (CRMD) Anti-Bacterial Envelope. TyRx Pharma, Inc.: Monmouth Junction, NJ, 2008; p K063091.
47. Choueka, J.; Charvet, J.; Koval, K.; Alexander, H.; James, K.; Hooper, K.; Kohn, J. Canine bone response to tyrosine-derived polycarbonates and poly(L-lactic acid). *J. Biomed. Mater. Res.* **1996**, 35–41.
48. Bourke, S.; Kohn, J. Polymers derived from the amino acid L-tyrosine: polycarbonates, polyarylates and copolymers with poly(ethylene glycol). *Adv. Drug Delivery Rev.* **2003**, 447–466.
49. Bourke, S.; Kohn, J.; Dunn, M. Preliminary development of a novel resorbable synthetic polymer fiber scaffold for anterior cruciate ligament reconstruction. *Tissue Eng.* **2004**, 43–52.
50. Aamer, K.; Genson, K.; Kohn, J.; Becker, M. Impact of Polymer-Bound Iodine on Fibronectin Adsorption and Osteoblast Cell Morphology in Radiopaque Medical Polymers: Tyrosine-Derived Polycarbonate Blends as a Model System. *Biomacromolecules* **2009**, 2418–2426.

Downloaded by CORNELL UNIV on June 23, 2012 | http://pubs.acs.org
Publication Date (Web): November 18, 2010 | doi: 10.1021/bk-2010-1054.ch006

Chapter 6

Development of κ-Carrageenan Poly(acrylic acid) Interpenetrating Network Hydrogel as Wound Dressing Patch

Haydee Dalafu,[1] Modesto T. Chua,[2] and Soma Chakraborty[1,*]

[1]Chemistry Department, Ateneo de Manila University, Loyola Schools, Quezon City, Philippines
[2]Philippine Institute of Pure and Applied Chemistry, Loyola Schools, Loyola Heights, Quezon City, Philippines
[*]schakraborty@ateneo.edu

Interpenetrating network (IPN) of κ-carrageenan and poly(acrylic acid) was fabricated. Polyacrylic acid was synthesized as well as crosslinked in the presence of κ-carrageenan followed by crosslinking the κ-carrageenan in the presence of sodium ion. In order to fabricate glycidyl trimethyl ammonium chloride(Quat 188) modified κ-carrageenan IPN, κ-carrageenan was first coupled with Quat 188 in the presence of base followed by the fabrication of IPN. Analysis of the DSC thermogram revealed that the rigidity of the IPN improved with the increment of the κ-carrageenan content. Modification of κ-carrageenan further increased the rigidity. The IPNs swelled almost 300% in aqueous medium to form the hydrogels. Swelling was more pronounced in basic pH than in acidic pH. These hydrogels could incorporate approximately 94% of the prototype drug $AgNO_3$ in 30min from aqueous medium.

Introduction

Marine based polysaccharides are widely used in the food and pharmaceutical industry because of their biocompatibility and low toxicity. Some of these polysaccharides are polyelectrolytes and show great potential to interact with guest molecules and therefore are attractive materials as delivery vehicles for pharmaceutical attributes and food products. One such polysaccharide is

In Biomaterials; Kulshrestha, A., et al.;
ACS Symposium Series; American Chemical Society: Washington, DC, 2010.

carrageenan, a generic name for a family of natural, watersoluble galactans that are isolated from red seaweeds (*Rhodophycae*) mostly of genus *Chondrus, Euchema, Gigartina* and *Iridaea*. They are abundant and extensively produced by seaweed farmers in the Asia- Pacific region. Asia-Pacific region accounts for around 47% of total carrageenan production in the world of which the Philippines, is the largest producer and meets approximately 80% of the world supply (*1*).

Carrageenans, the linear sulfated polysaccharides consist of alternating 3-linked-β-D-galactopyranose and 4-linked-α-D-galactopyranose units. They differ from each other in sulfate content/position as well as in the presence of an anhydrous bridge on one of the monomers. Depending on the number and position of the sulphate hemi ester groups in the repeating dissacharide sequence, carrageenan has been classified as κ-carrageenan, ι-carrageenan and λ-carrageenan.

Carrageenans are widely used in the food industry as viscosity, gel, or texture enhancers stabilizers, and fat substitutes. They are incorporated into a wide range of products such as yogurt, chocolate milk, jellies, relishes, sauces, frozen desserts, cheese, and meat products. Among them κ-carrageenan, produced form *Kappaphycus cottonii*, forms a firm clear, strong and rigid gels and has been widely studied for drug delivery and other applications in biotechnology sectors. Certain cations such as K^+, Rb^+, Cs^+, Na^+ are found to induce conformational changes in κ-carrageenan, with initial coil to helix transition and subsequent aggregation in the form of gel (*2*, *3*).

Gelled κ-carrageenan in the form of hydrogel and micro/nanoparticles as controlled drug delivery vehicle has been studied extensively. It has been found that the drug release rate is strongly dependent on the characteristics of the gel structure (*4*). Microbeads of κ-carrageenan crosslinked by epichlorohydrin has been studied as a potential drug carrier (*5*). Basic butylated methacrylate copolymer/kappa-carrageenan interpolyelectrolyte complex has been studied for the release of ibuprofen (*6*). Hydrogels based on radiation induced copolymerization of N-isopropylacrylamide and κ- carrageenan has also been investigated as controlled release vehicle (*7*). Good film forming ability of κ-carrageenan can also be explored for the development of patches for the treatment of topical wounds due to burn.

Hydrogel patches are finding wide applications for burn and injury dressings (*8*, *9*). These dressings have water content in excess of 90% and have capacity to absorb wound exudates. They are expected have a cooling effect on the burn wound and thus reduce the severity of the pain. It is supposed to provide moist environment, soften any slough, providessterile cover and regulates the oxygen supply to the wound site to enable faster healing. Being transparent in nature, the progress of the wound healing can be observed without removing the dressing. In many cases, the use of hydrogels has been observed to prevent scar formation as well as to flatten old scars.

This research work explored the scope of fabrication of polyacrylic acid kappa-carrageenan interpenetrating network hydrogel for wound dressing from the burn as well as controlled delivery of therapeutic agent to expedite the healing process.

Downloaded by CORNELL UNIV on June 23, 2012 | http://pubs.acs.org
Publication Date (Web): November 18, 2010 | doi: 10.1021/bk-2010-1054.ch006

Polyacrylic acid(PAA) forms a hydrogel with superabsorbent properties (*10*). κ-carrageenan on the other hand, forms a gel. Thus in the IPN hydrogel of PAA with k-carragennan, PAA is expected to enhance the moisture retention ability and κ-carragennan to maintain the integrity of the patch. The system is expected to show good adhesion with the dermal layer due to the bio-adhesiveness of polyacrylic acid (*11*). This research also involves fabrication of IPN of PAA with modified kappa-carrageenan. Quat 188 (glycidyl trimethyl ammonium chloride) was used as the modifier in order to impart antimicrobial property to the wound patch. Quat 188 has proven antimicrobial property (*12*).

$AgNO_3$ was used as the model drug for incorporation in the hydrogel. Silver nitrate, when used with minimal amount only, can control burn wound sepsis.(*13*) Further growth of bacterial proteins is inhibited through precipitation of silver chloride

Downloaded by CORNELL UNIV on June 23, 2012 | http://pubs.acs.org
Publication Date (Web): November 18, 2010 | doi: 10.1021/bk-2010-1054.ch006

Materials

κ-Carrageenan was obtained from Rico Carrageenan. N,N-Methylenebisacrylamide (NN'MBA) was purchased from Fluka, NaOH was from J.T. Baker. Acrylic Acid (AA) and Quat 188 were obtained from Rohm and Haas Company and potassium persulfate from Aldrich. The chemicals were used as received.

Instrumental Methods

Shimadzu FTIR 820/PC was used to characterize the Quat 188 modified κ-carageenan by IR analysis. Samples for analysis were prepared by pelletizing the product with anhydrous KBr. Pellets were prepared from powdered samples mixed with dry KBr in the ratio of 1:100 (sample:KBr). The spectra were recorded in a transmitance mode from 4500 to 450 cm^{-1}.

Differential Scanning Calorimetry analysis of the samples was carried out using Shimadzu DSC-50 in a nitrogen atmosphere. Aluminum pans were used for the samples and reference pan. The rate of heating was 10°C/min from 20°C to 300°C. 5mg of hydrogel was placed in the pan per run. The hydrogels were dried at 40°C for 48h prior to use.

Inductively coupled plasma spectrometry was used to study the loading and release behaviours of the hydrogels with $AgNO_3$ as the model drug. The supernatant liquid from the drug loading and release experiments were subjected to ICP-spectrometry using Shimadzu ICPS 7510 instrument. 2 mL supernatant liquid sample was digested with 0.02 mL concentrated HNO_3 followed by adjustment with 5mL distilled water. Ar was used as the carrier gas with the flow rate of 0.7 L/min. It was also used as the cooling gas with the flow rate of 1.4 L/min. Silver ion was analyzed at 328.068 nm. Amount of silver ion was quantified using calibration curve method.

Downloaded by CORNELL UNIV on June 23, 2012 | http://pubs.acs.org
Publication Date (Web): November 18, 2010 | doi: 10.1021/bk-2010-1054.ch006

Methods

Modification of κ-Carrageenan with Glycidyl Trimethyl Ammonium Chloride (Quat 188)

0.5 g (1.18 mmoles) κ-carrageenan along with 0.665 g (3.54 mmoles) Quat 188 was added to a test tube with 15mL of deionized water. After the mixture has been homogenized by stirring, 0.88mL of 4 M NaOH solution (3.54 mmoles) was added. The modification was performed at 70°C for 48 hours with continuous stirring. After the reaction, the modified κ-carrageenan was allowed to settle at room temperature and was washed with hot acetonitrile three times to remove unreacted Quat 188. The product was filtered by vacuum filtration with Whatmann 4 filter paper and then dried with a blow drier.

Synthesis of Semi-IPN of Crosslinked Poly(acrylic acid) with κ-Carrageenan

Simultanious synthesis and crosslinking of PAA was performed in a round bottom flask in the presence of unmodified and modified κ-carrageenan. In a typical synthesis of 10% (by mol) crosslinked PAA, AA (0.10g, 1.39 mmoles) and κ-carrageenan (0.59g, 1.39 mmoles) were transferred in a round bottom flask containing 15mL of distilled water. The system was homogenized by stirring at room temperature using a magnetic stirrer. The crosslinking agent, NN'MBA(0.02g, 10 mol % w.r.t AA), was then added followed by the addition of $K_2S_2O_8$(4mg, 0.0148 mmoles) free radical initiator. The reaction mixture was stirred again at room temperature to make it homogenous. The homogenous reaction mixture was placed in a temperature-regulated water bath set at 70°C. The reaction was performed for 6 hours under constant stirring, The gels were then washed with deionized water three times to remove $K_2S_2O_8$, after which the samples were collected into small molds and dried at 40°C until a constant dry weight was obtained. κ-Carrageenan component of the semi-IPN was further crosslinked to form full IPN.

Crosslinking κ-Carrageenan To Form a Full-IPN

In order to synthesize full-IPN of κ-carrageenan and PAA, after the 6-hour synthesis of the semi-IPN described in the previous section, κ-carrageenan was crosslinked by adding 0.35mL of a NaOH solution (1.4×10^{-3} mols) followed by stirring at room temperature for 4h.

After crosslinking κ-carrageenan, the samples were collected into small molds and dried at 40°C until a constant dry weight was obtained. The amount of κ-carrageenan was varied to produce 1:1 and 5:1 κ-carrageenan – PAA mole ratio IPNs.

Swelling Test

The swelling behaviors of the synthesized Semi-IPNs were studied by allowing the dry hydrogels (0.1g) to swell in 15 mL of deionized water (pH 5.5)

Downloaded by CORNELL UNIV on June 23, 2012 | http://pubs.acs.org
Publication Date (Web): November 18, 2010 | doi: 10.1021/bk-2010-1054.ch006

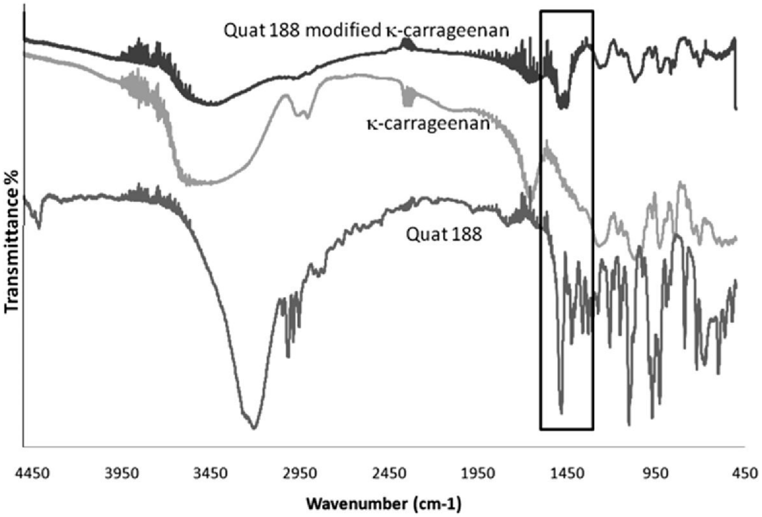

Figure 1. FTIR Spectra of Quat 188, κ-carrageenan and Quat 188 modified κ-carrageenan

and 0.2M pH 7 phosphate buffer solution. The percent swelling of the systems was computed as the function of time. At a given time % swelling is given by

$$\% \text{ Swelling} = \frac{W_t - W_0}{W_0} \times 100$$

Where W_t is the weight of the swelled hydrogel at time t and W_0 is the weight of the dry hydrogel.

Drug Incorporation

$AgNO_3$ as the model drug was incorporated in the hydrogel. The hydrogel was allowed to equilibrate in 2mL of deionized water for 30 minutes. This was followed by addition of 1mL of 0.001% (w/v) (10 µg/mL) of drugs in deionized water. The system was allowed to equilibrate for another for 30 minutes. The hydrogel with drugs was ultracentrifuged at 10,000 rpm for 30 minutes to allow the hydrogel to settle down. The supernatant was analyzed for the presence of residual drug that has not been incorporated in the hydrogel using ICP-OES technique.

Drug Release

The drug loaded hydrogel, after a quick washing with deionized water, was soaked in 5mL of deionized water and allowed to equilibrate for one hour. The supernatant was then decanted out and was analyzed for the amount of drug released from the hydrogel. ICP was used to analyze the presence of Ag^+ in the solution.

Results and Discussion

Quat 188 Modification

κ-Carrageenan was modified with Quat 188 in order to provide antimicrobial property to the hydrogel, which is important for the wound dressing application. The product obtained by the reaction of Quat 188 with κ-carrageenan was characterized using FTIR spectroscopy. The IR spectra of native κ-carrageenan, Quat 188 and Quat 188 modified κ-carrageenan are shown in Figure 1.

It can be observed that Quat 188 modified κ-carrageenan showed a peak at 1500cm^{-1} which is unique to the NH_2 scissoring. This absorption peak can be seen for the Quat 188 whereas it is absent for κ-carrageenan. Appearance of NH_2 scissoring for the modified κ-carrageenan is the evidence for the successful attachment of the Quat 188 to the κ-carrageenan chains. Furthermore, the IR spectrum of the acetonitrile washed of the product did not show the presence of residual Quat 188, indicating that the reaction between Quat 188 and κ-carrageenan was complete in 48h.

Strength of PAA κ-Carrageenan Semi-IPN

Semi-IPNs of κ-carrageenan and PAA that was fabricated by crosslinking PAA in the presence of κ-carrageenan were immersed in deionized water. The systems swelled rapidly and then ruptured. The time to rupture got delayed with the increase of the amount of crosslinker from 10-30 mol% wrt AA, however the system was not strong enough to act as the wound patch.

Strength of PAA, Na^+ Crosslinked κ-Carrageenan IPN

In order to enhance the rigidity of the system full IPN of PAA κ-carrageenan was fabricated by further crosslinking the κ-carrageenan chains of the semi-IPN in the presence of Na^+. NaOH solution was added to the semi-IPN that was crosslinked with 30 mol% of NN'MBA. The system was stirred at room temperature. At the initial stage of stirring white colored agglomerates were observed at several parts of the reaction pot which disappeared gradually over time. 4h of continuous stirring produced a homogenous mixture with no agglomeration.

Furthermore it was observed that the hydrogel swelled in deionized water without rupturing. Hence PAA- κ-carrageenan system was studied further as full IPN of PAA and κ-carrageenan with two different mole ratio of PAA and κ-carrageenan.

Rigidity of PAA κ-Carrageenan IPN

Two types of IPNs were fabricated by varying the ratio of PAA and κ-carrageenan. Transition temperature of two types of dry hydrogels was determined by DSC technique and compared with the transition temperature of κ-carrageenan. As shown in Fig 2 the transition temperature of the IPN (96.27°C) where the ratio of PAA to κ-carrageenan was 1:1 is lower than the transition

Downloaded by CORNELL UNIV on June 23, 2012 | http://pubs.acs.org
Publication Date (Web): November 18, 2010 | doi: 10.1021/bk-2010-1054.ch006

Downloaded by CORNELL UNIV on June 23, 2012 | http://pubs.acs.org
Publication Date (Web): November 18, 2010 | doi: 10.1021/bk-2010-1054.ch006

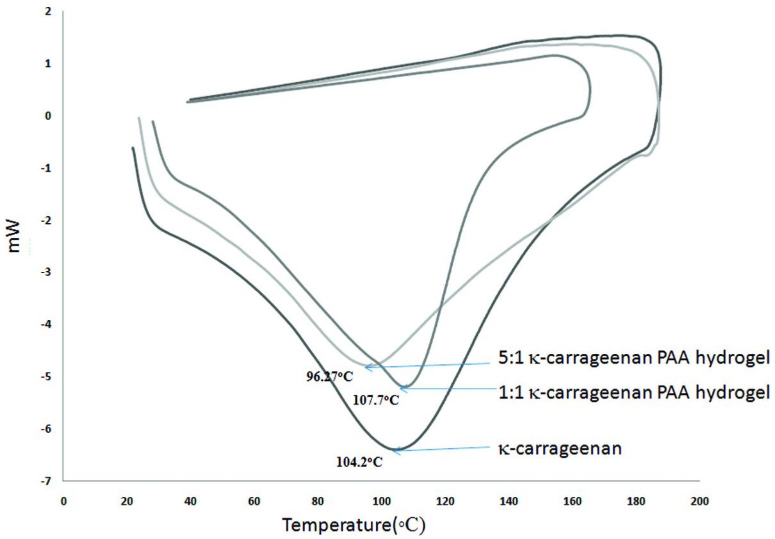

Figure 2. DSC profile of κ-carrageenan PAA IPN with different amount of κ-carrageenan, keeping the PAA amount constant

temperature of κ-carrageenan (104.2°C). Lowering of transition temperature can be attributed to the tremendous moisture absorbing capacity of PAA. Moisture absorbed by PAA that could not be removed by drying might have acted as plasticizer and lowered the transition temperature. However on increasing the amount of κ-carrageenan by changing the ratio of amount of κ-carrageenan: PAA to 5:1, the transition temperature increased to 107.7°C, indicating that κ-carrageenan in crosslinked form enhances the structural integrity of the hydrogel.

When the transition temperature of κ-carrageenan and Quat 188 modified κ-carrageenan was compared, it was observed that modified κ-carrageenan undergoes transition at higher temperature (113.1°C) over the unmodified one as seen in Figure 3. This transition temperature got lowered to 112°C when IPN was fabricated from modified κ-carrageenan and PAA in the ratio of 5:1 respectively, most probably due to the plasticization effect of PAA as discussed earlier. However this transition temperature still remained higher than the transition temperature of κ-carrageenan and PAA with similar composition. This observation reveals that apart from imparting antimicrobial property, Quat 188 can also impart rigidity to the hydrogel patch and can prevent its rupturing.

Swelling Kinetics

Modified and unmodified κ-carrageenan PAA IPNs were subjected to swell as function of time and pH. It was observed that the hydrogels swelled rapidly after immersion in the soaking medium, reached a saturation point beyond which no further swelling was observed. The hydrogels swelled more with the increment of the pH as seen in Figure 4. Maximum swelling was observed at

Downloaded by CORNELL UNIV on June 23, 2012 | http://pubs.acs.org
Publication Date (Web): November 18, 2010 | doi: 10.1021/bk-2010-1054.ch006

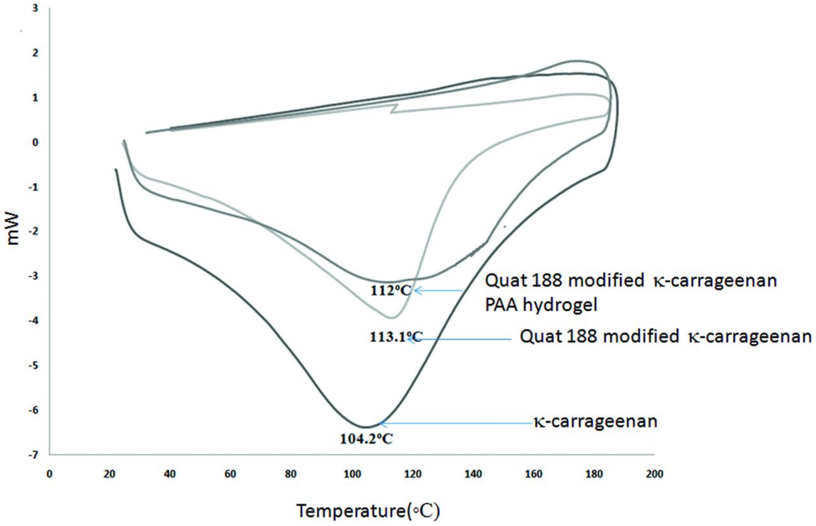

Figure 3. DSC profile of Quat 188, Quat 188 modified κ-carrageenan and Quat 188 modified κ-carrageenan PAA IPN

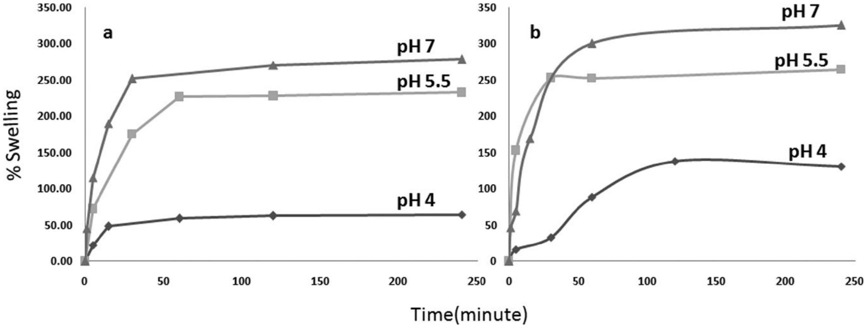

Figure 4. Swelling curves κ-carrageenan PAA IPN hydrogel as function of pH (a) κ-carrageenan to PAA ratio is 1:1 (b) κ-carrageenan to PAA ration is 5:1

pH 7, approximately 300%. This can be attributed to the repulsion between the carboxylate ions of PAA that are formed at higher pH.

It has also been observed that there is marginal increment in swelling with the increased amount of κ-carrageenan in the system. This is probably due to the presence of more –OH groups from the κ-carrageenan that interacted with the water molecules.

When the swelling of the 5:1 κ-carrageenan PAA hydrogel was compared 5:1 Quat 188 modified κ-carrageenan PAA hydrogel at pH 5.5, it was observed that unmodified κ-carrageenan hydrogel swelled more than the modified κ-carrageenan hydrogel as shown in Figure 5. Less swelling of the modified κ-carrageenan hydrogel can be attributed to the more integrated form of the IPN network as revealed by the DSC thermogram.

Downloaded by CORNELL UNIV on June 23, 2012 | http://pubs.acs.org
Publication Date (Web): November 18, 2010 | doi: 10.1021/bk-2010-1054.ch006

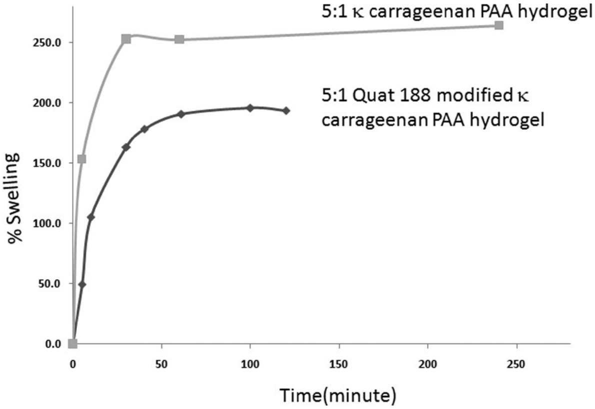

Figure 5. Swelling curves Quat 188 modified κ-carrageenan PAA IPN and κ-carrageenan PAA IPN hydrogel in pH 5.5

Table 1. Encapsulation and release of $AgNO_3$ from κ-carrageenan PAA IPN

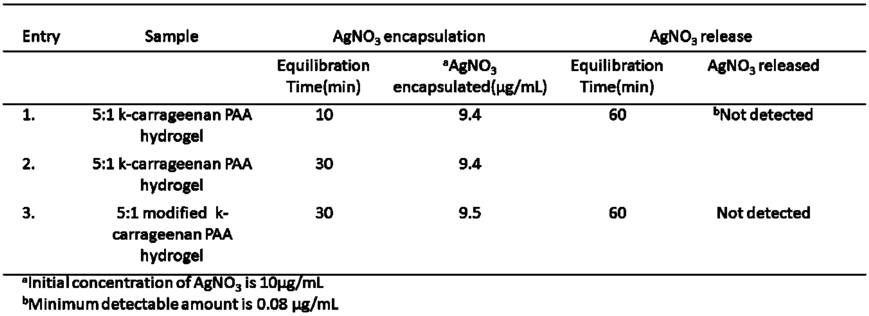

Entry	Sample	$AgNO_3$ encapsulation		$AgNO_3$ release	
		Equilibration Time(min)	[a]$AgNO_3$ encapsulated(μg/mL)	Equilibration Time(min)	$AgNO_3$ released
1.	5:1 k-carrageenan PAA hydrogel	10	9.4	60	[b]Not detected
2.	5:1 k-carrageenan PAA hydrogel	30	9.4		
3.	5:1 modified k-carrageenan PAA hydrogel	30	9.5	60	Not detected

[a] Initial concentration of $AgNO_3$ is 10μg/mL
[b] Minimum detectable amount is 0.08 μg/mL

Since these hydrogels have the potential to hold large amount of water, they are expected to be effective towards providing cooling sensation to the site of dermal injury.

Drug Encapsulation and Release

$AgNO_3$ which is used for the treatment of wound due to burn was incorporated in the hydrogels by equilibrating the swelled hydrogel in $AgNO_3$ solution. Amount of $AgNO_3$ released from the hydrogel was estimated by allowing the drug loaded hydrogel to equilibrate in deionized water for 1h. ICP-spectometry analysis was performed to determine the concentration of $AgNO_3$ in deionized water. The amount of drug encapsulated and released by the hydrogels is given in Table 1.

As shown in Table 1, most of the drug (94%) got incorporated in first 10 min of equilibration both for the modified and unmodified κ-carrageenan PAA IPN. However 100% drug loading was not achieved in spite of increasing the equilibration time from 10 min to 30 min for the unmodified κ-carrageenan PAA IPN.

Though efficient drug loading was possible using the fabricated IPNs, these IPNs did not release the drug when the drug loaded hydrogels were equilibrated in deionized water for 1h. Chelation of the Ag^+ ions by the hydroxyl ions of carrageenan might have prevented the release of $AgNO_3$. Increase in the equilibration time might have allowed the release of the drug.

Conclusion

κ-carrageenan and PAA can interpenetrate to form IPN hydrogels. Strength of the dry hydrogels increased with the increase in κ-carrageenan content. Modification of κ-carrageenan by coupling with Quat 188 further improved the dry strength of the hydrogels. These IPN hydrogels swelled almost 300 times. Swelling enhanced as the pH of the soaking medium became more basic. The hydrogels encapsulated 94% of the drug AgNO3 when equilibrated in deionized water for 10 minutes. However no release was observed in deionized water. Increase of equilibration time or tailoring of the IPN by changing the κ-carrageenan to PAA ratio, the amount of crosslinker might facilitate more drug release.

Since these hydrogels can retain a large amount of water and also can encapsulate silver nitrate in a short period of time, the can be explored as dermal patch for the treatment of wound due to burn.

Acknowledgments

Authors would like to acknowledge chemistry department, Ateneo de Manila University for supporting this project.

References

1. http://www.fao.org/docrep/006/Y4765E/y4765e09.htm.
2. MacArtain, P. J.; Jacquier, C.; Dawson, K. A. *Carbohydr. Polym.* **2003**, *53*, 395–400.
3. Nickerson, M. T.; Paulson, A. T. *Carbohydr. Polym.* **2005**, *61*, 231–237.
4. Mangione, M. R.; Giacomazza, D.; Cavallaro, G.; Bulone, D.; Martorana, V.; San Biagio, P. L. *Biophys. Chem.* **2007**, *129* (1), 18–22.
5. Keppeler, S.; Ellis, A.; Jacquier, J. C. *Carbohydr. Polym.* **2009**, *78*, 973–977.
6. Prado, H. J.; Matulewicz, M. C.; Bonelli, P.; Cukierman, A. L. *Eur. J. Pharm. Biopharm.* **2008**, *70*, 171–178.
7. Zhai, M.; Zhang, Y.; Ren, J.; Yi, M.; Ha, H.; Kennedy, J. F. *Carbohydr. Polym.* **2004**, *58*, 35–39.
8. Blanco, M. D.; Bernardo, M. V.; Teijon, C. R.; Sastre, L.; Teijon, J. M. *Int. J. Pharm.* **2003**, *255* (1−2), 99–107.
9. Boucarda, N.; Viton, C.; Agay, D.; Mari, E.; Roger, T.; Chancerelle, Y.; Domard, A. *Biomaterials* **2007**, *28* (24), 3478–3488.
10. Lin, J.; Wu, J.; Yang, Z.; Pu, M. *Macromol. Rapid Commun.* **2001**, *22* (6), 422–424.

Downloaded by CORNELL UNIV on June 23, 2012 | http://pubs.acs.org
Publication Date (Web): November 18, 2010 | doi: 10.1021/bk-2010-1054.ch006

11. Cui, F.; Qian, F.; Yin, C. *Int. J. Pharm.* **2006**, *316* (1−2), 154–161.
12. Kim, J.; Lee, J.; Lee, T.; Park, W. *Int. J. Biol. Macromol.* **2003**, *32*, 23–37.
13. Morris, F.; Bondoc, C.; Burke, J. *J. Surg.* **2008**, *41*, 108–111.

Downloaded by CORNELL UNIV on June 23, 2012 | http://pubs.acs.org
Publication Date (Web): November 18, 2010 | doi: 10.1021/bk-2010-1054.ch006

Chapter 7

Absorbable Polyurethanes

Rao S. Bezwada[*]

Bezwada Biomedical LLC, 15-1 Ilene Court, Hillsborough, New Jersey, 08844, USA
[*]Rao@bezwadabiomedical.com

Downloaded by UNIV OF DELAWARE MORRIS LIB on June 23, 2012 | http://pubs.acs.org
Publication Date (Web): November 18, 2010 | doi: 10.1021/bk-2010-1054.ch007

For the first time, a number of hydrolytically degradable aromatic isocyanates including diisocyanates are synthesized. These highly reactive diisocyanates are similar to MDI but are biodegradable and have tunable hydrolytic degradation profiles. What distinguishes these isocyanates from the commonly used isocyanate, MDI, is the presence of a hydrolytically degradable linkage bridging the aromatic rings instead of the non-degradable methylene group. Absorbable polyurethanes with hydrolytically degradable hard segments were prepared from these isocyanates. Physical and mechanical properties of absorbable polyurethanes along with their hydrolytic degradation profiles is presented and discussed.

1. Polyurethanes

Polyurethanes are segmented block copolymers containing blocks of low molecular weight polyesters or polyethers linked together via a urethane group. Depending on their composition and structure, they can exist in linear form (thermoplastic polyurethanes), cross-linked (thermosetting polyurethanes) and expanded (urethane foams) (*1*).

Polyurethanes are prepared via reaction between three monomers: a) an isocyanate, b) a macroglycol or polyol and 3) a chain extender or curative. The reaction advances with the nucleophilic attack on the carbon atom of the isocyanate group by a nucleophilic group (OH, NH_2) present in various compounds such as alcohols and amines. Attack by an alcohol results in the formation of a urethane group (-NH-CO-O-). In the case of amines, urea (-NH-CO-NH-) bonds are formed and poly(urea-urethanes) are obtained.

In Biomaterials; Kulshrestha, A., et al.;
ACS Symposium Series; American Chemical Society: Washington, DC, 2010.

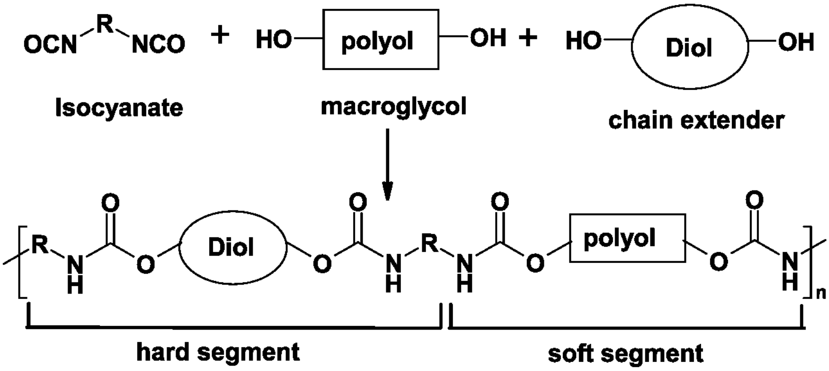

Figure 1. Polyurethane synthesis.

As shown in Figure 1, thermoplastic polyurethane comprises of two segments: a) *hard segment* formed by the reaction between isocyanate and chain extender and b) a *soft segment* formed by the reaction between isocyanate and a macroglycol. Segmented polyurethanes can be prepared in two different ways: a) in a one step process wherein the isocyanate, chain extender and macroglycol are mixed together in one step, or b) in a two step process in which prepolymers are first synthesized by reacting isocyanates with macroglycol and then this prepolymer is reacted with a chain extender to form high molecular weight polyurethane. The two-step process is used more in the preparation of medical grade segmented polyurethanes.

In contrast to the soft segment, which is elastic, the hard segment has a rigid nature, either glass or semi-crystalline. Due to incompatibility between the two segments, these materials are characterized by a separation of phases in the solid state; the resulting two-phase structure is formed by aggregates or domains of hard segments dispersed in the elastomeric matrix of the soft segment. Hard segments, dispersed in a matrix of soft segments, act as reinforcing particles and behave as physical cross-linking sites, which are reversible at high temperatures, giving the material elastomeric characteristics. Furthermore, these materials can undergo typical processing of the polymeric materials and once cooled, they behave again as chemically crosslinked rubber.

Figure 2 displays the structures and names of some common commercially important isocyanates used in polyurethane production. As shown, they can be aromatic or aliphatic. 4,4′-methylenebis(phenylisocyanate) (MDI) is the most commonly used aromatic isocyanate used in the polyurethane industry. It is a highly reactive isocyanate, in fact, so reactive that in many cases, a catalyst is not required for polyurethane synthesis.

Aromatic isocyanates are generally more reactive (*2*) than aliphatic isocyanates and yield polyurethanes with mechanical properties superior to those of aliphatic polyurethanes (*3*). This is attributed to the ability of aromatic polyurethanes to form much stronger intermolecular bonds than aliphatic polyurethanes. The hard segments in aromatic polyurethanes tend to be semicrystalline or crystalline in nature. Contrary to this, hard segments

Downloaded by UNIV OF DELAWARE MORRIS LIB on June 23, 2012 | http://pubs.acs.org
Publication Date (Web): November 18, 2010 | doi: 10.1021/bk-2010-1054.ch007

Downloaded by UNIV OF DELAWARE MORRIS LIB on June 23, 2012 | http://pubs.acs.org
Publication Date (Web): November 18, 2010 | doi: 10.1021/bk-2010-1054.ch007

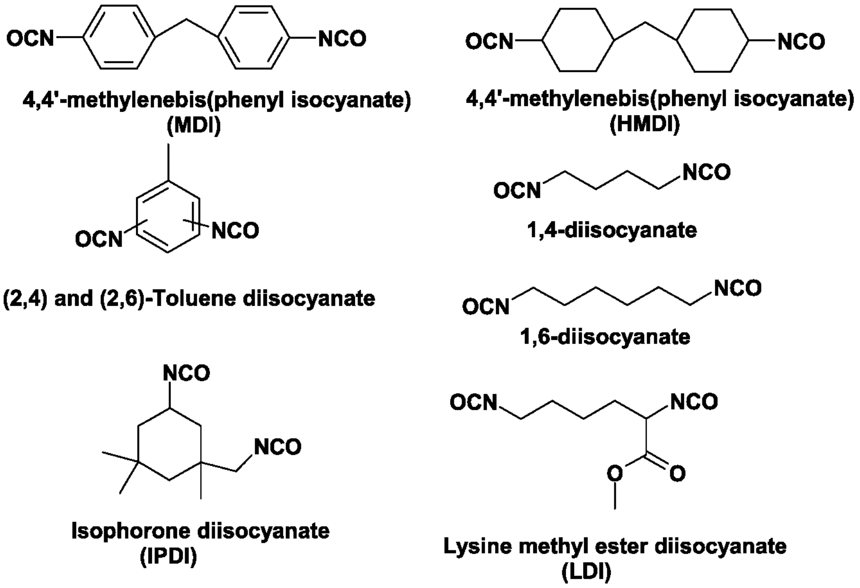
OCN
NCO
4,4'-methylenebis(phenyl isocyanate)
(MDI)
OCN
NCO
4,4'-methylenebis(phenyl isocyanate)
(HMDI)
OCN
NCO
(2,4) and (2,6)-Toluene diisocyanate
OCN
NCO
1,4-diisocyanate
OCN
NCO
1,6-diisocyanate
NCO
NCO
Isophorone diisocyanate
(IPDI)
OCN
NCO
O
O
Lysine methyl ester diisocyanate
(LDI)

Figure 2. Isocyanates of commercial importance.

Table 1. Selected commercial medical grade polyurethanes (see color insert)

Manufacturer	Trade Name	Isocyanate	Chain Extender	Polyol
Technical Polymers	Elastane	MDI	1,4-Butanediol	PTMEG
DSM PTG	Biospan	MDI	Diamine	Polyether
Lubrizol	Tecoflex	HMDI	1,4-Butanediol	Polyether
DSM PTG	Bionate	MDI	Diamine	Polycarbonate
Dow Chemical	Pellethane	MDI	1,4-Butanediol	PTMEG

DSM PTG: DSM Polymer Technology Group, PTMEG: Poly (tetramethyelene ether) glycol, MDI: 4,4'-diphenylmethane diisocyanate, HMDI: Hydrogenated MDI

containing aliphatic isocyanates do not have the ability to crystallize. Since more crystalline hard segments help more phase separation in the copolymer, mechanical properties of aromatic polyurethanes are better than those of aliphatic polyurethanes.

Although both aromatic and aliphatic polyurethanes are used in commercial biomedical-grade polyurethanes, as shown in Table 1, the majority of the medical grade polyurethanes are based on aromatic diisocyanate, MDI.

Downloaded by UNIV OF DELAWARE MORRIS LIB on June 23, 2012 | http://pubs.acs.org
Publication Date (Web): November 18, 2010 | doi: 10.1021/bk-2010-1054.ch007

2. Absorbable Polyurethanes

Biostable polyurethanes represent a diverse family of materials with the versatility of being rigid, semi-rigid and flexible (*1*, *4*, *5*). They are used in a wide variety of biomedical applications (*4–10*), including short-term medical devices (catheters, endotracheal tubes and cannulas), long-term implantable devices (vascular prostheses, intra-aortic balloons), tissue engineering scaffolds, infusion pumps and cardiac pacemakers. This is attributed to their excellent biocompatibility, outstanding hydrolytic stability, superior abrasion resistance, excellent physical strength, high flexural endurance and ease of processability (*4–11*).

There is a great demand for high strength elastomeric absorbable polymers for various biomedical applications in recent years. These biomedical applications include tissue-engineering applications such as artificial veins, skin, nerve guides and meniscus prostheses. In this regards, polyurethane class of polymers are viable candidates for elastomeric absorbable materials. However, relatively little research has been done so far at developing absorbable polyurethanes for biomedical applications. Several papers were published in the early 1980's describing polyurethane/polylactide blends as degradable materials for skin substitutes, vascular prostheses and nerve regeneration guides. However, in these cases the polyurethane portion of the blend was non-degradable and served only to provide favorable mechanical properties (*12*). Subsequent work by Bruin et al. (*13*) involved the synthesis of crosslinked polyurethane networks incorporating a lactide or glycolide, and an epsilon-caprolactone joined by a lysine-based diisocyanate. These polymers displayed good elastomeric properties and were found to degrade within 26 weeks in vitro and 12 weeks in vivo (subcutaneous implantation in guinea pigs). However, a drawback of this approach is that the highly crosslinked polymer may not be processed by standard techniques such as solution casting or melt processing, as is the case for typical linear, segmented polyurethanes. Furthermore, Cohn et al. (*14*) developed a series of elastomeric polyester-polyether-polyurethane block copolymers intended for use as surgical articles. Beckmann et al. (*15*) developed polyurethane based biodegradable adhesive from multi-isocyanate functional molecules and multifunctional precursor molecules with terminal groups selected from hydroxyl and amino groups. Woodhouse et al. (*16*) developed absorbable polyurethanes from lysine diisocyanate and lysine triisocyanate and polyols. Fuller et al. (*17*) developed absorbable polyurethanes based on biodegradable isocyanates from diols and nitrobenzoic acid. However, synthetic methods used by Fuller et al. to prepare these biodegradable polyisocyanates may be quite cumbersome and cost ineffective. Aliphatic poly(ester-urethane)s with tunable degradation rates and mechanical properties were developed from alternating blocks of crystalline poly[R-3-hydroxybutyric acid-co-R-3-hydroxyvaleric acid]-diol (PHB) and amorphous poly[glycolide-co-caprolactone]-diol linked by aliphatic isocyanates (LDI and 2,2,4-trimethyl-hexamethlene diisocyanate) (*19*, *20*). Similarly, Gunatillake et al (*21–25*) developed biodegradable poly(ester-urethanes) from LDI and polyester polyols.

Downloaded by UNIV OF DELAWARE MORRIS LIB on June 23, 2012 | http://pubs.acs.org
Publication Date (Web): November 18, 2010 | doi: 10.1021/bk-2010-1054.ch007

Table 2. Comparison between prior art and our state-of-the-art (see color insert)

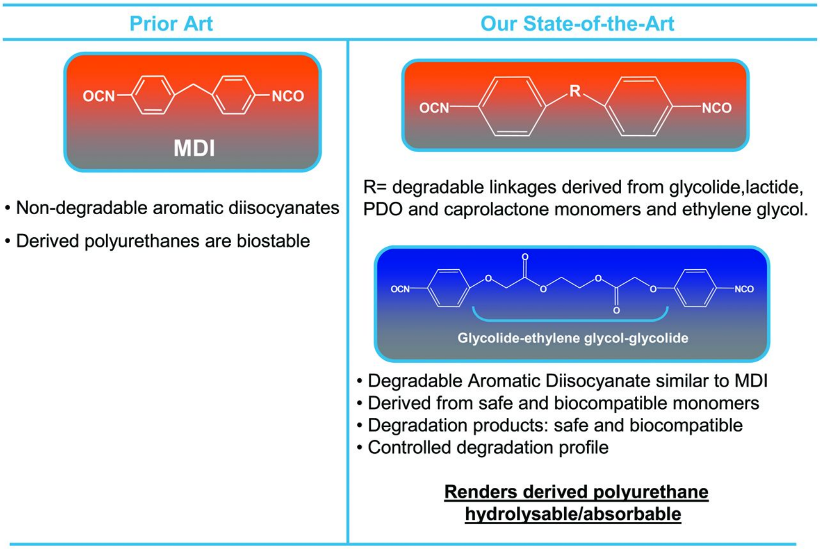
OCN
NCO
R
OCN
NCO
O
O
O
O
OCN
NCO

Prior Art	Our State-of-the-Art
MDI • Non-degradable aromatic diisocyanates • Derived polyurethanes are biostable	R= degradable linkages derived from glycolide,lactide, PDO and caprolactone monomers and ethylene glycol. Glycolide-ethylene glycol-glycolide • Degradable Aromatic Diisocyanate similar to MDI • Derived from safe and biocompatible monomers • Degradation products: safe and biocompatible • Controlled degradation profile **Renders derived polyurethane hydrolysable/absorbable**

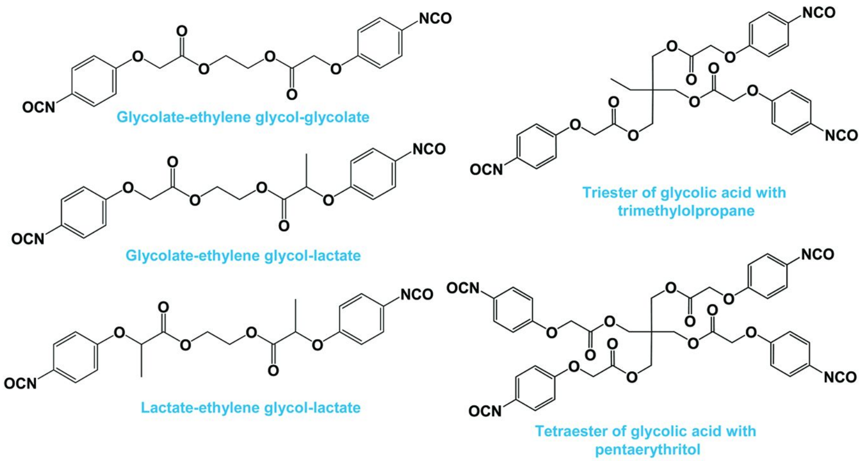
NCO
OCN
Glycolate-ethylene glycol-glycolate
NCO
OCN
Glycolate-ethylene glycol-lactate
NCO
OCN
Lactate-ethylene glycol-lactate
NCO
NCO
OCN
Triester of glycolic acid with trimethylolpropane
OCN
NCO
NCO
OCN
Tetraester of glycolic acid with pentaerythritol

Figure 3. Examples of hydrolytically degradable aromatic isocyanates (see color insert)

However, all these absorbable polyurethanes suffered from the following drawbacks: a) they did not have hydrolysable hard segments (b) the rate of formation of polyurethane is very slow, and this is attributed to the low reactivity of the isocyanates; and (c) they did not have tunable physical and mechanical properties, and controllable hydrolytic degradation profiles.

In the present paper, we report the synthesis of hydrolytically degradable aromatic diisocyanates and absorbable polyurethanes with hydrolytically degradable hard segments. The mechanical properties are compared with those of present day biostable polyurethanes based on non-degradable aromatic isocyanates. Furthermore, the hydrolytic degradation profiles of these polyurethanes are compared as function of the type and soft segment content.

2.1. Hydrolytically Degradable Aromatic Isocyanates

Highly reactive isocyanates that are similar to MDI but are biodegradable and have tunable hydrolytic degradation profiles were synthesized (*12*, *18*, *26*, *27*). What distinguishes these isocyanates from the commonly used isocyanate, MDI, is the presence of a hydrolytically degradable linkage bridging the aromatic rings instead of the non-degradable methylene group. Furthermore, the degradable linkage in these isocyanates is derived from safe and biocompatible glycolic acid, lactic acid, caprolactone, p-dioxanone and diols, examples of which are shown in Figure 3. A comparison between the prior art and our state-of-the-art is given below in Table 2.

In the following section, synthesis and characterization of three hydrolytically degradable diisocyanates is described. These isocyanates are labeled as BB002 BB003 and BB004 as shown in Figure 4. Out of these only BB002 and BB004 diisocyanates were used as the precursor for preparing absorbable polyurethanes of the present study.

Downloaded by UNIV OF DELAWARE MORRIS LIB on June 23, 2012 | http://pubs.acs.org
Publication Date (Web): November 18, 2010 | doi: 10.1021/bk-2010-1054.ch007

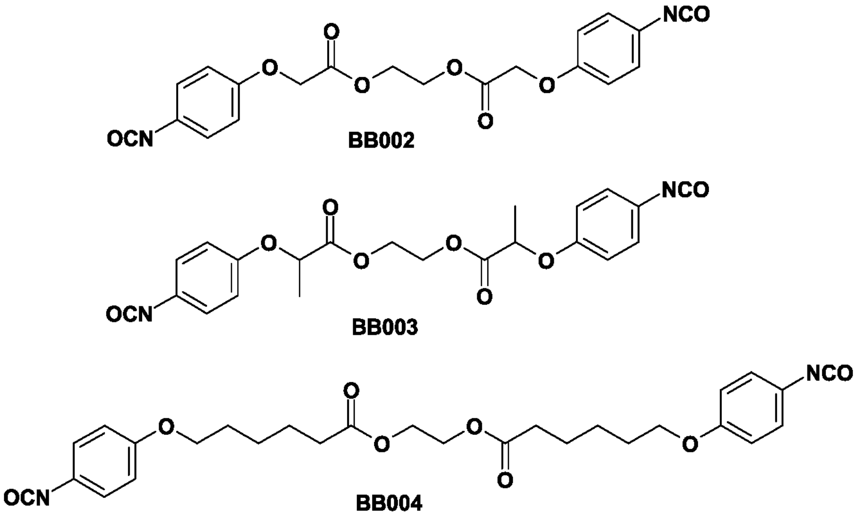

Figure 4

2.2. Synthesis and Characterization of Hydrolytically Degradable Isocyanates

2.2.1. Synthesis of BB002

Step 1: Synthesis of Methyl (4-Nitro phenoxy) acetate (1)

Downloaded by UNIV OF DELAWARE MORRIS LIB on June 23, 2012 | http://pubs.acs.org
Publication Date (Web): November 18, 2010 | doi: 10.1021/bk-2010-1054.ch007

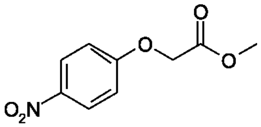

To a mixture of 4-nitrophenol (100 g, 719 mmol) and anhydrous K_2CO_3 (400 gm, 2.894 mol) in anhydrous acetone (950 ml) was added methyl chloroacetate (114 g, 1.050 moles) and refluxed for 12 hours. Acetone was distilled off and water (1500 ml) was added. Crude **1** was filtered, dried and recrystallised from a mixture of ethyl acetate: hexane (1:5) to give pure **1** (110 g, 72.5%) as a white fluffy powder with a melting point between 97-98°C

Step 2: Synthesis of (4-Nitrophenoxy) acetic acid (**2**)

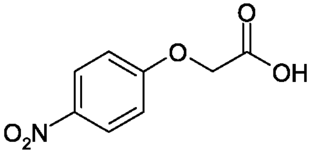

Methyl (4-nitrophenoxy) acetate **1** (100 g, 474 mmol) was refluxed in conc. HCl (1 L) for 8 hours. The reaction mass was cooled to room temperature and crude 2 was filtered, dried and recrystallized from a mixture of ethyl acetate:hexane (1:5) to give pure **2** (86 g, 92.1%) as a white shining powder with a melting point between 186-188°C.

Step 3: Synthesis of (4-Nitrophenoxy)-acetic acid-2-hydroxy-ethyl ester (**3**)

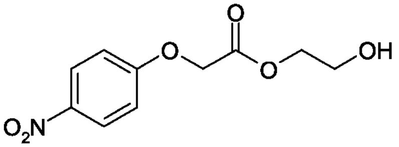

Dry HCl gas was passed through a mixture of (4-nitrophenoxy) acetic acid 2 (100 g, 507 mmol) and ethylene glycol (300 ml) for 1 hour. During HCl gas bubbling the temperature rose to 60°C. The crude reaction mass was poured onto ice (2 kg). Crude **3** was filtered, dried and purified by column chromatography on silica gel using hexane: ethyl acetate (95:5) to give pure **3** (70 g, 57.4%) as a white powder with a melting point between 74-76°C. ^{1}HNMR ($CDCl_3$) δ 3.70 (m, 2H, CH_2), 4.28 (m, 2H, $OCOCH_2$), 4.56 (6m, 1H, OH), 4.80 (s, 2H, OCH_2), 7.00 (d, 2H, Ar), 8.16 (d, 2H, Ar)

Step 4: Synthesis of (4-Nitrophenoxy)-acetic acid-2-[2-(4-nitrophenoxy)-acetoxy]-ethyl ester (**4**)

Downloaded by UNIV OF DELAWARE MORRIS LIB on June 23, 2012 | http://pubs.acs.org
Publication Date (Web): November 18, 2010 | doi: 10.1021/bk-2010-1054.ch007

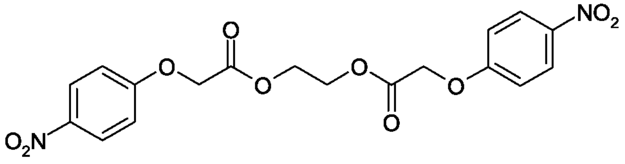

To a mixture of (4-nitrophenoxy) acetic acid 2 (80 g, 406 mmol) and (4-nitrophen-oxy)-acetic acid-2-hydroxyethyl ester 3 (80 g, 332 mmol) in anhydrous dichloromethane (2 L) under nitrogen atmosphere was added a solution of 1,3-di-cyclohexyl carbodiimide (128 g, 620 mmol) in anhydrous dichloromethane (750 ml) drop wise. The reaction mixture was stirred at room temperature for 8 hours. The solids were filtered off and dichloromethane distilled off to get crude 4. The crude 4 was purified by column chromatography on silica gel using hexane:ethyl acetate (95:5) to get pure 4 (75 grams, 54%) as a white powder with a melting point between 138-139°C.

Step 5: Synthesis of (4-Amino-phenoxy)-acetic acid-2-[2-(4-amino-phenoxy)-acetoxy]-ethyl ester (5)

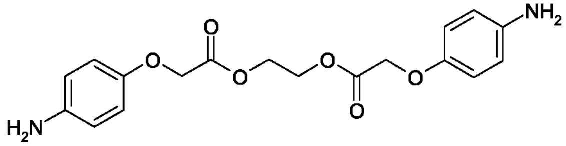

(4-Nitrophenoxy)-acetic acid-2-[2-(4-nitrophenoxy)-acetoxy]-ethyl ester 4 (100 g, 238 mmol) was dissolved in dry dimethyl formamide (500 ml) in a pressure vessel, palladium on carbon (5%, 22 g) was added, and the mixture stirred under an atom-sphere of hydrogen (4 kg) for 6 hours. The catalyst was removed by filtration and ice water (2.5 L) was added to the filtrate. Crude 5 was filtered off, dried and recrystallized in a mixture of methanol: chloroform (1:1) to give pure 5 (65 g, 78%) as a light brown shining powder with a melting point between 124-126°C. ^{1}HNMR ($CDCl_3$) δ 4.40 (s, 2H, $OCOCH_2$), 4.50 (s, 2H, OCH_2), 6.54 (d, 2H, Ar), 6.70 (d, 2H, Ar), 7.26 (s, 2H, NH_2)

Step 6: Synthesis of (4-Isocyanatophenoxy)-acetic acid 2-[2-(4-isocyanatophenoxy)-acetoxy]-ethyl ester (6)

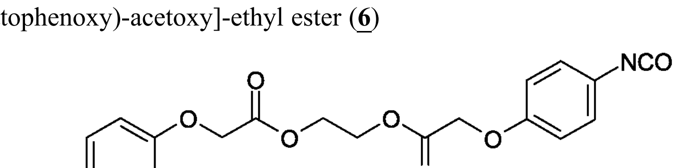

(4-Aminophenoxy)-acetic acid 2-[2-(4-aminophenoxy)-acetoxy]-ethyl ester 5 (5 g, 14.3 mmol) were dissolved in dry dioxane (80 ml) under nitrogen atmosphere and cooled to below 20°C. A solution of triphosgene (7 g, 23.6 mmol) in dry dioxane (20 ml) was added drop wise. The mixture was heated slowly to 75-80°C and maintained for 2 ½ hours. The condenser was then arranged for distillation

Downloaded by UNIV OF DELAWARE MORRIS LIB on June 23, 2012 | http://pubs.acs.org
Publication Date (Web): November 18, 2010 | doi: 10.1021/bk-2010-1054.ch007

and solvent removed by distillation at atmospheric pressure until the volume of the reaction mixture was reduced to approximately one third. Fresh dry dioxane (50 ml) was added and the solvent was distilled off under vacuum. The residue was re-evaporated two times from dry dioxane to give crude **6**. Crude 6 was recrystallized from a mixture of toluene: hexane (1:3) to give pure **6** (2.6 g, 44.2%) as a white powder with a melting point between 96-98°C [BB002]. ^{1}HNMR ($CDCl_3$) δ 4.45 (s, 2H, $OCOCH_2$), 4.62 (s, 2H, OCH_2), 6.85 (d, 2H, Ar), 7.04 (s, 2H, Ar); IR: 2274 cm^{-1}

2.2.2. Synthesis of BB003

Step 1: Synthesis of 2-(4-Nitrophenoxy)-propionic acid methyl ester (7)

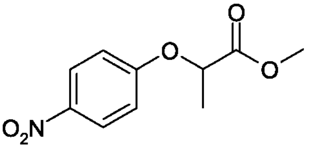

To a mixture of 4-nitrophenol (200 g, 1.439 mol), anhydrous K_2CO_3 (800 g, 5.789 mol) and sodium iodide (10 g, 66.7 mmol) in anhydrous acetone (2.75 L) was added methyl 2-chloropropionate (264 g, 2.154 mol) and refluxed for 20 hours. Acetone was distilled off and water (3 L) was added. Crude 7 was filtered, dried and recrystallised from a mixture of ethyl acetate: hexane (1:5) to give pure 7 (100 g, 31%) as a white fluffy powder with a melting point between 83-84°C.

Step 2: Synthesis of 2-(4-Nitrophenoxy)-propionic acid (**8**)

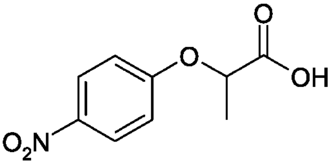

2-(4-Nitrophenoxy) propionic acid methyl ester 7 (50 g) and conc. HCl (500 ml) were refluxed for 8 hours. The reaction mass was cooled to room temperature. Crude **8** was filtered, dried and recrystallised from a mixture of ethyl acetate: hexane (1:5) to give pure **8** (40 g, 85.3%) as a white powder with a melting point between 139-141°C.

Step 3: Synthesis of 2-(4-Nitrophenoxy)-propionic acid 2-hydroxy-ethyl ester (**9**)

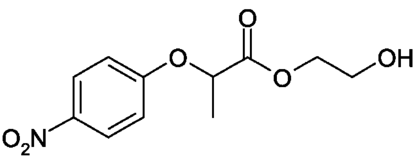

Downloaded by UNIV OF DELAWARE MORRIS LIB on June 23, 2012 | http://pubs.acs.org
Publication Date (Web): November 18, 2010 | doi: 10.1021/bk-2010-1054.ch007

Dry HCl gas was passed through a mixture of 2-(4-nitrophenoxy)-propionic acid 8 (45 g, 213 mol) and ethylene glycol (135 ml) for 1 ½ hours. During HCl gas bubbling the temperature rose to 60°C. The crude reaction mass was poured onto cold water (600 ml). Crude 9 was extracted into chloroform, dried over Na_2SO_4, distilled and purified by column chromatography on silica gel using hexane as eluant to give pure 9 (28 g, 56.8%) as a syrup. ^{1}HNMR ($CDCl_3$) δ 1.62 (d, 3H, CH_3), 2.64 (bs, 1H, OH), 3.68 (m, 2H, CH_2), 4.20 (m, 2H, CH_2), 4.82 (q, 1H, OCH), 6.85 (d, 2H, Ar), 8.05 (d, 2H, Ar).

Step 4: Synthesis of 2-(4-Nitrophenoxy)propionic acid 2-[2-(4-nitrophenoxy)propionyloxy]ethyl ester (**10**)

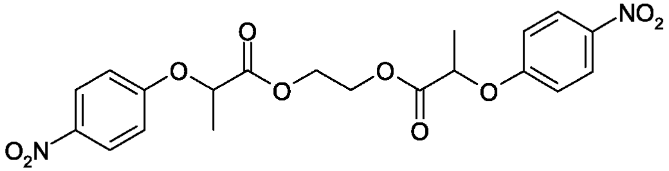

To a mixture of 2-(4-nitrophenoxy)-propionic acid 8 (25 g, 118.5 mmol) and 2-(4-nitrophenoxy)propionic acid 2-hydroxyethyl ester 9 (25 g, 108 mmol) in anhydrous dichloromethane (625 ml) under nitrogen atmosphere was added dropwise a solution of 1,3-dicyclohexyl carbodiimide (40 g, 194 mmol) in anhydrous dichloromethane (250 ml). The reaction mixture was stirred at room temperature for 8 hours. The solids were filtered off and dichloromethane distilled off to get crude 10. The crude 10 was purified by column chromatography on silica gel using hexane as eluant to get pure 10 (17 g, 35.1%) as a white powder with a melting point between 117-120°C. ^{1}HNMR (DMSO) δ 1.50(d, 3H, CH_3), 4.36 (s, 2H, $OCOCH_2$), 5.22 (q, 1H, OCH), 7.08 (d, 2H, Ar), 6.16 (d, 2H, Ar)

Step 5: Synthesis of 2-(4-Aminophenoxy)-propionic acid 2-[2-(4-aminophenoxy)-propionyloxy]-ethyl ester (**11**)

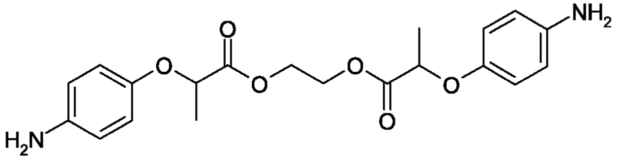

2-(4-Nitrophenoxy)-propionic acid 2-[2-(4-nitrophenoxy)propionyloxy]-ethyl ester 10 (50 g, 89.3 mmol) was dissolved in dry dimethylformamide (400 ml) in a pressure vessel. Palladium on carbon (5%, 12.5 g) was added, and the mixture stirred under an atmosphere of hydrogen (4 kg) for 4 hours. Catalyst was removed by filtration and ice water (3 L) was added to the filtrate. Crude 11 was extracted into ethyl acetate, dried over Na_2SO_4, and distilled and purified by column chromatography on silica gel using chloroform as eluant to give pure 11 (25 g, 58%) as a syrup. ^{1}HNMR ($CDCl_3$) δ 1.52 (d, 3H, CH_3), 3.30 (bs, 2H, NH_2), 4.30(s, 2H, $OCOCH_2$), 4.56 (q, 1H, OCH), 6.50 (d, 2H, Ar), 6.66 (d, 2H, Ar)

Downloaded by UNIV OF DELAWARE MORRIS LIB on June 23, 2012 | http://pubs.acs.org
Publication Date (Web): November 18, 2010 | doi: 10.1021/bk-2010-1054.ch007

Step 6: Synthesis of 2-(4-Isocyanatophenoxy)-propionic acid 2-[2-(4-isocyanatophenoxy)-propionyloxy]-ethyl ester (**12**)

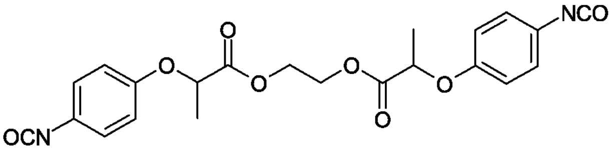

2-(4-Aminophenoxy)-propionic acid 2-[2-(4-aminophenoxy)-propionyloxy]-ethyl ester **11** (5.3 g, 13.6 mmol) was dissolved in dry dioxane (80 ml) under nitrogen atmosphere and cooled to below 20°C. A solution of triphosgene (7 g, 23.6 mmol) in dry dioxane (20 ml) was added drop wise. The mixture was heated slowly to 75-80°C and maintained for 2 ½ hours. The condenser was then arranged for distillation and solvent removed by distillation at atmospheric pressure until the reaction mixture volume was reduced to approximately one third. Fresh dry dioxane (50 ml) was added and the solvent then distilled off under vacuum. The residue was re-evaporated two times from dry dioxane to give pure **12** (4 g, 66.5%) as a light brown liquid. ^{1}HNMR ($CDCl_3$) δ1.60 (d, 3H, CH_3), 4.41 (s, 2H, $COOCH_2$) 4.68 (q, 1H, OCH), 6.84 (d, 2H, Ar), 7.00 (d, 2H, Ar)

2.2.3. Synthesis of BB004

Step 1: Synthesis of 6-(4-Nitrophenoxy)-hexanoic acid methyl ester (**13**)

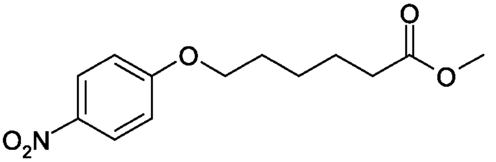

To a mixture of 4-nitrophenol (150 g, 1.079 moles), potassium carbonate (600 g, 4.341 moles) and sodium iodide (10 g, 66.7 mmol) in anhydrous acetone (2.1 L) was added methyl 6-bromohexanoate (156 g, 746.41 mmol) with and heating to reflux for 48 hours. Acetone was distilled off and water (2 L) was added. Crude **13** was filtered, dried and recrystallised from a mixture of ethyl acetate: hexane (1:6) to get pure **13** (130 g, 45.1%) as a white powder with a melting point between 84-86°C

Step 2: Synthesis of 6-(4-Nitrophenoxy)-hexanoic acid (**14**)

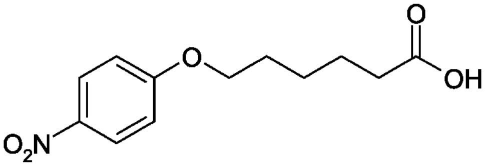

Downloaded by UNIV OF DELAWARE MORRIS LIB on June 23, 2012 | http://pubs.acs.org
Publication Date (Web): November 18, 2010 | doi: 10.1021/bk-2010-1054.ch007

6-(4-nitrophenoxy)-hexanoic acid methyl ester **13** (125 g, 468.16 mmol) was refluxed in conc. HCl (1250 ml) for 16 hours. The reaction mixture was cooled to room temp., filtered, dried and recrystallised from a mixture of ethyl acetate: hexane (1:6) to get pure **14** (95 g, 80.2%) as a white powder with a melting point between 104-107°C.

Step 3: Synthesis of 6-(4-Nitrophenoxy)-hexanoic acid 2-hydroxy-ethyl ester (**15**)

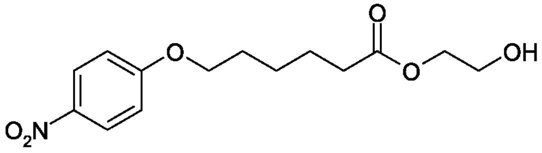

Dry HCl gas was passed through a mixture of 6-(4-nitrophenoxy)-hexanoic acid **14** (50 g, 197.62 mmol) and ethylene glycol (200 ml) was passed dry HCl gas for one hour. During HCl gas bubbling the temperature rose to 60°C. The crude reaction mass was poured onto ice (1 kg), extracted in to ethyl acetate, washed with water (2x250 ml), dried over sodium sulphate and distilled to get crude **15**, which was purified by column chromatography on silica gel using benzene as eluant to get pure **15** (46 g, 78.3) as a light yellow syrup.

Step 4: Synthesis of Ethane-1,2-diyl bis (6-(4-nitrophenoxy) hexanoate (**16**)

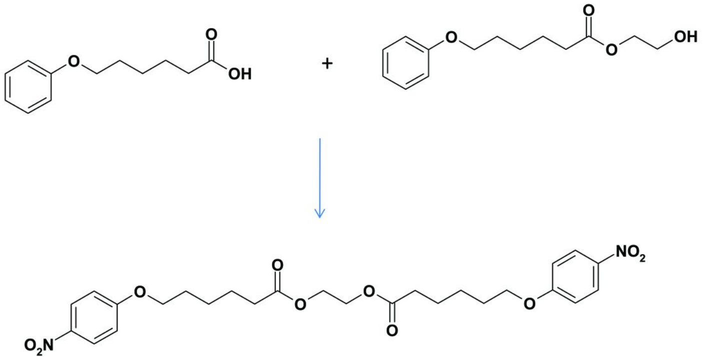

Ethane-1,2-diyl bis (6-(4-nitrophenoxy) hexanoate **16** was prepared using the procedure very similar to synthesis of compound **4**.

Step 5: Synthesis of 6-(4-Amino-phenoxy)-hexanoic acid 2-[6-(4-amino-phenoxy)-hexanoyloxy]-ethyl Ester (**17**)

Downloaded by UNIV OF DELAWARE MORRIS LIB on June 23, 2012 | http://pubs.acs.org
Publication Date (Web): November 18, 2010 | doi: 10.1021/bk-2010-1054.ch007

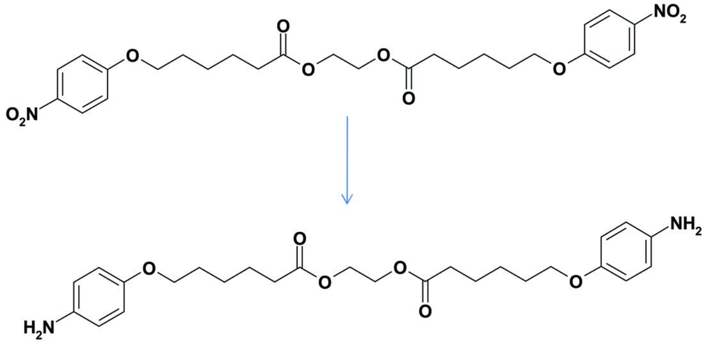

6-(4-Amino-phenoxy)-hexanoic acid 2-[6-(4-amino-phenoxy)-hexanoyloxy]-ethyl Ester **17** was prepared using the procedure very similar to synthesis of compound **5**.

Step 6: Synthesis of Ethane-1, 2-diyl bis (6-(4-Isocyanatophenoxy) hexanoate (**18**)

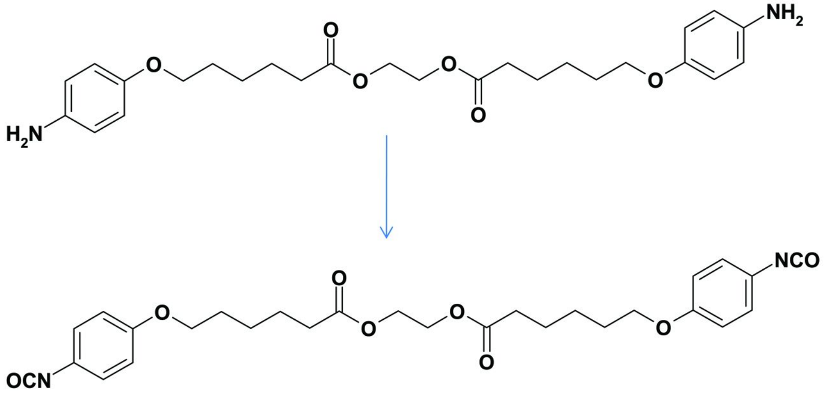

Ethane-1, 2-diyl bis (6-(4-Isocyanatophenoxy) hexanoate **18** was prepared using the procedure very similar to synthesis of compound **6**. The resulting dicaprolactone diisocyanate [BB-004] is a crystalline powder with a melting point of 65-68°C.

3. Synthesis of Absorbable Polyurethanes

3.1. Materials

Hydrolytically degradable aromatic diisocyanates BB002 and BB004 were synthesized. The isocyanate content was determined using standard ASTM (*28*) procedures. Polycaprolactonediol (PCL diol) having M_n of 530 and 2,000 were obtained from Sigma-Aldrich, Milwaukee, WI. Polyethyleneglycol (PEG) having M_n of 4,600 was obtained from Sigma-Aldrich, Milwaukee, WI. Both of them were used as the soft segment (SS) components in the polyurethane synthesis. The exact molecular weights of the diols were determined by using procedures

Downloaded by UNIV OF DELAWARE MORRIS LIB on June 23, 2012 | http://pubs.acs.org
Publication Date (Web): November 18, 2010 | doi: 10.1021/bk-2010-1054.ch007

described in ASTM D4274 (*29*). 1,4-butanediol (BD) was obtained from BASF, Mount Olive, NJ. Figure 5 displays the structures of polyols and chain extender used in polyurethane synthesis. All diols were dried to below 100 ppm moisture content prior to use in synthesis. Stannous octoate obtained from Aldrich was used as the catalyst. Anhydrous dimethylacetamide (DMAc) was used as solvent for the polyurethane synthesis reactions. Phosphate buffer salt (mixture of sodium phosphate dibasic and potassium phosphate monobasic: 12 g packets) was purchased from Fisher Scientific. One liter of the PBS buffer solution was prepared by dissolving one 12 g pack in 1 liter of DI water. The resultant solution had a pH of 7.39 at 37°C (~ 0.06M), which was adjusted to 7.34 ±0.02 with appropriate amounts of 0.1 M phosphoric acid at 37°C.

3.2. General Procedure for Synthesis of Polyurethanes (*27*)

Polyurethane solutions with varying soft segment contents were synthesized at 20 or 30 wt% concentration levels in two steps at 50-55°C. In the first step, the soft segment polyol was reacted with isocyanate in anhydrous DMAc under nitrogen atmosphere. In the second step, this prepolymer is reacted with chain extender 1,4-butanediol. The progress of the reaction was monitored by following consumption of isocyanate using method described in ASTM D5155. The resultant viscous polyurethane solutions were casted into films on silicone coated Mylar sheets using a device coater. The cast films were dried overnight using forced air at 50°C and the dry films were peeled-off from the Mylar sheet. Figure 6 depicts the representative structure of the synthesized absorbable polyurethanes.

3.3. Characterization of Absorbable Polyurethanes

Molecular Weight Determination

Molecular weights of synthesized polyurethanes were determined by GPC on Waters 150-C ALC system (Milford, MA) at 40°C. All the molecular weights were measured relative to polystyrene standards. All samples were run using Dimethylformamide (DMF) as solvent and DMF w/LiBr (Lithium Bromide) (0.05M) as the system mobile phase at 1 ml/min.

Tensile Strength

Uniaxial tensile strength of films was determined on an Instron 5566 instrument using ASTM D1708 methods. For this purpose, dog bone samples of gauge length of 0.9”, test width of 0.186” and thickness varying between 4-10 mils were stretched at a uniform strain rate of 4 in/min until the point of failure. The data reported are average of 5 specimens for each of the reported polyurethanes (*27*).

Downloaded by UNIV OF DELAWARE MORRIS LIB on June 23, 2012 | http://pubs.acs.org
Publication Date (Web): November 18, 2010 | doi: 10.1021/bk-2010-1054.ch007

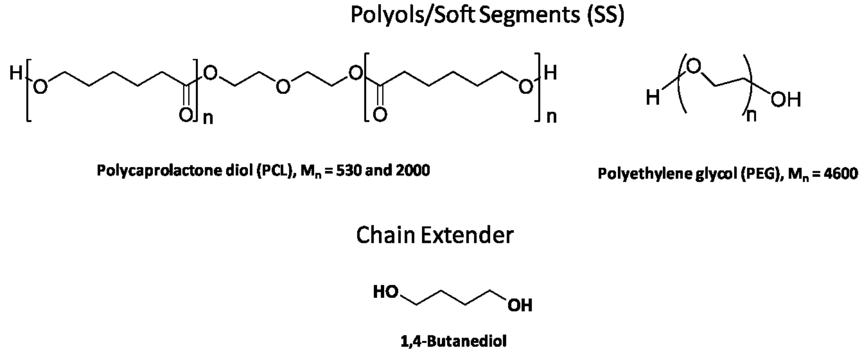
Polyols/Soft Segments (SS)
Polycaprolactone diol (PCL), Mn = 530 and 2000
Polyethylene glycol (PEG), Mn = 4600
Chain Extender
1,4-Butanediol

Figure 5. Polyols and Chain extender used in polyurethane synthesis

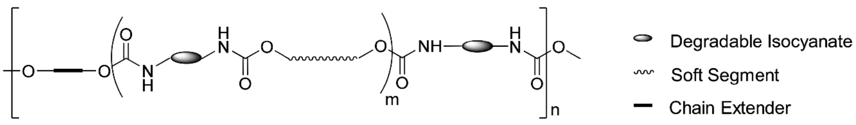

Figure 6. Representative Structure of Absorbable Polyurethanes

In Vitro Hydrolytic Degradation Studies

In-vitro hydrolytic degradation studies (*27*) of the absorbable polyurethane films were conducted using test guidelines described in ISO 10993-13 (*30*). Film samples weighing between 0.1 to 0.2g were immersed in phosphate buffer solution (PBS) having a pH of 7.34± 0.02 at 37°C. The ratio of buffer to solid film weight was 100:1. The samples were withdrawn after every seven days for 6 weeks. The moist and dry weights of these samples were measured. The moist weights of the samples were measured after blotting the surface moisture with lintless wipes. The GPC molecular weights were also measured relative to polystyrene standards using procedure described above. The selected absorbable polyurethanes were subjected to real-time degradation tests at physiological temperature of 37±1°C for 5 weeks (35 days).

4. Results and Discussions

Absorbable polyurethanes were synthesized using BB002 and BB004 diisocyanates, PCL 530 and PEG 4600 polyols and 1,4-butanediol as the chain extender. Table 3 to 7 displays the molecular weights and physical properties of polyurethanes derived from isocyanates BB002 and BB004. As can be seen, molecular weights of the synthesized polyurethanes were very high. They ranged between 300,000 and 500,000 Daltons.

Downloaded by UNIV OF DELAWARE MORRIS LIB on June 23, 2012 | http://pubs.acs.org
Publication Date (Web): November 18, 2010 | doi: 10.1021/bk-2010-1054.ch007

Table 3. Effect of SS Content (wt %) on Physical Properties of PU using BB002, PCL-530 & 1,4-Butanediol (see color insert)

Isocyanate	SS Content (wt%)	Polyurethane M_w/(PI)	PI	Maximum Tensile strength, (psi)	Elongation at Break (%)
BB002	20	160774	1.4	2971	387
BB002	30	355195	1.7	4772	551

Table 4. Effect of SS Content (wt %) on Physical Properties of PU using BB004, PCL-530 & 1,4-Butanediol (see color insert)

Isocyanate	SS Content (wt%)	Polyurethane Mol wt (PI)	PI	Maximum Tensile strength, (psi)	Elongation at Break (%)
BB004	20	274887	1.5	6117	632
BB004	30	497182	1.8	7054	651

Table 5. Effect of Molecular weight of soft segment on physical properties of PU using BB002, PCL (30 wt %) & 1,4-Butanediol (see color insert)

Isocyanate	PCL mol wt	Polyurethane Mol wt (PI)	Maximum Tensile strength, (psi)	Elongation at Break (%)	Modulus (secant 50%) (psi)
BB002	530	355220 (1.7)	4772	551	2275
BB002	2000	371952 (1.6)	7577	531	4363

Table 6. Effect of Molecular weight of soft segment on physical properties of PU using BB004, PCL (30 wt %) & 1,4-Butanediol (see color insert)

Isocyanate	PCL mol wt	Polyurethane Mol wt & (PI)	Maximum Tensile strength, (psi)	Elongation at Break (%)	Modulus (secant 50%) (psi)
BB004	530	497182	7054	651	2395
BB004	2000	362681	6830	651	3455

Downloaded by UNIV OF DELAWARE MORRIS LIB on June 23, 2012 | http://pubs.acs.org
Publication Date (Web): November 18, 2010 | doi: 10.1021/bk-2010-1054.ch007

Table 7. Effect of type of soft segment (30 wt %) on physical properties of PU using BB002 using PCL and PEG respectively as soft segment (see color insert)

Isocyanate	SS type	Polyurethane Mol wt & (PI)	Maximum Tensile strength, (psi)	Elongation at Break (%)	Modulus (secant 50%) (psi)
BB002	PEG 4600	341824	7012	513	4057
BB002	PCL 2000	371952	7577	531	4363

Table 8. Comparison of tensile properties of Absorbable polyurethane prepared from BB002 versus commercial biostable polyurethane (see color insert)

Polyurethane	Isocyanate	Polyol/Soft Segment	Maximum Tensile strength, (psi)	Elongation at Break (%)	Modulus (secant 50%) (psi)
Absorbable Polyurethane	BB002	PEG 4600	7012	513	4057
Commercial Biostable Polyurethane	MDI	Polycarbonate diol	8326	362	3408

Table 3 and Table 4 shows the effect of content of polycaprolactone diol (M_n 530) based soft segment on the physical properties of polyurethane derived from BB002 and BB004 isocyanates respectively. As can be seen from both table 3 and table 4, higher content of soft segment results in better physical properties. Furthermore, polyurethane prepared from isocyanate BB004 has higher tensile strength as compared to polyurethanes derived from isocyanate BB002. Similarly, table 5 and 6 depicts the effect of molecular weight of soft segment on the physical properties of polyurethane. As shown in table 5, higher molecular weight of soft segment did not result in a significant increase in the molecular weight of the polyurethane derived from BB002. However, it resulted in relatively higher tensile strength of the polyurethane. Surprisingly, as shown in table 6, increase in molecular weight of soft segment resulted in a decrease in the molecular weight and tensile strength of the polyurethane derived from BB004.This can be partially attributed to the differences in the chemical structures of the isocyanates BB002 and BB004. However, the tensile modulus of polyurethanes derived from higher molecular weight soft segment with both BB002 and BB004 was higher than that prepared from low molecular weight soft segment.

The type of soft segment also had a significant effect on the tensile properties of these absorbable polyurethanes. For example, as shown in table 7, polyurethane derived from polycaprolactone based soft segment has a higher molecular weight and a relatively higher maximum tensile stress and modulus as compared to polyurethane comprised of polyethylene glycol based polyurethane using BB002 isocyanate and 1,4-butanediol chain extender.

Downloaded by UNIV OF DELAWARE MORRIS LIB on June 23, 2012 | http://pubs.acs.org
Publication Date (Web): November 18, 2010 | doi: 10.1021/bk-2010-1054.ch007

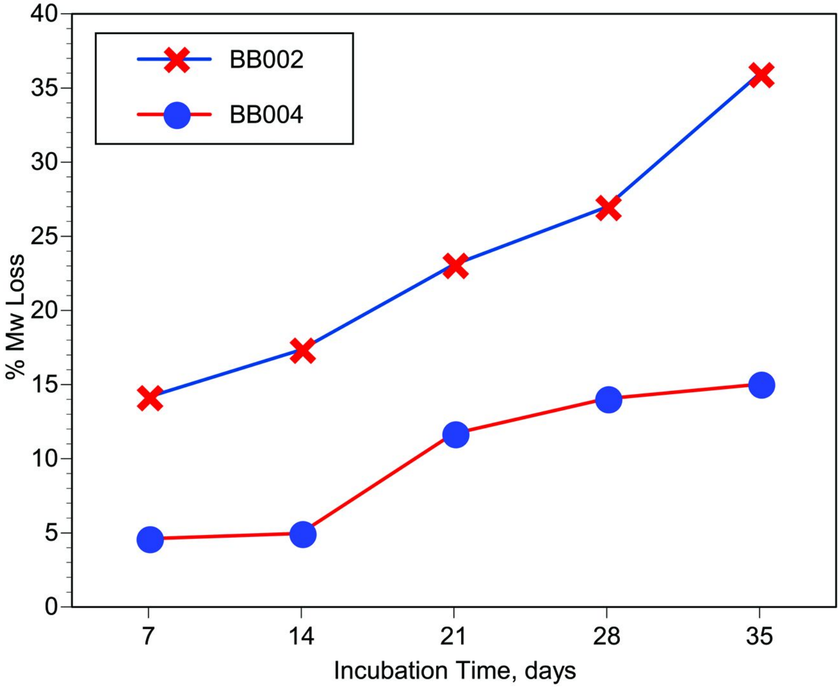

Figure 7. Comparison of in vitro hydrolytic degradation at 37°C of absorbable polyurethane prepared from BB002 vs BB004 with PCL-530 (30%) (see color insert)

In general, majority of these synthesized polyurethanes exhibited tensile and elongation properties similar to that of commercially available medical grade polyurethanes. For example, as shown in Table 8 below, absorbable polyurethane derived from isocyanate BB002, chain extender 1,4-butanediol and polyethyleneglycol polyol of average molecular weight 4600 has a maximum tensile strength of 7000 psi and elongation at break of 513%. This is comparable to commercially available medical grade biostable polyurethane derived from MDI, polycarbonate diol and 1,4-butanediol.

4.1. Hydrolytic Degradation Studies

In-vitro hydrolytic degradation of the polyurethanes was carried out under physiological (37°C) conditions using PBS buffer solution of pH 7.34. The rate of degradation was monitored by measuring the changes in molecular weights relative to polystyrene standards using Gel Permeation Chromatography. Figure 7 compares the percent (%) loss in the molecular weight of absorbable polyurethanes prepared from BB002 and BB004 isocyanates using PCL-530 (30% soft segment) polyol for a period of 35 days (5 weeks). As can be seen, polyurethane based on BB002 hydrolyses faster than BB004 based absorbable polyurethane. This is attributed to the presence of glycolic acid based degradable linkage in BB002 that has the propensity to hydrolyze faster than the caprolactone based degradable

Downloaded by UNIV OF DELAWARE MORRIS LIB on June 23, 2012 | http://pubs.acs.org
Publication Date (Web): November 18, 2010 | doi: 10.1021/bk-2010-1054.ch007

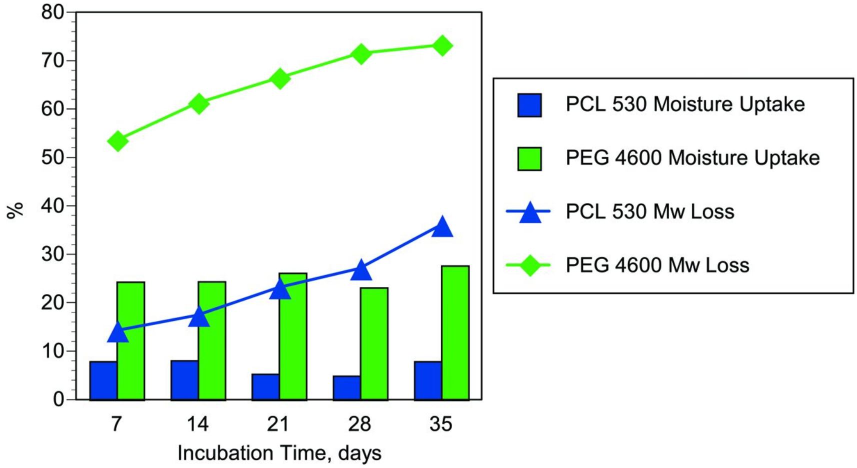

Figure 8. Comparison of in vitro hydrolytic degradation at 37°C of absorbable polyurethane prepared from BB002 isocyanate using PCL-530 vs. PEG 4600 polyol (see color insert)

linkage in BB004. This shows that the hydrolytic degradation rate of developed absorbable polyurethanes can be controlled by varying the chain length of the degradable linkage of the isocyanates and/or by varying the safe and biocompatible molecule within the degradable linkage of the isocyanate, i.e. replacing glycolide with lactide or p-dioxanone, and the like.

Similarly, Figure 8 compares the moisture uptake and hydrolytic degradation behavior at 37°C of BB002 isocyanate based absorbable polyurethanes wherein one of the polyurethane has a polycaprolactone (PCL 530) polyol based soft segment and the other polyurethane has a PEG 4600 polyol based soft segment. The hard segment of both the polyurethanes under study was derived from 1,4-butanediol. As can be seen, moisture uptake by polyurethane films increased from 5-8% by weight for PCL polyol based polyurethane to ~25% by weight for PEG containing polyurethane. This dramatic increase facilitates faster degradation of PEG based polyurethane. While the molecular weight of PCL based polyurethane decreased by only 32% in 5 weeks, it decreased by 72% in PEG based absorbable polyurethane. Hence, the rate of hydrolytic degradation can be further controlled by the type of soft segment in the polyurethane backbone.

A number of extensive additional studies on these absorbable polyurethanes are underway in our laboratories. The results of these studies will be a part of separate publication.

5. Conclusions

For the first time, a number of hydrolytically degradable aromatic isocyanates including diisocyanates were synthesized. These highly reactive diisocyanates are similar to MDI but are biodegradable and have tunable hydrolytic degradation profiles.

These aromatic diisocyanates were further used as precursors to develop polyurethanes. The polyurethanes derived from these isocyanates are not only absorbable, but also possess for the first time, hydrolytically degradable hard segments. Furthermore, the hydrolytic degradation rate of these absorbable polyurethanes can be easily controlled by varying the chain length of the hydrolytically degradable linker and by varying the safe and biocompatible molecule within the degradable linkage i.e., replacing glycolide with caprolactone and the like. For example, the rate of hydrolytic degradation of absorbable polyurethane prepared from BB002 (with a glycolic acid based linker) is faster than the rate of hydrolytic degradation of absorbable polyurethane prepared from BB004 (with a caprolactone-based linker). Furthermore, the developed absorbable polyurethanes exhibited high molecular weights, high tensile strength and high elongation at break. The tensile properties of some of the synthesized absorbable polyurethanes are comparable to that of commercial biostable polyurethanes. Moreover, these absorbable polyurethanes are expected to degrade into safe and biocompatible degradation products, unlike polyurethanes derived from MDI.

These absorbable polyurethanes are expected to find use in a number of biomedical applications including absorbable tissue adhesives and sealants, adhesion prevention barrier, absorbable scaffolds for tissue engineering, absorbable coatings and controlled release of drugs

Downloaded by UNIV OF DELAWARE MORRIS LIB on June 23, 2012 | http://pubs.acs.org
Publication Date (Web): November 18, 2010 | doi: 10.1021/bk-2010-1054.ch007

Acknowledgments

The author would like to thank James Parakka, Ananth V Iyer and Robert Ward of DSM Polymer technology group for the hydrolytic degradation data and results from polyurethane characterization studies.

References

1. Guelcher, S. A.; Hollinger, J. O.. Biomedical Engineering Series: An introduction to Biomaterials; *Polyurethanes*; CRC Press: Boca Raton, FL, 2006; p 161.
2. Szycher, M. *Szycher's Handbook of Polyurethanes*; CRC Press: Boca Raton, FL, 1999 (Reactivity of aromatic isocyanate faster).
3. Frisch, K.; et al. In *Advances in Urethane Science and Technology* Frisch, K, Reegen, S., Eds.; Technomic Publishing: Lancaster, 1971; p 49 (mechanical properties superior).
4. Lelah, M. D.; Cooper, J. L. *Polyurethanes in Medicine*; CRC Press: Boca Raton, FL, 1986 (Biostability, Durability, Medical applications).
5. Stokes, K.; McVenes, R. Polyurethane elastomer Stability. *J. Biomater. Appl.* **1995**, *9*, 321 (Biostability, Durability, Medical applications).
6. Ward, R. S; et al. The effect of Phase separation and End Group Chemistry on the in vivo biostability of polyurethanes. *ASAIO J.* **1996**, *42* (2), 17.
7. Gunatillake, P. A.; et al. Designing Biostable Polyurethane Elastomers for Biomedical Implants. *Aust. J. Chem.* **2003**, *56* (6), 545.

8. Spaans, C. J.; et al. Solvent-free fabrication of microporous polyurethane-amide and polyurethane-urea scaffolds for repair and replacement of the knee joint meniscus. *Polym. Prepr.* **1999**, *40*, 589.
9. Thomas, V.; et al. In vitro studies on the effect of physical- crosslinking on the biological performance of aliphatic poly(urethane urea) for blood contact applications. *Biomacromolecules* **2001**, *2*, 588.
10. Hoffman, D.; et al. Safety and intracardiac function of a silicone-polyurethane elastomer designed for vascular use. *Clin. Mater.* **1993**, *13*, 95.
11. Oertel, G. *Polyurethane Handbook*; Hanser Gardner Publications: Berlin, 1994.
12. Bezwada, R. S. Bioabsorbable and biocompatible polyurethanes and polyamides for medical devices. U.S. Patent 7772352.
13. Bruin, P.; et al. Design and synthesis of biodegradable poly(ester-urethane) elastomer networks composed of non-toxic building blocks. *Makromol. Chem. Rapid. Commun.* **1988**, *9*, 589.
14. Cohn, D.; et al. U.S. Patent No. 6579951.
15. Beckmann, E.; et al. Medical adhesive and methods of tissue adhesion. U.S. Patent publication number 2004/0170597A1.
16. Woodhouse, K. A.; et al. Biodegradable Polyurethanes. U.S. Patent 221997.
17. Fuller, W. D.; et al. Metabolically acceptable polyisocyanate adhesive. U.S. Patent 4829099.
18. Bezwada, R. S.; et al. Bioabsorbable polymers from bioabsorbable polyisocyanates and uses thereof. U.S. Patent publication 2009/0292029A1.
19. Saad, B.; et al. New versatile, elastomeric, degradable polymeric materials for medicine. *Int. J. Biol. Macromol.* **1999**, *25*, 293.
20. Borkenhagen, M.; et al. In vivo performance of a new biodegradable polyester urethane system used as a nerve guidance channel. *Biomaterials* **1998**, *19*, 2155.
21. Gunatillake, P. A.; et al. Biodegradable Polyurethane/urea compositions. Australia Patent WO 2004/009227 A2, 2004.
22. Gunatillake, P. A.; et al. Injectable Biodegradable Polyurethanes for tissue engineering: Effect of phosphorylcholine. Abstract presented at 7th world biomaterials congress, Sydney, Australia, 2004.
23. Gunatillake, P. A.; et al. Injectable Biodegradable Polyurethanes for Cartilage repair: Evaluation of biocompatibility and biodegradability. Transactions of the 7th World Biomaterials Congress, Sydney, Australia, 2004; 1618.
24. Gunatillake, P. A.; et al. Recent Developments in Biodegradable Synthetic Polymers. *Biotechn. Annu. Rev.* **2006**, *12*, 301–347.
25. Adhikari, R.; et al. Biodegradable injectable polyurethanes: Synthesis and evaluation for orthopedic applications. *Biomaterials* **2008**, *29* (28), 3762–3770.
26. Bezwada, R. S. Synthesis and characterization of bioabsorbable polyurethanes from novel isocyanates. *PMSE Prepr.* **2006**, *95*, 1054.
27. Parraka, J.; et al. Bioresorbable Polyurethanes with Degradable Hard Segments. Poster 616, Society for Biomaterials Annual Meeting, 2009.

Downloaded by UNIV OF DELAWARE MORRIS LIB on June 23, 2012 | http://pubs.acs.org
Publication Date (Web): November 18, 2010 | doi: 10.1021/bk-2010-1054.ch007

28. ASTM. ASTM D4274-05 Standard Test methods for Polyurethane Raw materials: Determination of Isocyanate Content of Aromatic Isocyanates. 2007; Vol 08.03.
29. ASTM. ASTM D4274-05 Standard Test methods for Polyurethane Raw materials: Determination of Hydroxyl numbers of Polyols. 2007, Vol 08.02.
30. ISO. ISO 10993-13 Biological Evaluation of Medical Devices-Part 13; Identification and Quantification of Degradation Products from Polymeric Medical Devices. ISO 10993-13, 198, p 10.

Downloaded by UNIV OF DELAWARE MORRIS LIB on June 23, 2012 | http://pubs.acs.org
Publication Date (Web): November 18, 2010 | doi: 10.1021/bk-2010-1054.ch007

Downloaded by UNIV OF GUELPH LIBRARY on June 23, 2012 | http://pubs.acs.org
Publication Date (Web): November 18, 2010 | doi: 10.1021/bk-2010-1054.ch008

Chapter 8

Formation and Characterization of Chitosan-Based Coatings on Stainless Steel

**Gary Halada,[1,*] Prashant Jha,[1] Karl Nelson,[2] Wei Zhao,[2]
Chad S. Korach,[2] Aaron Neiman,[3] So-Jeung Lee,[1] and Eric Mintzer[4]**

**[1]Department of Materials Science and Engineering, Stony Brook University,
Stony Brook, NY 11794-2275
[2]Department of Mechanical Engineering, Stony Brook University,
Stony Brook, NY 11794-2300
[3]Department of Biochemistry and Cell Biology, Stony Brook University,
Stony Brook, NY 11794-5215
[4]Kings Park High School, Kings Park, NY 11754-3963
[*]ghalada@notes.cc.sunysb.edu**

Chitosan, the second most abundant organic material on earth, is a bio-polymer found in crustaceans, fungi, insects, bacterial spore coats and other natural sources and has been successfully used in medical applications, such as wound dressings and delivery of pharmaceuticals, and in environmental treatment applications, such as sorption of heavy metals. Chitosan provides a low cost and safe base material for development of functionalized coatings. A strong scientific underpinning is needed if such ‘green’ biomaterials are to be developed and used effectively for engineering applications. In particular, it is important to understand mechanisms for creating composite chitosan-based materials with strong interfaces. In this paper, we demonstrate the formation of adherent, durable layers of chitosan on stainless steel substrates, through a recently developed electrochemical method. Spectroscopic (X-ray diffraction and FTIR and Raman spectroscopies) and mechanical testing (atomic force acoustic microscopy, microscratch tests and tribotesting) are used to characterize the structure and properties of the deposited materials. Chitosan-based layers are formed relatively quickly, and demonstrate a number of properties which suggest new

In Biomaterials; Kulshrestha, A., et al.;
ACS Symposium Series; American Chemical Society: Washington, DC, 2010.

engineering applications, including environmental, biomedical and mechanical uses.

Introduction

Chitosan, a linear polysaccharide of 2-amino-2-deoxy-D-glucopyranose obtained by deacetylation of chitin from crustacean, mollusks, insects and fungi, is the second most abundant natural biopolymer (after cellulose). It has found a broad range of applications in the form of powder, flakes, beads, and occasionally fibers and membranes in the pharmaceutical, food processing and medical industries due to its biocompatibility and non-toxicity, its excellent gel and film-forming ability, and its chemical reactivity as a natural polycation (*1*). While the biomedical (e.g. tissue engineering (*2*)) and pharmaceutical applications (e.g. drug delivery) have been exploited for some time, the potential uses of chitosan-based biomaterials in industry (e.g. as a support for catalysts or substrate in organic electronics) have been hindered by questions of stability, variability in properties, and methods and extent of production (*3*). Surfaces for flexible electronics, sensors and device development (*4*) require both the elasticity of polymeric materials (relatively low Young's modulus) coupled with good toughness and environmental durability as well as the ability to provide a strong interconnect to metallic structures (*5*). The potential for chitosan as a hierarchal soft-interconnect for nano-scale components have also recently been pointed out (*6*). This refers to the ability to use chitosan, processed using a similar electrochemical technique to that which is described below, as a means to assemble soft nanoscale components at specific locations.

In particular, durability and mechanical toughness as well as adhesion to metal substrates have remained challenges to chitosan application. For example, silane coupling agents were needed to create a bond between a chitosan film and titanium substrates used in dental implants (*7*). This required a complex process involving several chemical treatments (including curing at elevated temperature, reaction with a cyano-oxysilane coupling agent and overnight exposure to a glutaraldehyde cross-linking agent) – a process which one would hope to avoid for industrial applications. Chitosan and chitosan loaded with an antibiotic (gentamicin), has been applied to stainless steel bone screws, and found to be biocompatible and to inhibit growth of bacteria (*8*). These researchers also used a method for deposition involving silane (to promote adhesion) and glutaraldehyde (a cross-linking agent). We have used a deposition method which does not require adhesion promoters due to the nature of the electrochemical process.

A number of reviews of the extent and mechanism of metal ion sorption by chitosan-based materials have been published over the past decade (*9*). The amine groups of chitosan are noted to be reactive sites for metal ions, through the free electron pair on nitrogen. Protonated amine groups are noted to electrostatically sorb metal anions (for example oxyanions such as chromate). Since polysaccharides, including chitosan, are known to bind to chromate, molybdate and other oxyanions in solution, it is likely that an initial chitosan layer created through electrostatic interaction with a cathodically charged stainless

Downloaded by UNIV OF GUELPH LIBRARY on June 23, 2012 | http://pubs.acs.org
Publication Date (Web): November 18, 2010 | doi: 10.1021/bk-2010-1054.ch008

steel surface will adhere due to the association of Cr(VI) and Mo(VI) with amine groups. The contribution of this phenomenon to initial film formation and enhancement of mechanical properties, including adhesion, represents an important focus of our research.

Electrochemical Deposition

Through the use of electrochemical formulation of chitosan-based composites, we reduce the need for enzymes and chemical processing steps involving non-renewable solvents (resulting in a more sustainable process). The method for electrochemically-induced deposition is based upon cathodic polarization of the electrode on which deposition is to occur – a process which has long been shown to create a region of higher pH (due to hydrogen evolution) (*10*). Since the pKa value for the amino groups in chitosan is approximately 6.3, chitosan becomes deprotonated and hence insoluble when pH >6.3. In the case of electrochemically-induced deposition, the high pH region formed at negative electrode due to hydrogen evolution deprotonates the chitosan in solution which then becomes immobilized at the surface. Fernandez, et al., showed that cathodic polarization of a gold patterned electrode in slightly acidic (pH 5.5) solutions of chitosan resulted in formation of a hydrogel-like deposit (*11*). Variations in current density allowed for some control over deposited amounts, and the ability to create localized deposits (on patterned conductors) was cited as a means to integrate hydrogels into microelectromechanical systems (MEMS). A recent study has shown that chitosan layers can be formed electrochemically on a graphite electrode. This study used Raman analysis to identify the progress of coating formation, and monitor de-acetylization of the resulting layer with time (*12*). These methodologies offers distinct advantages over past approaches for chitosan deposition requiring drying or spin casting and the use of potentially hazardous chemicals.

In addition to creating a region of elevated pH, we hypothesize that the cathodic potential at the stainless steel surface would also serve to initially and very rapidly attract cationic chitosan to create a thin bound layer (through the same mechanisms by which chitosan creates complexes with chromate). Continued cathodic polarization would create conditions for deposition of additional layers of chitosan through the deprotonation/desolubilization mechanism.

Downloaded by UNIV OF GUELPH LIBRARY on June 23, 2012 | http://pubs.acs.org
Publication Date (Web): November 18, 2010 | doi: 10.1021/bk-2010-1054.ch008

Experimental

Electrochemically-Induced Deposition

1.5g low molecular weight chitosan (Sigma Aldrich, 75-85% deacetylated) was added to 120mL of DI water and was stirred in a flask. 1M HCl was added drop wise, and the pH was periodically tested, until it reached approximately 2. The solution was stirred overnight until all the chitosan dissolved. A fine frit was used to filter the solution to remove any impurities. After filtration 1M NaOH was slowly added until the solution reached a pH of around 5. The solution was stored in a refrigerator to prevent fungal growth and returned to room temperature for use in further experiments.

The working electrode was polished 304 stainless steel. Several materials have been explored as electrode substrates, but stainless steels (in the 300 series) appear to provide the best experimental surfaces for deposition (due to their thin passive layer, which allows for strong film adhesion). The passive film on stainless steels is composed of an inner layer of kinetic metal oxide barriers and oxyhydroxides, with an outer layer enriched in oxyanions. Since polysaccharides, including chitosan, are known to bind to chromate and other oxyanions in solution, it is likely that an initial chitosan layer created through electrostatic interaction with a cathodically charged stainless steel surface will adhere due to the association of Cr (VI) with amine groups. Deposition on 304 stainless steel (18%Cr, 8%Ni, bal. Fe) at a cathodic potential is rapid, and 10 minutes provides a thick layer of approximately 20-50 microns.

Pt wire was used as the counter electrode. Gamry Instruments Reference 600 was used to perform the electrochemistry and Gamry Instrument Framework was the software used. Controlled Potential Coulometry at a voltage of -2V was applied for 5 min. The resulting gel was exposed to UV light (20 W at 6 cm) for 20-25 minutes. A recent study indicates photopolymerization of chitosan with organic ligands using UV wavelengths (*13*). While further analysis is required, our preliminary work shows this process results in a stable layer, with good adhesion and mechanical properties (*14*).

Downloaded by UNIV OF GUELPH LIBRARY on June 23, 2012 | http://pubs.acs.org
Publication Date (Web): November 18, 2010 | doi: 10.1021/bk-2010-1054.ch008

X-ray Diffraction (XRD)

Powder XRD was performed on a Philips CM1728 diffractometer with a Cu Kα source (wavelength 1.5418 A). The dried films of electrochemically deposited chitosan were peeled off using a razor blade and ground using mortar and pestle. The sample is then placed in the vacuum filtration system and is washed with 100ml of water prior to XRD to remove any contaminants or residual NaCl from the deposition process. Powders are scanned from $2\theta \approx 12$ to 80 degrees (Powders cannot be scanned at a lower angle due to limitations of sample mounting.).

Raman Spectroscopy

Raman spectroscopy was performed to investigate chemical bonding in the deposited chitosan films. A Thermo Nicolet Almega spectrometer was operated in microspectroscopy mode (using a 10x objective and 50 micron slit) with a 532nm wavelength laser operated at 30 mW. 128 scans were averaged over a range of 3600 cm^{-1} Raman shift (from 400 to 4000 cm^{-1}).

Fourier Transform Infrared Spectroscopy (FTIR)

Dried samples were used for FTIR analysis without any additional sample preparation. A Nicolet Model Magna 760 FTIR spectrometer was used in diffuse reflectance mode to obtain spectra from 2000 cm^{-1} to 650 cm^{-1}. Data resolution was set to 2-4 cm^{-1} and summed over 256 scans to improve the signal-to-noise ratio.

Atomic Force Acoustic Microscopy (AFAM)

Atomic force acoustic microscopy (AFAM) was used to measure the Young's modulus of the deposited films. The AFM used was an NT-MDT SolverProM and samples were insonified by mounting on an ultrasonic transducer (*15*). Semi-contact cantilevers with normal contact loads on the order of 1 µN were used.

Microscratch Testing

Electrochemically deposited chitosan films on stainless steel substrates were measured for cohesive and adhesive strength, and the coefficient of friction utilizing a microscratch technique. The indenter used for all tests was a diamond Rockwell with a 5 µm included radius of curvature at the tip as measured by atomic force microscopy. All substrates used were adhered with an epoxy glue to guarantee no sample translation during scratch testing. The scanning speed was set at 2 µm/sec. for all scans, and topography scans were performed with a normal load of 0.1 mN. Scratch scans were linear ramped loads from a 'zero' load of 0.1 mN (topography load) to a specified maximum normal load of 300 mN. Loading rate (1.33 mN/sec.) is determined by the ratio of the maximum load to the ramped loading length, multiplied by the scanning speed, and was held constant for all tests.

To identify the extent of elastic and plastic deformation of the film and the substrate, pre- and post- scratch topography scans were performed over the scratch length with the same diamond scratch indenter. After the initial topography scan, tests began with a 50 µm topography scan which is used as a data leveling region when compared with the pre- and post-scratch topography data. The linear ramped loading began after 50 µm and extends 450 µm along the sample surface before the conclusion of the scan. The post-scratch topography scan commenced at this point during the test. During all tests the depth, load, and friction forces were instrumented, and recorded using a data acquisition system. In situ friction coefficients are calculated which are compared with the depth data. From this analysis, changes in friction coefficient, along with depth changes, can be correlated with different regimes of coating cohesion and adhesion.

Tribotesting

Electrochemically deposited chitosan films on stainless steel substrates were used in a triob-tester to measure coefficients of friction at higher speeds. All tests were performed unlubricated in a CETR UMT-2 tribotester at linear speeds of 48 and 255 mm/sec at a normal load of ~1 N. The test consists of a stainless steel ball in contact with the chitosan coated substrate, which is mounted to a rotating platen.

Downloaded by UNIV OF GUELPH LIBRARY on June 23, 2012 | http://pubs.acs.org
Publication Date (Web): November 18, 2010 | doi: 10.1021/bk-2010-1054.ch008

Downloaded by UNIV OF GUELPH LIBRARY on June 23, 2012 | http://pubs.acs.org
Publication Date (Web): November 18, 2010 | doi: 10.1021/bk-2010-1054.ch008

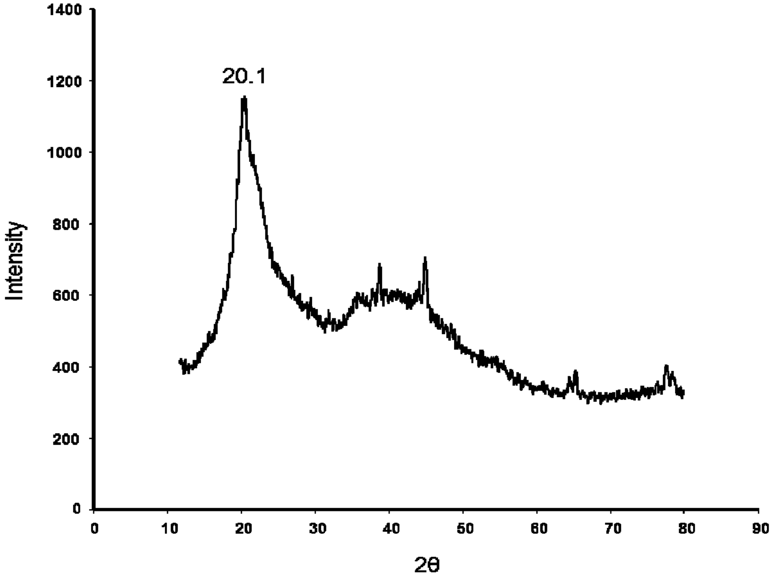

Figure 1. Powder XRD spectrum from electrodeposited chitosan layer following removal from the stainless steel substrate.

Results and Discussion

XRD

Typical diffraction spectra from electrochemically deposited chitosan (Figure 1) shows a large asymmetric peak at 2θ = 20.1 degrees. Normally, a second scattering peak at approximately 10 degrees would appear, but, as stated earlier, the system used for analysis did not permit measurements at angles below 2θ ≈ 12 degrees. A broad peak also appears, centered around 40 degrees (with several small sharper peaks at 38 and 43 degrees). XRD of chitosan powder shows a similar broad peak at 19.8 degrees, while chemically formed (at elevated pH) layers of chitosan often shows a similar broad peak between 20 and 21.5 degrees (*16*). The overall shape of the peak at 20 degrees, with a slight shoulder as opposed to a more pronounced shoulder or even second peak on the high angle side is very similar to what is observed from high molecular weight chitosan powder (600,000-800,000 MW) with a high degree of deacetylization (*17*). As the powder used in solution was low molecular weight, this is a strong indication of cross-linking or polymerization during the electrodeposition process.

The overall strength of the peak at 20 degrees indicates a high degree of crystallinity in the deposited chitosan. Studies have shown that precipitated and oven-dried chitosan films usually show far less crystallinity as compared to chitosan powder prior to processing (*18*). Our data indicates that the electrochemical deposition process results in a more highly crystalline layer than those processed by oven or freeze-drying following chemical precipitation.

Downloaded by UNIV OF GUELPH LIBRARY on June 23, 2012 | http://pubs.acs.org
Publication Date (Web): November 18, 2010 | doi: 10.1021/bk-2010-1054.ch008

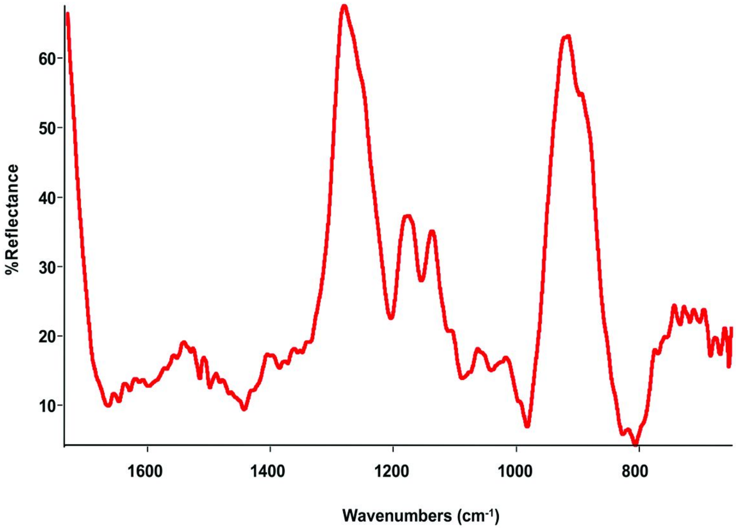

Figure 2. FTIR spectrum from electrochemically deposited and UV exposed chitosan on 304 stainless steel substrate

The small peaks between 35 and 45 degrees may also indicate some short range ordering in the electrodeposited structure which will be investigated further.

Spectroscopic

Reflectance FTIR spectroscopy from the surface (Figure 2) of electrochemically deposited chitosan shows peaks characteristic of chitosan. The peak at 1585cm^{-1} can be attributed to the NH_2 stretching vibration, that at 1442 cm^{-1} is from C-C stretching in rings, the peak at 1203 cm^{-1} can be from NH deformation, while the peak at 1154 cm^{-1} is from C-O-C stretching (*19*). In addition, a cyclic ether asymmetric peak and a peak due to OH deformation can be seen at 1020 and 805 cm^{-1} respectively. The large peak at 950 - 965 cm^{-1} may be due to CN stretching with some possible contributions from partial oxidation of amine bonds.

Overall, the analysis shows that there are no major changes in chitosan structure, though some broadening of the peaks may be due to complexation and some possible surface oxidation. There is some evidence of carboxyl formation (peak at 1663 cm^{-1}) in the FTIR spectrum. It is possible that surface oxidation of the chitosan layer may be enhanced through the UV processing stage of film formation. A recent study by Sionkowska, et al., considered the effects of UV exposure on the surface of properties of chitosan films (*20*). While no structural change was noted from UV irradiation, contact angle and surface free energy measurements did show a change in wettability and polarity indicating surface photo-oxidation. The degree of oxidation could not be detected, as surface sensitivity of techniques used to analyze the post-irradiated surface was limited.

The Raman spectrum from electrochemically-deposited and UV exposed chitosan (Figure 3) shows a number of prominent peaks at 1150 cm^{-1} (C-O-C

Downloaded by UNIV OF GUELPH LIBRARY on June 23, 2012 | http://pubs.acs.org
Publication Date (Web): November 18, 2010 | doi: 10.1021/bk-2010-1054.ch008

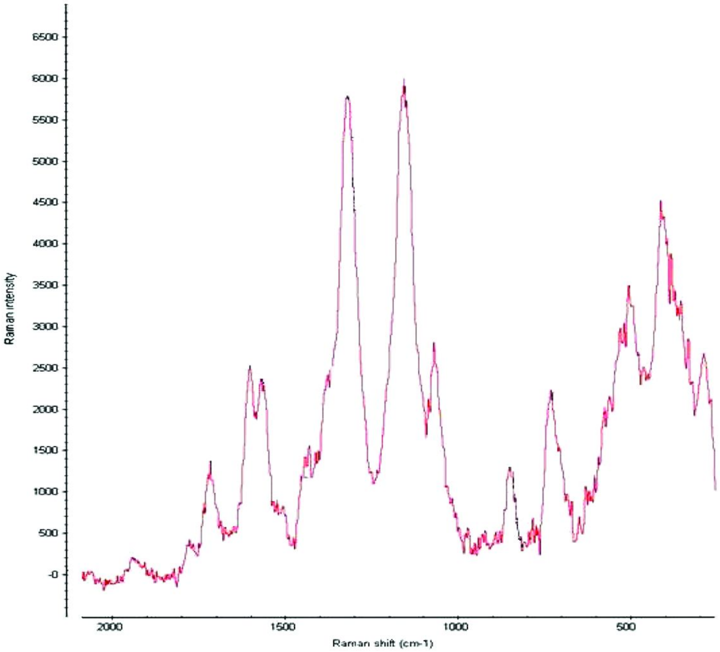

Figure 3. Raman spectrum from electrochemically-deposited/UV treated chitosan layers on 304 SS.

stretch); 1318 cm^{-1} (acetyl; amide III); 504 cm^{-1} and 850 cm^{-1} (C-C-O vibrational bands); 725 cm^{-1} (CO bend); and 1564 and 1601 cm^{-1} (amide II, NH deformation). All these peaks are consistent with chitosan flakes or dried coatings. There is also a peak which can be attributed to carboxylic functionality at 1715 cm^{-1}, in agreement with FTIR data which may be the result of photo-oxidation. Analysis of UV-exposed versus non-UV exposed deposited layers indicates an enhancement in peaks related to oxidized species in the exposed samples.

The Raman spectra from the electrochemically deposited coatings indicate a higher intensity in the primary amine bands, and occasionally in the phenolic region, as compared to the stock powder. The FTIR spectra indicate bound hydroxide. For the most part, the vibrational spectra verify the chitosan layer composition, with evidence of amino and phenolic changes consistent with surface binding (to the metal substrate).

Atomic Force Acoustic Microscopy

Atomic Force Acoustic Microscopy is used to measure nano-scale material elasticity (E). Based on five different spatial location measurements on three separate films deposited on stainless steel, the Young's modulus of the coating was determined to be 5-6 GPa using AFAM (similar to polyethylene), using a 4th order body of revolution contact model.

Downloaded by UNIV OF GUELPH LIBRARY on June 23, 2012 | http://pubs.acs.org
Publication Date (Web): November 18, 2010 | doi: 10.1021/bk-2010-1054.ch008

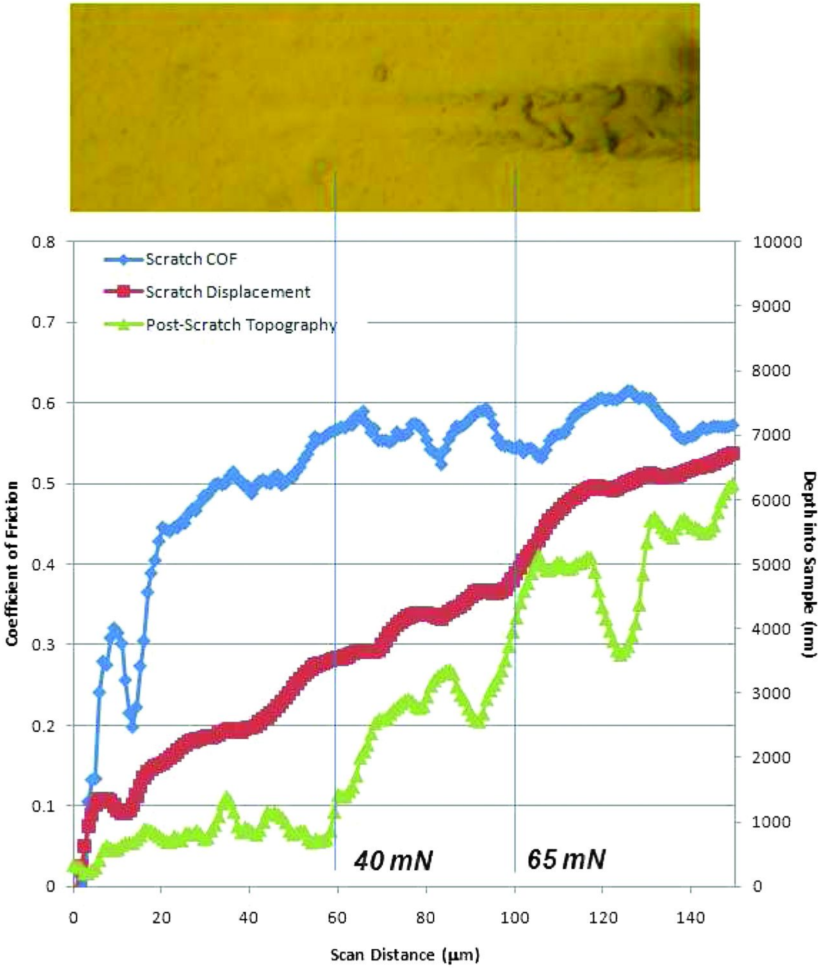

Figure 4. Results of microscratch testing of electrochemically-deposited, UV-treated chitosan coating on 304 stainless steel (with optical image of scratch at top).

Scratch Test

Films formed on stainless steel were measured for cohesive and adhesive strength and coefficient of friction utilizing a microscratch technique (Figure 4). A diamond tip is used to scratch the chitosan surface at a rate of 2 μm/s from a ‘zero’ load of 0.1 mN (topography load) to a specified maximum normal load. Pre- and post-scratch topography scans were performed over the scratch length to identify the extent of elastic and plastic deformation of the film and the substrate. In situ friction coefficients (COFs) are calculated which are compared with the depth data, and changes in COFs can be correlated with different regimes of coating cohesion and adhesion.

Downloaded by UNIV OF GUELPH LIBRARY on June 23, 2012 | http://pubs.acs.org
Publication Date (Web): November 18, 2010 | doi: 10.1021/bk-2010-1054.ch008

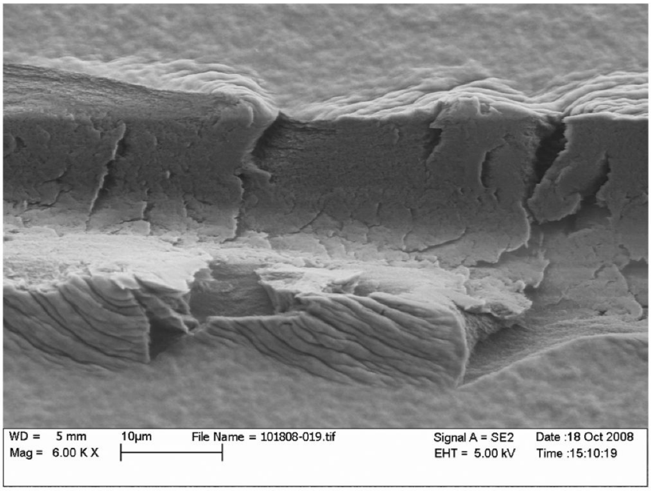

Figure 5. Scanning electron micrograph of electrochemically deposited chitosan). At heaviest loading (and deepest area of scratch), no metal substrate could be observed.

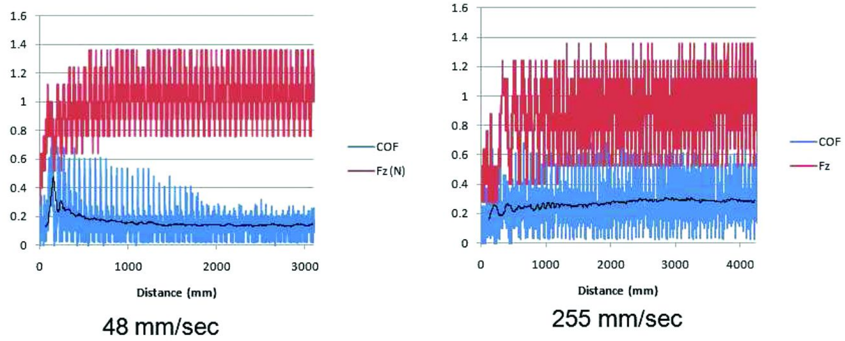

48 mm/sec

255 mm/sec

Figure 6. Results of stainless steel ball friction tests on electrochemically-deposited chitosan coatings.

To physically observe the post-scratch surface, high resolution optical and scanning electron microscopy is used (Figure 5). Residual depth of the scratch can be calculated and the location of coating delamination recorded. Additionally, the range of loads associated with coating cohesive failure prior to coating removal from the substrate is identified. These loads were located within a region of constant COF, which indicates the friction forces are strongly dependent on the contact area. The constant COF can be explained by the stress release in the form of surface fractures, which are identified from post-scratch microscopy. The COF increased prior to cohesive failure up to a normal load of 13 mN, at which point an average value of 0.57 was achieved. The leveling off of the COF coincides with the visible permanent scratch deformation of the chitosan film. This indicates that the chitosan film is capable of withstanding significant plastic deformation due to shear up to a normal load of 13 mN and a lateral load of ~7.5 mN. Prior to this, plastic deformation is observed for the film an order of 4 times smaller, and is attributed to normal compressive loading of the film. This region indicates significant elastic recovery, up to 75%, of the chitosan. Based on the applied loads, indenter geometry, and chitosan film properties, the contact pressures were on the order of 1 GPa.

Tribotest

Higher speed friction tests (48 mm/s to 255 mm/s) were conducted on coatings using a stainless steel ball test in an unlubricated environment at a contact pressure of 65-90 MPa (Figure 6). The resulting COF was found to range from 0.16 to 0.27 (values between that of steel on smooth, clean graphite (0.1) and polystyrene (0.3)). No wear of the films was observed for the short test duration (3-4 m). The low COF is useful for improved durability in sliding applications, such as in biomedical coatings (*21*). AFAM was used to measure nano-scale material elasticity (E) of the coating used in the test, finding the Young's modulus to be 5-7 GPa, a value comparable to polystyrene and other polymeric materials, and similar to the films used for the scratch test. This is an important development as dried chitosan membranes are normally brittle and cross-linking additives must be used to improve flexibility and durability in use.

Conclusions

Electrochemically deposited coatings of chitosan on 304 stainless steel, with minimum surface preparation, yield very good mechanical and adhesion properties. Spectroscopic and mechanical data indicates that cationic chitosan is attracted from the immediate vicinity to the cathodically-polarized surface where we propose that an initial, strongly bound layer is formed through complexation between NH_2 groups and chromate oxyanions in the outermost layer of the passive film. Through a deprotonation mechanism, chitosan is deposited from solution due to the pH gradient near the stainless steel electrode surface. The dried coating develops with a chemistry similar to high molecular weight deacetylated chitosan, with some additional oxidation of functional groups (which may play a role in cross-linking and mechanical properties). The structure formed also seems to possess a higher degree of crystallinity than non-electrochemically formed films. The precise crystalline structure formed is currently under study, as is the role of oxidized C and N in the film.

Scratch and wear tests indicate that the electrodeposited chitosan films have a strong adherence to the stainless steel substrate, have a high amount of elastic recovery, and undergo plastic deformation and cohesive failure prior to delamination. This indicates the capability of the chitosan films to provide a good resistance to high contact stresses with little to no permanent deformation. Higher speed tribotesting revealed a lower friction coefficient, and was comparable to the COFs found in the lower contact pressure regime of the microscratch tests.

Overall, electrochemically-drive deposition of chitosan onto 304 stainless steel substrates, accompanied by UV-exposure and drying, results in a structure

Downloaded by UNIV OF GUELPH LIBRARY on June 23, 2012 | http://pubs.acs.org
Publication Date (Web): November 18, 2010 | doi: 10.1021/bk-2010-1054.ch008

Downloaded by UNIV OF GUELPH LIBRARY on June 23, 2012 | http://pubs.acs.org
Publication Date (Web): November 18, 2010 | doi: 10.1021/bk-2010-1054.ch008

with beneficial mechanical and adhesive properties relevant to various engineering and biomedical applications. Ongoing research into enhancement of interfacial chemistry and properties for new applications will focus on variations in deposition parameters and solution chemistry as well as substrate materials and preparation.

References

1. Yao, K. D.; Peng, T.; Yin, Y. J.; Xu, M. X.; Goosen, M. F. A. Microcapsules /microspheres related to chitosan. *J. Macromol. Sci., Rev. Macromol. Chem. Phys.* **1995**, *C35*, 155–180.
2. Kim, I.-Y.; Seo, S.-J.; Moon, H.-S.; Yoo, M.-K.; Park, I.-Y.; Kim, B.-C.; Cho, C.-S. Chitosan and its derivatives for tissue engineering applications. *Biotechnol. Adv.* **2008**, *26* (1), 1–21.
3. Guibal, E. Heterogeneous catalysis on chitosan-based materials: A review. *Prog. Polym. Sci.* **2005**, *30*, 71–109.
4. Lumelsky, J.; Shur, M. S.; Wagner, S. Sensitive skin. *IEEE Sens. J.* **2001**, *1* (1), 41–51.
5. Lacour, S. P.; Jones, J.; Wagner, S.; Li, T.; Suo, Z. Stretchable Interconnects for Elastic Electronic Surfaces. *Proc. IEEE* **2005**, *93* (8).
6. Payne, G. F.; Raghavan, S. R. Chitosan: a soft interconnect for hierarchal assembly of nano-scale components. *Soft Matter* **2007**, *3*, 521–527.
7. Bumgardner, J .D.; Wiser, R.; Elder, S. H.; Jouett, R.; Yang, Y.; Ong, J. L. Contact angle, protein adsorption and osteoblast precursor cell attachment to chitosan coatings bonded to titanium. *J. Biomater. Sci., Polym. Ed.* **2003**, *14* (12), 1401–1409(9).
8. Greene, A. H.; Bumgardner, J. D.; Yang, Y.; Moseley, J.; Haggard, W. O. Chitosan-coated stainless steel screws for fixation in contaminated fractures. *Clin. Orthop. Relat. Res.* **2008**, *466*, 1699–1704.
9. Guibal, E. Interactions of metal ions with chitosan-based sorbents: a review. *Sep. Purif. Technol.* **2004**, *38*, 43–74.
10. Dahms, H.; Croll, I. M. The anomalous codeposition of nickel-iron alloys. *J. Electrochem. Soc.* **1965**, *112*, 771–775.
11. Fernandez, R.; Wu, L.-Q.; Chen, T.; Yi, H.; Rubloff, G. W.; Ghodssi, R.; Bentley, W. E.; Payne, G. F. Electrochemically-induced deposition of a polysaccharide hydrogel onto a patterned surface. *Langmuir* **2003**, *19*, 4058–4062.
12. Dreyer, E. Masters Thesis, University of Maryland, 2006.
13. Davidenko, N. Photopolymerisation Of Acrylic Acid And Chitosan Gels (I). Influence Of Preparation Method On The Formation And Kinetic Behaviour Of Interpenetrating Complexes. *Lat. Am. Appl. Res.* **2007**, *37*, 247.
14. Halada, G. P.; Jha, P.; Nelson, K.; Korach, C. S.; Neiman, A. Formation and characterization of chitosan-based composite coatings. Abstract PMSE 375, 238th National American Chemical Society meeting, Washington, DC, August 16th–20th, 2009

15. Zhao, W.; Singh, R. P.; Korach, C. S. Effects of environmental degradation on near-fiber nanomechanical properties of carbon fiber epoxy composites. *Composites, Part A* **2009**, *40*, 675–678.
16. Caixia, L.; Zihua, Y.; Zhiyun, L.; Yunke, W. Preparation and characterization of hydroxyapatite/chitosan-sodium alginate composite materials. http://www.chemistrymag.org/cji/2006/088053pe.htm (Vol. 8, no. 8, p 53, 2006).
17. Nunthanid, J.; Puttipipatkhachorn, S.; Yamamoto, K.; Peck, G. E. Physical Properties and Molecular Behavior of Chitosan Films. *Drug Development and Industrial Pharmacy* **2001**, *27* (2), 143–157.
18. Jaworska, M.; Sakurai, K.; Gaudon, P.; Guibal, E. Influence of chitosan characteristics on polymer properties. I: Crystallographic properties. *Polym. Int.* **2003**, *52*, 198–205.
19. Felt, O.; Buri, P.; Gurny, R. Chitosan: a unique polysaccharide for drug delivery. *Drug Dev. Ind. Pharm.* **1998**, *24* (11), 979–993.
20. Sionkowska, A.; Kaczmarek, H.; Wisniewski, M.; Skopinska, J.; Lazare, S.; Tokarev, V. The Influence of UV Irradiation on the Surface of Chitosan Films. *Surf. Sci.* **2006**, *600*, 3775–3779.
21. Ramakrishnan, S.; Mayer, J.; Wintermantel, E.; Leong, K. W. Biomedical applications of polymer-composite materials: a review. *Compos. Sci. Technol.* **2001**, *61* (9), 1189–1224.

Downloaded by UNIV OF GUELPH LIBRARY on June 23, 2012 | http://pubs.acs.org
Publication Date (Web): November 18, 2010 | doi: 10.1021/bk-2010-1054.ch008

Downloaded by DUKE UNIV on June 23, 2012 | http://pubs.acs.org
Publication Date (Web): November 18, 2010 | doi: 10.1021/bk-2010-1054.ch009

Chapter 9

Cyclic Dithiocarbonates: Novel in Situ Polymerizing Biomaterials for Medical Applications

Ankur S. Kulshrestha, Walter R. Laredo, Tom Matalenas, and Kevin L. Cooper*

Advanced Technologies and Regenerative Medicine LLC, Somerville, New Jersey, NJ 08876
***KCooper2@its.jnj.com**

Cyclic dithiocarbonates as a new class of in-situ gelling biomaterials is reported. Cyclic dithiocarbonates with degradable ester linkages were synthesized and characterized. PEG based cyclic dithiocarbonates were also prepared. These cyclic dithiocarbonates were reacted with amines such as spermidine and Jeffamines at room temperature to form cross-linked networks. Furthermore, no addition of any catalyst or solvent is required to facilitate gelation. Gelation occurred from seconds to a couple of minutes for both PEG based and ester-linked cyclic dithiocarbonates. Biocompatibility of the cross-linked polymers formed as a result of the reaction of PEG as well as ester linkage containing dithiocarbonates with spermidine as the cross-linker was studied using a intramuscular rat model. Rats were implanted with pre-polymerized discs and euthanized at 3 and 28 days (N=4 per time point). Necrosis surrounding the implant was measured and was found to be average 200 microns at day 3 which becomes negligible at later time points (28 days). This is similar to a low molecular weight PLGA [poly(lactide-co-glycolide)] drug depot and hence could be deemed acceptable for some biomedical applications where the thickness of tissue is greater than 200 microns. The cyclic dithiocarbonates and the cross-linked gels derived from them described in this communication are anticipated to have a number of potential biomedical and pharmaceutical applications

In Biomaterials; Kulshrestha, A., et al.;
ACS Symposium Series; American Chemical Society: Washington, DC, 2010.

> such as to encapsulate and thereby deliver bioactive agents, cells or genes to a desired site, in tissue engineering applications as supports for cells, in wound healing as tissue sealants or adhesives, as coating materials to coat the surfaces of the implantable medical devices to affect the surface properties.

1. Introduction

The development of injectable, fast curing, in-situ gelling biomaterials that can be delivered to the body cavity in a fluid form and can solidify on site via polymerization yielding appropriate physical properties have been of intense interest in recent years. The fluidity of these biomaterials not only enhances their ease of use but also reduces their invasiveness associated with applications such as tissue engineering and drug delivery.

Various synthetic methodologies to prepare these kind of biomaterials have been reported in the literature. All these synthetic methodologies aim to develop biocompatible, chemically versatile materials capable of maintaining sustained, localized drug delivery or acting as a scaffold for incorporation of biologically active molecules or cells to either enhance (i.e tissue regeneration) or limit tissue growth (i.e.adhesion prevention) (*1*). These methodologies include ionic crosslinking of alginate (*2*), thermally induced physical crosslinking of pluronics (*3*) and poly(NIPAM-co-acrylic acid) (*4*) and enzymatic or pH induced gelation of chitosan (*5*). Unfortunately, most of the materials prepared using the synthetic methodologies described above have poor mechanical properties due to limited control on gelation kinetics and hence limit the potential of their practical use in medical and pharmaceutical applications.

Covalent crosslinking is recognized as a much more viable route to prepare biomaterial networks with mechanical properties similar to that of native tissues. This is reflected in the wide participation of many research groups in this area and the resulting large number of publications. For example, Temenoff et al. (*6*) developed thermally crosslinked oligo(poly(ethyleneglycol) fumarate) hydrogels to support osteogenic differentiation of encapsulated marrow stromal cells. Anseth and co workers developed photocrosslinked polyanhydrides (*7*) and thiol-acrylate photopolymers (*8*) as in situ forming biomaterial for orthopaedic applications. However, the molecules used to generate the active radical centers and initiate chain growth polymerization can be cytotoxic and in certain applications, such as cell, protein and DNA encapsulation residual initiator molecules are problematic. As an alternative to thermally and photoinitiated crosslinked in situ forming degradable networks, Hubbell and coworkers (*9*) developed degradable networks formed through the Michael addition type reactions between thiol and acrylate, acrylamide and vinyl sulfone group. Although the Michael addition reaction eliminated the need to add any initiators but the network gelation rates to achieve optimal crosslinking efficiency were considerably slower than the photoinitiated chain polymerizations.

We are currently investigating alternative crosslinking chemistries to photocrosslinking and Michael addition that spontaneously afford a gel within a

Downloaded by DUKE UNIV on June 23, 2012 | http://pubs.acs.org
Publication Date (Web): November 18, 2010 | doi: 10.1021/bk-2010-1054.ch009

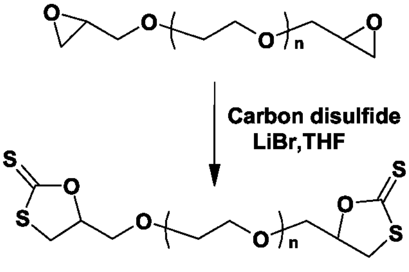

Scheme 1. Synthesis of PEG dithiocarbonates from PEG diglycidyl ether.

Downloaded by DUKE UNIV on June 23, 2012 | http://pubs.acs.org
Publication Date (Web): November 18, 2010 | doi: 10.1021/bk-2010-1054.ch009

few minutes at room temperature without any added catalyst. Herein, we report for the first time the application of cyclic dithiocarbonates as a new class of in situ polymerizing biomaterials. Cyclic dithiocarbonates have been reported in the literature (*10a–10d*) to have high reactivity and selectivity, especially for amines and forms crosslinked networks spontaneously at room temperature with amines without addition of any catalyst. The crosslinking is reported to occur as a result of the formation of disulfide linkages formed by the autooxidation of the thiol groups produced during the reaction (*10d*). These characterstics motivated us to study them as fast curing in situ gelling materials for biomedical applications. Cyclic dithiocarboonates are formed by the reaction of oxiranes with carbon disulfide (*10e*). Although compounds and polymers containing dithiocarbonate groups are reported in the literature to have application as ingredients for coatings, adhesives, inks, sealing agents and photoresist materials but there has been no report so far of their biomedical application. This paper describes for the first time the synthesis of polyethyleneglycol based as well as ester linkage containing degradable cyclic dithiocarbonates, the formation of crosslinked materials from these dithiocarbonate precursors and the biocompatibility of these crosslinked materials.

Poly(ethyleneglycol) dithiocarbonates of number average molecular weights 200, 500 and 1000 were synthesized from corresponding commercially available poly(ethyleneglycol) diglycidyl ether by the addition of carbon disulfide in presence of lithium bromide catalyst using tetrahydrofuran solvent at room temperature as shown in Scheme 1. Figure 3 displays the ^{1}H NMR spectra of cyclic dithiocarbonate of Polyethyleneglycol diglycidylether. The PEG based cyclic dithiocarbonates were fully characterized by ^{1}H NMR and ^{13}C NMR spectroscopy. The details of the synthesis and characterization of the PEG dithiocarbonates are described in section 3.

In order to prepare cyclic dithiocarbonates with degradable ester linkage, the precursor diglycidyl ester was synthesized from glycidol and the acid chloride (*11*, *12*). For example, cyclic dithiocarbonate of diglycidyl sebacate was synthesized by the addition of Carbon disulfide to the diglycidyl sebacate formed from sebacoyl chloride and glycidol as shown in Scheme 2. The cyclic dithiocarbonate of diglycidyl sebacate and the precursor diglycidyl sebacate were fully characterized by ^{1}H NMR and ^{13}C NMR spectroscopy as shown in section 3. Figures 4 and 5 display the ^{1}H NMR and ^{13}C NMR spectra respectively of cyclic dithiocarbonate of diglycidyl sebacate.

Downloaded by DUKE UNIV on June 23, 2012 | http://pubs.acs.org
Publication Date (Web): November 18, 2010 | doi: 10.1021/bk-2010-1054.ch009

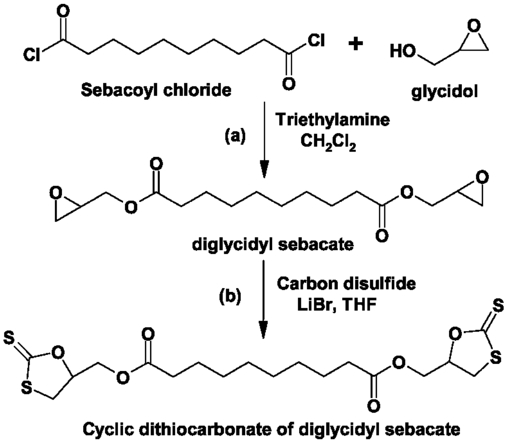
Sebacoyl chloride
glycidol
(a)
Triethylamine
CH_2Cl_2
diglycidyl sebacate
(b)
Carbon disulfide
LiBr, THF
Cyclic dithiocarbonate of diglycidyl sebacate

Scheme 2. Synthesis of degradable cyclic dithiocarbonate.

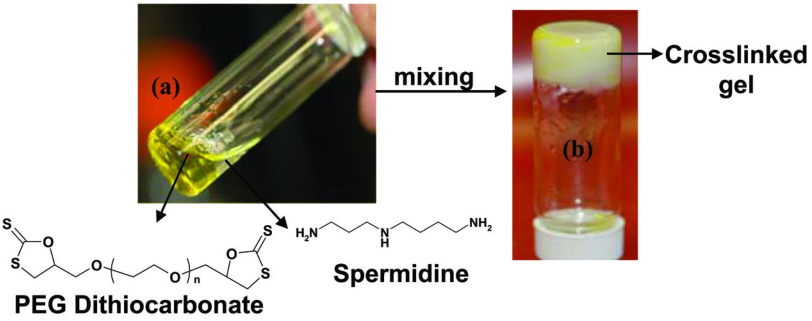
(a)
mixing
Crosslinked gel
(b)
PEG Dithiocarbonate
Spermidine

Figure 1. Formation of crosslinked gel from PEG dithiocarbonate and Spermidine after mixing at room temperature.

To prepare the crosslinked gel, the synthesized PEG based cyclic dithiocarbonate of average molecular weight 500 was reacted with either Spermidine or a 1:1 combination of PEG based amines (Jeffamine XTJ-504 and HK-511) as crosslinkers at room temperature in absence of any catalyst and solvent. The molar ratio of amine to the dithiocarbonate in all the formulations was 1:1. Furthermore, Spermidine was assumed to react as a triamine in the formulation where it was used as a crosslinker. The gelation time was monitored by measuring the storage modulus (G′) as well as the loss modulus (G″) at 37°C. The gel point was taken to be the point of interection of G′ and G″. The time for the formation of gel varied from few seconds to a couple of minutes depending on the amine used. Thus, when spermidine was used as a crosslinker, the gel formed within a minute as shown in Figure 1, whereas when 1:1 combination of Jeffamines HK-511 and XTJ-504 was used the gel formation took 5 minutes. Furthermore, the gels formed from exhibited viscoelastic properties. For example, the complex modulus for the crosslinked gel formed from PEG dithiocarbonate and Jeffamines was 3.5x 10^4. Detailed rheological studies are currently in progress in our laboratory and will be reported later as a part of the full paper.

Downloaded by DUKE UNIV on June 23, 2012 | http://pubs.acs.org
Publication Date (Web): November 18, 2010 | doi: 10.1021/bk-2010-1054.ch009

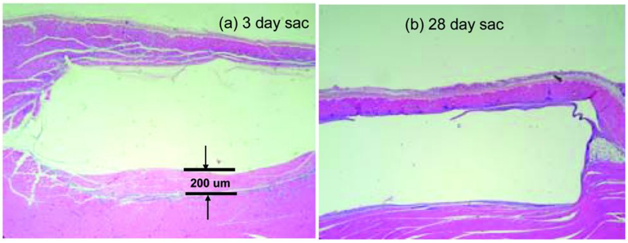

Figure 2. Histological photomicrographs of intramuscular skin of rat after (a) 3 days and (b) 28 days of implantation of prepolymerized crosslinked disks formed from the reaction of PEG based cyclic dithiocarbonates with spermidine as the crosslinker showing mild tissue necrosis similar to that observed in PLGA drug depots after 3 days which completely disappears after 28 days of implantation. Similar results were obtained from the implantation of prepolymerized crosslinked disks using ester linkage containing dithiocarbonates with spermidine as the cross-linker.

Similar results were obtained when reactions were done between the ester linkage containing degradable cyclic dithiocarbonate of diglycidyl sebacate and the amines except that Poly(ethyleneglycol) of average molecular weight 200 was used as a solvent to dissolve the cyclic dithiocarbonate of diglycidyl sebacate.

In order to determine the biocompatibility of the crosslinked polymers formed as a result of the reaction of Poly(ethyleneglycol)dithiocarbonates and ester linkage containing dithiocarbonates respectively with spermidine as the crosslinker, two sets of tissue reaction studies were performed. These preliminary studies were performed in rats intramuscularly. Four rats were used per time point with two sacs of 3 and 28 days. The crosslinked polymers were implanted as pre-polymerizaed discs. This was done in this study to eliminate any variability in polymerization from animal to animal. Three histological photomicrographs are shown in figure 2. Figure 2a and 2b are histological photomicrographs after 3 and 28 days of implantation of crosslinked polymer formed from PEG dithiocarbonate and spermidine as the crosslinker. The center clear portion in the two photomicrographs is where the polymer disc was located. The disc was lost during processing. The important aspect to observe between these two photomicrographs is the degree of necrosis surrounding the implant. In the fig 2a the necrosis averaged 200 microns. This is similar to a low molecular weight PLGA drug depot and hence could be deemed acceptable for some applications where the thickness of tissue is greater than 200 microns. In the fig 2b, the necrosis was negligible in this case. Hence, based on these results it is believed that unreacted amines leach out of the polymer discs in the first few days and cause the tissue reactions that were observed here after 3 days which becomes negligible at later time points (28 days). The results of the same biocompatibility studies with the crosslinked polymers obtained from ester linkage containing dithiocarbonates with spermidine were same. Work is in progress in our lab to optimize the formulations to reduce the leachables to further improve the tissue reactions so that they can be studied for their efficacy in several appropriate biomedical applications.

Downloaded by DUKE UNIV on June 23, 2012 | http://pubs.acs.org
Publication Date (Web): November 18, 2010 | doi: 10.1021/bk-2010-1054.ch009

2. Experimental

2.1. Materials

Polyethylene glycol diglycidyl ether of molecular weight 200 and 500 were purchased from Aldrich and were used without further purification. Sebacoyl chloride, diglycolyl chloride, glycidol, carbon disulfide, spermidine, anhydrous dichloromethane, anhydrous tetrahydrofuran and lithium bromide were purchased from Aldrich Chemical Company in the highest possible purity and used as received. Hexanes and Acetone were purchased from Fisher Scientific Co. Branched PEG based amines i.e Jeffamines (XTJ-504, T-403) were received as a gift from Huntsman Corporation, Alabama.

2.2. Instrumental Methods

2.2.1. Nuclear Magnetic Resonance (NMR)

The precursor cyclic dithiocarbonates were characterized using proton (^1H) and gated ^{13}C NMR spectroscopy. Spectra were recorded on a Varian Unity NMR spectrometer at 400 MHz and 100 MHz, respectively, in *d*-chloroform as solvent. ^1H NMR chemical shifts in parts per million (ppm) are reported downfield from 0.00 ppm using tetramethylsilane (TMS) as an internal reference. The concentration of the synthesized cyclic dithiocarbonates was ~10% w/v in *d*-chloroform. The instrument parameters for ^1H NMR experiments were as follows: 3.4 s acquisition time, temperature 300K, spectral width 6000 Hz, 32 transients. ^{13}C NMR chemical shifts were referenced relative to *d*-chloroform at 77.0 ppm. The concentration of the synthesized polymers was ~25% w/v in *d*-chloroform. The instrument parameters for ^{13}C NMR experiments were as follows: 1.19 s acquisition time, temperature 300K, spectral width 25 000 Hz, number of scans 5 000.

3. Synthesis and Characterization

3.1. Synthesis and Characterization of Bis [(2-thioxo-1, 3-oxathiolan-5-yl) methyl] Decanedioate

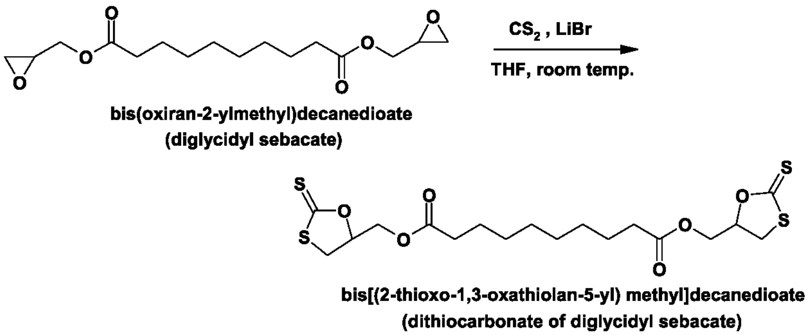
CS$_2$, LiBr
THF, room temp.
bis(oxiran-2-ylmethyl)decanedioate
(diglycidyl sebacate)
bis[(2-thioxo-1,3-oxathiolan-5-yl) methyl]decanedioate
(dithiocarbonate of diglycidyl sebacate)

Downloaded by DUKE UNIV on June 23, 2012 | http://pubs.acs.org
Publication Date (Web): November 18, 2010 | doi: 10.1021/bk-2010-1054.ch009

Into a flame dried 1000 mL round flask equipped with nitrogen inlet was dissolved bis (oxiran-2-ylmethyl) decanedioate (15.4g, 49mmol) and 700mg of Lithium bromide catalyst (Aldrich, Milwaukee, WI) in 200 mL of anhydrous Tetrahydrofuran (Aldrich, Milwaukee, WI). To this magnetically stirred solution was added dropwise Carbon disulfide (8.96g, 118mmol) from a flame dried addition funnel. The reaction mixture was left for stirring at room temperature for 24 hours. After the reaction, tetrahydrofuran solvent was rotoevaporated under reduced pressure and the resultant product was purified by column chromatography using silica gel (70-230 mesh, 60A^O, Aldrich, Milwaukee) and 50/50 hexane/acetone as the mobile phase. The resultant dithiocarbonate was isolated as a yellow colored liquid, which turns gradually into a yellow creamy solid. The dithiocarbonate was characterized by ^{1}H NMR and ^{13}C NMR spectroscopy using a Varian Unity Plus 400 MHz Spectrometer. ^{1}H NMR (400MHz,$CDCl_3$), δ=1.297-1.393 (bm, 8H), δ=1.642 (bm, 4H), δ=2.348 (t, 4H), δ=3.534-3.632 (dd, 2H), δ=3.642-3.722, (dd, 2H), δ=4.352-4.422 (bm, 2H), δ=4.454-4.532 (dd, 2H), δ=5.297-5.395 (bm, 2H). ^{13}C NMR (100MHz, $CDCl_3$) 24.9 ppm, 29.48 ppm, 34.13ppm, 36.21ppm, 63.85ppm, 89ppm, 173.51 ppm, 212ppm.

3.2. Synthesis and Characterization of Bis [(2-thioxo-1, 3-oxathiolan-5-yl) methyl] 2,2′-Oxydiacetate

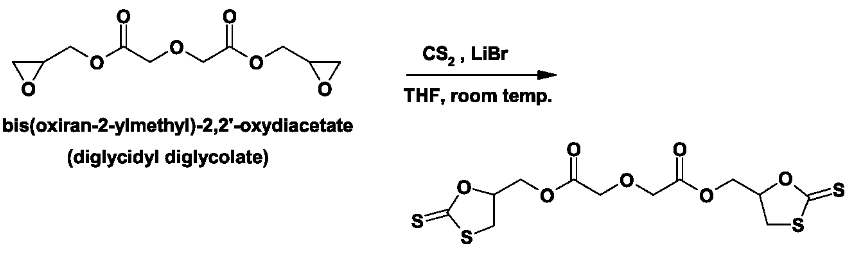

bis(oxiran-2-ylmethyl)-2,2'-oxydiacetate
(diglycidyl diglycolate)

bis[(2-thioxo-1,3-oxathiolan-5-yl) methyl]2,2'-oxydiacetate
(dithiocarbonate of diglycidyl diglycolate)

Into a flame dried 1000 mL round flask equipped with nitrogen inlet was dissolved bis (oxiran-2-ylmethyl) 2,2′-oxydiacetate (26.0g, 106 mmol) and 700mg of Lithium bromide catalyst (Aldrich, Milwaukee, WI) in 200 mL of anhydrous Tetrahydrofuran (Aldrich, Milwaukee, WI). To this magnetically stirred solution was added dropwise Carbon disulfide (19.31g, 253 mmol) from a flame dried addition funnel. The reaction mixture was left for stirring at room temperature for 20 hours. After the reaction, tetrahydrofuran solvent was rotoevaporated under reduced pressure and the resultant product was purified by column chromatography using silica gel (70-230 mesh, 60A^O, Aldrich, Milwaukee) and 30/70 hexane/acetone as the mobile phase. The resultant dithiocarbonate was isolated in 86% yield as a yellow orange colored viscous liquid. The dithiocarbonate was characterized by ^{1}H NMR spectroscopy using a Varian Unity Plus 400 MHz Spectrometer. ^{1}H NMR (400MHz,$CDCl_3$), δ=3.53-3.63 (dd, 2H), δ=3.64-3.72 (dd, 2H), δ =4.29(s, 4H), δ=4.42-4.53 (bm, 4H), δ=5.29-5.39 (bm, 2H).

3.3. Synthesis and Characterization of PEG 200 Dithiocarbonate

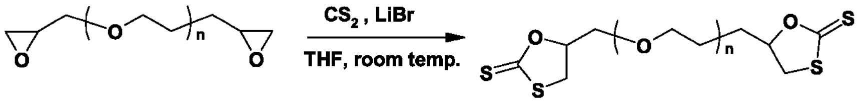

Into a flame dried 1000 mL round flask equipped with nitrogen inlet was dissolved Poly(ethylene glycol) diglycidyl ether (50.0g, 250 mmol) (average M_n ca. 200, Polysciences, PA), and 500mg of Lithium bromide catalyst (Aldrich, Milwaukee, WI) in 200 mL of anhydrous Tetrahydrofuran (Aldrich, Milwaukee, WI). To this magnetically stirred solution was added dropwise Carbon disulfide (45.70g, 600 mmol) from a flame dried addition funnel. The reaction mixture was left for stirring at room temperature for 16 hours. After the reaction, tetrahydrofuran solvent was rotoevaporated under reduced pressure and the resultant product was purified by column chromatography using silica gel (70-230 mesh, 60A^{O}, Aldrich, Milwaukee) and 50/50 hexane/acetone as the mobile phase. The resultant polymer was isolated as a yellow colored liquid. The polymeric dithiocarbonate was characterized by ^{1}H NMR and ^{13}CNMR spectroscopy using a Varian Unity Plus 400 MHz Spectrometer. ^{1}H NMR (400MHz,$CDCl_3$), δ=3.53-3.74 (bm, 4H), δ=3.75-3.83 (bm, 1H), δ3.84-3.92 (bm, 1H), δ=3.92-4.11 (bm, 1H), δ=5.32-5.21(bm, 2H). ^{13}C NMR (100MHz, $CDCl_3$) 36.3, 44.2, 69.3, 70.1, 70.6, 71.0, 79.7, 89.8, 212.4 ppm.

3.4. Synthesis and Characterization of PEG 500 Dithiocarbonate

Into a flame dried 1000 mL round flask equipped with nitrogen inlet was dissolved Poly(ethylene glycol) diglycidyl ether (100.0g, 191.8 mmol) (average M_n ca. 500, Aldrich, Milwaukee, WI), and 833mg of Lithium bromide catalyst (Aldrich, Milwaukee, WI) in 200 mL of anhydrous tetrahydrofuran (Aldrich, Milwaukee, WI). To this magnetically stirred solution was added dropwise carbon disulfide (35.0g, 460.3 mmol) from a flame dried addition funnel. The reaction mixture was left for stirring at room temperature for 16 hours. After the reaction, tetrahydrofuran solvent was rotoevaporated under reduced pressure and the resultant product was purified by column chromatography using silica gel (70-230 mesh, 60A^{O}, Aldrich, Milwaukee) and 50/50 hexane/acetone as the mobile phase. The resultant polymer was isolated as a yellow colored liquid. The polymeric dithiocarbonate was characterized by ^{1}H NMR and ^{13}CNMR spectroscopy using a Varian Unity Plus 400 MHz Spectrometer. ^{1}H NMR (400MHz,$CDCl_3$), δ=3.53-3.74 (bm, 4H), δ=3.75-3.83 (bm, 1H), δ=3.84-3.92 (bm, 1H), δ=3.92-4.11 (bm, 1H), δ=5.32-5.21(bm, 2H). ^{13}CNMR (100MHz, $CDCl_3$) 36.3, 44.2, 69.3, 70.1, 70.6, 71.0, 79.7, 89.8, 212.4 ppm.

Downloaded by DUKE UNIV on June 23, 2012 | http://pubs.acs.org
Publication Date (Web): November 18, 2010 | doi: 10.1021/bk-2010-1054.ch009

Downloaded by DUKE UNIV on June 23, 2012 | http://pubs.acs.org
Publication Date (Web): November 18, 2010 | doi: 10.1021/bk-2010-1054.ch009

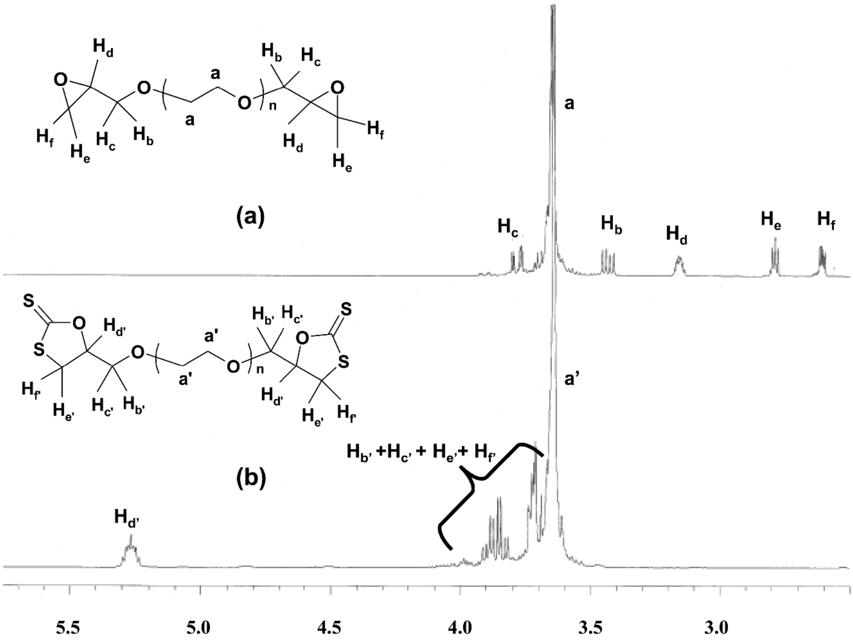

Figure 3. ^{1}*H NMR spectra (400 MHz, d-chloroformCDCl*$_3$*) of (a) Polyethyleneglycol diglycidyl ether (b) Cyclic dithiocarbonate of Polyethyleneglycol diglycidylether.*

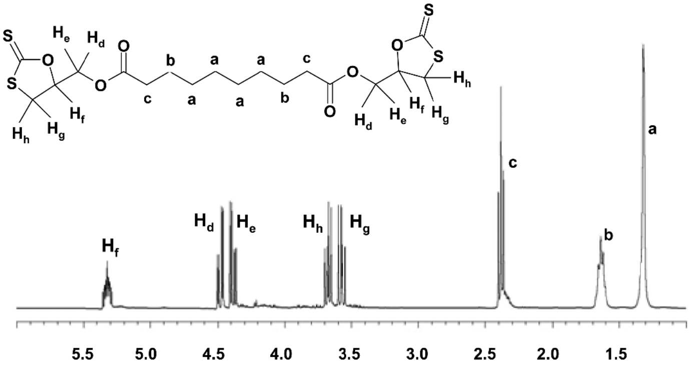

Figure 4. ^{1}*H NMR spectra (400 MHz, d-chloroform) of cyclic dithiocarbonate of diglycidyl sebacate containing degradable ester linkages.*

Downloaded by DUKE UNIV on June 23, 2012 | http://pubs.acs.org
Publication Date (Web): November 18, 2010 | doi: 10.1021/bk-2010-1054.ch009

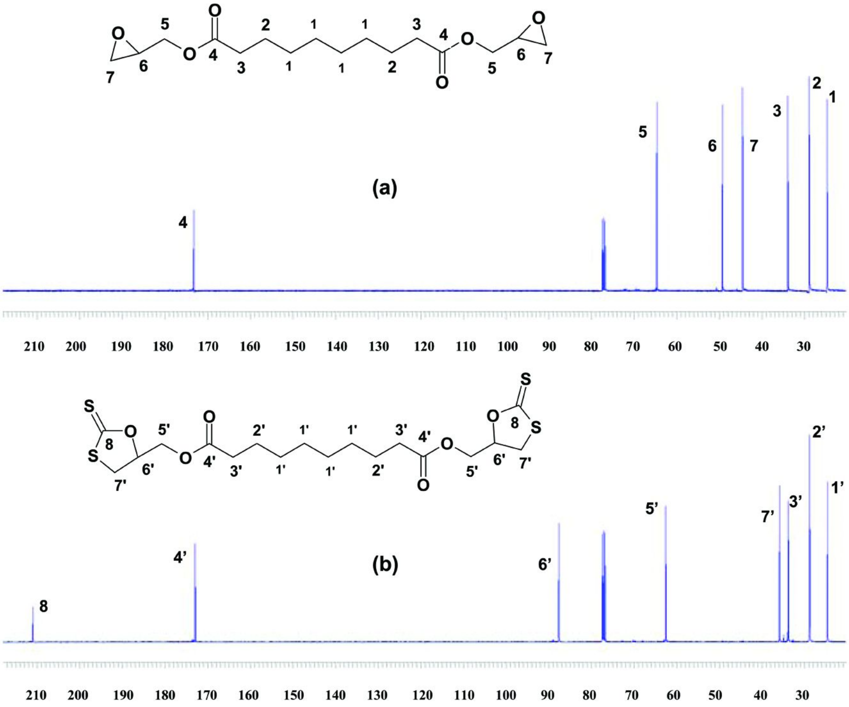

Figure 5. Expanded region of ^{13}C NMR (100 MHz) spectra recorded in d-chloroform that shows signals corresponding to (A) diglycidyl sebacate and (B) cyclic dithiocarbonate of diglycidyl sebacate.

4. Conclusions

In summary, cyclic dithiocarbonates as a new class of in situ polymerizing biomaterials is reported. The curing of these dithiocarbonates with amines occurs at room temperature without addition of any catalyst. Furthermore, addition of solvent is not necessary in some cases to dissolve the dithiocarbonates. We believe that the cyclic dithiocarbonates and the crosslinked gels derived from them can have various potential biomedical applications such as to encapsulate and thereby deliver bioactive agents, cells or genes to a desired site, in tissue engineering applications as supports for cells, to coat the surfaces of the implantable medical devices to affect the surface properties.

Acknowledgments

We wish to acknowledge Johnson & Johnson Corporate Office of Science and Technology for their Financial Support. Authors would like to thank Neil Cowley for carrying out the GPC, Tricia Twaddle, Wei Kong and John Mathews for animal studies and Susan Trenka-Benthin for Histological studies.

References

1. Gutowska, A.; Jeong, B.; Jasionowski, M. *Anat. Rec.* **2001**, *263* (4), 342.
2. Kuo, C. K.; Ma, P. X. *Biomaterials* **2001**, *22* (6), 511.
3. Cao, Y. L.; Ibarra, C.; Vacanti, C. *Tissue Engineering: Methods and Protocols*; Humana Press: 1999.
4. (a) Kim, S.; Healy, K. E. *Biomacromolecules* **2003**, *4* (5), 1214. (b) Shim, W. S.; Yoo, J. S.; Bae, Y. H.; Lee, D. S. *Biomacromolecules* **2005**, *4* (5), 1214
5. Chen, T. H.; Embree, H. D.; Brown, E. M.; Taylor, M. M.; Payne, G. F. *Biomaterials* **2003**, *24* (17), 2831.
6. Temenoff, J. S.; Park, H.; Jabbari, E.; Conway, D. E.; Sheffield, T. L.; Ambrose, C. G. *Biomacromolecules* **2004**, *5* (1), 5.
7. (a) Pohusta, A. K.; Burdick J. A.; Mortisen, D. J.; Padera, R. F.; Ruehlman D.; Yaszemski, M. J.; Anseth, K. S. *J. Biomed. Mater. Res.* **2003**, *64A*, 62. (b) Burkoth A. K.; Anseth K. S. *Biomaterials* **2002**, *23* (22), 4307.
8. Rydholm, A. E.; Bowman, C. N.; Anseth, K. S. *Biomaterials* **2005**, *26*, 4495.
9. (a) Elbert, D. L.; Hubbell, J. A.; *Biomacromolecules* **2001**, *2* (2), 430. (b) Elbert, D. L.; Pratt A. B.; Lutolf, M. P.; Halstenberg S.; Hubbell, J. A. *J. Controlled Release* **2001**, *76* (1−2), 11. (c) Lutolf, M. P.; Hubbell, J. A. *Biomacromolecules* **2003**, *4* (3), 713. (d) Lutolf, M. P.; Tirelli, N.; Cerritelli, S.; Cavalli, L.; Hubbell, J. A. *Bioconjugate Chem.* **2001**, *12* (6), 1051. (e) Vernon B.; Tirelli, N.; Bachi, T.; Haldimann, D.; Hubbell, J. A. *J. Biomed. Mater. Res., Part A* **2003**, *64A* (3), 447.
10. (a) Murayama, T.; Hotta, I.; Hanrahan, B. *Polym. Prepr.* **2003**, *44* (1), 156. (b) Choi, W.; Sanda, F.; Kihara, N.; Endo, T. *J. Polym. Sci., Part A: Polym. Chem.* **1998**, *36*, 79. (c) Choi, W.; Nakajima, M.; Sanda, F.; Endo, T. *Macromol. Chem. Phys.* **1998**, *199*, 1909. (d) Moriguchi, T.; Endo, T. *Macromolecules* **1995**, *28*, 5386. (e) Kihara, N.; Nakawaki, Y.; Endo, T. *J. Org. Chem.* **1995**, *60*, 473.
11. Kulshrestha, A. K.; et al. Dithiocarbonate containing macromers and polymers derived from such macromers. U.S. Patent No. 7572929.
12. Kulshrestha, A. K.; et al. Cyclic dithiocarbonates: Novel in situ gelling biomaterials. Abstracts of Papers, 238th ACS National Meeting, Washington, DC, United States, August 16−20, 2009, PMSE-139.

Downloaded by DUKE UNIV on June 23, 2012 | http://pubs.acs.org
Publication Date (Web): November 18, 2010 | doi: 10.1021/bk-2010-1054.ch009

Chapter 10

Synthesis of Morpholine-2,5-dione Monomers for the Preparation of Polydepsipeptides

Mena Abdelmelek,[1] Mary Nguyen,[1] Valerie Bradford,[2] Brent Iverson,[2] and Laura Suggs[1,*]

[1]Department of Biomedical Engineering, University of Texas at Austin
[2]Department of Chemistry and Biochemistry, University of Texas at Austin
[*]laura.suggs@mail.utexas.edu

Biomaterials derived from synthetic polymers have traditionally been used for a variety of tissue engineering applications, however current research focuses on biologically functionalizing materials to improve various physical characteristics. Our laboratory has investigated the synthesis and characterization of polydepsipeptides (PDPs), which combine both synthetic and biologically relevant chemical groups. PDPs are prepared from a cyclic intermediate, the morpholine dione (MD). Here, we describe the synthesis of MDs using solid phase synthesis in an attempt to control racemization and improve purity with respect to prior solution phase synthesis methods.

Polydepsipeptides: Hybrids of Synthetic and Natural Materials

Polydepsispeptides (PDPs) represent an important class of biomaterials. PDPs can be considered as ‘hybrids’ with characteristics of both poly(α-hydroxy acids) and polypeptides, which make them ideal candidates for tissue engineering and biomedicine (Figure 1). The basis of this assertion is three-fold: PDPs are bioresorbable and biocompatible due to the biologic origin of their components and degradation products, bear pendant functional groups that can be derivatized, and are capable of spontaneous assembly into novel secondary structures due to the occurrence of amino acid residues at regular intervals. Langer and colleagues synthesized RGD-modified PDP, poly(lactic acid-*co*-lysine) (PLAL) (*1*). Their results illustrated an increase in cellular adhesion and proliferation of bovine

In Biomaterials; Kulshrestha, A., et al.;
ACS Symposium Series; American Chemical Society: Washington, DC, 2010.

aortic endothelial cells compared to PLA films. Similarly, Yan *et al.* synthesized RGD-modified poly[Lac-*co*-(Glc-*alt*-*L*-Lys)] and demonstrated improved cellular adhesion, viability, and morphological properties of RSC96 cells compared to culture on poly-*D,L*-lactic acid (PDLLA) films (*2*).

PDPs resemble both poly(α-hydroxy acid)s and polypeptides, while possessing features that circumvent the limitations of either material. For instance, poly(lactic-co-glycolic acid) (PLGA) lacks pendant functional groups that can serve as attachment sites for drugs, crosslinking agents, or protein ligands. Additionally, PLGA and other poly(α-hydroxy acid)s are unable to assemble into higher order structures primarily because they are synthesized as random copolymers which inhibits the formation of regularly occurring structural units. On the other hand, synthetic polypeptides bear chemically labile functional groups and are capable of higher order structural assembly. However, their use as implantable materials has been limited due to factors such as low solubility, thermal instability, and immunogenicity (*3–5*).

Morpholine Diones: A Historical Perspective

The synthesis of PDPs is similar to that of poly(lactones), in which a cyclic intermediate, in this case a morpholine-2,5-dione (MD), is opened upon polymerization. Ring-opening polymerization of MDs has been studied extensively for the preparation of a variety of PDPs. Readers interested in a thorough review of the synthesis and characterization of MDs are directed to a recent review (*6*). The main concerns associated with this synthesis include successful attachment of pendant groups, racemization at the 3- and 6-position, purity and product yield. The next section will focus on the progression of adding functionality to the 3- and 6-positions of the MD (Figure 2), specifically the identity of the peptide and hydroxy acid, and the effects on polymerization and yield.

Initial reports of MDs consisted of relatively simple functionality at the 3- and 6-position (Figure 3). For example, the MDs synthesized by Shalaby and Koelmel were based on glycolic acid and glycine or alanine (*7*). Helder et al. incorporated a methyl group to the 6-position, rendering a PDP with alternating lactic acid and glycine components (*8*, *9*). The MD was recovered as yellow oil and recrystallized six times from ethyl acetate in 39% yield. Polymerization was carried out while varying the amount of stannous octoate initiator and polymerization time at 130°C. The molecular weights of the polymer were on the order of 2×10^4 which was considerably lower than poly(*L*-lactide) synthesized in a similar manner (MW~10^5). Investigators maintained that the sample with the longest polymerization time did not form a polymer, specifically due the presence of residual solvent and uncyclized intermediates. Substitution at various positions of MDs can also affect polymerization. For example, Yonezawa et al. found that MDs substituted at the 4-position did not polymerize (*10*).

The stereochemistry of the MD at the 3- and 6-position is relatively difficult to control and affects the mechanical properties of the final polymer. Feijen et al. synthesized functionalized PDPs based on aspartic acid, lysine, and

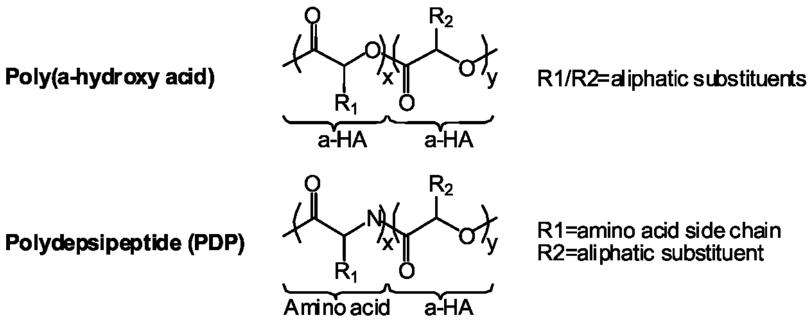

Figure 1. Structural comparisons between poly(α-hydroxy acid)s and PDPs.

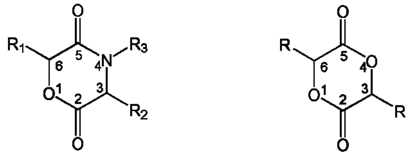

Figure 2. General structure of morpholine-2,5-dione (left, R_3=H in most cases) compared to six-membered lactones (right)

cysteine side chains (*11*). The intermediates were cyclized with two methods: dry heating the sodium salts of the appropriate linear intermediates or with triethylamine (TEA) in DMF at 100°C. While the MDs synthesized with TEA gave lower yields (29% to 58%) compared to the dry heating method (23% to 83%), they had greater optical purity. In addition, the later method was contaminated with numerous side products, which could not be removed by recrystallization or column chromatography. Fung and Glowaky synthesized optically active 3-substitued MDs with glycolic acid and alanine, leucine, or phenylalanine functionality for the development of optically active PDPs to improve the crystallinity of analogous racemic PDPs (*12*). The polymerization of (L)-3-methylmorpholine-2,5-dione gave semi-crystalline poly(*L*-Ala-alt-Glc) whereas polymerization of (D,L)-3-methylmorpholine-2,5-dione yielded amorphous poly(*D,L*-Ala-alt-Glc).

The rotational identity of the amide bonds can also affect ring formation. Feijen et al. described the synthesis of 3,6-alkyl substituted MDs inspired by lactic acid and glycine, alanine, and valine (*13*, *16*, *17*). MD yields ranged from 4% for (S)-3-isopropylmorpholine-2,5-dione to 83% for (S)-3-methyl-(*R,S*)-6-methylmorpholine-2,5-dione. The low yields observed for several MDs were attributed to the high cis-trans rotational barrier of acyclic, nonalkylated amide bonds (~90 KJ/mol). They suggested that for successful cyclization of linear intermediates to occur, a less favorable cis conformation should be adopted as opposed to the preferred trans conformation of linear amides.

To avoid racemization during cyclization, In't Veld et al. investigated a mechanism to synthesize optically pure MDs derived from *L*-aspartic acid and *L*-lactic acid intended to promote ring-closure of linear intermediates (*11*). In addition, Jörres et al. synthesized optically active 3,6-alkyl-substituted MDs by

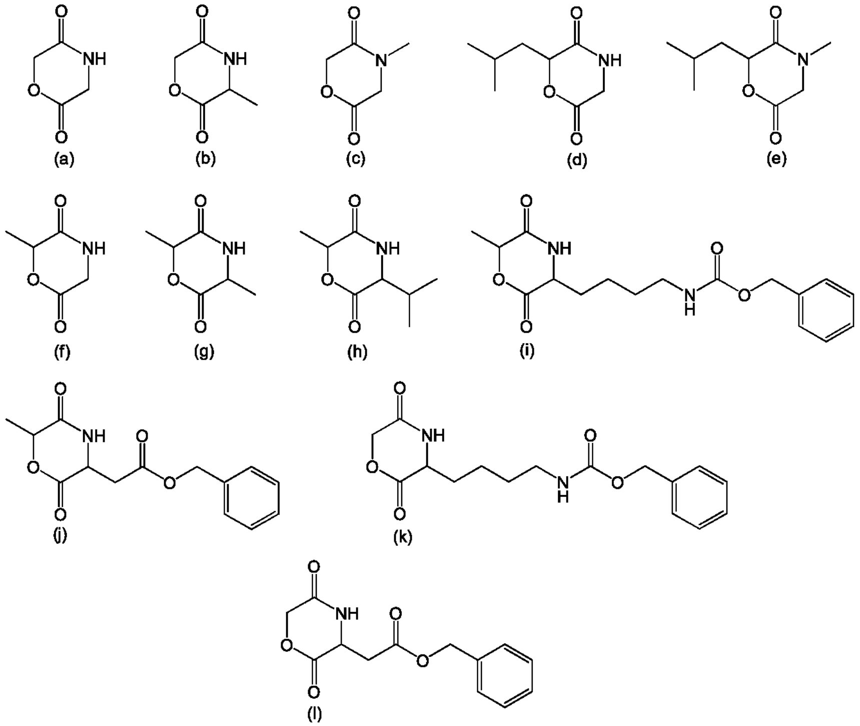

Figure 3. Substituted MDs, developed by the groups of Shalaby (7) (a,b,c), Yonezawa (10) (d,e), In't Veld (11, 13)(f,g,h,i,j), and Ouchi (14, 15)(k,l).

condensation of an amino acid sodium salt with an α-hydroxy acid/ester followed by acid catalyzed cyclization (*18*, *19*). The investigators also extensively detailed the homopolymerization of an MD based on lactic acid and valine using stannous octoate as a catalyst or stannous acetylacetonate as an initiator (*20*). Results indicated that the extent of racemization was dependent on the catalyst or choice of the initiator. Furthermore, the stereochemistry of the peptide region was maintained upon polymerization.

MDs subjected to ring-opening homopolymerization would yield PDPs with alternating amino acid and α-hydroxy acid residues while ring-opening copolymerization of MDs in conjunction with lactones would yield random PDP copolymers. For example, Ouchi and coworkers reported the first successful homopolymerization of a variety of MDs based on glycolic acid with a variety of functional pendant groups (*14*, *15*, *21–36*). Specifically, poly(Glc-alt-Asp), poly(Glc-alt-Lys), and poly(Glc-alt-Glu) were obtained by MDs synthesized in solution (*21*). The 3-substituted cyclo[Glc-Asp(OBz)], cyclo[Glc-Lys(Z)], and cyclo[Glc-Glu(OBz)] MDs were obtained in respective yields of 24.9%, 11.4%, and 20.2%. Each MD was homopolymerized using stannous octoate at 115°C producing the protected PDPs, which were subsequently deprotected with either TFMSA-thioanisole/TFA or HBr/Acetic acid. The resulting PDPs, poly(Glc-alt-Asp), poly(Glc-alt-Lys), and poly(Glc-alt-Glu), were obtained in yields of 78.5%, 78.6%, and 70.5%, respectively. These investigators later reported the synthesis of protected copolymers of polylactide and PDPs with similar methods to those previously stated (*22*, *23*, *25*).

Solid Phase Organic Synthesis of Morpholine Diones

The previous discussion focused on the synthesis of MDs in solution. However, solid phase organic synthesis (SPOS) can be used to eliminate racemization and purity issues that have been described during the cyclization process. Scott et al. developed 3,4,6-substituted MDs for creating combinatorial libraries of small heterocyclic compounds (*37*). The α-bromocarboxylic acid of interest was conjugated to a Wang resin with diisopropylcarbodiimide and dimethylaminopyridine. The resin-bound amine was then acylated with another α-bromocarboxylic acid using DIPEA and PyBrop. Treatment of the resin-bound intermediate with TFA causes the molecule to cyclize either by acid catalysis in solution or by cyclative cleavage from the solid support, both of which were reported as possible mechanisms.

Our work presents a novel platform for obtaining MDs with high purity while maintaining the stereochemistry of the side chains at the 3- and 6-position (Scheme 1). SPOS provides a simplified means for synthesizing and derivatizing a wide variety of organic molecules and oligomeric compounds. A reaction on solid phase typically involves a molecule covalently bound to an insoluble support to which reactants can be added in excess for a given time and later washed away by filtering the mixture. This allows reactions on solid phase supports to be driven to completion and then separated from the reactants and any side products. Thus, compounds synthesized on solid phase supports can be recovered in high yields and high purity following cleavage from the support.

Materials

Fmoc-Lysine(Z)-OH, Fmoc-Aspartic acid(OBzl)-OH, 4-dimethylaminopyridine (DMAP), and *N*-cyclohexylcarbodiimide,*N′*-methyl-polystyrene were purchased from EMD Biosciences. Trityl chloride resin and di-isocarbodiimide (DIC) were purchased from Anaspec while Piperidine was purchased from Alfa Aesar. *L*-lactic acid (crystalline, 99%) (L) was from Biosynth. *N,N*-diisopropylethylamine (99.5%) (DIPEA) and *R*-mandelic acid (M) were from Acros Organics. Trifluroacetic acid (TFA), dichloromethane (DCM), dimethylformamide (DMF), isopropanol, and petroleum ether were purchased from Fisher Scientific.

Synthesis of Morpholine-2,5-dione

Trityl chloride resin (500 mg) was suspended in excess DCM. The α-hydroxy acid (8 mol) was diluted with DCM and mixed with DIPEA (0.99 mol). The solution was introduced to the swollen beads and mixed for 2 hours at room temperature. The resulting resin **(1)** was washed with DCM. The Fmoc-amino acid (4 mol) and DMAP (0.05 mol) was dissolved in a mixture of DCM and DMF

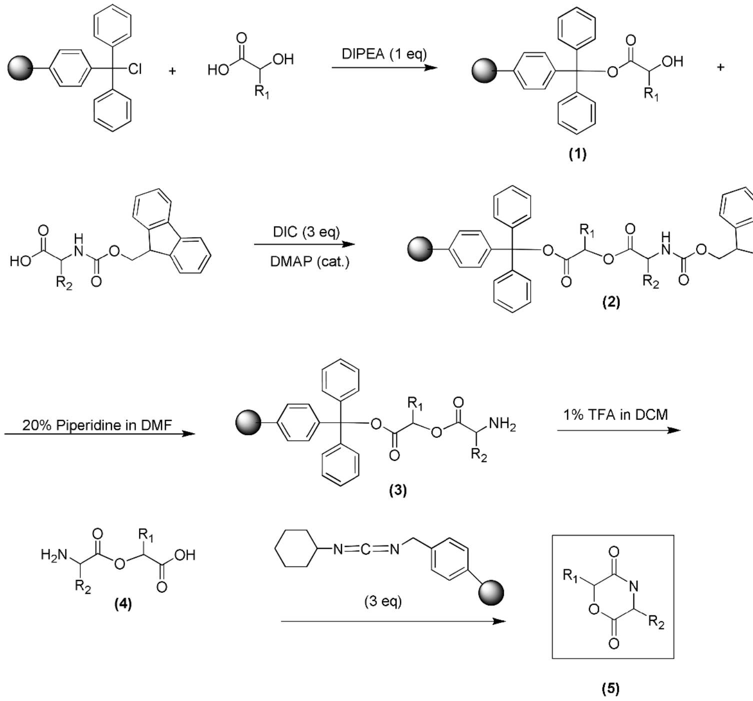

Scheme 1. SPOS of MD consisting of (1) loading of α-hydroxy acid, (2) coupling of Fmoc-amino acid, (3) amino acid deprotection, (4) cleavage from the resin, and (5) intramolecular cyclization.

and added to the resin. DIC (3 mol) was introduced to the reaction vessel and mixed for 1.5 hours at room temperature. The resin **(2)** was washed with DCM, DMF, and DCM. The Fmoc-protecting group was removed from the *N*-terminal with 20% piperidine in DMF. The solution was mixed for 15 minutes at room temperature. The resin **(3)** was washed with DCM, DMF, and DCM. The resin was cleaved with 1% TFA in DCM. The solution was mixed for 20 minutes at room temperature, filtered, and concentrated. The linear monomer **(4)** was dissolved in excess DCM. Carbodiimide-polystyrene resin (3 eq) was added to the mixture. The reaction stirred overnight at room temperature. The solution was filtered, and DCM was removed. The material was extracted from isopropanol and concentrated **(5)**. The MDs were analyzed with using mass spectroscopy (MS) in DCM and H-NMR in DMSO. All had a Mass/Calculated Mass ratio of 1. Quantitative yields of the final MD product which were obtained a mixture of diastereomers are reported in Table 1.

The synthetic mechanism for MDs is fairly straightforward in terms of SPOS methods. The desired α-hydroxy acid is covalently bound to a trityl chloride resin via a standard S_N1 reaction with DIPEA to avoid hydroxyl deprotonation. The desired Fmoc-amino acid is coupled to the resin-bound α-hydroxy acid with DIC and a catalytic amount of DMAP. The reaction forms a urea side product which is readily washed away with DMF. The protecting groups on both the *N*-

Table 1. NMR data from SPOS of MDs

Cyclo(Lac-Lyz(Z)):

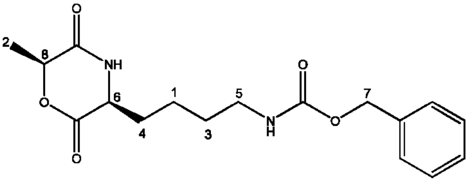

^{1}H NMR$^{a)}$ (DMSO-d_6 with TMS, 400 MHz, ppm) δ=1.34-1.42 (m, 2H, CH$_2$-1), 1.37 (d, J=6.9 Hz, 3H, CH$_3$-2), 1.46 (m, 2H, CH$_2$-3), 1.60-1.82 (m, 2H, CH$_2$-4), 2.98 (t, J=5.9 Hz, CH$_2$-5), 4.10-4.27 (m, 0.4H, CH-6), 4.30 (t, J=5.6 Hz, 0.6H, CH-6), 5.00 (s, 2H, CH$_2$Ph-7), 5.07 (q, J=6.9 Hz, 0.6H, CH-8), 5.15-5.22 (m, 0.4H, CH-8), 7.25 (t, J=5.1 Hz, 1H, carbamate NH), 7.28-7.39 (m, 5H, $H_{aromatic}$), 8.46 (s, 1H, amide NH). Percentage Yield: 36%

a) consistent with literature'[18, 38]

Cyclo(Man-Lyz(Z)):

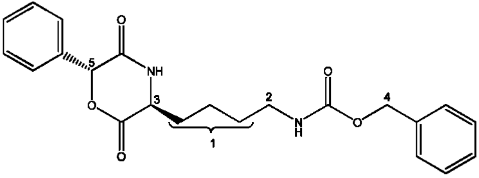

^{1}H NMR (DMSO-d6, 300 MHz, ppm) δ=1.30-1.86 (m, 6H, 3 CH$_2$'s-1), 3.0 (d, J = 5.9 Hz, CH$_2$-2), 4.18 (t, J = 4.6 Hz, 0.68H, CH-3), 4.39 (t, J = 4.6 Hz, 0.32H, CH-3), 5.0 (s, 2H, CH$_2$Ph-4), 5.8 (m, 0.22H, CH-5), 6.04 (m, 0.78H, CH-5), 7.22-7.54 (m, 10H, $H_{aromatic}$), 8.31 (s, 1H, carbamate NH), 8.68, 8.77 (s, 1H, amide NH). Percentage Yield: 5%

Cyclo(Lac-Asp(OBz)):

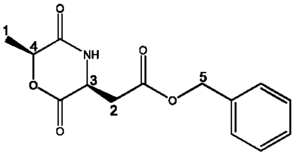

^{1}H NMR (DMSO-d6, 400 MHz, ppm) δ= 1.38 (d, J = 6.4 Hz, 2.3H, CH3=1), 1.46 (d, J = 6.9 Hz, 0.8H, CH3-1), 2.89 (d, J = 4.9 Hz, 2H, CH2-2), 4.58 (m, 0.27H, CH-3), 4.66 (t, 5.0 Hz, 0.73H, CH-3), 4.89-4.93 (q, J = 6.6 Hz, 0.46H, CH-4), 5.11 (s, 2H, CH2Ph-5), 5.15 (q, J = 6.7 Hz, 0.64H, CH-4), 7.35 (m, 5H, $H_{aromatic}$), 8.49 (s, 0.3H, NH), 8.56 (s, 0.7H, NH). Percentage Yield: 46%

b) consistent with literature[39]

Cyclo(Man-Asp(OBz)):

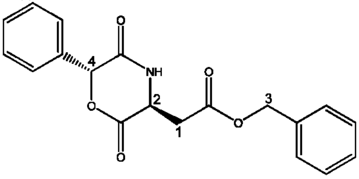

^{1}H NMR (DMSO-d6 with TMS, 500 MHz, ppm) δ = 2.89-3.12 (m, 2H, CH2-1), 4.58 (t, J = 4.4 Hz, 0.6H, CH-2), 4.81 (t, J = 5.1 Hz, 0.4H, CH-2), 5.16 (s, 2H, CH2Ph-3), 5.93 (s, 0.64H, CH-4), 6.14 (s, 0.46H, CH-4), 7.38 (m, 10H, $H_{aromatic}$), 8.76 (d, 1H, NH). Percentage Yield: 5%

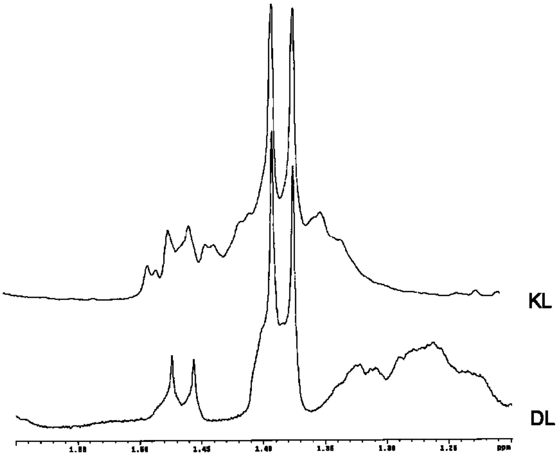

Figure 4. The leaching of the CDI beads via DCM are a by-product in the final MD product. The chemical shifts of cyclo(Lac-Lys) (KL) and Cyclo(Lac-Asp) (DL) are illustrated above.

and *C*-terminal are readily cleaved by treating the resin with 20% piperidine in DMF (v/v) or with 0.1% to 1% trifluoroacetic acid (TFA) in DCM respectively. Cyclization of the linear monomers occurs on a carbodiimide(CDI)-functionalized polystyrene resin in dilute solvent conditions (1-3 mL DCM/mg monomer). The CDI group on the resin deprotonates the carboxyl group of the monomer and sequesters the carboxylate anion. The intramolecular amine then attacks the activated acid-CDI complex, thus cyclizing the molecule while simultaneously cleaving the final product from the resin. The urea side product remains bound to the resin, and the final product is recovered upon filtration and removal of DCM.

The data demonstrate that MDs can be adequately synthesized using the prescribed solid phase approach. MS samples reveal relatively high composition of the cyclic monomers, indicating the lack of by-products after purification. The results from the H-NMR analysis is similar to previous results, specifically for cyclo(Lac-Lys(Z)) (*18*, *38*) and cyclo(Lac-Asp(OBz) (*39*). A closer investigation of the spectra reveals that racemization occurs at both stereocenters leading to the formation of diastereomers, particularly in MDs containing aspartic acid. The racemization may be due to the use of DMAP during esterification which has been reported to manifest such changes (*40*, *41*). It is suggested that smaller molar equivalents of DMAP be investigated to determine the effects on the diastereomeric ratio of the final MD product. Other condensation reagents such as 1-(mesitylene-2-sulfonyl)-3-nitro-1H-1,2,4-triazole (MSNT) may be an appropriate alternative during esterification as it has been shown to minimize racemization of Fmoc-amino acids prone to enantiomerization (*42*).

Impurities around 1-1.5 ppm and various downfield regions on the ^{1}H NMR spectra are most likely residual polystyrene and/or urea from prolonged exposure to the polystyrene-supported carbodiimide resin during cyclization (Figure 4). Attempts to eliminate impurities by precipitating the MDs from petroleum ether using isopropanol may have also contributed to the observed racemization. At any rate, optimization of the purification method may improve the product yield.

The ambition of this research was to provide a simplified means of synthesizing PDPs consisting of any aliphatic-substituted α-hydroxy acid and any α-amino acid from commercially available reagents. Common issues that have been presented repeatedly in MD literature include successful attachment of pendant groups, racemization at the 3- and 6-position, and purity and product yield. The methods described employ solid phase synthetic techniques, offering significant advantages over previously reported methods. Primarily, SPOS eliminates many of the difficulties associated with solution phase synthesis such as loss of product during intermediate steps, separation of reactants and side products from reaction mixtures, incomplete reactions, and purification following synthesis.

References

1. Cook, A. H.; Hrkach, J. S.; Gao, N. N.; Johnson, J. M.; Pajvani, U. B.; Cannizzaro, S. M.; Langer, R. Characterization and development of RGD-peptide-modified poly(lactic acid-co-lysine) as an interactive, resorbable biomaterial. *J. Biomed. Mater. Res.* **1997**, *35* (4), 513–523.
2. Yan, Q. J.; Li, J.; Li, S. P.; Yin, Y. X.; Zhang, P. Synthesis and RGD peptide modification of poly{(lactic acid)-co-[(glycolicacid)-alt-(L-lysine)]}. *E-Polymers* **2008**, 12.
3. Ratner, B. D.; Hoffman, A. S.; Schoen, F. J.; Lemons, J. E. *Biomaterials Science An Introduction to Materials in Medicine*; 2nd ed.; Elsevier Academic Press: 2004.
4. Chow, D.; Nunalee, M. L.; Lim, D. W.; Simnick, A. J.; Chilkoti, A. Peptide-based biopolymers in biomedicine and biotechnology. *Mater. Sci. Eng. R-Reports* **2008**, *62* (4), 125–155.
5. Zheng, B.; Haynie, D. T.; Zhong, H.; Sabnis, K.; Surpuriya, V.; Pargaonkar, N.; Sharma, G.; Vistakula, K. Design of peptides for thin films, coatings and microcapsules for applications in biotechnology. *J. Biomater. Sci., Polym. Ed.* **2005**, *16* (3), 285–299.
6. Feng, Y. K.; Guo, J. T. Biodegradable Polydepsipeptides. *Int. J. Mol. Sci.* **2009**, *10* (2), 589–615.
7. Shalaby, W.; Koelmel, D. F. Copolymers of p-dioxanone and 2,5-morpholinediones and surgical devices form therefrom having accelerated absorption characteristics. 4441496, April 10, 1984.
8. Helder, J.; Feijen, J.; Lee, S. J.; Kim, S. W. Copolymers of D,L-lactic acid and glycine. *Makromol. Chem., Rapid Commun.* **1986**, *7* (4), 193–198.
9. Helder, J.; Kohn, F. E.; Sato, S.; van den Berg, J. W.; Feijen, J. Synthesis of poly[oxyethylidenecarbonylimino(2-oxoethylene)] [poly(glycine-D,L-lactic acid)] by ring opening polymerization. *Makromol. Chem., Rapid Commun.* **1985**, *6* (1), 9–14.
10. Yonezawa, N.; Toda, F.; Hasegawa, M. Synthesis of polydepsipeptides: Ring-opening polymerization of 6-isopropylmorpholine-2,5-dione and

6-isopropyl-4-methylmorpholine-2,5-dione. *Die Makromolekulare Chemie, Rapid Communications* **1985**, *6* (9), 607–611.

11. In't Veld, P. J. A.; Dijkstra, P. J.; Feijen, J. Synthesis of biodegradable polyesteramides with pendant functional-groups. *Makromol. Chem., Macromol. Chem. Phys.* **1992**, *193* (11), 2713–2730.
12. Fung, F.; Glowaky, R. C. Bioabsorbable polydepsipeptide, preparation and use thereof. 4916209, 1987.
13. In't Veld, P. J. A.; Dijkstra, P. J.; Vanlochem, J. H.; Feijen, J. Synthesis of alternating polydepsipeptides by ring-opening polymerization of morpholine-2,5-dione derivatives. *Makromol. Chem., Macromol. Chem. Phys.* **1990**, *191* (8), 1813–1825.
14. Ouchi, T.; Seike, H.; Miyazaki, H.; Tasaka, F.; Ohya, Y. Synthesis of a block copolymer of L-lactide and depsipeptide with pendant thiol groups. *Des. Monomers Polym.* **2000**, *3* (3), 279–287.
15. Ouchi, T.; Shiratani, M.; Jinno, M.; Hirao, M.; Ohya, Y. Synthesis of poly[(glycolic acid)-alt-(l-aspartic acid)] and its biodegradation behavior in-vitro. *Makromol. Chem., Rapid Commun.* **1993**, *14* (12), 825–831.
16. In't Veld, P. J. A.; Shen, Z. R.; Takens, G. A. J.; Dijkstra, P. J.; Feijen, J. Glycine glycolic acid-based copolymers. *J. Polym. Sci., Part A: Polym. Chem.* **1994**, *32* (6), 1063–1069.
17. In't Veld, P. J. A.; Ye, W. P.; Klap, R.; Dijkstra, P. J.; Feijen, J. Copolymerization of epsilon-caprolactone and morpholine-2,5-dione derivatives. *Makromol. Chem., Macromol. Chem. Phys.* **1992**, *193* (8), 1927–1942.
18. Jorres, V.; Keul, H.; Hocker, H. Aminolysis of α-hydroxy acid esters with α-amino acid salts; first step in the synthesis of optically active 2,5-morpholinediones. *Macromol. Chem. Phys.* **1998**, *199* (5), 825–833.
19. Hartwig, W.; Schollkopf, U. Asymmetric syntheses via heterocyclic intermediates .16. Enantioselective synthesis of α-alkyl-alpha-phenylglycines by alkylation of 3,6-dihydro-3-phenyl-2h-1,4-oxazin-2-ones chirally substituted at c-6. *Liebigs Ann. Chem.* **1982** (11), 1952–1970.
20. Jorres, V.; Keul, H.; Hocker, H. Polymerization of (3S,6S)-3-isopropyl-6-methyl-2,5-morpholinedione with tin octoate and tin acetylacetonate. *Macromol. Chem. Phys.* **1998**, *199* (5), 835–843.
21. Ouchi, T.; Nozaki, T.; Okamoto, Y.; Shiratani, M.; Ohya, Y. Synthesis and enzymatic hydrolysis of polydepsipeptides with functionalized pendant groups. *Macromol. Chem. Phys.* **1996**, *197* (6), 1823–1833.
22. Ouchi, T.; Nozaki, T.; Ishikawa, A.; Fujimoto, I.; Ohya, Y. Synthesis and enzymatic hydrolysis of lactic acid depsipeptide copolymers with functionalized pendant groups. *J. Polym. Sci., Part A: Polym. Chem.* **1997**, *35* (2), 377–383.
23. Ouchi, T.; Seike, H.; Nozaki, T.; Ohya, Y. Synthesis and characteristics of polydepsipeptide with pendant thiol groups. *J. Polym. Sci., Part A: Polym. Chem.* **1998**, *36* (8), 1283–1290.
24. Ouchi, T.; Hamada, A.; Ohya, Y. Biodegradable microspheres having reactive groups prepared from L-lactic acid-depsipeptide copolymers. *Macromol. Chem. Phys.* **1999**, *200* (2), 436–441.

25. Tasaka, F.; Miyazaki, H.; Ohya, Y.; Ouchi, T. Synthesis of comb-type biodegradable polylactide through depsipeptide-lactide copolymer containing serine residues. *Macromolecules* **1999**, *32* (19), 6386–6389.
26. Ouchi, T.; Miyazaki, H.; Tasaka, F.; Hamada, A.; Ohya, Y. Architecture of polymer micelles from block-copolymers of lactide and depsipeptide as drug carriers. *Abstr. Pap. Am. Chem. Soc.* **2000**, *220*, U283–U283.
27. Ouchi, T.; Miyazaki, H.; Arimura, H.; Tasaka, F.; Hamada, A.; Ohya, Y. Synthesis of biodegradable amphiphilic AB-type diblock copolymers of lactide and depsipeptide with pendant reactive groups. *J. Polym. Sci., Part A: Polym. Chem.* **2002**, *40* (9), 1218–1225.
28. Ouchi, T.; Toyohara, M.; Arimura, H.; Ohya, Y. Preparation of poly(L-lactide)-based microspheres having a cationic or anionic surface using biodegradable surfactants. *Biomacromolecules* **2002**, *3* (5), 885–888.
29. Ohya, Y.; Matsunami, H.; Yamabe, E.; Ouchi, T. Cell attachment and growth on films prepared from poly(depsipeptide-co-lactide) having various functional groups. *J. Biomed. Mater. Res., Part A* **2003**, *65A* (1), 79–88.
30. Arimura, H.; Ohya, Y.; Ouchi, T. The formation of biodegradable polymeric micelles from newly synthesized poly(aspartic acid)-block-polylactide AB-type diblock copolymers. *Macromol. Rapid Commun.* **2004**, *25* (6), 743–747.
31. Ohya, Y.; Matsunami, H.; Ouchi, T. Cell growth on the porous sponges prepared from poly(depsipeptide-co-lactide) having various functional groups. *J. Biomater. Sci., Polym. Ed.* **2004**, *15* (1), 111–123.
32. Ouchi, T.; Ohya, Y. In *Design of lactide copolymers as biomaterials*; 2004; pp 453−462.
33. Ouchi, T.; Sasakawa, M.; Arimura, H.; Toyohara, M.; Ohya, Y. Preparation of poly[DL-lactide-co-glycolide]-based microspheres containing protein by use of amphiphilic diblock copolymers of depsipeptide and lactide having ionic pendant groups as biodegradable surfactants by W/O/W emulsion method. *Polymer* **2004**, *45* (5), 1583–1589.
34. Ohya, Y.; Toyohara, M.; Sasakawa, M.; Arimura, H.; Ouchi, T. Thermosensitive biodegradable polydepsipeptide. *Macromol. Biosci.* **2005**, *5* (4), 273–276.
35. Ohya, Y.; Nakai, T.; Nagahama, K.; Ouchi, T.; Tanaka, S.; Kato, K. The synthesis and biodegradability of poly(lactide-random-depsipeptide)-PEG-Poly(lactide-random-depsipeptide) ABA-type triblock copolymers. *J. Bioact. Compat. Polym.* **2006**, *21* (6), 557–577.
36. Nagahama, K.; Ueda, Y.; Ouchi, T.; Ohya, Y. Exhibition of soft and tenacious characteristics based on liquid crystal formation by introduction of cholesterol groups on biodegradable lactide copolymer. *Biomacromolecules* **2007**, *8* (12), 3938–3943.
37. Scott, B. O.; Siegmund, A. C.; Marlowe, C. K.; Pei, Y. Z.; Spear, K. L. Solid phase organic synthesis (SPOS): A novel route to diketopiperazines and diketomorpholines. *Mol. Diversity* **1996**, *1* (2), 125–134.
38. Barrera, D. A.; Zylstra, E.; Lansbury, P. T.; Langer, R. Copolymerization and degradation of poly(lactic acid co-lysine). *Macromolecules* **1995**, *28* (2), 425–432.

39. Feng, Y.; Klee, D.; Hocker, H. Synthesis of poly[(lactic acid)-alt- or co-((S)-aspartic acid)] from (3S,6R,S)-3-[(benzyloxycarbonyl)methyl]6-methylmorpholine-2,5-dione. *Macromol. Chem. Phys.* **2002**, *203* (5−6), 819–824.
40. HarthFritschy, E.; Cantacuzene, D. Esterification of 9-fluorenylmethoxycarbonyl-glycosylated serine and cysteine derivatives with an hydroxymethyl resin. *J. Pept. Res.* **1997**, *50* (6), 415–420.
41. Le, H. T.; Mayer, M.; Thoret, S.; Michelot, R. Incorporation of Thioamide Linkages into a Growing Peptide under SPPS Conditions Improved by Salt Effects. *Int. J. Pept. Protein Res.* **1995**, *45* (2), 138–144.
42. Nielsen, J.; Lyngso, L. O. Combinatorial solid-phase synthesis of balanol analogues. *Tetrahedron Lett.* **1996**, *37* (46), 8439–8442.

Downloaded by OHIO STATE UNIV LIBRARIES on June 23, 2012 | http://pubs.acs.org
Publication Date (Web): November 18, 2010 | doi: 10.1021/bk-2010-1054.ch011

Chapter 11

Nitric Oxide and Drug Releasing Hydrolysable Macromers, Oligomers and Polymers

Rao S. Bezwada[*]

Bezwada Biomedical LLC, 15-1 Ilene Court, Hillsborough, New Jersey, USA, 08844
[*]Rao@bezwadabiomedical.com

New nitric oxide (NO) and drug releasing macromers, oligomers and polymers useful for biomedical applications were prepared. These NO and drug releasing macromers and oligomers are comprised of a drug molecule and a NO releasing moiety linked to each other via a hydrolytically degradable linker. This hydrolytically degradable linker is comprised of repeat units derived from safe and biocompatible molecules such as glycolic acid, lactic acid, p-dioxanone and caprolactone that are key components of all commercially available absorbable medical devices. NO and drug releasing macromers and oligomers developed by our research group are expected to have controllable hydrolysis profiles and enhanced functionality. The controlled release profiles represent slow, moderate and/or rapid release of drug and nitric oxide. This release may be targeted to one or more specific organs or parts of the body. Furthermore, these macromers and oligomers are anticipated to degrade into safe and biocompatible molecules. Moreover, hydrolytic degradation of some specific NO and drug releasing absorbable macromers and oligomers release the drug molecule as such with no change in chemical structure. This preserves the activity and efficacy of the drug molecule and provides extended therapeutic properties to the substrate when incorporated in a polymer matrix or applied as part of a coating on the substrate. These NO and drug releasing macromers and oligomers have a great potential for use in numerous therapeutic and biomedical applications including (a) treatment of cardiovascular, gastrointestinal, inflammatory and respiratory

diseases, (b) therapies for central nervous system disorders and sexual dysfunctioning, (c) NO releasing anti-proliferative agents to prevent restenosis, (d) key components of coatings for medical devices to prevent platelet aggregation and adhesion, and (e) key components of anti-microbial, wound healing and pharmaceutical formulations for controlled release applications.

1. Nitric Oxide : Biological Importance

Downloaded by OHIO STATE UNIV LIBRARIES on June 23, 2012 | http://pubs.acs.org
Publication Date (Web): November 18, 2010 | doi: 10.1021/bk-2010-1054.ch011

Nitric oxide (NO) is a vital biological molecule. It plays a significant role (*1–6*) in diverse biological processes, such as host defense, cardiovascular regulation, signal transduction, neurotransmission and wound healing. NO also plays an important role in many diseases, including cardiovascular, gastrointestinal, inflammatory and respiratory diseases, and medical conditions such as central nervous disorders and sexual dysfunctioning, by influencing many biochemical and physiological reactions.

NO is a well known inhibitor of platelet adhesion, activation and smooth cell proliferation (*7–10*). Continuous release of NO from the surface of endothelial cells effectively prevents the adhesion /activation of platelets on normal blood vessel walls. Agents that release or generate NO locally have been proposed as systemic drugs to prevent and treat restenosis (*11*) and thrombus formation in an individual that have come into contact with medical devices such as cardiovascular drug-eluting stents, diagnostic catheters, guide wires, guide catheters, intra-aortic balloon pump catheters, intravascular sensors, extra-corporeal blood loop circuits, intravenous grafts/shunts and adhesion prevention barriers.

In addition to helping body cells to communicate with each other by transmitting signals (*12*, *13*) throughout the entire body, NO assists the immune system at fighting off bacteria (*4*) and defending against tumors (*7*, *14*, *15*). Furthermore, it helps reduce inflammation and regulate blood pressure (*12*) by dilating arteries. NO released from wound resident cells also plays an important role in unique cell signaling pathways and re-establishment of microcirculation as new vascularized tissue is formed. Moreover, NO is anti-inflammatory (*16*) and hence valuable for indwelling medical devices such as urethral or Total Parenteral Nutritional Catheters.

In light of its significant biological role and beneficial therapeutic properties, researchers have sought various ways to deliver NO to damaged tissue and to tissues and organs at risk of injury. One approach for providing a therapeutic level of NO at an injury site is to increase systemic NO levels prophylactically. This can be accomplished by stimulating endogenous NO production or using exogenous NO sources. Methods to regulate endogenous NO release have primarily focused on activation of synthetic pathways using excess amounts of NO precursors like L-arginine, or increasing expression of nitric oxide synthase (NOS) using gene therapy (*17*). However, these methods have not been proven effective in preventing restenosis. Regulating endogenously expressed NO using gene therapy techniques (*18*) remain highly experimental and has not yet proven safe and effective.

Exogenous NO sources such as pure NO gas are highly toxic, short-lived and relatively insoluble in physiological fluids (*19*). Consequently, Nitric oxide-releasing compounds suitable for in vivo applications have been developed by a number of investigators (*1*, *20*). This includes organic nitrate pro drugs such as nitroglycerin (*20*), isosorbide dinitrate (*20*), NO donor aspirin (*20*) and Naproxen (*20*), nitrosothiols (*20*, *21*), nitroprusside (*20*, *22*), N-Diazenium diolates (*1*, *23–26*), and Zeolites (*27*) Nitric oxide-releasing compounds with sufficient stability at body temperatures to be useful as therapeutics were ultimately developed by Keefer et al. (*12*, *24*) and Hrabie et al (*28*). However, N-diazeniumdiolate small molecules and polymers incorporating them have the potential to form carcinogenic nitrosamines (*29*). The nitrosothiols have been shown to be unstable and labile to standard sterilization methods, and nitroprusside is difficult to sterilize. Both nitrosothiols and nitroprusside require metabolism to release NO and are subject to tolerance formation (*19*). Chen et al (*30*) reported NO releasing biodegradable polymers derived from [1,4] oxazepan-7-one suitable for use as medical devices and coatings for medical devices. Raulli et al (*31*) described multi-phased nitric oxide and anti-proliferative drug eluting polymer coatings for medical devices wherein the NO is released by a NO donor selected from a group consisting of C-diazeniumdiolates, O-diazenium diolates, N-diazenium diolates, nitrosothiols, organic nitrates and nitrites, nitroprusside and other iron nitrosyl compounds, ruthenium/NO or other metal/NO complexes, heterocyclic N-oxides, C-nitroso compounds, oximes, N-hydroxyguanidines and N-hydroxyureas, and other nitric oxide releasing compounds. However, all these NO donors do not provide us with a controlled release of NO.

Nitric oxide-donor compounds and compositions comprising them can be useful for treating cardiovascular disorders, gastrointestinal disorders, hepatic disorders and for inhibiting platelet adhesion were developed by Nicoletta et al. (*32*). However, the Nicoletta et al. disclosure does not relate to and also does not provide macromers and oligomers that release nitric oxide and, optionally, drug molecule. Furthermore, the Nicoletta disclosure does not relate to and also does not provide compositions comprising NO and drug releasing macromers and oligomers, combinations thereof and their blends with absorbable and non-absorbable polymers for applications in medical devices and medical device coatings. Moreover, the Nicoletta disclosure also does not teach art by which the rate of release of NO can be controlled.

In summary, although, work has been carried out in the past to develop NO donors and NO donor drug molecules, the work suffers from the following disadvantages (*32*, *33*) (a) the rate of release of nitric oxide and drug molecule cannot be controlled (b) some of the NO donors reported so far release toxic and carcinogenic nitrosamines upon decomposition under oxygenated conditions (c) some of the NO donors release NO radical, which is rapidly consumed by hemoglobin and is toxic to individuals with arteriosclerosis and (c) NO donors reported in the literature have short lives and they rapidly lose their ability to deliver NO under physiological conditions for extended periods of time or to control the amount of NO delivered. In light of the above drawbacks, therefore, there is a need for new molecules and compositions capable of delivering NO

Downloaded by OHIO STATE UNIV LIBRARIES on June 23, 2012 | http://pubs.acs.org
Publication Date (Web): November 18, 2010 | doi: 10.1021/bk-2010-1054.ch011

Downloaded by OHIO STATE UNIV LIBRARIES on June 23, 2012 | http://pubs.acs.org
Publication Date (Web): November 18, 2010 | doi: 10.1021/bk-2010-1054.ch011

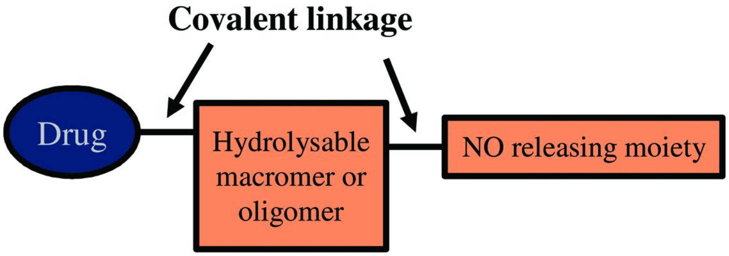

Figure 1. General structure of NO and drug releasing macromers and oligomers developed by Bezwada Biomedical, LLC (see color insert)

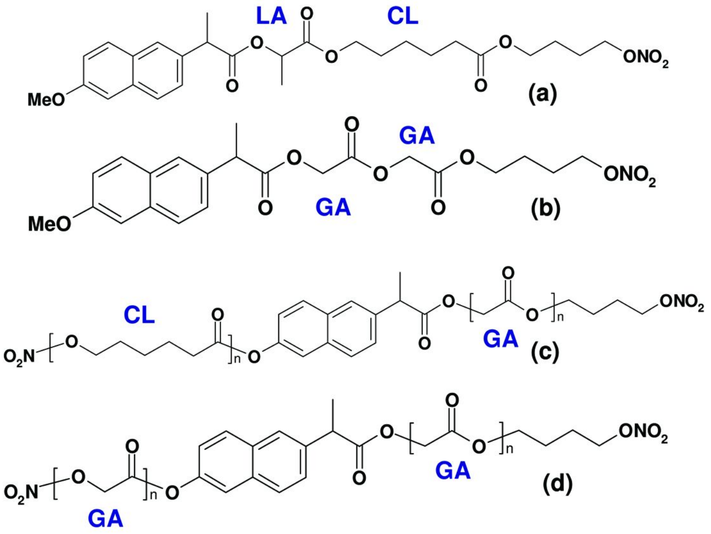

Figure 2. (a)-(d) NO and Naproxen releasing macromers and oligomers with varying hydrolytic degradation rates, wherein GA, LA and CL represents glycolic acid, lactic acid and caprolactone repeat units (see color insert)

and drug to treatment sites in a controlled manner and which can overcome these shortcomings.

The present work is directed towards overcoming these challenges by providing NO and drug releasing macromers and oligomers wherein the rate, extent and site of release of NO and the drug molecule can be controlled independently of each other. NO and drug releasing macromers and oligomers of the present work are expected to have highly controllable hydrolysis profiles, increased solubility, improved bioavailability, improved efficacy and enhanced functionality. The controlled release profiles represent slow, moderate and/or rapid release of drug and nitric oxide. This release may be targeted to one or more specific organs or parts of the body. The hydrolytic degradation of some specific NO and drug releasing macromers and oligomers of the present work will typically release drug molecule as such with no change in native chemical structure and efficacy. The present work is expected to provide greater control

Downloaded by OHIO STATE UNIV LIBRARIES on June 23, 2012 | http://pubs.acs.org
Publication Date (Web): November 18, 2010 | doi: 10.1021/bk-2010-1054.ch011

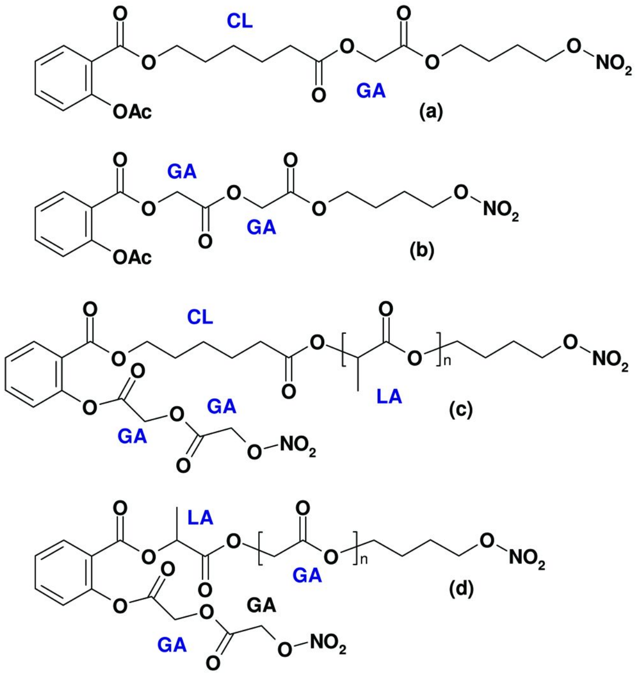

Figure 3. NO and Aspirin releasing macromers and oligomers with varying hydrolytic degradation rates, wherein GA, LA and CL represents glycolic acid, lactic acid and caprolactone; repeat unit Ac represents an acetyl group. (see color insert)

of the bioavailability of the drug and nitric oxide while retaining the inherent biological properties of both.

2. Nitric Oxide and Drug Releasing Hydrolysable Macromers and Oligomers

Nitric oxide and drug releasing hydrolysable macromers and oligomers represented by a general structure depicted in Figure 1, below were synthesized (*33*). As shown, these macromers and oligomers are comprised of a drug molecule and a NO releasing moiety, linked to each other via a hydrolytically degradable linker. This hydrolytically degradable linker is comprised of repeat units derived from safe and biocompatible hydroxy acid molecules such as glycolic acid, lactic acid, open chain p-dioxanone and open chain caprolactone. These hydroxy acids are base materials of a range of absorbable and biocompatible polymers and copolymers, such as poly (lactide) (PLA), poly(glycolide) (PGA), poly(caprolactone) (PCL), poly(p-dioxanone) (PDS), poly(lactide-co-glycolide) and poly(glycolide-co-caprolactone). These polymers and copolymers are the key components of a majority of absorbable medical devices, ranging from sutures, staples, orthopedic screws and implantable surgical devices to tissue engineering scaffolds.

Downloaded by OHIO STATE UNIV LIBRARIES on June 23, 2012 | http://pubs.acs.org
Publication Date (Web): November 18, 2010 | doi: 10.1021/bk-2010-1054.ch011

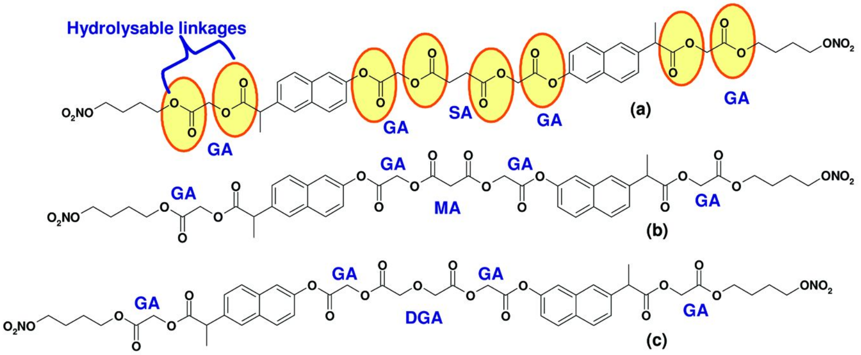

Figure 4. NO and Naproxen releasing macromers containing two molecules of naproxen per macromer, wherein GA, SA, MA and DGA represents glycolic acid, succinic acid, malonic acid and diglycolic acid, respectively (see color insert)

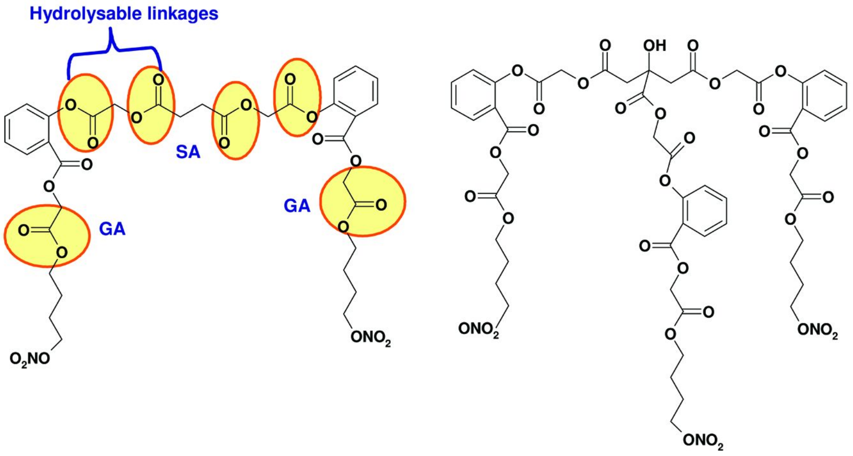

Figure 5. NO and Aspirin releasing macromers containing two and three molecules of Aspirin per macromer, wherein GA and SA represent glycolic acid and succinic acid, respectively (see color insert)

Figure 2 (a)–(d) shows the structures of NO and Naproxen releasing macromers and oligomers. Similarly, Figure 3 (a)-(d), below, shows the structures of NO and Aspirin releasing macromers and oligomers. The rate of hydrolysis of these NO and drug releasing macromers and oligomers will depend upon a number of factors, including the number of repeat units in the linker as well as the choice of the safe and biocompatible molecules from which the repeat units are derived. For example, NO and drug releasing macromers and oligomers comprised of a degradable linker containing repeat units derived from glycolic acid will hydrolyze faster than those comprised of repeat units derived from p-dioxanone. Similarly, NO and drug releasing macromers and oligomers comprised of a degradable linker containing repeat units derived from lactic acid and caprolactone should take much longer to hydrolyze than the ones wherein

Downloaded by OHIO STATE UNIV LIBRARIES on June 23, 2012 | http://pubs.acs.org
Publication Date (Web): November 18, 2010 | doi: 10.1021/bk-2010-1054.ch011

the degradable linker is comprised of repeat units derived from glycolic acid and dioxanone. Furthermore, it is expected that the rate of hydrolysis will vary with variation in the number of repeat units in the degradable linker. Thus, the desired time range may be obtained by altering the number of repeat units in the linker as well as by the choice of the safe and biocompatible molecules from which the repeat units are derived. For example, NO and Naproxen releasing oligomers with structure 2(d) will hydrolyze faster than oligomers with structure 2(c). Similarly, NO and Naproxen releasing macromers of structure 2(b) will hydrolyze faster than oligomers with structure 2(a).

In addition to macromers and oligomers comprising one drug molecule per macromer or oligomer, macromers and oligomers comprising two or more drug molecules functionalized with a NO releasing moiety covalently linked to each other via a hydrolysable macromer or an oligomer were also synthesized. For example, Figure 4 below depicts the structures of NO and Naproxen releasing macromers containing two molecules of Naproxen per macromer. Similarly, Figure 5 below depicts the structures of NO and Aspirin releasing macromers containing two or more Aspirin molecules per macromer.

As shown in Figures 2 to 5, NO and drug releasing macromers and oligomers developed by our research group are expected to have controllable hydrolysis profiles, increased solubility, improved bioavailability, improved efficacy and enhanced functionality. The controlled release profiles represent slow, moderate and/or rapid release of drug and nitric oxide. This release may be targeted to one or more specific organs or parts of the body. Furthermore, these macromers and oligomers developed by our group are anticipated to degrade into safe and biocompatible molecules. Moreover, hydrolytic degradation of some specific NO and drug releasing absorbable macromers and oligomers will release the drug molecule as such with no change in chemical structure. This will preserve the activity and efficacy of the drug molecule and is anticipated to provide extended therapeutic properties to the substrate when incorporated in a polymer matrix or applied as part of a coating on the substrate.

3. Polymers Bearing NO and Drug Releasing Pendant Groups

In addition to NO and drug releasing macromers and oligomers, we have also developed polymers bearing NO and drug releasing pendant groups. In order to prepare these polymers, we first developed monomers such as diols having the NO releasing and/or biologically active agent releasing moieties. Figure 6 (a) and (b) depict the structures of NO and naproxen and NO and Aspirin releasing hydrolytically degradable diols, respectively. These diol monomers having the NO releasing and/or biologically active agent releasing moieties can be reacted with isocyanates to prepare polyurethanes, as depicted in Figure 7, below. In a similar fashion, polyesters bearing NO and drug releasing pendant groups were prepared via reaction of diol monomers with diacids, as shown in Figure 8, below. Polymers bearing NO and drug releasing pendant groups with varying molecular weights were developed. Furthermore, the frequency of occurrence of

Downloaded by OHIO STATE UNIV LIBRARIES on June 23, 2012 | http://pubs.acs.org
Publication Date (Web): November 18, 2010 | doi: 10.1021/bk-2010-1054.ch011

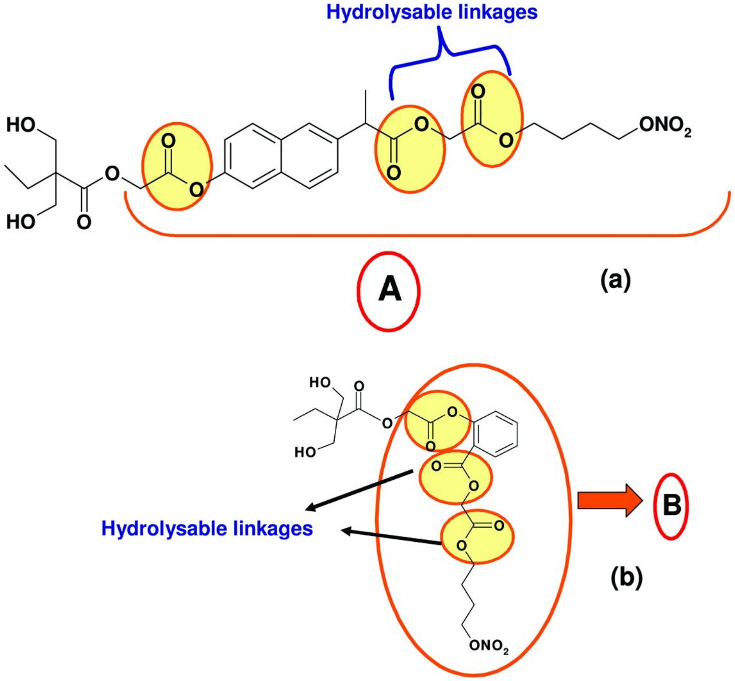
Hydrolysable linkages
HO
HO
O
O
O
O
O
O
O
O
ONO2
A
(a)
HO
O
HO
O
O
O
O
O
O
O
Hydrolysable linkages
ONO2
B
(b)

Figure 6. (a) NO and Naproxen releasing hydrolytically degradable diol monomer (b) NO and Aspirin releasing hydrolytically degradable diol monomer (see color insert)

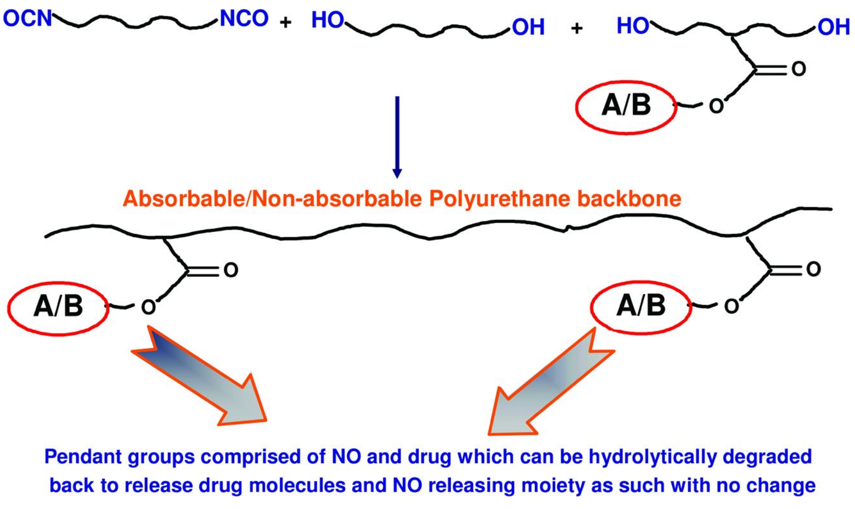
OCN
NCO
+
HO
OH
+
HO
OH
O
A/B
O
Absorbable/Non-absorbable Polyurethane backbone
O
A/B
O
O
A/B
O
Pendant groups comprised of NO and drug which can be hydrolytically degraded back to release drug molecules and NO releasing moiety as such with no change

Figure 7. Polyurethanes bearing NO and drug releasing pendant groups (see color insert)

pendant groups along the polymer backbone was also controlled. These NO and drug releasing polymers will find potential use in a number of biomedical and

Downloaded by OHIO STATE UNIV LIBRARIES on June 23, 2012 | http://pubs.acs.org
Publication Date (Web): November 18, 2010 | doi: 10.1021/bk-2010-1054.ch011

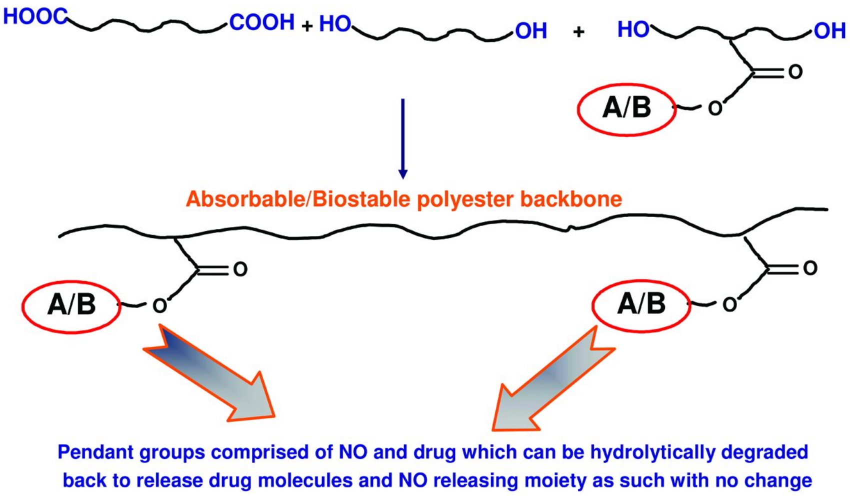
HOOC
COOH
+
HO
OH
+
HO
OH
O
A/B
O
Absorbable/Biostable polyester backbone
O
A/B
O
A/B
O
O
Pendant groups comprised of NO and drug which can be hydrolytically degraded
back to release drug molecules and NO releasing moiety as such with no change

Figure 8. Polyesters bearing NO and drug releasing pendant groups (see color insert)

pharmaceutical applications such as NO and drug-eluting stents, medical device coatings, transdermal patches for wound healing, and controlled delivery.

4. Synthesis of NO Releasing Macromers

Example 1: Synthesis of 2-(6-Methoxy-naphthalen-2-yl)-propionic acid benzyloxy-carbonyl methyl ester

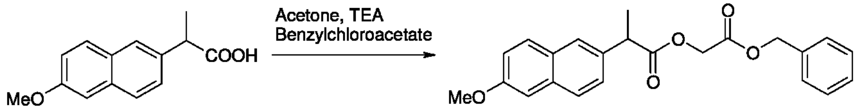
MeO
COOH
Acetone, TEA
Benzylchloroacetate
MeO
O
O
O
O
O

To a mixture of Naproxen (25 grams, 108.56 mmol) and triethylamine (23 ml, 165.01 mmol) in acetone (150 ml) was added benzyl chloroacetate (24 grams, 132.15 mmol) drop wise, and the mixture was stirred at 50°C temperature for three hours. The reaction mixture was poured onto cold water, and crude 2-(6-Methoxy-naphthalen-2-yl)-propionic acid benzyloxy-carbonyl methyl ester was filtered, dried and purified by recrystallizing from a mixture of ethyl acetate: hexane (1:5) to give pure 2-(6-Methoxy-naphthalen-2-yl)-propionic acid benzyloxycarbonyl methyl ester (39 grams) as a white powder. m.p: 95.3-97.3°C. The pure product was characterized using ^{1}H NMR spectroscopy in $CDCl_3$: δ 1.60 (d, 3H, CH_3), 3.80(m, 4H, CH and OCH_3), 4.56(q, 2H, OCH2), 5.12(q, 2H, OCH2), 7.06(m, 2H, Ar), 7.30(m, 6H, Ar), 7.64(m, 3H, Ar)

Example 2: Synthesis of 2-(6-Methoxy-naphthalen-2-yl)-propionic acid carboxymethyl ester

Downloaded by OHIO STATE UNIV LIBRARIES on June 23, 2012 | http://pubs.acs.org
Publication Date (Web): November 18, 2010 | doi: 10.1021/bk-2010-1054.ch011

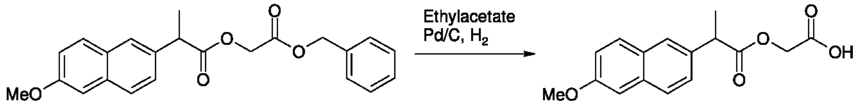

To a solution of 2-(6-methoxy-naphthalen-2-yl)-propionic acid benzyloxy carbonyl methyl ester (45 grams, 119.04 mmol) in ethyl acetate (200 ml), was added 50% wet Palladium on carbon (10%, 9 grams), and the mixture was stirred under an atmosphere of hydrogen (4 Kg) overnight in a pressure vessel. The catalyst was removed by filtration and ethyl acetate was distilled under vacuum. The crude product was precipitated by adding hexane, filtered, dried, and purified by recrystallization in a mixture of ethyl acetate: hexane (1:5) to get pure 2-(6-Methoxy-naphthalen-2-yl)-propionic acid carboxymethyl ester (30 grams) as a white powder with a melting point of 131-132.5°C. The pure product was characterized using ^{1}H NMR spectroscopy in $CDCl_3$: ^{1}H NMR ($CDCl_3$) δ 1.60(d, 3H, CH_3), 3.88(s, 1H, OCH_3), 3.94(m, 1H, CH), 4.54(q, 2H, OCH2), 7.06(m, 2H, Ar), 7.39(d, 1H, Ar), 7.64(m, 3H, Ar).

Example 3: Synthesis of 2-(6-Methoxy-naphthalen-2-yl)-propionic acid 4-bromo-butoxy carbonyl methyl ester

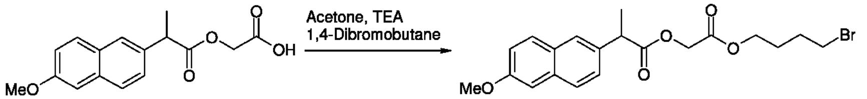

To a mixture of 2-(6-Methoxy-naphthalen-2-yl)-propionic acid carboxymethyl ester (30 grams, 104.16 mmol) and triethylamine (21.9 ml, 157.12 mmol) in acetone (200 ml) was added 1,4-dibromobutane (90 grams, 416.85 mmol) drop wise, and the mixture stirred at room temperature for 24 hours. The reaction mixture was poured onto cold water and crude 2-(6-Methoxy-naphthalen-2-yl)-propionic acid 4-bromo-butoxy carbonyl methyl ester was extracted into dichloromethane. After drying over sodium sulphate, dichloromethane was distilled off under reduced pressure, and the residue was purified by column chromatography using hexane as an eluant to get 18 grams of 2-(6-Methoxy-naphthalen-2-yl)-propionic acid 4-bromo-butoxy carbonyl methyl ester as light brown syrup. The pure product was characterized using ^{1}H NMR spectroscopy in $CDCl_3$: δ 1.52(d, 3H, CH_3), 1.62(m, 4H, CH_2 X_2), 3.16(t, 2H, CH_2), 3.82(m, 4H, CH and OCH_3), 3.98(t, 2H, CH_2), 4.46(q, 2H, OCH2), 7.00(m, 2H, Ar), 7.30(d, 1H, Ar), 7.58(m, 3H, Ar).

Example 4: Synthesis of 2-(6-Methoxy-naphthalen-2-yl)-propionic acid 3-nitrooxy-propoxy carbonyl methyl ester

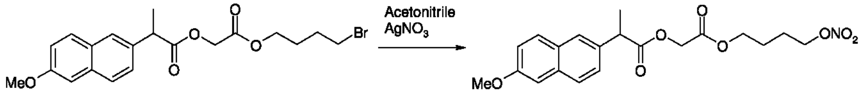

To a solution of 2-(6-Methoxy-naphthalen-2-yl)-propionic acid 4-bromo-butoxy carbonyl methyl ester (15 grams, 35.46 mmol) in acetonitrile (150

Downloaded by OHIO STATE UNIV LIBRARIES on June 23, 2012 | http://pubs.acs.org
Publication Date (Web): November 18, 2010 | doi: 10.1021/bk-2010-1054.ch011

ml) was added Silver nitrate (8.7 grams, 51.21 mmol), and the mixture was left for stirring with reflux overnight. The reaction mixture was filtered and washed with acetonitrile, dried over sodium sulphate, the solvent distilled off under reduced pressure, and the residue was purified by column chromatography using hexane: ethyl acetate (8:2) as eluant to get 13 grams of 2-(6-Methoxy-naphthalen-2-yl)-propionic acid 3-nitrooxy-propoxy carbonyl methyl ester as a light yellow syrup. The pure product was also characterized using ^{1}H NMR spectroscopy in $CDCl_3$: δ 1.62(m, 7H, CH_2 X $_2$ and CH_3), 3.92(s, 3H, OCH_3), 3.97(q, 1H, CH), 4.12(t, 2H, CH_2), 4.32(t, 2H, CH_2), 4.61(s, 2H, OCH2), 7.16(m, 2H, Ar), 7.43(d, 1H, Ar), 7.73(m, 3H, Ar)

Example 5: Synthesis of 2-(6-Hydroxy-naphthalen-2-yl)-propionic acid

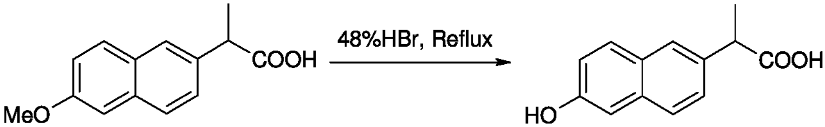

A mixture of Naproxen (500 grams, 2.774 mmol) and 48% HBr solution (1500 ml) was refluxed for 10 Hours, poured onto ice water (3000 ml), and stirred for 30 minutes. Crude 2-(6-hydroxy-naphthalen-2-yl)-propionic acid was filtered, dried and recrystallised from a mixture of ethyl acetate and hexane (1:5) to give pure 2-(6-hydroxy-naphthalen-2-yl)-propionic acid (380 grams, 81%) as a white powder with a melting point of 186-188°C.

Example 6: Synthesis of 2-(6-Hydroxy-naphthalen-2-yl)-propionic acid methyl ester

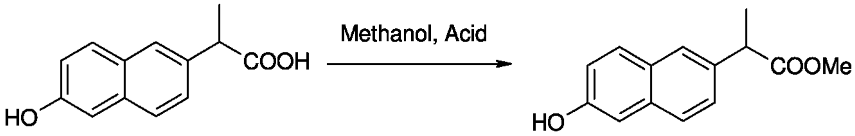

To a solution of methanol (2100 ml) and sulphuric acid (84 ml) was added 2-(6-Hydroxy-naphthalen-2-yl)-propionic acid (420 grams, 1.944 mmol). The reaction mixture was refluxed for 6 Hours. Methanol (1000 ml) was distilled, and the cooled reaction mass was poured onto ice water to yield crude 2-(6-hydroxy-naphthalen-2-yl)-propionic acid methyl ester which was filtered, dried and recrystallized using a (1:5) mixture of ethyl acetate: hexane to yield pure product (400 grams, 89.5% yield) as a white fluffy powder with a melting point of 89.5-92°C. The pure product was characterized using ^{1}H NMR spectroscopy in $CDCl_3$ δ 1.60(d, 3H, CH_3), 3.70(s, 3H, Ester), 3.88(q, 1H, CH), 5.36(bs, 1H, OH), 7.08(m, 2H, Ar), 7.48(m, 1H, Ar), 7.65(m, 3H, Ar)

Example 7: Synthesis of 2-[6-(2-Chloro-acetoxy)-naphthalen-2-yl]-propionic acid methyl ester

Downloaded by OHIO STATE UNIV LIBRARIES on June 23, 2012 | http://pubs.acs.org
Publication Date (Web): November 18, 2010 | doi: 10.1021/bk-2010-1054.ch011

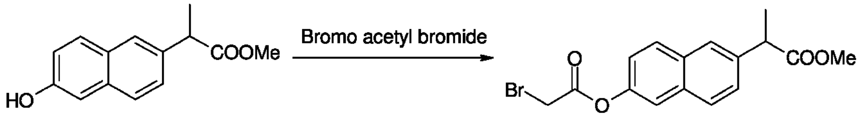

To a solution of 2-(6-hydroxy-naphthalen-2-yl)-propionic acid methyl ester (20 grams, 86.95 mmol) and pyridine (10.3 grams, 130.43 mmol) in dichloromethane (200 ml) maintained at 0-5°C under N_2 atmosphere was added dropwise bromoacetyl chloride (19.6 grams, 173.54 mmol). The reaction was stirred at the same temperature for one hour. The reaction mixture was washed with water (2x500ml) and 5% solution of sodium carbonate followed by drying over sodium sulphate and distillation to get crude compound, which was purified by column chromatography using hexane as eluant to get pure 2-[6-(2-bromo-acetoxy)-naphthalen-2-yl]-propionic acid methyl ester (14 grams) as a dark brown syrup. The pure product was characterized using ^1H NMR spectroscopy in $CDCl_3$ δ 1.55(d,3H,CH_3), 3.65(s,3H,Ester), 3.82(q,1H, CH), 4.08(s, 2H, OCH_2) 7.20(dd, 1H, Ar), 7.4(dd,1H, Ar),7.57(d, 1H,Ar), 7.72(d, 1H,Ar), 7.78(d, 1H, Ar), 7.84(d,1H, Ar).

Example 8: Synthesis of 2-[6-(2-Nitrooxy-acetoxy)-naphthalen-2-yl]-propionic acid methyl ester

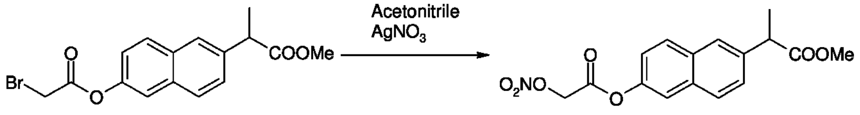

To a solution of 2-[6-(2-bromo-acetoxy)-naphthalen-2-yl]-propionic acid methyl ester (14 grams, 39.88 mmol) in acetonitrile (150 ml) was added silver nitrate (20.2 grams, 118.91 mmol). The solution was stirred at room temperature overnight followed by stirring at 45- 50°C for 4-6hrs. The reaction mixture was filtered and washed with acetonitrile, dried over sodium sulphate, and the solvent was distilled off under reduced pressure. The residue was purified by column chromatography using a mixture of Hexane: Ethyl acetate (8:2) as eluant, followed by recrystallisation from a mixture of toluene: hexane to get 5.5 grams 2-[6-(2-Nitrooxy-acetoxy)-naphthalen-2-yl]-propionic acid methyl ester as off white powder. The pure product was characterized using ^1H NMR spectroscopy in $CDCl_3$ δ 1.56(d,3H,CH_3), 3.65(s, 3H,Ester), 3.90(q,1H, CH), 5.258(s, 2H, OCH_2) 7.20(dd, 1H, Ar), 7.4(dd,1H, Ar), 7.57(d, 1H,Ar), 7.72(d, 1H,Ar), 7.78(d, 1H, Ar), 7.84(d,1H, Ar). The pure product has a melting point of 72-74°C.

Example 9: Synthesis of 2-(6-hydroxy-naphthalen-2-yl)-propionic acid

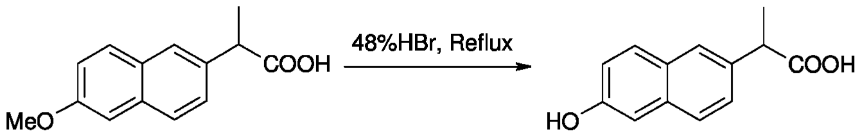

Downloaded by OHIO STATE UNIV LIBRARIES on June 23, 2012 | http://pubs.acs.org
Publication Date (Web): November 18, 2010 | doi: 10.1021/bk-2010-1054.ch011

To a mixture of Naproxen (500 grams, 2.774 mmol) and 48% HBr (1500 ml) was refluxed for 10 hours. It was poured onto ice water (3000 ml) and stirred for 30 minutes. Crude 2-(6-Hydroxy-naphthalen-2-yl)-propionic acid was filtered, dried and recrystallized from a mixture of ethyl acetate and hexane (1:5) to yield pure product (380 grams, 81%) as a white powder with a melting point of 186-188°C

Example 10: Synthesis of 2-(6-hydroxy-naphthalen-2-yl)-propionic acid benzyloxy carbonyl methyl ester

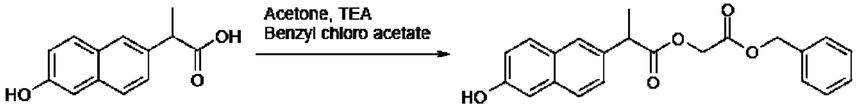

To a mixture of 2-(6-hydroxy-naphthalen-2-yl)-propionic acid (50 grams, 231.48 mmol), triethylamine (33 ml, 236.76 mmol) in acetone (500 ml) was added benzyl chloroacetate (45 grams, 243.77 mmol) drop wise, and the mixture stirred at 50°C temperature for three hours. The reaction mixture poured onto cold water, crude 2-(6-hydroxy-naphthalen-2-yl)-propionic acid benzyloxy carbonyl methyl ester extracted into ethyl acetate, washed with water, dried over sodium sulphate, the solvent distilled off, and purified by column chromatography with hexane: ethyl acetate as eluant to give pure 2-(6-hydroxy-naphthalen-2-yl)-propionic acid benzyloxy carbonyl methyl ester (41 grams) as a white powder with a melting point of 104-106.5°C. The pure product was characterized using ^{1}H NMR spectroscopy in $CDCl_3$ δ 1.57(d, 3H, CH_3), 3.88(q, 1H, CH), 4.60(q, 2H, OCH2), 5.10(q, 2H, OCH2), 7.04(m, 2H, Ar), 7.27(m, 7H, Ar), 7.60(m, 3H, Ar).

Example 11: Synthesis of 2-(6-hydroxy-naphthalen-2-yl)-propionic acid carboxy methyl ester

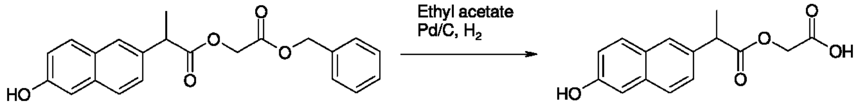

To a solution of 2-(6-Hydroxy-naphthalen-2-yl)-propionic acid benzyloxy carbonyl methyl ester (41 grams, 112.63 mmol) in ethyl acetate (400 ml) in a pressure vessel was added 50% wet palladium on carbon (10%, 9 grams) and the mixture was stirred overnight under an atmosphere of hydrogen (5 Kg) at a temperature of 50°C. The catalyst was removed by filtration and ethyl acetate distilled off (50%) under vacuum, and the product precipitated by adding hexane, filtered and dried to get pure 2-(6-hydroxy-naphthalen-2-yl)-propionic acid carboxy methyl ester (30 grams) as a white powder with a melting point of 186-188.5°C. The pure product was characterized using ^{1}H NMR spectroscopy in $CDCl_3$ δ 1.60(d, 3H, CH_3), 3.88(s, 1H, OCH_3), 3.94(m, 1H, CH), 4.54(q, 2H, OCH2), 7.06(m, 2H, Ar), 7.39(d, 1H, Ar), 7.64(m, 3H, Ar).

Example 12: Synthesis of 2-(6-hydroxy-naphthalen-2-yl)-propionic acid 4-bromo-butoxy carbonyl methyl ester

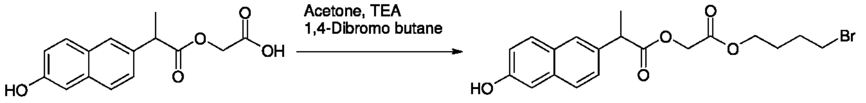

To a mixture of 2-(6-hydroxy-naphthalen-2-yl)-propionic acid carboxy methyl ester (30 grams, 138.88 mmol) and triethylamine (24 ml, 172.19 mmol) in acetone (300 ml) was added dropwise 1,4-dibromo butane (96.5 grams, 446.90 mmol) drop wise followed by stirring at room temperature for 24 hours. The reaction mixture was poured onto cold water, crude 2-(6-hydroxy-naphthalen-2-yl)-propionic acid 4-bromo-butoxy carbonyl methyl ester was extracted into ethyl acetate, and dried over sodium sulphate. Ethyl acetate was distilled off under reduced pressure and the residue was purified by column chromatography using hexane as eluant to yield 24 grams of 2-(6-Hydroxy-naphthalen-2-yl)-propionic acid 4-bromo-butoxy carbonyl methyl ester as a light brown syrup. The pure product was characterized using ^1H NMR spectroscopy in $CDCl_3$ δ 1.60(d, 3H, CH_3), 1.74(m, 4H, CH_2 X_2), 3.22(t, 2H, CH_2), 3.90(q, 1H, CH), 4.08(t, 2H, CH_2), 4.55(q, 2H, OCH2), 7.02(m, 2H, Ar), 7.30(d, 1H, Ar), 7.58(m, 3H, Ar)

Example 13: Synthesis of 2-(6-hydroxy-naphthalen-2-yl)-propionic acid 4-bromo-butoxy carbonyl methyl ester

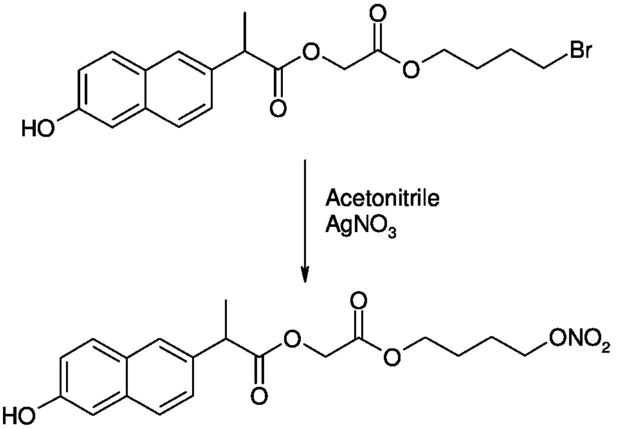

To a solution of 2-(6-hydroxy-naphthalen-2-yl)-propionic acid 4-bromo-butoxy carbonyl methyl ester (20 grams, 48.89 mmol) in acetonitrile (200 ml) was added Silver nitrate (12.4 grams, 72.99 mmol), and the mixture stirred at reflux temperature overnight. The reaction mixture was filtered and washed with acetonitrile, dried over sodium sulphate, the solvent distilled off under reduced pressure, residue re-dissolved in dichloro methane, and the salts filtered off; then the organic layer was washed with water (2x 50 ml), dried over Sodium sulphate, the solvent distilled off under reduced pressure, and the residue was purified by column chromatography using hexane: ethyl acetate (8:2) as an eluant to get 17 grams of 2-(6-hydroxy-naphthalen-2-yl)-propionicacid 4-nitrooxy-butoxy carbonyl methyl ester white powder.

Downloaded by OHIO STATE UNIV LIBRARIES on June 23, 2012 | http://pubs.acs.org
Publication Date (Web): November 18, 2010 | doi: 10.1021/bk-2010-1054.ch011

Downloaded by OHIO STATE UNIV LIBRARIES on June 23, 2012 | http://pubs.acs.org
Publication Date (Web): November 18, 2010 | doi: 10.1021/bk-2010-1054.ch011

Example 14: Synthesis of 2-[6-(2-Bromo-acetoxy)-naphthalen-2-yl]-propionic acid 4-nitrooxy-butoxy carbonyl methyl ester

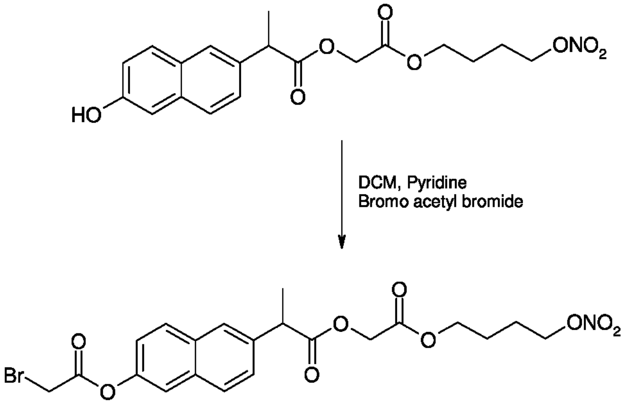

To a solution of 2-(6-hydroxy-naphthalen-2-yl)-propionic acid and 4-nitrooxy-butoxy carbonyl methyl ester (17 grams, 43.48 mmol) and pyridine (5.7 ml, 66.38 mmol) in dichloromethane (200 ml) maintained at 0-5°C under N_2 atmosphere was added dropwise bromo acetyl bromide (5.6 ml, 64.36 mmol). The reaction mixture was stirred at the same temperature for one hour. The reaction mixture was washed with water (2x25 ml) and a solution of 5% Sodium carbonate (3x25 ml). The solution was dried over sodium sulphate and the solvent was distilled off to get crude 2-[6-(2-Bromo-acetoxy)-naphthalen-2-yl]-propionic acid 4-nitrooxy-butoxy carbonyl methyl ester.

Example 15: Synthesis of 2-[6-(2-Nitrooxy-acetoxy)-naphthalen-2-yl]-propionic acid 4-nitrooxy-butoxy carbonyl methyl ester

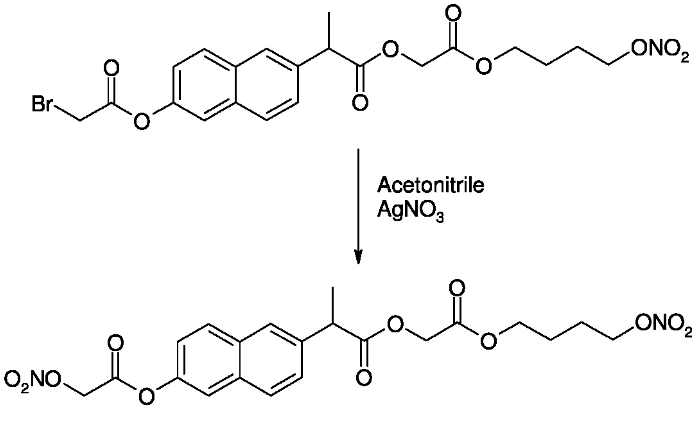

To a solution of 2-[6-(2-Bromo-acetoxy)-naphthalen-2-yl]-propionic acid 4-nitrooxy-butoxy carbonyl methyl ester (15 grams, 29.35 mmol) in acetonitrile (150 ml) was added silver nitrate (10 grams, 58.86 mmol), and the mixture stirred at 40°C temperature for 24 hours. The reaction mixture was

Downloaded by OHIO STATE UNIV LIBRARIES on June 23, 2012 | http://pubs.acs.org
Publication Date (Web): November 18, 2010 | doi: 10.1021/bk-2010-1054.ch011

filtered and washed with acetonitrile, dried over sodium sulphate, the solvent distilled off under reduced pressure, and the residue was purified by column chromatography using hexane:ethyl acetate (8:2) as eluant to get 10 grams of 2-[6-(2-nitrooxy-acetoxy)-naphthalen-2-yl]-propionic acid 4-nitrooxy-butoxy carbonyl methyl ester as a light yellow syrup.

Example 16: Synthesis of 2-Acetoxy-benzoic acid benzyloxy carbonyl methyl ester

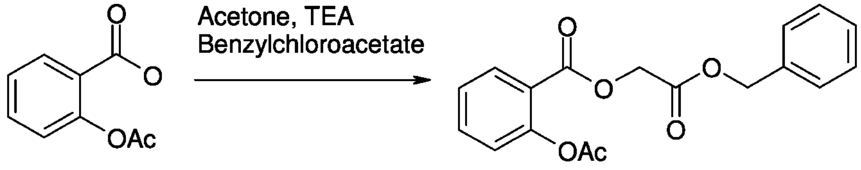

To a mixture of Aspirin (25 grams, 138.77 mmol) and triethylamine (29 ml, 208.06 mmol) in acetone (250 ml) was added dropwise benzyl chloro acetate (30.75 grams, 166.56 mmol), followed by stirring at 50°C for five hours. The reaction mixture was poured onto cold water, crude 2-Acetoxy-benzoic acid benzyloxy carbonyl methyl ester was filtered, dried and purified by recrystallisation from a (1:4) mixture of chloroform: hexane to give pure 2-Acetoxy-benzoic acid benzyloxy carbonyl methyl ester (25 grams) as a white powder with a melting point of m.p: 91-92.5°C. The pure product was characterized using ^{1}H NMR spectroscopy in $CDCl_3$ δ2.30(s, 3H, OAc), 4.82(s, 2H, CH_2), 5.20(s, 2H, CH2), 7.10(d, 1H, Ar), 7.32(m, 6H, Ar), 7.56(t, 1H, Ar), 8.18(d, 1H, Ar).

Example 17: Synthesis of 2-Acetoxy-benzoic acid carboxymethyl ester

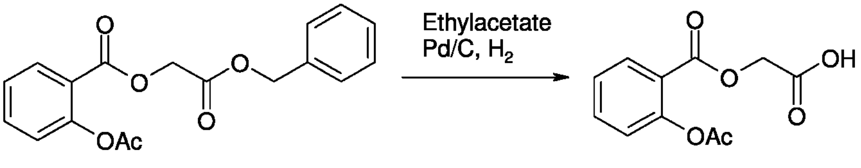

2-Acetoxy-benzoic acid benzyloxy carbonyl methyl ester (50 grams, 152.43 mmol) was dissolved in ethyl acetate (150 ml) in a pressure vessel and 50% wet palladium on carbon (10%, 10 grams) was added. The reaction mixture was stirred under an atmosphere of hydrogen (4 Kg) for 14 hours. The catalyst was removed by filtration and ethyl acetate was distilled off under vacuum. The crude was precipitated by adding hexane followed by filtration, drying and purification by recrystallisation using a (1:6) mixture of ethyl acetate: hexane to yield pure 2-Acetoxy-benzoic acid carboxymethyl ester (32 grams) as a white powder with a melting point of 130-131.5°C. The pure product was characterized using ^{1}H NMR spectroscopy in DMSO-d_6 δ 2.28(s, 3H, OAc), 4.8(s, 2H, CH_2), 7.24(d, 1H, Ar), 7.55(t, 1H, Ar), 7.74(t, 1H, Ar), 8.10(d, 1H, Ar), 13.20 (bs, 1H, COOH)

Downloaded by OHIO STATE UNIV LIBRARIES on June 23, 2012 | http://pubs.acs.org
Publication Date (Web): November 18, 2010 | doi: 10.1021/bk-2010-1054.ch011

Example 18: Synthesis of 2-Acetoxy-benzoic acid 4-bromo-butoxy carbonyl methyl ester

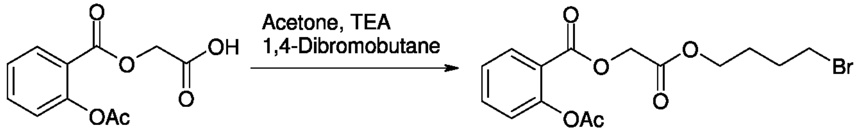

To a mixture of 2-acetoxy-benzoic acid carboxymethyl ester (30 grams, 126.05 mmol), and triethylamine (26.5 ml, 190.12 mmol) in acetone (200 ml) was added dropwise 1,4-dibromo butane (109 grams, 504.86 mmol). The reaction mixture was left for stirring at room temperature for 24 hours. The reaction mixture was poured onto cold water and crude 2-acetoxy-benzoic acid 4-bromobutoxy carbonyl methyl ester was extracted into dichloromethane followed by drying over sodium sulphate. Dichloromethane was distilled off under reduced pressure and the residue was purified by column chromatography using hexane as eluant to get 32 grams of 2-acetoxy-benzoic acid 4-bromo-butoxy carbonyl methyl ester as a light yellow liquid. The pure product was characterized using ^{1}H NMR spectroscopy in $CDCl_3$ δ 1.88(m, 4H, CH_2X_2), 2.32(s, 3H, OAc), 3.39(t, 2H, CH_2), 4.20(t, 2H, CH_2), 4.75(s, 2H, CH_2), 7.10(d, 1H, Ar), 7.23(t, 1H, Ar), 7.50(t, 1H, Ar), 8.10(d, 1H, Ar)

Example 19: Synthesis of 2-Acetoxy-benzoic acid 4-nitrooxy-butoxy carbonyl methyl ester

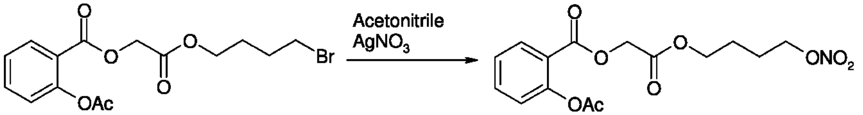

To a solution of 2-Acetoxy-benzoic acid 4-bromo-butoxy carbonyl methyl ester (20 grams, 53.61 mmol) in acetonitrile (150 ml) was added silver nitrate (13.6 grams, 80.06 mmol). The reaction mixture was refluxed for four hours. The reaction mixture was filtered and washed with acetonitrile, dried over sodium sulphate followed by distillation of solvent under reduced pressure. The residue was purified by column chromatography using hexane as eluant to get 15 grams of 2-acetoxy-benzoic acid 4-nitrooxy-butoxy carbonyl methyl ester as a light yellow liquid. The pure product was characterized using ^{1}H NMR spectroscopy in $CDCl_3$ δ1.80(m, 4H, CH_2X_2), 2.34(s, 3H, OAc), 4.22(t, 2H, CH_2), 4.44(t, 2H, CH_2), 4.80(s, 2H, CH_2), 7.14(d, 1H, Ar), 7.34(t, 1H, Ar), 7.60(t, 1H, Ar), 8.08(d, 1H, Ar.

Example 20: Synthesis of Bromo-acetic acid 2-formyl-phenyl ester

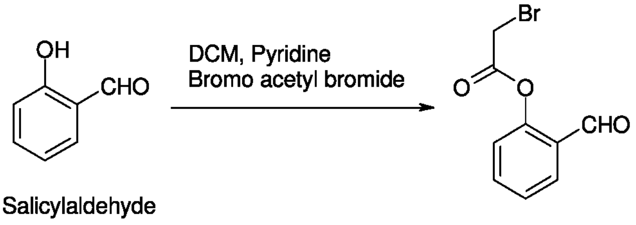

To a solution of Salicylaldehyde (50 grams, 409.4 mmol) and pyridine (48.5 grams, 815.25 mmol) in dichloromethane (500ml) maintained at 0-5°C under nitrogen atmosphere was added dropwise bromoacetyl bromide (210.6 grams, 1042 mmol). The reaction mixture was stirred for one hour at the same temperature. The reaction mixture was washed with 1000 ml of water and 1500 ml of 5% sodium bicarbonate solution, dried over sodium sulphate followed by distillation of solvent under reduced pressure to get 60.0 grams of bromo-acetic acid 2-formyl-phenyl ester.

Example 21: Synthesis of Nitrooxy-acetic acid 2-formyl-phenyl ester

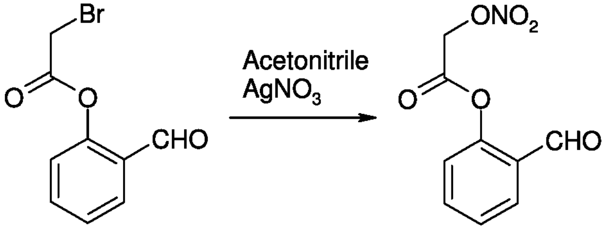

To a solution of bromoacetic acid 2-formyl-phenyl ester (10 grams, 41.15 mmol) in acetonitrile (150 ml) was added silver nitrate (14.0 grams, 82.41 mmol). The reaction mixture was stirred at room temperature for 35-38 hours. The reaction mixture was then filtered and washed with acetonitrile, dried over sodium sulphate, and the solvent was distilled off under reduced pressure to leave the residue which was purified by column chromatography using hexane: ethyl acetate (8:2) as eluant to yield 3.0 grams of nitrooxy-acetic acid 2-formyl-phenyl ester as brown syrup. The pure product was characterized using ^{1}H NMR spectroscopy in $CDCl_3$ δ 5.25(s, 2H, OCH_2), 7.20 (d, 1H, Ar), 7.53(dd, 1H, Ar), 7.63(dd, 1H, Ar), 7.90(d, 1H, Ar).

Example 22: Synthesis of 2-(2-Nitrooxy-acetoxy)-benzoic acid

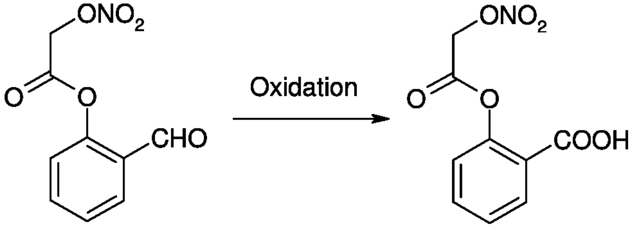

Downloaded by OHIO STATE UNIV LIBRARIES on June 23, 2012 | http://pubs.acs.org
Publication Date (Web): November 18, 2010 | doi: 10.1021/bk-2010-1054.ch011

To a solution of nitrooxyacetic acid-2-formyl-phenyl ester (3.0 grams, 13.3mmole) in acetone (50.0ml) was added potassium permanganate (3.0grams, 18.95 mmol) at 0°C and stirred at the same temperature for 5-6 hours. Oxalic acid (15grams) was added to the reaction mixture and the reaction mixture was washed with acetone followed by filtration, the solution was dried over sodium sulphate and the solvent was distilled off under reduced pressure. The residue was dissolved in dichloromethane and the organic layer was washed with water and dried over sodium sulphate. The solvent was distilled off under reduced pressure, purified by column chromatography using a mixture of hexane: ethyl acetate (8:2) as an eluant to yield 1.0 grams of product (an off-white powder). The product is purified further to yield 2-(2-nitrooxy-acetoxy)-benzoic acid.

Downloaded by OHIO STATE UNIV LIBRARIES on June 23, 2012 | http://pubs.acs.org
Publication Date (Web): November 18, 2010 | doi: 10.1021/bk-2010-1054.ch011

Example 23: Synthesis of 2-hydroxy-benzoic acid benzyloxy carbonyl methyl ester

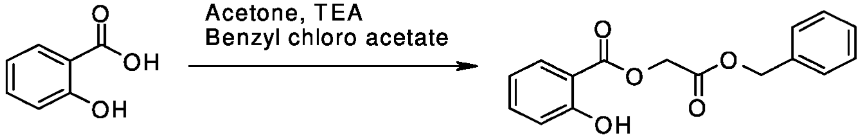

To a mixture of Salicylic acid (100 grams, 724 mmol) and triethylamine (152 ml, 1.09 mmol) in acetone (500 ml) was added dropwise benzyl chloroacetate (147 grams, 796.32 mmol). The solution was stirred at 50°C temperature for four hours. The reaction mixture was poured onto cold water and the isolated crude 2-hydroxy-benzoic acid benzyloxy carbonyl methyl ester was filtered, dried and purified by recrystallising from a mixture of ethyl acetate: hexane (1:4) to yield pure 2-hydroxy-benzoic acid benzyloxy carbonyl methyl ester (50 grams) as a white powder with a melting point of 75.5-77°C.

Example 24: Synthesis of 2-Hydroxy-benzoic acid carboxymethyl ester

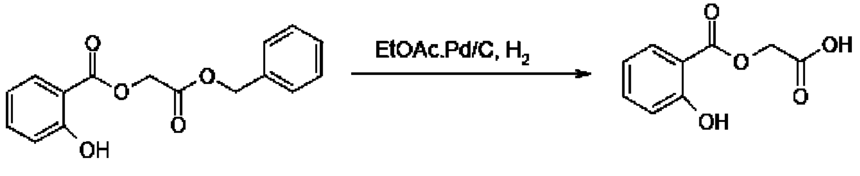

To a solution of 2-hydroxy-benzoic acid benzyloxy carbonyl methyl ester (55 grams, 192.31 mmol) in ethyl acetate (300 ml) in a pressure vessel was added 50% wet Palladium on carbon (10%, 15 grams). The reaction mixture was stirred under an atmosphere of hydrogen (4 Kg) for 16 hours. The catalyst was removed by filtration and ethyl acetate was distilled off under vacuum to yield crude 2-hydroxy-benzoic acid carboxymethyl ester, which was precipitated from hexane. The precipitate was filtered, dried and purified by recrystallisation from a mixture of ethyl acetate: hexane (1:6) to yield 33 grams of pure 2-hydroxy-benzoic acid carboxymethyl ester as a white powder. The pure product was characterized using ^{1}H NMR spectroscopy in DMSO-d_6 δ 4.85(s, 2H, CH_2), 7.00(m, 2H, Ar), 7.55(t, 1H, Ar), 7.85(d, 1H, Ar), 10.30 (bs, 1H, OH). The pure product has a melting point of 131-132.5°C.

Example 25: Synthesis of 2-hydroxy-benzoic acid 4-bromo-butoxy carbonyl methyl ester

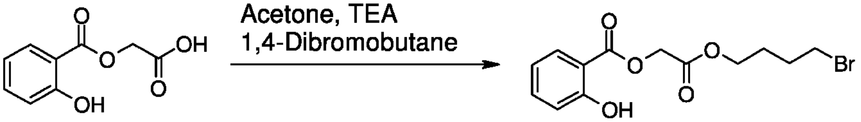

To a mixture of 2-hydroxybenzoic acid carboxy methyl ester (33 grams, 168.37 mmol), and triethylamine (36 ml, 258.29 mmol) in acetone (400 ml) was added dropwise 1,4-dibromo butane (146 grams, 676.24 mmol). The reaction mixture was stirred at 40°C for 16 hours. The reaction mixture was poured onto cold water to yield crude 2-Hydroxy-benzoic acid 4-bromobutoxy carbonyl methyl ester which was extracted into dichloro methane and dried over sodium sulphate. The solvent was distilled off under reduced pressure and the residue was purified by column chromatography using a mixture of hexane:ethyl acetate (9:1) as eluant to yield 40 grams of 2-hydroxybenzoic acid-4-bromo-butoxy carbonyl methyl ester as a light yellow liquid. The pure product was characterized using ^{1}H NMR spectroscopy in ^{1}H NMR ($CDCl_3$) δ 1.95 (m, 4H, CH_2X_2), 3.40(t, 2H, CH_2), 4.25(t, 2H, CH_2), 4.85(s, 2H, CH_2), 6.90(m, 2H, Ar), 7.5(t, 1H, Ar), 7.90(d, 1H, Ar), 10.35(s, 1H, OH).

Example 26: Synthesis of 2-Hydroxy-benzoic acid 4-nitrooxy-butoxy carbonyl methyl ester

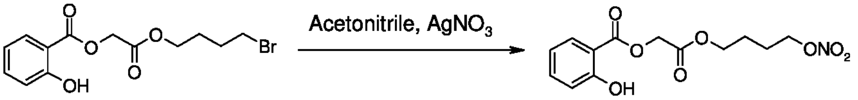

To a solution of 2-hydroxy-benzoic acid 4-bromo-butoxy carbonyl methyl ester (30 grams, 90.63 mmol) in acetonitrile (300 ml) was added silver nitrate (30 grams, 176.57 mmol) and stirred at 50°C temperature for eight hours. The reaction mixture was filtered and washed with acetonitrile, dried over sodium sulphate, the solvent distilled off under reduced pressure ,and the residue was dissolved in dichloromethane, filtered off the salts; organic layer washed with water (2x 50 ml), dried over sodium sulphate, distilled under vacuum, and precipitated with hexane to yield 23 grams of 2-hydroxy-benzoic acid 4-nitrooxy-butoxy carbonyl methyl ester as an off-white powder. The pure product was characterized using ^{1}H NMR spectroscopy in ^{1}H NMR ($CDCl_3$) δ 1.85(m, 4H, CH_2 X_2), 4.25(t, 2H, CH_2), 4.55(t, 2H, CH_2), 4.85(s, 2H, CH_2), 6.90(m, 2H, Ar), 7.5(t, 1H, Ar), 7.90(d, 1H, Ar), 10.30(s, 1H, OH). The pure product has a melting point of 84-86.5°C.

Example 27: Synthesis of 2-(2-Bromo-acetoxy)-benzoic acid 4-nitrooxy-butoxy carbonyl methyl ester

Downloaded by OHIO STATE UNIV LIBRARIES on June 23, 2012 | http://pubs.acs.org
Publication Date (Web): November 18, 2010 | doi: 10.1021/bk-2010-1054.ch011

Downloaded by OHIO STATE UNIV LIBRARIES on June 23, 2012 | http://pubs.acs.org
Publication Date (Web): November 18, 2010 | doi: 10.1021/bk-2010-1054.ch011

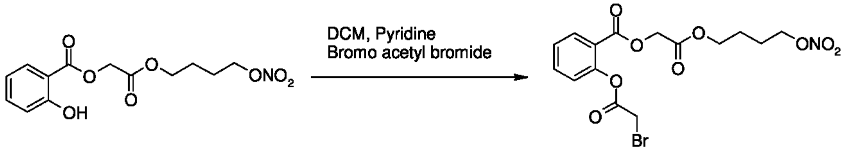

To a solution of 2-hydroxy-benzoic acid 4-nitrooxy-butoxy carbonyl methyl ester (20 grams, 63.89 mmol) and pyridine (8 ml, 98.91 mmol) in dichloromethane (300 ml) maintained at 0-5°C under N_2 atmosphere was added dropwise bromoacetyl bromide (8ml, 91.95 mmol). The reaction mixture was stirred at the same temperature for two hours. The reaction mixture was washed with water (200 ml) and a 5% solution of sodium carbonate (300 ml). The solution was dried over sodium sulphate and solvent was distilled off to yield crude 2-hydroxy-benzoic acid 4-nitrooxy-butoxy carbonyl methyl ester as light brown syrup The pure product was characterized using ^{1}H NMR spectroscopy in ^{1}H NMR ($CDCl_3$) δ 1.70(m, 4H, CH_2X_2), 4.15(t, 4H, CH_2), 4.35(s, 2H, CH_2), 4.70(s, 2H, CH_2), 7.05(d, 1H, Ar), 7.30(t, 1H, Ar), 7.55(t, 1H, Ar), 8.05(d, 1H, Ar).

Example 28: Synthesis of 2-(2-Nitrooxy-acetoxy)-benzoic acid 4-nitrooxy-butoxy carbonyl methyl ester

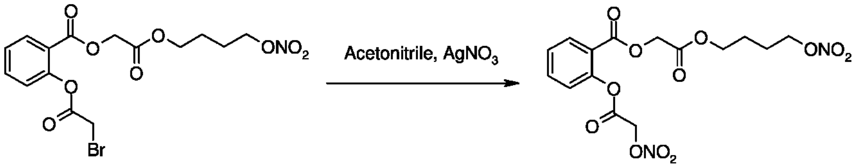

To a solution of 2-(2-bromoacetoxy)-benzoic acid-4-nitrooxy-butoxy carbonyl methyl ester (15 grams, 35.85 mmol) in acetonitrile (150 ml) was added Silver nitrate (12.2 grams, 71.81 mmol). The solution was stirred at 50°C temperature for twenty four hours. The reaction mixture was filtered, washed with acetonitrile, and dried over sodium sulphate. The solvent was distilled off under reduced pressure. The residue was dissolved in dichloromethane, and the salts were filtered off. The organic layer was washed with water (2x 50 ml), dried over sodium sulphate, distilled under vacuum to yield 2-(2-nitrooxy-acetoxy)-benzoic acid 4-nitrooxy-butoxy carbonyl methyl ester, which was purified by column chromatography using a mixture of hexane: ethyl acetate (9:1). The product was further precipitated with hexane to yield 7.5 grams of 2-(2-nitrooxy-acetoxy)-benzoic acid 4-nitrooxy-butoxy carbonyl methyl ester as a white powder. The pure product was characterized using ^{1}H NMR spectroscopy in ^{1}H NMR ($CDCl_3$) δ δ1.75(m, 4H, CH_2X_2), 4.20(t, 2H, CH_2), 4.45(t, 2H, CH_2), 4.80(s, 2H, CH_2), 5.30(s, 2H, CH_2), 7.15(d, 1H, Ar), 7.45(t, 1H, Ar), 7.65(t, 1H, Ar), 8.15(d, 1H, Ar).

Downloaded by OHIO STATE UNIV LIBRARIES on June 23, 2012 | http://pubs.acs.org
Publication Date (Web): November 18, 2010 | doi: 10.1021/bk-2010-1054.ch011

5. Conclusions

Nitric Oxide and drug releasing macromers and oligomers were prepared. These NO and drug releasing macromers and oligomers are comprised of a drug molecule and a NO releasing moiety covalently linked to each other via a hydrolytically degradable linker. This hydrolytically degradable linker is comprised of repeat units derived from safe and biocompatible molecules such as glycolic acid, lactic acid, p-dioxanone and caprolactone, which are key components of all commercially available absorbable medical devices. These macromers and oligomers have tunable hydrolytic degradation profiles and hence the rate of release of NO and drug molecules can be controlled. Furthermore, these macromers and oligomers are anticipated to degrade into safe and biocompatible molecules upon hydrolysis. Hydrolytically degradable macromers and oligomers comprising two or more drug molecules, functionalized with a NO releasing moiety, were also synthesized. This serves to release the drug molecule as such without any change in chemical structure, activity and efficacy. The active portion of these macromers and polymers are expected to have improved bioavailability, increased solubility and better control on degradation rates. Absorbable polymers, including polyurethanes, polyesters and polyesteramides bearing pendant NO and drug releasing groups, were also synthesized. These absorbable polymers are expected to find use in a number of biomedical and pharmaceutical applications, such as NO and drug-eluting stents, medical device coatings, transdermal patches for wound healing, and controlled delivery. These NO and drug releasing macromers and oligomers may also find use in preparing a variety of therapeutic formulations for treatment of cardiovascular diseases, osteoarthritis, respiratory diseases, diabetic retinopathy, hypertension, pain and inflammation. Detailed studies to evaluate physical and mechanical property as well as biocompatibility of these polymers is currently in progress in our laboratories and results will be reported in a separate publication.

References

1. Meyerhoff, M. E.; et al. Polymers incorporating nitric oxide releasing/generating substances for improved biocompatibility of blood contacting medical devices. *Biomaterials* **2005**, *26*, 1685–93.
2. Mowery, K. A.; et al. Preparation and Characterization of Hydrophobic Polymeric films that are thromboresistant via Nitric Oxide Release. *Biomaterials* **2000**, *21*, 9–21.
3. Annich, G. M.; et al. Reduced platelet activation and thrombosis in extracorporeal circuits coated with nitric oxide release polymers. *Crit. Care Med.* **2000**, *28*, 915–20.
4. Fang, F. C. *Nitric Oxide and Infection*; Kluwer Academic/Plenum Publishers: New York, 1999
5. Green, S. J.; et al. Encapsulated and non-encapsulated nitric oxide generators used as anti-microbial agents. U.S. Patent No. 5814666.

6. Masters, K. S. B.; et al. Effects of nitric oxide releasing poly(vinyl alcohol) hydrogel dressings on dermal wound healing in diabetic mice. *Wound Rep. Reg.* **2002**, *10*, 286–94.
7. Fitzhugh, A. L.; et al. Highly-crosslinked, extremely hydrophobic nitric oxide-releasing polymers and methods for their manufacture and use. U.S. Patent No. 7226582 B2.
8. Bohl, K. S.; et al. Nitric Oxide-generating polymers reduce platelet adhesion and smooth muscle cell proliferation. *Biomaterials* **2000**, *21* (22), 2273–8.
9. Groves, P. H.; et al. The effects of exogenous nitric oxide on smooth muscle cell proliferation following porcine carotidangioplasty. *Cardiovasc. Res.* **1995**, *30*, 87–96.
10. Radomski, M. W.; et al. The role of nitric oxide and cGMP in platelet adhesion to vascualr endothelium. *Biochem. Biophys. Res. Commun.* **1987**, *148*, 1482.
11. Buergler, J. M.; et al. Use of Nitric oxide-eluting polymer-coated stents for prevention of restenosis in pigs. *Coron. Artery Dis.* **2000**, *11* (4), 351.
12. Keefer, L. K.; et al. Nitic Oxide releasing medical devices. U.S. Patent No. 7425218 B2.
13. Ignarro, L. J.; et al. Nitric Oxide. A novel signal transduction mechanism for transcellular communication. *Hypertension (Dallas)* **1990**, *16*, 477–43.
14. Hibbs, J. B.; et al. A cytotoxic activated macrophage effector molecule. *Biochem. Biophys. Res. Commun.* **1988**, *157*, 87.
15. Steuhr, D. J.; et al. Nitric Oxide: A Macrophage product responsible for cytostasis and Respiratory inhibition in tumor target cells. *J. Exp. Med* **1989**, *169*, 1543.
16. Smith, D. J.; et al. Polymeric Wound healing accelerators. U.S. Pat. No. 5,519,020.
17. U.S. Patent Nos. 5,945,452, 5,891,459 and 5,428,070.
18. U.S. Patent Nos. 5,268,465, 5,468,630 and 5,658,565.
19. WHO Task Group on environmental health criteria for oxides of nitrogen, Oxides of nitrogen, Environmental health criteria 4 (WHO Geneva 1977).
20. Miller, M. R.; et al. Recent developments in nitric oxide donor drugs. *Br. J. Pharmacol.* **2007**, *151*, 305.
21. U.S. Patent Nos. 5,380,758, 5,574,068 and 5,583,101 Nitrosothiols.
22. Herzog, W. R.; et al. U.S. Patent No. 6,656,217.
23. Smith, D. J.; et al. Nitric Oxide releasing Polymers Containing the [N(O)NO] Group. *J. Med.Chem.* **1996**, *39*, 1148–1156.
24. Keefer, L. K.; et al. U.S. Patent Nos. 4954526, 5039705, 5155137, 5212204, 5250550, 5366997, 5405919 and 5650447.
25. Zhang, H.; et al. Nitric Oxide Releasing Silicone Rubbers with improved blood compatibility: preparation, characterization and in vivo evaluation. *Biomaterials* **2002**, *23*, 1485.
26. Schoenfisch, M. H.; et al. Improving the thromboresistivity of chemical sensors via nitric oxide release: fabrication and in vivo evaluation of NO releasing oxygen sensing catheters. *Anal. Chem.* **2000**, *72*, 1119–26.
27. Wheatley, P. S.; et al. NO releasing zeolites and their anti-thrombotic properties. *J. Am. Chem. Soc.* **2006**, *128*, 502.

Downloaded by OHIO STATE UNIV LIBRARIES on June 23, 2012 | http://pubs.acs.org
Publication Date (Web): November 18, 2010 | doi: 10.1021/bk-2010-1054.ch011

28. Hrabie, J. A.; et al. New Nitric Oxide/Releasing Zwitterions derived from Polyamines. *J. Org. Chem.* **1993**, *58*, 1472–6.
29. Maragos, C. M.; et al. Complexes of NO with nucleophiles as agents for the controlled biological release of nitric oxide. *J. Med. Chem.* **1991**, *34*, 3242.
30. Chen, M.; et al. U.S. Patent Application Publication No. 20080220048.
31. Raulli, R.; et al. WO Patent Application Publication No. 2007053578.
32. Nicoletta, A.; et al. Nitric Oxide donor compounds. U.S. Patent Publication No. 2010/0099729 A1.
33. Bezwada, R. S. Controlled release of nitric oxide and drugs from functionalized macromers and oligomers. U.S. Patent Publication No. 2010/0209469 A1.

Downloaded by OHIO STATE UNIV LIBRARIES on June 23, 2012 | http://pubs.acs.org
Publication Date (Web): November 18, 2010 | doi: 10.1021/bk-2010-1054.ch011

Downloaded by UNIV OF DELAWARE MORRIS LIB on June 23, 2012 | http://pubs.acs.org
Publication Date (Web): November 18, 2010 | doi: 10.1021/bk-2010-1054.ch012

Chapter 12

Metalloporphyrin based Biomimetic Catalysts for Materials Synthesis and Biosensing

**Subhalakshmi Nagarajan,[3] Ferdinando F. Bruno,[4]
Lynne Samuelson,[4] Jayant Kumar,[2,3] and Ramaswamy Nagarajan[1,3,*]**

**[1]Department of Plastics Engineering, [2]Physics and Applied Physics, [3]Center for Advanced Materials, University of Massachusetts, Lowell, MA 01854
[4]U.S Army Natick Soldier Research, Development and Engineering Center, Natick, MA
*Ramaswamy_Nagarajan@uml.edu**

With the increase in popularity of enzyme catalysis, there has been a demand for the development of novel biomimetics that can emulate naturally occurring enzymes and serve as surrogate catalysts. Metal containing porphyins have been used as catalysts for mediating a number of chemical transformations. Metalloporphyrins play vital roles in catalyzing important biological transformations. Iron porphyrins in particular are attractive candidates for the synthesis of biomimics due to their biocompatibility, easy availability and the ability to tune their structure and hence catalytic activity through chemical and enzymatic modifications. This chapter discusses recent advances in the use of porphyrins as biomimetic catalysts for polymer syntheses, biosensing and in the removal of toxic waste.

Introduction

Driven by the discovery of new enzymes and efficient processes for the production of the enzymes, biocatalysis has emerged to be very promising in numerous applications. The steady increase in use of biocatalysts as viable alternative to conventional catalysts has spurred interest in development of versatile low-cost biomimetic alternatives.

In Biomaterials; Kulshrestha, A., et al.;
ACS Symposium Series; American Chemical Society: Washington, DC, 2010.

Downloaded by UNIV OF DELAWARE MORRIS LIB on June 23, 2012 | http://pubs.acs.org
Publication Date (Web): November 18, 2010 | doi: 10.1021/bk-2010-1054.ch012

Biocatalysis has played a vital role in the evolution of biological life. The origin of catalysis can be traced to the origin of life. Living systems are capable of carrying out chemical transformations efficiently using bioderived catalysts. The importance of enzymes were first elucidated by Lazzaro Spallanzani in 1783. Spallanzani showed that gastric digestion is not a purely physical action, but involved a factor called "pepsin". Several years later it was identified that pepsin was indeed secreted by the stomach glands in an inactive form called pepsinogen. Hydrochloric acid present in the gastric juice converted pepsinogen to active pepsin. The term enzyme was used for the first time in 1876 due to the pioneering work of German physiologist Wilhelm Friedrich Kühne. Kühne discovered the biological activity of trypsin and subsequently proposed the term "Enzym". It was not until 1893, when Wilhelm Ostwald defined the term "catalyst". Nobel laurearte Hermann Emil Fischer in 1890 proposed a "Lock and Key Model" to visualize the substrate and enzyme interaction. While the use of natural catalysts by humans to accomplish chemical transformations predates most recorded history, the systematic study of biocatalysis has only been started in the last century.

The number of enzymes known to mankind has significantly risen from around 700 in the 1960s to over 3000 in the 1990s. Enzymes can be broadly classified based on their catalytic activities into six categories. Enzyme Classification (EC) number is used to numerically categorize the enzymes by virtue of the chemical reaction they catalyze. The EC number for each of the enzymes is denoted in parentheses.

1. **Oxidoreductases (EC 1):** As the name suggests, these enzymes catalyze a variety of oxidation-reduction reactions including oxidations of alcohols, aldehydes and several dehydrogenation reactions. It has been reported that more than one-third of all documented enzymatic reactions are catalyzed by oxidoreductases (*1*).
2. **Transferases (EC 2):** catalyze the transfer of a functional moiety/group from one molecule to another. Transferases catalyze reactions involving transfer of nitrogenous groups, aldehydic/ketonic groups, phosphorous, sulfur and selenium containing groups
3. **Hydrolases (EC 3):** are involved in hydrolysis of a number of chemically important bonds/molecules.
4. **Lyases (EC 4):** catalyze elimination or addition reactions involving double bonds.
5. **Isomerases (EC 5):** are known to catalyze various isomerization reactions including racemization.
6. **Ligases (EC 6):** catalyze coupling reactions between biomolecules /macromolecules. This is usually accompanied by the hydrolysis of a chemical bond.

Hydrolases and oxidoreductases account for more than 70% of all research on enzyme catalysis clearly emphasizing the versatility of these enzymes (*2*). Oxidoreductases are further classified into 22 sub-classes. Among these

Downloaded by UNIV OF DELAWARE MORRIS LIB on June 23, 2012 | http://pubs.acs.org
Publication Date (Web): November 18, 2010 | doi: 10.1021/bk-2010-1054.ch012

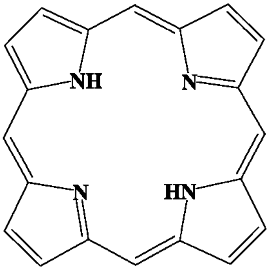

Figure 1. General Structure of a porphyrin ring

sub-classes, peroxidases (EC 1.11) are oxidoreductases produced by a number of microorganisms and plants.

However from an industrial application-standpoint, a slew of reservations have already been voiced regarding the viability of enzyme catalysis. The main concerns are related to the limitations in availability, stability, substrate specificity and the requirement of co-factors for efficient catalysis.

Recombinant DNA technology has allowed for more efficient production and targeted modification of enzymes. On the other hand, there has also been a dramatic increase in the design of biomimetic catalysts, which can mimic the action of naturally occurring enzymes. A literature search on “biomimetic catalysts” reveals a five fold increase in the number of publications over the last 20 years. This growing interest can be attributed to the rising need for development of biomimetics synthesized preferably using biocompatible methods. These biomimetic catalysts are often challenged to outperform chemical catalysts both at the laboratory and industrial scale and also work in biological applications.

Naturally occurring peroxidases catalyze a variety of reactions including polymerization in the presence of oxidants such as hydrogen peroxide. However, some of the peroxidases possess limited stability at lower pH conditions which are required for several oxidative polymerization reactions. In addition, high cost and low stability at higher temperatures impedes widespread use of these enzymes.

In this context, porphyrins are considered to be attractive starting materials for design of biomimetic catalysts. Porphyrins are organic pigments of both natural and synthetic origin and usually consist of four pyrrolic rings linked by four methine bridges to form a macrocycle (fig. 1). Porphyrins are known to bind and form complexes with a number of metals. In addition, metalloporphyrins (metal containing porphyrins) are one of the most widely studied class of compounds which play important roles in major biochemical, enzymatic, and photochemical processes. Hence, metalloporphyrins and their derivatives have been seen as attractive starting materials for the syntheses of a number of biomimetic catalysts.

In nature, metalloporphyrins such as cytochrome P-450 are able to efficiently catalyze reactions such as hydroxylation of hydrocarbons, in spite of the relative inertness of the C-H bond (*3*).

With the ultimate aim of mimicking cytochrome P450 and other compounds used by biological systems, several strategies have been adopted for the design and synthesis of biomimetic catalysts based on porphrins or metal containing porphyrins (metalloporphyrins). Broadly, these strategies have focused on augmenting the catalytic reactivity of porphyrins. They include the introduction of metal binding sites in the active site of a protein (*4–7*), chemical modification of prosthetic groups (*8–11*), and covalent attachment of chemical entities (metal co-factors) to overcome some of limitations in terms of stability or to increase the catalytic activity of these compounds (*12–14*). The following sections will summarize research on the use of metalloporphyrins as catalysts for polymerization of various classes of monomers.

Metalloporphyrins as Catalysts

Downloaded by UNIV OF DELAWARE MORRIS LIB on June 23, 2012 | http://pubs.acs.org
Publication Date (Web): November 18, 2010 | doi: 10.1021/bk-2010-1054.ch012

Metalloporphyrins have been explored as catalysts for polymerization of a wide variety of monomers such as alkyl methacrylates, lactones, epoxides, and olefins through different mechanisms. The reactivity of metal-centered radical species and organometallic derivatives has been gainfully utilized in the control of radical polymerization by catalytic chain transfer and living radical polymerization. Copper (II) tetraphenyl porphyrin and silver tetraphenyl porphyrin have also been found to catalyze the "living-like" radical polymerization of styrene (*15*). Various metal containing porphyrins (*16*) have also been investigated as catalytic chain transfer agents in free radical polymerizations. Aluminum porphyrins (*17*), zinc N-methylporphyrins (*18*), manganese (*19*) and titanium porphyrins (*20*) have been used as initiators for polymerization. Results indicate that aluminum porphyrins are the most efficient initiators for the polymerization of a wide range of monomers. The readers are directed towards several good review articles and papers for reactions involving the use of aluminum porphyrins as initiators (*20–22*).

Redox chemistry in nickel containing porphyrins have been the subject of interest after the discovery that nickel tetrapyrrole factor 430 (F430), was a key cofactor involved in the conversion of carbon dioxide to methane by methanogenic bacteria. Nickel (II) meso-5,10,15,20-tetraphenylporphyrin (Ni(II)TPP)/methylaluminoxane (MAO) has been used as a catalyst for the polymerization of styrene (*23*) acrylate monomers (*24*) and for the copolymerization of styrene and butadiene (*25*). Cobalt porphyrins are also effective in catalyzing the polymerization of vinyl monomers to form alternating copolyperoxides as depicted in fig. 2.

When a solution of a vinyl monomer containing a cobalt porphyrin, namely 5,10,15,20-tetraphenyl-21H, 23H-porphinecobalt(II) pyridine complex [CoTPP(Py)], is exposed to air at room temperature, an alternating copoly peroxide is obtained (*26*). CoTPP(Py) was found to catalyze the oxidation of styrene, α-methylstyrene, methyl methacrylate to their corresponding polyperoxides namely polystyrene peroxide, polymethylstyrene peroxide, and poly(methyl methacrylate) peroxide respectively. Interestingly, polymerization was found to be instantaneous in both air and O_2 without any induction period. In the presence of O_2, CoTPP(Py) complex is known to exist as a 1:1 oxygen adduct. The polymerization reaction is initiated by the addition reaction of the adduct to the alkene producing free radicals. Cobalt porphyrins have also been used as a catalyst for polymerization of indene (*27*) and methyl methacrylate

Downloaded by UNIV OF DELAWARE MORRIS LIB on June 23, 2012 | http://pubs.acs.org
Publication Date (Web): November 18, 2010 | doi: 10.1021/bk-2010-1054.ch012

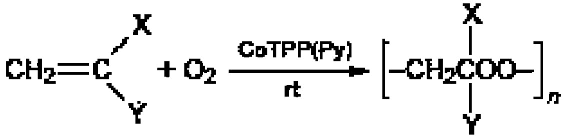

Figure 2. Biomimetic polymerization of vinyl monomers catalyzed by cobalt porphyrin.

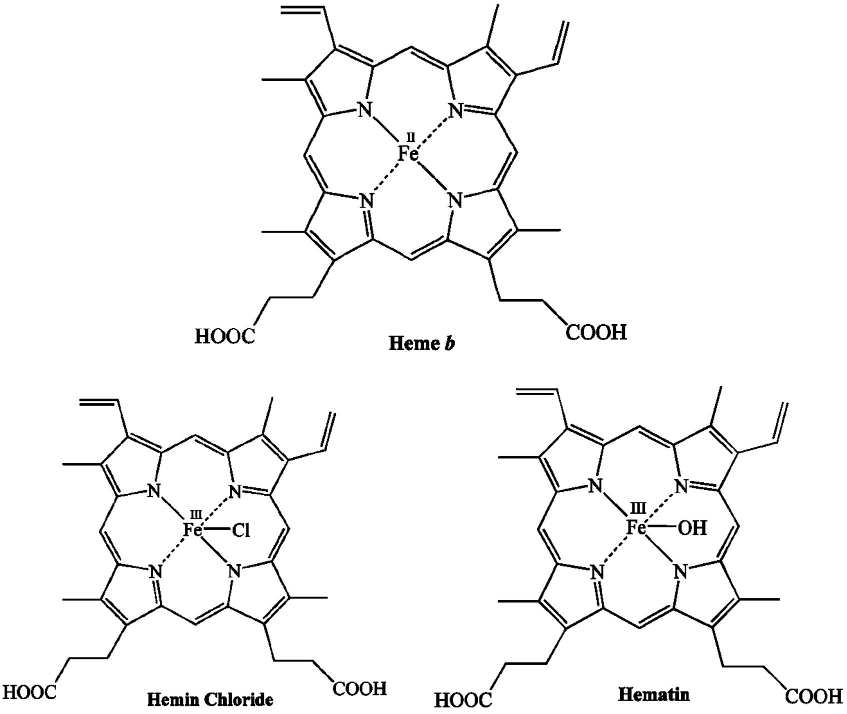

Figure 3. Structures of heme, hematin and hemin chloride.

(MMA) (*28*).This review will focus on the recent developments in iron containing porphyrins and their derivatives used as biomimetic catalysts particularly in oxidative polymerization

Among metal containing porphyrins, iron containing porphyrins have elicited tremendous amount of research interest owing to their unique biological functions. These include the transport of electrons (e.g., cytochrome b5), the transport of oxygen (e.g., hemoglobin), and the catalysis of redox reactions (e.g., cytochrome P450). Despite the differences in the chemistry, all of these proteins have iron protoporphyrin IX (heme) as their prosthetic group. The structure of heme *b* is shown in fig. 3.

Oxidation of the iron to the ferric state yields hemin or ferric protoporphyrin. Anionic groups tend to co-ordinate with the axial positions leading to a square pyramidal geometry. When the anion bound is hydroxide, the resulting compound is referred to as hematin and hemin chloride, when a chloride ion is bound to the Iron.

Heme proteins are without doubt one of the most important class of versatile biological macromolecules possessing a range of catalytic and molecular recognition abilities.

Peroxidases versus Hematin as Catalysts for Polymerization

The dramatic increase in the use of polymeric materials in commercial and industrial applications is in large part due to discoveries of new classes of polymers (e.g. conducting polymers) (*29–32*), new syntheses routes for polymer design (e.g. living polymerization), and efficient catalysts of polymerization reactions (e.g. Ziegler−Natta catalysts) (*33*).

With a forseable increase in environmental regulation, the widespread use of polymers has also necessitated the development of more environmentally conscious pathways (use of both benign catalysts and routes) to synthesize these polymers. For example, phenol-formaldehyde resins are widely used owing to their excellent chemical and thermal stability. However, concerns about the continued use of phenol-formaldehyde resins due to the high toxicity of formaldehyde, has triggered investigations into alternative routes for their synthesis (*34*). There is clearly an imminent need for the development of other milder, environmentally safe synthetic routes and alternative catalysts which can mediate these reactions under relatively benign conditions.

Naturally occurring plant peroxidases have been successfully used as catalysts for the syntheses of a wide range of conducting polymers such as polyaniline (*35*), Poly(ethylene dioxythiophene) (PEDOT) (*36*, *37*) and polyphenols (*38*). While peroxidases can catalyze the polymerization of these compounds, more research is needed to reduce the cost of utilizing them for industrial processes.

It is well known that the peroxidases which catalyze oxidative polymerization reactions contain heme as the active catalytic site (*39*). Iron containing porphyrins are attractive since they contain the heme group but lack the protein environment normally present in peroxidases, thus making them more suitable for use as catalysts at extreme pH conditions. Iron porphyrins such as hemin chloride and hematin are being explored as alternative catalysts for the polymerization of a wide range of monomers.

Hemin chloride has been shown to catalyze the polymerization of phenols (*40*, *41*). However the poor catalytic activity has led to several efforts to augment the catalytic activity including encapsulation of hemin chloride in a beta-cyclodextrin matrix (*42*) or by simply mixing hemin chloride with a hydrogel formed by the self assembly of two amino acids (*43*). The latter approach was found to increase the catalytic activity of hemin in both aqueous and organic solvents.

Wang *et al* (*44*) have tethered hemin to a N-isopropylacrylamide (NIPAAm) hydrogel. The hydrogel was not active at lower pH conditions and optimal catalytic activity was observed at pH 9-10.

Downloaded by UNIV OF DELAWARE MORRIS LIB on June 23, 2012 | http://pubs.acs.org
Publication Date (Web): November 18, 2010 | doi: 10.1021/bk-2010-1054.ch012

Downloaded by UNIV OF DELAWARE MORRIS LIB on June 23, 2012 | http://pubs.acs.org
Publication Date (Web): November 18, 2010 | doi: 10.1021/bk-2010-1054.ch012

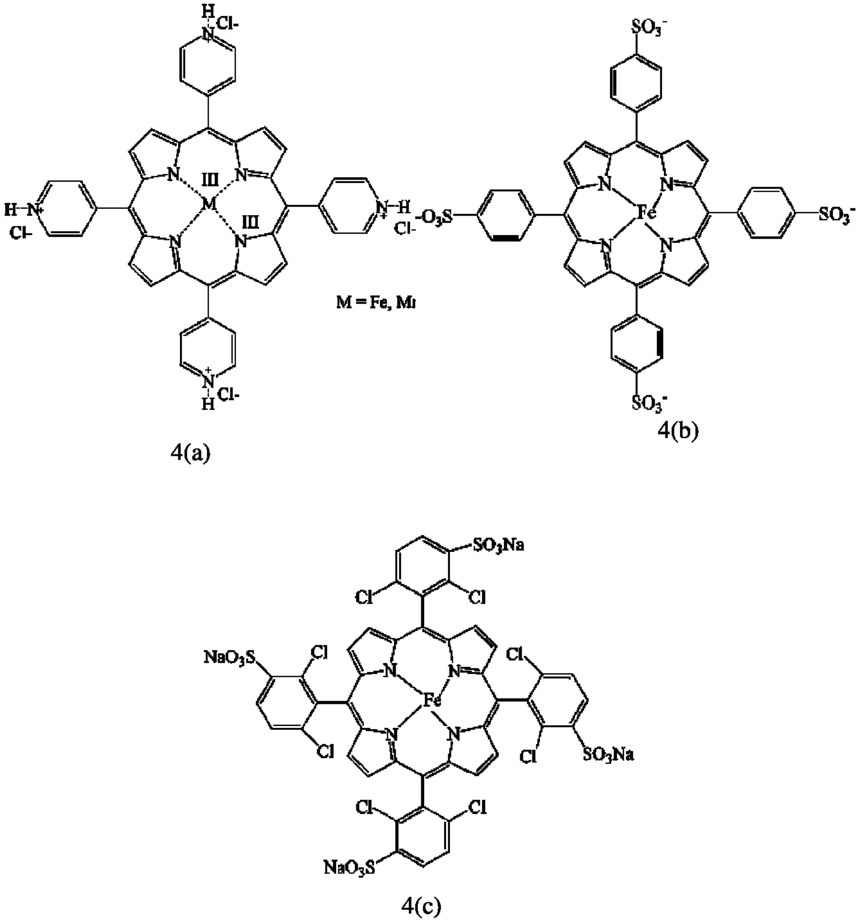
M = Fe, Mn
Cl-
N-H
III
M
Fe
SO3-
SO3Na
NaO3S
Cl

4(a)

4(b)

4(c)

Figure 4. Structure of some synthetic analogues of porphyrin.

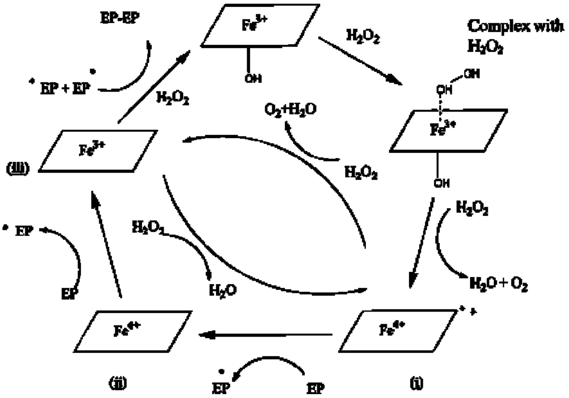
Fe3+
H2O2
Complex with H2O2
OH
Fe3+
O2+H2O
H2O2
H2O2
H2O+O2
Fe4+
(i)
Fe4+
(ii)
EP
•EP
Fe3+
(iii)
EP-EP
•EP + EP•
H2O2
H2O
•EP
EP

Figure 5. Proposed mechanism for the hematin catalyzed polymerization of phenols.

Downloaded by UNIV OF DELAWARE MORRIS LIB on June 23, 2012 | http://pubs.acs.org
Publication Date (Web): November 18, 2010 | doi: 10.1021/bk-2010-1054.ch012

Synthetic analogues of iron containing porphyrins have also been prepared in an effort to mimic hemeproteins. Iron (III) tetrapyridylporphyrin, manganese (III) tetrapyridylporphyrin and cobalt (III) tetrapyridylporphyrin (4a, fig. 4) and Iron (III) tetra (p-sulfonated phenyl) porphyrin [(Fe(III)TPPS] (4b, fig. 4) have been found to oxidatively catalyze the polymerization of aniline (*45*) and iron(III)5,10,15,20-tetrakis-(2′,6′-dichloro-3′-sulfonatophenyl)porphyrin (4c, fig. 4) was used as a catalyst for the polymerization of acrylamide (*46*).

The preparation of these synthetic analogues often involves use of multi-step syntheses and/or complex purification procedures.

For biological compatibility, it would be beneficial if these biomimetic catalysts are synthesized using benign routes. Hemoglobin (Hb) is the major heme protein of red blood cells and is known to act as a biomimetic peroxidase. Hb was shown to catalyze the oxidative polymerization of aniline using sulphonated polystyrene (SPS), ligninsulfonate (LGS) (*47*) and sodium dodecyl sulphate (*48*) as templates. Polyaniline with conductivities ranging from $2x10^{-3}$ -$11x10^{-3}$ S/cm^{-1} were observed (*49*). However Hemoglobin contains proteins associated with the hematin active site. The possibility of hematin directly as a catalyst for polymerization has also been explored.

Akkara *et al* (*50*) have reported on the use of hematin as a catalyst for the polymerization of ethylphenol. A mechanism for the hematin catalyzed polymerization has been proposed (fig. 5) with the intermediate states involved believed to be similar to the intermediate states observed in the mechanism of horseradish peroxidase (HRP)-catalyzed polymerization. Hematin was also used as a catalyst for the polymerization of styrene and methyl methacrylate (MMA) (*51*) (fig. 6). The polymerization reactions involved the use of 2, 4-pentanedione and were carried out in DMF or in a sodium carbonate buffer.

The insolubility of hematin at lower pH conditions however prevents widespread use of this catalyst at low pH conditions which are required for many oxidative polymerization reactions. Roy *et al* (*52*) developed a water-soluble catalyst by the esterification reaction between poly(ethylene glycol) (PEG) and hematin. The esterification reaction was carried out in DMF in the presence of N,N′-carbonyldiimidazole and 1,8 diazabicyclo[5.4.0] undec-7-ene (DBU). This novel biomimetic catalyst was effective in catalyzing the polymerization of a number of monomers. Please refer to the section on the "applications of porphyrins and related biomimics" for a detailed description of the polymers synthesized using this biomimetic catalyst.

This PEG-Hematin has been used to synthesize polyphenols (*53*) under aqueous conditions using various templates (*54*). PEG-hematin was also used as a catalyst for the polymerization of sodium styrene sulphonate (*55*) (fig. 7).

Use of PEG-hematin led to the formation of a high molecular weight polymer (M_n~ 223,520) in comparison to polystyrene sulphonate obtained with HRP catalysis (M_n~136,431). While this catalyst was effective, the purification of the reaction mixture is complex. The reaction is carried out in DMF in which both hematin and the final ester, PEG-Hematin are soluble. Further, since the esterification reaction is performed at room temperature, hematin can exist in a substantially aggregated form.

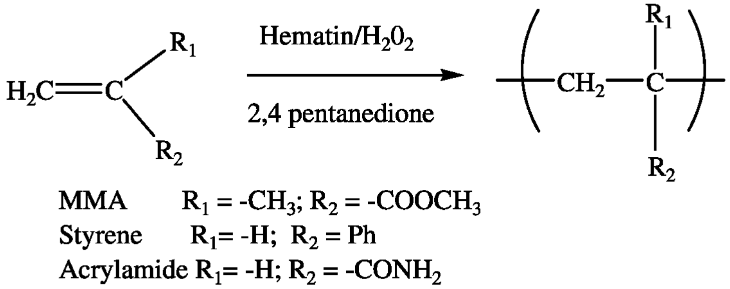

MMA R_1 = $-CH_3$; R_2 = $-COOCH_3$
Styrene R_1= -H; R_2 = Ph
Acrylamide R_1= -H; R_2 = $-CONH_2$

Figure 6. Polymerization of vinyl monomers using hematin as a catalyst in presence of 2,4-pentanedione and/or H_2O_2.

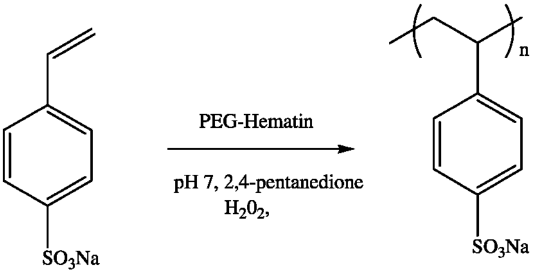

Figure 7. Polymerization of sodium styrene sulfonate catalyzed by PEG-Hematin.

Nagarajan *et al* (*56*) have developed a more facile route to the synthesis of the PEG-hematin involving the use of lipases to accomplish the esterification reaction between hematin and PEG. Novozyme -435 is a lipase known to catalyze esterification, amidation and transesterification reactions under solventless conditions (*57*).

The reaction was carried out by simply mixing both PEG and hematin. The mono functionalized PEG used offers better control over functionalization. The reaction work–up was simple and involves pouring the reaction mixture into slightly acidic water. Hematin is insoluble in water at slightly acidic conditions, precipitates out of solution and is filtered off and unreacted PEG is removed by dialysis. However, one of the disadvantages of the pegylated hematin was that it was prone to hydrolysis especially at a low pH.

In order to overcome this limitation, Nagarajan *et al* (*58*) have modified hematin with methoxypolyethylene glycol amine ($MPEGNH_2$). Amidation is a one-step lipase catalyzed reaction (fig. 8). As shown in fig. 9, even at pH 1 the amidated hematin was stable and water-soluble. The catalytic activity of iron porphyrins (*43*) and peroxidases have been evaluated using the peroxidase assay developed by Willstaeter (*59*, *60*). This assay measures the rate of formation of purpurogallin from pyrogallol when catalyzed by peroxidases (fig. 10).

In order to verify that the catalytic center in the amidated hematin was intact, the activity of the amidated hematin in catalyzing the oxidative transformation of pyrogallol to purpurogallin was monitored and compared with native hematin.

Downloaded by UNIV OF DELAWARE MORRIS LIB on June 23, 2012 | http://pubs.acs.org
Publication Date (Web): November 18, 2010 | doi: 10.1021/bk-2010-1054.ch012

Downloaded by UNIV OF DELAWARE MORRIS LIB on June 23, 2012 | http://pubs.acs.org
Publication Date (Web): November 18, 2010 | doi: 10.1021/bk-2010-1054.ch012

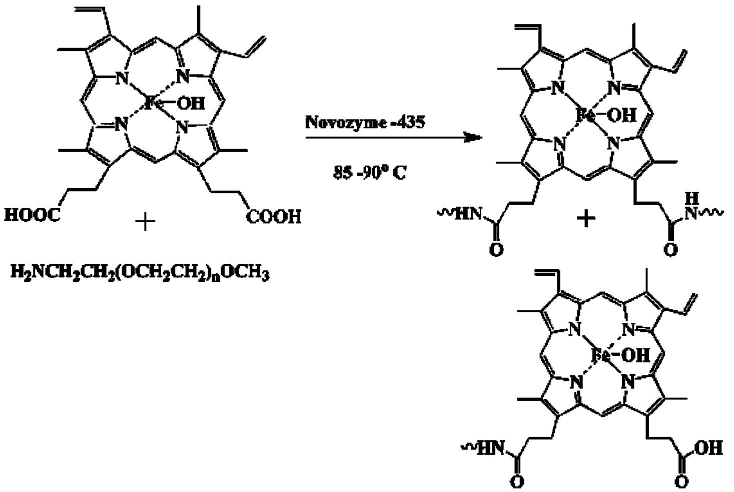
Fe-OH
HOOC
COOH
+
$H_2NCH_2CH_2(OCH_2CH_2)_nOCH_3$
Novozyme-435
85-90° C
HN
H N
O
OH

Figure 8. Scheme for the amidation of hematin with MPEGNH$_2$

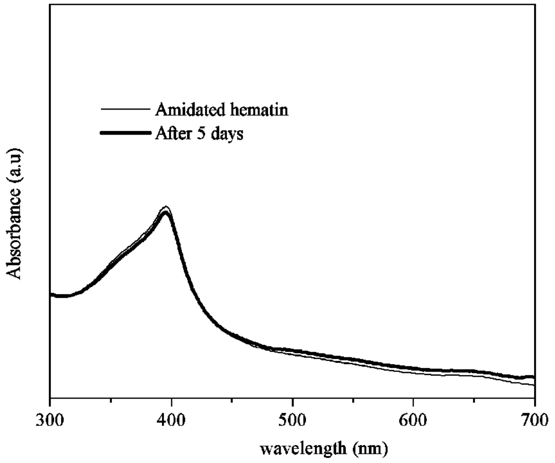

Figure 9. Stability of amidated hematin at pH 1.

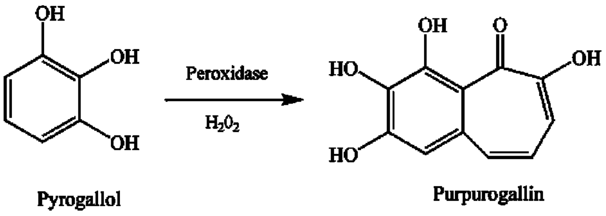
OH
OH
OH
Peroxidase
H_2O_2
Pyrogallol
HO
HO
OH
O
OH
Purpurogallin

Figure 10. Scheme for the oxidative transformation of pyrogallol to purpurogallin.

The formation of purpurogallin was monitored at 420nm using UV-Visible Spectroscopy. As seen in fig. 11, the amide functionalized hematin was active and could catalyze the transformation of pyrogallol to purpurogallin. In contrast, hematin by itself could not catalyze the formation of purpurogallin under identical conditions due to its poor solubility at this pH. It is evident that the iron porphyrins can serve as versatile catalysts. The next section will review some of the applications of polymers synthesized using these biomimetic catalysts.

Applications of Porphyrin and Related Biomimic Catalysts

Syntheses of Electrically Conducting Polymers Using Porphyrin Catalysis for Biosensing Applications

Inherently conducting polymers exhibit tremendous potential in the area of modification, manipulation and sensing of biological molecules/processes owing to their unique combination of properties including redox tenability.

The structures of commonly used conducting polymers are shown in fig. 12. Conducting polymers have been used in several biological applications including glucose and cholesterol sensors, amino acid discrimination, modulation of enzyme activity, detection of specific sequence(s) of DNA and in numerous other areas (*61–65*)

In sensing of DNA hybridization, obtaining an electrical/spectral signal during or after the process of hybridization is often the most crucial issue. Electrochemical transduction involving electroactive materials have shown considerable promise in the development of faster, less tedious and more portable detection systems. Among the conducting polymers, PEDOT and polypyrrole have shown promise for biosensing (*66*) including DNA sensors (*67*). However for use in biological applications, it is imperative that these conducting polymers are synthesized in relatively benign conditions using catalysts compatible with biological systems.

Among the biomimic catalysts, the pegylated hematin described in earlier sections was found to be efficient in catalyzing the polymerization of aniline in the presence of SPS (*52*) or lignin sulphonate (LGS) to form a thermally stable and electrically conductive poly(aniline) [PANI]/SPS or PANI/LGS complexes (*68*).

Figure 13 shows the UV –Visible spectra for the formation of PANI over time when catalyzed by PEG-Hematin. The PEG-Hematin was also able to catalyze the polymerization of phenol and the synthesis of conducting copolymers of EDOT and pyrrole (PPYR) in presence of SPS (*69*).

As shown in fig. 14, while the monomers have no significant absorption beyond 350nm, a broad peak is seen after the addition of PEG-hematin and hydrogen peroxide. This was the first report on use of a biomimetic iron containing porphyrin for the synthesis of copolymers of EDOT and pyrrole. More detailed investigations on using biological polyelectrolytes such as DNA for the syntheses of these conducting polymers is being evaluated in our laboratories.

Downloaded by UNIV OF DELAWARE MORRIS LIB on June 23, 2012 | http://pubs.acs.org
Publication Date (Web): November 18, 2010 | doi: 10.1021/bk-2010-1054.ch012

Downloaded by UNIV OF DELAWARE MORRIS LIB on June 23, 2012 | http://pubs.acs.org
Publication Date (Web): November 18, 2010 | doi: 10.1021/bk-2010-1054.ch012

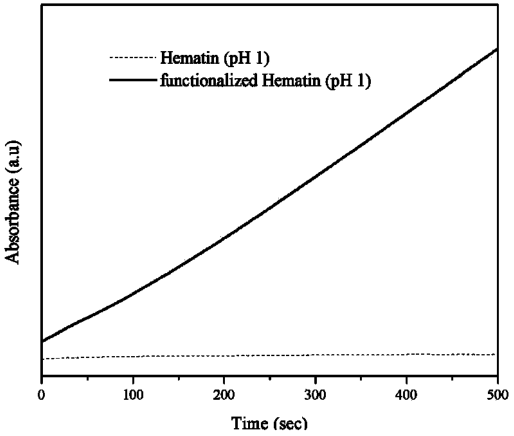

Figure 11. Efficiency of amidated hematin and hematin in catalyzing the oxidative transformation of pyrogallol to purpurogallin.

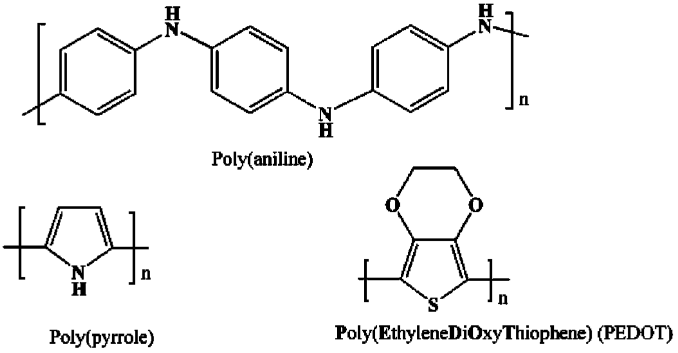

Figure 12. Chemical structures of some of the common conducting polymers.

Use of Porphyrin Derivatives in Removal of Toxic Wastes

Chemical contamination of soil and water is a widespread problem faced by many countries worldwide. Current methods are based on either physical separations, chemical and biological treatment. Physical treatment methods often involve separation of waste material according to the physical properties such as size or hydrophobicity. Biological methods take advantage of the catabolic and anabolic processes in microbial organisms and utilize them to either degrade waste or convert waste into innoculous matter. Storage and handling of some of these microorganisms may be an issue of concern. Chemical treatment methods are still probably the most widely used route for removing harmful waste. Use of enzymatic methods however has several advantages over both chemical and biological routes.

Downloaded by UNIV OF DELAWARE MORRIS LIB on June 23, 2012 | http://pubs.acs.org
Publication Date (Web): November 18, 2010 | doi: 10.1021/bk-2010-1054.ch012

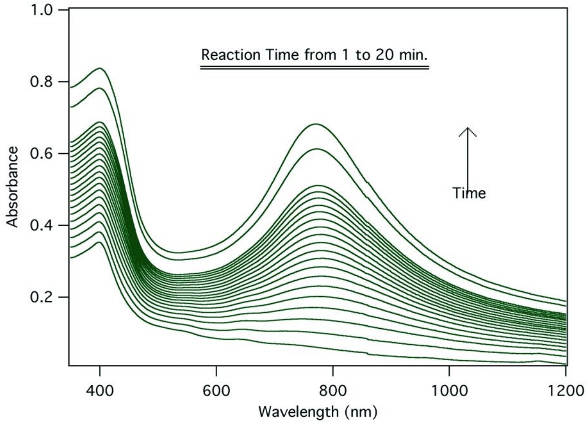

Figure 13. UV-Visible spectra depicting the formation of polyaniline by PEG-Hematin catalysis.

Enzyme catalyzed reactions can be carried out under relatively mild conditions (moderate temperatures and atmospheric pressure). In contrast, chemical treatment methods often require harsher conditions. The rate of enzyme catalyzed reactions are several orders of magnitude higher than traditional chemical reactions. This can certainly help in speeding up waste removal. Finally, the high specificity of enzymes can minimize formation of other undesirable byproducts.

Phenols and their derivatives are one of the major organic pollutants from a variety of industrial processes (*70*). Alkylphenols are used extensively in petroleum refining, resins, plastics, dyes, and pulp (*71*). Since most phenols are toxic, they need to be removed from effluents before disposal. Current methods include solvent extraction, microbial degradation, adsorption on activated carbon and chemical oxidation (*72*, *73*).

The use of enzyme based methodologies for the removal of organic compounds from aqueous solutions was first explored by Klibanov *et al* (*74*, *75*). The authors reported the use of HRP to remove more than 25 aromatic amines and phenols. However, it was found that the costs of removing wastes from 1 m^3 of foundry waste water containing around 3.5mmol dm^{-3} of phenols was around US $ 50 taking into the account of costs of pure HRP and hydrogen peroxide (*76*). Wilberg *et al* (*76*) have given a detailed summary of the costs associated with purification processes using HRP as an enzyme. It appears that the purity of the enzyme seems to play a vital role in the cost of the treatment.The high cost associated with the enzymatic process compared to commercial Fenton processes behooves research focused on more economical and efficient catalysts.

Some of the naturally occuring iron porphyrins are relatively abundant and have been shown to catalyze oxidative oligomerization of phenols and in some cases, aromatic amines. Hence it is plausible that these can potentially serve as economical surrogates to naturally occuring peroxidases. A water soluble, iron(III) meso-tetra-(2,6-dichloro-3-sulfonatophenyl)-porphyrinate [Fe-(TDCPPS)Cl] was synthesized (*77*) and was found to be effective in catalyzing the transformation of phenol containing monomers such as catechol (*78*), caffeic acid and p-coumaric acid (*79*). These biomimetic catalysts were found to help in toxicity reduction of olive mill waste water by oxidative coupling of toxic, small-molecule phenol containing impurities resulting in the formation of macromolecules, which can be easily separated (*80*). Since the optimal activity of hematin and other iron containing porphyrins is observed around pH 11, they have the potential to serve as catalysts for reducing toxins in industrial waste.

Porphyrin Derivatives for Biosensing Applications

Scientific literature is abound with the use of porphyrins as sensing elements for the fabrication of a variety of sensors (*81–84*). This section will discuss developments in the use of porphyrins and related compounds for sensing compounds of biological significance. While heme proteins have been known to play critical roles in transport of oxygen in living systems, research in the last decade has also shown that these proteins also serve as efficient biosensors in a number of biological organisms (*85*). For example, heme based *FixL* proteins in *rhizobia* are known to sense oxygen efficiently (*86–88*). The mechanism of sensing is believed to be initiated by the binding of the analyte to the heme, which then induces an conformational change in the protein that ultimately regulates binding to DNA or alters enzymatic activity. Additionally, heme proteins have been shown to sense carbon monoxide (CO) (*89*) and Nitric Oxide (NO) (*90*).

Nitric Oxide Sensors

NO is a important biological molecule known to play important roles in several biological processes (*91*) including immune responses (*92*). Deficiency of NO has been related to a number of disorders including cardiovascular disease. Various methods such as electron paramagnetic resonance, chemiluminescence, UV-visible spectroscopy have been used for the detection of NO. The low half life of NO under-*in-vivo* conditions and the ability of NO to rapidly react with O_2 to form NO^{2-} and NO^{3-} present significant challenge in the design of a biocompatible NO sensor. A crucial aspect for the design of a monomeric/polymeric porphyrin based electrochemical sensor is the current generated by NO oxidation must be several orders of magnitude higher than current which is produced by other species present *in-vivo*.

The intrinsic ability of the porphyrins to bind specifically to NO has been used to fabricate porphyrin based NO sensors. For example, it is well-known that *Cytochrome-c* has the unique ability to bind NO but is unable to form such stable complexes with O_2. Hence metalloporphyrins have been modified and evaluated for their ability to specifically and selectively detect NO. Malinksi *et al* (*93*) reported the use of electropolymerized nickel porphyrin film electrode for in situ amperometric detection of nitric oxide in biological systems. A polymeric porphyrinic film based on tetrakis(3-methoxy-4-hydroxyphenyl)porphyrin was used for the fabrication of NO sensor. The authors coated carbon fibers with thin polymeric nickel porphyrin layers and used Nafion to minimize detection

Downloaded by UNIV OF DELAWARE MORRIS LIB on June 23, 2012 | http://pubs.acs.org
Publication Date (Web): November 18, 2010 | doi: 10.1021/bk-2010-1054.ch012

Downloaded by UNIV OF DELAWARE MORRIS LIB on June 23, 2012 | http://pubs.acs.org
Publication Date (Web): November 18, 2010 | doi: 10.1021/bk-2010-1054.ch012

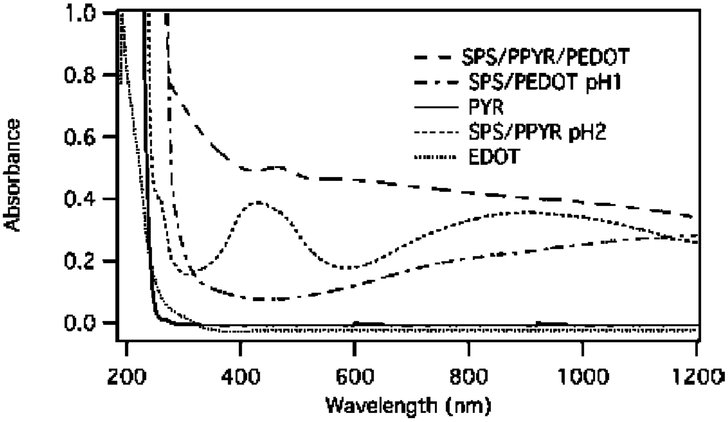

Figure 14. UV-spectra for the pyrrole EDOT copolymers obtained using PEG-Hematin as a catalyst.

of nitrite and thereby improve the sensitivity of the sensor. The sensor, which could be operated both in the amperometric or voltametric mode was reported to exhibit a linear response upto 300μM concentration of NO and a detection limit of 10nM. Since then, there have been several reports on the use of this metalloporphyrin biosensor for determination of NO. The reader is directed to a review article (*94*) and papers in this area (*95–99*). Porphyrin based sensors have been successfully used for the detection of NO in tissue, lung and heart (*100*). Although porphyrin based electrodes coated on to carbon fibers have been demonstrated to be effective, some studies have also shown that carbon fibers tethered with porphyrins (without a coordinated metal) can also be used to detect NO with significant sensitivity, and in some cases, the carbon fiber in a stand-alone mode could detect NO (*101*, *102*).

Several other metalloporphyrins such as manganese porphyrin, cobalt porphyrin (*103*) were hence employed as catalysts for construction of NO sensors. Manganese(II)-meso-tetracarboxyphenyl porphyrin (fig. 15a) was attached to a pyrrole unit and this complex was found to detect NO at concentrations upto 1x10^{-7}M (*104*). Nickel (II) porphyrins (fig. 15b) have been found to be efficient for detecting NO at concentrations from 5 to 30μM (*105*). Biomimetic sensors based on iron porphyrin in combination with Gallium Arsenide have been fabricated for the detection of NO (*106*). Carbon microelectrodes functionalized with Fe, Mn and Co protoporphyrins have been shown to be efficient electrochemical sensors in detecting NO (*107*).

In general, it was found that in, that the sensitivity of detection greatly relied on the quality of the final polymeric film, the purity of the monomeric porphyrin and the potential range of polymerization. The sensitivity and selectivity of the porphyrinic NO sensors varied significantly from electrode to electrode and depended not only on the potential at which NO oxidizes, but also ligation to the central metal in the porphyrin.

Downloaded by UNIV OF DELAWARE MORRIS LIB on June 23, 2012 | http://pubs.acs.org
Publication Date (Web): November 18, 2010 | doi: 10.1021/bk-2010-1054.ch012

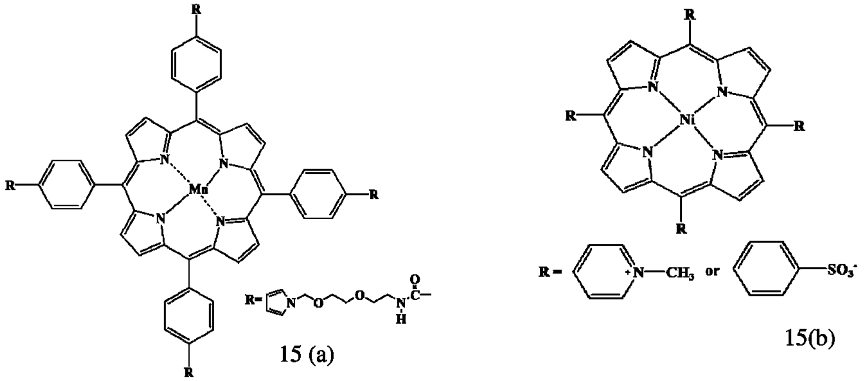

15 (a)

15(b)

Figure 15. Structures of synthetic porphyrins used for detecting NO.

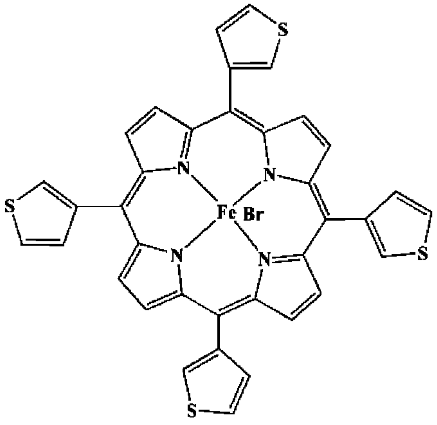

Figure 16. Structure of synthetic porphyrin used as a sensing element in electrochemical sensor for detection of superoxide anion radical.

Porphyrins in DNA Conformational Studies

DNA is a biological macromolecule known to adopt many conformations (Z-DNA, cruciform DNA) besides the classical B-form proposed by Watson and Crick. It is well-known that specific sequences of DNA can form "non-B-DNA" structures, such as left-handed Z-DNA, cruciform DNA, hairpins, and triplex and quadruplex DNA. The biological relevance of Z-DNA has been recently demonstrated by the discovery of proteins that bind specifically to Z-DNA (*108–111*).

The handedness of the different forms of the DNA can be distinguished using Circular dichroism (CD). B-DNA is characterized by a complex positive band centered at 274 nm and a negative Cotton effect at 253 nm, while Z-DNA exhibits a negative Cotton effect at 293 nm and a positive Cotton effect at 263 nm. Determination and sensing of Z-DNA based on these spectral differences, however, is hampered by other proteins which make the region below 300 nm in the CD spectra difficult to analyze.

Porphyrins have been used for recognizing the "handness" of a DNA helix (*112*). The non-covalent interactions of cationic or anionic water-soluble achiral porphyrins with chiral templates have been exploited to determine the handedness of biological matrices like DNA.

Cationic zinc (II) porphyrin has been shown to detect the higher energy conformation of DNA, i.e. Z-DNA (*113*). Nickel porphyrins have been shown to be efficient in selectively sensing Z-DNA and not B-DNA (*114*). By synthetically modifying porphyrins, they can serve as a valuable tool for studying oligonucleotide conformations.

Downloaded by UNIV OF DELAWARE MORRIS LIB on June 23, 2012 | http://pubs.acs.org
Publication Date (Web): November 18, 2010 | doi: 10.1021/bk-2010-1054.ch012

Electrochemical Sensing of Superoxide Anion Radical Using Porphyrin

Reactive oxygen species (ROS) such as the superoxide anion is required for normal cell growth. However, excess generation of ROS has been linked to several diseases including cancer (*115*). Hence, quantitative determination of ROS levels *in-vivo* is an area of increasing interest. Cytochrome-c (*cyt-c*) based sensors have been used for sensing ROS (*116*). Stability and handling issues associated with *cyt-c* have led to research on other efficient molecules. Hemin modified with pyrolytic graphite has been found to exhibit higher sensitivity to ROS when compared to cyt-c based sensors (*117*).

Synthetic polymeric iron porphyrin complexes have been used successfully in the design of electrochemical sensors for the detection of the superoxide anion radical (O^{2-}.). Yuasa *et al* (*118*) have used bromoiron (III) mesotetra(3-thienyl)porphyrin (fig. 16) as the sensing element which is formed by electropolymerization to give the corresponding sensing polymer. From these examples it is obvious that the utility of porphyrins extends beyond catalysis to chemical and biosensing applications. Development of other porphyrin derivatives (naturally derived or chemically synthesized) is obviously beneficial for a wide variety of applications.

Conclusion

As the demand for efficient and environmentally benign biobased catalysts increases, there is an obvious need for the design of effective, inexpensive biomimetic alternatives useful in a broad range of applications. This review chapter provides an overview of porphyrins as a peroxidase mimic and their use as an attractive bio-based starting material for catalyzing oxidative polymerization reactions, chemical and bionsensing and a slew of other applications. While there has been considerable amount of effort devoted to developing new biomimetic catalysts, a more indepth understanding of structure- property relationships can help in improving both the modification of naturally occurring porphyrins and the design of new and more efficient biomimetics. Further studies on the electrochemical behavior of the synthetic porphyrins and their analogues will aid in designing the next generation of "green" biomimetic catalysts.

Acknowledgments

Funding from the US Army Natick Research Development and Engineering Center is acknowledged. We thank Mr. Sethumadhavan Ravichandran for help with the manuscript.

References

1. Mu, F.; Pat, J.; Unkefer, P. J.; Unkefer, C. J.; Hlavacek, W. S. *Bioinformatics* **2006**, *22*, 3082–3088.
2. Anderson, E. M.; et al. *Biocatal. Biotransform.* **1998**, *16*, 181−204. Faber, K. *Biotransformations in organic chemistry*; 5th ed.; Springer:2004, p 22.
3. Ortiz de Montellano, P. R., Ed. *Cytochrome P450 Structure, Mechanism, and Biochemistry*, 3rd ed.; Kluwer: New York, 2005.
4. Qi, D.; Tann, C. M.; Haring, D.; Distefano, M. D. *Chem. Rev.* **2001**, *101*, 3081–3112.
5. van de Velde, F.; van Rantwijk, F.; Sheldon, R. A. *Trends Biotechnol.* **2001**, *19*, 73.
6. Sigman, J. A.; Kwok, B. C.; Lu, Y. *J. Am. Chem. Soc.* **2000**, *122*, 8192–8196.
7. Braha, O.; Walker, B.; Cheley, S.; Kasianowicz, J. J.; Song, L.; Gouaux, J. E.; Bayley, H. *Chem. Biol.* **1997**, *4*, 497–505.
8. Ozaki, S.; Ortiz de Montellano, P. R. *J. Am. Chem. Soc.* **1995**, *117*, 7056–7064.
9. Neya, S.; Funasaki, N.; Imai, K. *J. Biol. Chem.* **1988**, *263*, 8810–8815.
10. Hu, Y. Z.; Tsukiji, S.; Shinkai, S.; Oishi, S.; Hamachi, I. *J. Am. Chem. Soc.* **2000**, *122*, 241.
11. Hayashi, T.; Hitomi, Y.; Ando, T.; Mizutani, T.; Hisaeda, Y.; Kitagawa, S.; Ogoshi, H. *J. Am. Chem. Soc.* **1999**, *121*, 7747–7750.
12. Ma, S. K.; Lu, Y. *J. Inorg. Biochem.* **1999**, *74*, 217–243.
13. Ermacora, M. R.; Delfino, J. M.; Cuenoud, B.; Schepartz, A. *Proc. Natl. Acad. Sci.* **1992**, *89*, 6383–6387.
14. Sigman, D. S.; Bruice, T. W.; Mazumder, A.; Sutton, C. L. *Acc. Chem. Res.* **1993**, *26*, 98–104.
15. Asandei, A. D.; Moran, I. W.; Bruckner, C. *Polym. Prepr.* **2003**, *44*, 82–83.
16. (a) Gridnev, A. A.; Ittel, S. D. *Chem. Rev.* **2001**, *101*, 3611. (b) Gridnev, A. *J. Polym. Sci., Part A: Polym. Chem.* **2000**, *38*, 1753. (c) Gridnev, A.; Ittel, S. *Chem. Rev.* **2001**, *101*, 3611−3659. (d) Heuts, J. P. A.; Forster, D. J.; Davis, T. P.; Yamada, B.; Yamazoe, H.; Azukizawa, M. *Macromolecules* **1999**, *32*, 2511.
17. Inoue, S. *J. Polym. Sci., Part A: Polym. Chem.* **2000**, *38*, 2861–2871.
18. Aida, T.; Inoue, S. *J. Am. Chem. Soc.* **1983**, *105*, 1304–1309.
19. Takeda, N.; Inoue, S. *Makromol. Chem.* **1978**, *179*, 1377–1381.
20. Aida, T.; Inoue, S. *Acc. Chem. Res.* **1996**, *29*, 39–48.
21. Yasuda, T.; Aida, T.; Inoue, S. *Makromol. Chem., Rapid Commun.* **1982**, *3*, 585–588.
22. Yasuda, T.; Aida, T.; Inoue, S. *Macromolecules* **1983**, *16*, 1792–1796.

Downloaded by UNIV OF DELAWARE MORRIS LIB on June 23, 2012 | http://pubs.acs.org
Publication Date (Web): November 18, 2010 | doi: 10.1021/bk-2010-1054.ch012

23. Li, J.; Li, M.; Li, S.; Shi, L.; Ren, C.; Cui, D.; Wang, Y.; Tang, T . *Polym. Sci., Part B: Polym. Phys.* **2008**, *46*, 1240–1248.
24. Wayland, B. B.; Basickes, L.; Mukerjee, S.; Wei, M.; Fryd, M. *Macromolecules* **1997**, *30*, 8109–8112.
25. Endo, K.; Matsuda, Y. *Polym. Int.* **2001**, *50*, 59–62.
26. Jayaseharan, J.; Kishore, K. *J. Am. Chem. Soc.* **1998**, *120*, 825–826.
27. Nanda, A. K.; Kishore, K. *Macromolecules* **2001**, *34*, 1600–1605.
28. Nanda, A. K.; Kishore, K. *Polymer* **2001**, *42*, 2365–2372.
29. Heeger, A. J.; Schrieffer, J. R.; Su, W.-P. *Rev. Mod. Phys.* **1988**, *60*, 781–850.
30. Nalwa, H. S. In *Handbook of Organic Conductive Molecules and Polymers*; John Wiley & Sons Ltd.: Chichester, 1997; Vol. 1−4.
31. Skotheim, T. A.; Elsenbaumer, R. L.; Reynolds, J. R. In *Handbook of Conducting Polymers*; Marcel Dekker: New York, 1998; Vol. 1−2.
32. Burroughes, J. H.; Bradley, D. D. C.; Brown, A. R.; Marks, R. N.; MacKay, K.; Friend, R. H.; Burns, P. L.; Holmes, A. B. *Nature* **1990**, *347*, 539–541.
33. Ziegler, K.; Holzkamp, E.; Breil, H.; Martin, H. *Angew. Chem., Int. Ed. Engl.* **1955**, *67*, 541−547. Natta, G.; Pino, P.; Corradini, P.; Danusso, F.; Mantica, E.; Mazzanti, G.; Moraglio, G. *J. Am. Chem. Soc.* **1955**, *77*, 1708−1710.
34. Clary, J. J.; Gibson, J. E.; Waritz, R. S. Formaldehyde Toxicology. In *Epidemiology, Mechanisms*; Marcel Dekker: New York, 1983.
35. Liu, W.; Kumar, J.; Tripathy, S. K.; Senecal, K. J.; Samuelson, L. A. *J. Am. Chem. Soc.* **1999**, *121*, 71–78.
36. Nagarajan, S.; Kumar, J.; Bruno, F. F.; Samuelson, L. A.; Nagarajan, R. *Macromolecules* **2008**, *41*, 3049–3052.
37. Rumbau, V.; Pomposo, J. A.; Eleta, A.; Rodriguez, J.; Grande, H.; Mecerreyes, D.; Ochoteco, E. *Biomacromolecules* **2007**, *8*, 315–317.
38. Bruno, F. F.; Nagarajan, R.; Kumar, J.; Samuelson, L. A. *J. Macromol. Sci., Pure Appl. Chem.* **2002**, *A39* (10), 1061–1068.
39. Dawson, J. H. *Science* **1988**, *240*, 433–439.
40. Akita, M.; Tsutsumi, D.; Kobayashi, M.; Kise, H. *Biotechnol. Lett.* **2001**, *23*, 1827–1831.
41. Zhang, K.; Mao, L.; Cai, R. *Talanta* **2000**, *51*, 179–186.
42. Huang, Y. P.; Cai, R. X.; Mao, L. Y.; Huang, H. P. *Anal. Lett.* **2000**, *33*, 2883–2899.
43. Wang, Q.; Yang, Z.; Zhang, X.; Xiao, X.; Chang, C. K.; Xu, B. *Angew. Chem., Int. Ed.* **2007**, *46*, 4285–4289.
44. Wang, X.; Li, Y.; Chang, W. *Anal. Chim. Acta* **1999**, *400*, 135–142.
45. Nabid, M. R.; Sedghi, R.; Jamaat, P. R.; Safari, N. A.; Entezami, A. *J. Appl. Polym. Sci* **2006**, *102*, 2929–2934.
46. Angrish, C.; Chauhan, S. M. S. *ARKIVOC* **2004** (viii), 61–68.
47. Xing, H.; Shenggui1, L.; Zhao, M.; Zou, G. *J. Wuhan Univ. Technol., Mater. Sci. Ed.* **2008**, *23*, 809–815.
48. Xing, H.; Chen, D. M.; Zou, G. *Wuhan Univ. J. Nat. Sci.* **2005**, *10*, 460–464.
49. Xing, H.; Yu-Ying, Z.; Kai, T.; Guo-Lin, Z. *Synth. Met.* **2005**, *150*, 1–7.

Downloaded by UNIV OF DELAWARE MORRIS LIB on June 23, 2012 | http://pubs.acs.org
Publication Date (Web): November 18, 2010 | doi: 10.1021/bk-2010-1054.ch012

50. Akkara, J. A.; Wang, J.; Yang, D-P.; Gonsalves, K. E. *Macromolecules* **2000**, *33*, 2377–2382.
51. Kadokawa, J.-I.; Kokubo, A.; Tagaya, H. *Macromol. Biosci.* **2002**, *2*, 257–260.
52. Roy, S.; Nagarajan, R.; Bruno, F. F.; Tripathy, S. K.; Kumar, J.; Samuelson, L. A. *Polym. Mater. Sci. Eng.* **2001**, *85*, 202–203.
53. Bruno, F. F.; Nagarajan, S.; Nagarajan, R.; Kumar, J.; Samuelson, L. A. *Polym. Prepr.* **2007**, 660.
54. Bruno, F. F.; Nagarajan, R.; Sidhartha, J. S.; Yang, K.; Kumar, J.; Tripathy, S.; Samuelson, L. A *Mater. Res. Soc. Symp. Proc.* **2000**, *600*, 255.
55. Singh, A.; Roy, S.; Samuelson, L. A.; Bruno, F. F.; Nagarajan, R.; Kumar, J.; John, V.; Kaplan, D. K. *J. Macromol. Sci., Pure Appl. Chem.* **2001**, *A38* (12), 1219–1230.
56. Nagarajan, S.; Nagarajan, R.; Tyagi, R.; Kumar, J.; Bruno, F. F.; Samuelson, L. A. *J. Macromol. Sci., Pure Appl. Chem.* **2008**, *45*, 951–956.
57. Roxana, I.; Katsuya, K. *Tetrahedron Lett.* **2004**, *45*, 523–525.
58. Nagarajan, S.; Nagarajan, R.; Bruno, F. F.; Samuelson, L. A.; Kumar, J. *Green Chem.* **2009**, *11*, 334–338.
59. Willstaetter, R.; Stoll, A. *Liebigs Ann.* **1918**, *416*, 21.
60. Willstaetter, R.; Weber, H. *Ann. Chem.* **1926**, *449*, 156.
61. Brahim, S.; Narinesingh, D.; Guiseppi-Elie, A. *Biosens. Bioelectron.* **2002**, *17*, 53−59. Lu, W.; Zhou, D.; Wallace, G. G. *Anal. Commun.* **1998**, *35*, 245−248.
62. Lee, T. Y.; Shim, Y. B. *Anal. Chem.* **2001**, *73*, 5629–5632.
63. Garnier, F.; Korri-Youssoufi, H.; Srivastava, P.; Mandrand, B.; Delair, T. *Synth. Met.* **1999**, *100*, 89–94.
64. Brahim, S.; Narinesingh, D.; Guiseppi-Elie, A. *Anal. Chim. Acta* **2001**, *448*, 27–36.
65. Guo, H.; Knobler, C. M.; Kaner, R. B. *Synth. Met.* **1999**, *101*, 44–47.
66. Kros, A.; Van Hövell, S. W. F. M.; Sommerdijk, N. A. J. M.; Nolte, R. J. M. *Adv. Mater.* **2001**, *13*, 1555–1557.
67. Krishnamoorthy, K.; Gokhale, R. S.; Contractor, A. Q.; Kumar, A. *Chem. Commun.* **2004**, *7*, 820–821.
68. Roy, S.; Fortier, J. M.; Nagarajan, R.; Tripathy, S. K.; Kumar, J.; Samuelson, L. A.; Bruno, F. F. *Biomacromolecules* **2002**, *3*, 937–941.
69. Bruno, F. F.; Fosey, S.; Nagarajan, S.; Nagarajan, R.; Kumar, J.; Samuelson, L. A. *Biomacromolecules* **2006**, *7*, 586–589.
70. Jahnig, C. E.; Bertrand, R. R. *Chem. Eng. Prog.* **1976**, *72*, 51–56.
71. Guillette, L. J.; Gunderson, M. P. *Reproduction* **2001**, *122*, 857–864.
72. Lanouette, K. H. *Chem. Eng.* **1977**, *84*, 73. Throop, W. M. *J. Hazardous Mater.* **1977**, *1*, 319−329.
73. Klein, J. A.; Lee, D. D. *Biotechnol. Bioeng. Symp.* **1978**, *8*, 379–390.
74. Klibanov, A. M.; Alberti, B. N.; Morris, E. D.; Felshin, L. M. *J. Appl. Biochem.* **1980**, *2*, 414–421.
75. Klibanov, A. M.; Morris, E. D. *Enzyme Microb. Technol.* **1981**, *3*, 119–122.
76. Walberg, K.; Assenhaimer, C.; Rubio, J. J. *Chem. Technol. Biotechnol.* **2002**, *77*, 851–857.

Downloaded by UNIV OF DELAWARE MORRIS LIB on June 23, 2012 | http://pubs.acs.org
Publication Date (Web): November 18, 2010 | doi: 10.1021/bk-2010-1054.ch012

77. Piccolo, A.; Conte, P.; Tagliatesta, P. *Biomacromolecules* **2005**, *6*, 351–358.
78. Smejkalova, D.; Conte, P.; Piccolo, A. *Biomacromolecules* **2007**, *8*, 737–743.
79. Smejkalova, D.; Piccolo, A. *Environ. Sci. Technol.* **2006**, *40*, 1644–1649.
80. Celano, G.; Smejkalova, D.; Spaccini, R.; Piccolo, A. *Environ. Sci. Technol.* **2008**, *42*, 4896–4901.
81. Donato, M.; Nardis, S.; Stefanelli, M.; Paolesse, R.; Natale, C. D.; D'Amico, A. *J. Sens.* **2009**, *2009*; Article ID 856053; DOI: 10.1155/2009/856053.
82. Paolesse, R.; Lvova, L.; Nardsi, S.; Natale, C. D.; D'Amico, A.; Castro, F. L. *Microchim. Acta* **2008**, *163*, 103–112.
83. Winnischofer, H.; Toma, H. E.; Araki, K. *J. Nanosci. Nanotechnol.* **2006**, *6*, 1701–1709.
84. Toal, S. J.; Trogler, W. C. *J. Mater. Chem.* **2006**, *16*, 2871–2883.
85. Rodgers, K. R. *Curr. Opin. Chem. Biol.* **1999**, *3*, 158.
86. Gilles-Gonzalez, M. A.; Ditta, G.; Helinski, D. R. *Nature* **1991**, *350*, 170.
87. Gilles-Gonzalez, M. A.; Gonzalez, G.; Perutz, M..F.; Kiger, L.; Marden, M.; Poyart, C. *Biochemistry* **1994**, *33*, 8067.
88. Gong, W; Hao, B.; Mansy, S. S.; Gonzalez, G.; Gilles-Gonzalez, M. A.; Chan, M. K. *Proc. Natl. Acad. Sci. USA* **1998**, *95*, 15177.
89. Gong, W.; Hao, B.; Mansy, S. S.; Gonzalez, G.; Gilles-Gonzalez, M. A.; Chan, M. K. *Proc. Natl. Acad. Sci. USA* **1998**, *95*, 15177.
90. Garbers, D. L.; Lowe, D. G. *J. Biol. Chem.* **1994**, *269*, 30741.
91. Kuriyama, K.; Ohkuma, S. *Jpn. J. Pharmacol.* **1995**, *69*, 1–8.
92. Chakravortty, D.; Hensel, M. *Microbes Infect.* **2003**, *5*, 621–627.
93. Malinski, T.; Taha, Z. *Nature* **1992**, *358*, 676.
94. Bedioui, F.; Villeneuve, N. *Electroanalysis* **2003**, *15* (1), 5–18.
95. Kashevskii, A. V.; Lei, J.; Safronov, A. Y.; Ikeda, O. *J. Electroanal. Chem.* **2002**, *531*, 71.
96. Kashevskii, A. V.; Safronov, A. Y.; Ikeda, O. *J. Electroanal. Chem.* **2001**, *510*, 86.
97. Hayon, J.; Ozer, D.; Rishpon, J.; Bettelheim, A. *J. Chem. Soc., Chem. Commun.* **1994**, 619.
98. Ciszewski, A.; Kubaszewski, E.; Lozynski, M. The role of nickel as central metal in conductive polymeric porphyrin film for electrocatalytic oxidation of nitric oxide. *Electroanalysis* **1996**, *8*, 293.
99. Bedioui, F.; Trevin, S.; Albin, V.; Villegas, M. G. G.; Devynck, J. *Anal. Chim. Acta* **1997**, *341*, 177.
100. Kadish, K. M.; Smith, K. M.; Guilard, R. *The porphyrin handbook*; Vol. 4, pp 232−255.
101. Bedioui, F.; Trevin, S.; Devynck, J. The use of gold electrodes in the electrochemical detection of nitric oxide in aqueous solution. *J. Electroanal. Chem.* **1994**, *377*, 295–298.
102. Lantoine, F.; Trevin, S.; Bediousi, F.; Devynck, J. Selective and sensitive electrochemical measurement of nitric oxide in aqueous solution; discussion and new results. *J. Electroanal. Chem.* **1995**, *392*, 85–89.
103. Kashevskii, A. V.; Lei, J.; Safronov, A. Y.; Ikeda, O. Electrocatalytical properties of meso-tetraphenylporphyrin cobalt for nitric oxide oxidation in

Downloaded by UNIV OF DELAWARE MORRIS LIB on June 23, 2012 | http://pubs.acs.org
Publication Date (Web): November 18, 2010 | doi: 10.1021/bk-2010-1054.ch012

Downloaded by UNIV OF DELAWARE MORRIS LIB on June 23, 2012 | http://pubs.acs.org
Publication Date (Web): November 18, 2010 | doi: 10.1021/bk-2010-1054.ch012

methanolic solution and in nafion film. *J. Electroanal. Chem.* **2002**, *531*, 71–79.

104. Diab, N.; Schuhmann, W. *Electrochim. Acta* **2001**, *47*, 265–273.
105. Trévin, S.; Bedioui, F.; Devynck, J. *J. Electroanal. Chem.* **1996**, *408*, 261–265.
106. Wu, D. G.; Ashkenasy, G.; Shvarts, D.; Ussyshkin, R. V.; Naaman, R.; Shanzer, A.; Cahen, D. *Angew. Chem., Int. Ed.* **2000**, *39*, 4496–4500.
107. Li, C.-Z.; Alwarappan, S.; Zhang, W.; Nikki Scafa, N.; Zhang, X. *Am. J. Biomed. Sci.* **2009**, *1*, 274–282.
108. Herbert, A.; Alfken, J.; Kim, Y.-G.; Mian, I. S.; Nishikura, K.; Rich, A. *Proc. Natl. Acad. Sci. USA* **1997**, *94*, 8421–8426.
109. Kim, Y.-G.; Lowenhaupt, K.; Maas, S.; Herbert, A.; Schwartz, T.; Rich, A. *J. Biol. Chem.* **2000**, *275*, 26828–26833.
110. Kim, Y.-G.; Lowenhaupt, K.; Oh, D.-B.; Kim, K. K.; Rich, A. *Proc. Natl. Acad. Sci. USA* **2004**, *101*, 1514–1518.
111. Schwartz, T.; Rould, M. A.; Lowenhaupt, K.; Herbert, A.; Rich, A. *Science* **1999**, *284*, 1841–1845.
112. Balaz, M.; Klaus, B.-J.; Mammana, A.; Ellestad, G. A.; Nakanishi, K.; Berova, N. *Pure Appl. Chem.* **2007**, *79*, 801–809.
113. Balaz, M.; Napoli, M. D.; Holmes, A.E.; Mammana, A.; Nakanishi, K.; Berova, N.; Purrello, R. *Angew. Chem., Int. Ed.* **2005**, *44*, 4006–4009.
114. Alessandro D'Urso, A.; Mammana, A.; Balaz, M.; Holmes, A. E.; Berova, N.; Lauceri, R.; Purrell, R. *J. Am. Chem. Soc.* **2009**, *131*, 2046–2047.
115. Yuasa, M.; Oyaizu, K.; Horiuchi, A.; Ogata, A.; Hatsugai, T.; Yamaguchi, A.; Kawakami, H. *Mol. Pharm.* **2004**, *1*, 387–389.
116. McNeil, C. J.; Smith, K. A.; Bellavite, P.; Bannister, J. V. *Free Radical Res. Commun.* **1989**, *7*, 89–96.
117. Chen, J.; Wollenberger, U.; Lisdat, F.; Ge, B.; Scheller, F. W. *Sens. Actuators, B* **2000**, *70*, 115–120.
118. Yuasa, M.; Oyaizu, K.; Yamaguchi, A.; Ishikawa, M.; Eguchi, K.; Kobayashi, T.; Toyoda, Y.; Tsutsui, S. *Polym. Adv. Technol.* **2005**, *16*, 287–292.

Downloaded by DUKE UNIV on June 23, 2012 | http://pubs.acs.org
Publication Date (Web): November 18, 2010 | doi: 10.1021/bk-2010-1054.ch013

Chapter 13

Design of Highly Functional Antiferritin-Immunolatex by Hybridization of Antiferritin/Mixed-PEG Polymers onto Polystyrene Submicroparticles

Xiaofei Yuan,[1,2,3] Dolça Fabregat,[6] Keitaro Yoshimoto,[1,2,3] and Yukio Nagasaki[1,2,3,4,5,*]

[1]Graduate School of Pure and Applied Sciences, [2]Tsukuba Research Center for Interdisciplinary Materials Science (TIMS), [3]Tsukuba Advanced Research Alliance (TARA), [4]Master School of Medical Sciences, Graduate School of Comprehensive Human Sciences, University of Tsukuba, Ten-noudai 1-1-1, Tsukuba, Ibaraki 305-8577, Japan
[5]Satellite Laboratory of International Center for Materials Nanoarchitectonics (MANA) in National Institute for Materials Science (NIMS), Ten-noudai 1-1-1, Tsukuba, Ibaraki 305-8573, Japan
[6]Biokit Latex R&D Department, 08186 Lliçà d'Amunt, Barcelona, Spain
[*]nagasaki@nagalabo.jp

Pentaethylenehexamine-ended poly(ethylene glycol), N6-PEG comprising N6-PEG-5k (M_n = 6000 g/mol) and N6-PEG-2k (M_n = 2000 g/mol), was employed as a novel blocking agent to formulate stable and highly functional antiferritin-immunolatex (LAmP-s, s denotes antiferritin load). In comparison with the immunolatex complex (LAB-s), which were prepared in a similar manner except for using bovine serum albumin (BSA) as a blocking agent, the LAmP-s complex showed a difference only in the surface charge property, because of the altered surface treatment in the case of the LAmP-s (PEGylation) and LAB-s complexes (BSA covering). However, the nonspecific deposition level of BSA-FITC molecules was remarkably low for the LAmP-s complex. Simultaneously, the LAmP-s complex showed significantly higher reactivity (i.e., a high response yield and a low detention limit) compared to that of the LAB-s complex, not only in phosphate buffer (10 mM, pH =

7.4) but also in 100 % fetal bovine serum (FBS), as measured by the turbidimetric monitoring method. The electrical repulsion between the negatively charged LAB-s complex and the anionic antigen was the primary obstacle in the former case, and the overwhelming nonspecific deposition of contaminants from FBS onto the LAB-s complex, was the main reason in the latter case. Moreover, the PEGylation treatment allowed the LAmP-s complex to possess invariable size and reactivity for at least one month at 4 °C without salt, obviously demonstrating that the PEGylation technique is a promising method for constructing sensitive immunoassay systems.

Downloaded by DUKE UNIV on June 23, 2012 | http://pubs.acs.org
Publication Date (Web): November 18, 2010 | doi: 10.1021/bk-2010-1054.ch013

Introduction

Immunolatex agglutination test, of which the result can be rapidly evaluated with the naked eye, is a low-cost and user-friendly, needs no special equipment or skilled personnel, yields the result within 2 min (*1–3*), and is claimed to be the quickest and easiest immunoassay method. The formulation of immunolatex usually includes bovine serum albumin (BSA) to cover the residual hydrophobic particle surface after the sensitization of antibodies or antigens (*4–6*), with the purpose of stabilizing the particle and protecting it from any interfacial disturbance during assay. However, the inherent protein nature of BSA is an obstacle to this function (e.g., BSA is negatively charged under physiological conditions, as is unfavorable for dense covering of BSA molecules onto a negatively charged surface.), and a novel surface modification technique is required to solve the problem.

Poly(ethylene glycol) (PEG) is a well-known hydrophilic, flexible and neutral polymer of low toxicity. It has been widely used to stabilize various nano- and micro-scale particles. Additionally, since a PEG chain possesses low affinity for various bio-macromolecules, a PEGylated surface improves the performance of bio-diagnosis, especially in immunodiagnostic systems (*7–10*). In this case, the long chain length and high chain density of the PEG layer were both required, but increased polymer chain length is always accompanied by decreased polymer chain density, owing to the steric exclusion of the tethered PEG chains (*11*, *12*). A mixed-PEG chain layer with both long-chain (5k) and short-chain (2k) PEGs may resolve this trade-off relation, in that the long PEG chains retained the chain length of the layer, while the short ones easily occupied the inter-space between two long PEG chains to remarkably increase the total chain density of the layer (*7*, *13–15*). Besides, a PEG-chain layer may also create a suitable environment for specific types of bio-recognition (*16*, *17*). In view of these facts, we successfully designed and formulated a novel high-performance antiferritin-immunolatex particle, based on this special PEGylation technique instead of the traditional BSA surface treatment.

Formulation of Various Complexes and Immune Response Measurements

Figure 1 shows the preparation procedure of various forms of complex. Briefly, a carboxylated polystyrene submicroparticle (sMP) suspension (30 µl) was poured into a 1.5-ml plastic tube and diluted with 167 µl of NaH_2PO_4 solution (buffer B; 10 mM, pH = 4.8). Then, 3 µl of an 1-ethyl-3-[3-dimethylaminopropyl]carbodiimide hydrochloride (EDC) aqueous solution (12.5 mg/ml) were poured in followed by shaking for 20 min at 25°C to activate the surface carboxyl groups of the particles. The thus obtained activated sMPs were further diluted by 100 µl of phosphate buffer (buffer A; 10 mM, pH = 7.4) before mixing them (50 µl) with both buffer A (275 µl) and 10 µl of antiferritin solution in buffer A (0.514, 1.14, 1.71 and 2.28 mg/ml, separately corresponding to s = 0.45, 1.0, 1.5, and 2.0 mg/m^2), followed by 1h incubation with shaking to bind the antiferritin onto the particles. Then, such obtained sMP/antibody (LA) complex (300 µl), which was monodispersed again by ultra-sonication treatment, was reacted with N6-PEG-5k (150 µl, 0.3 % w/v) for 30 min to formulate sMP/antibody/PEG complex (LAP-s, s denotes the amount of antiferritin used to prepare the complex.), or successively reacted with N6-PEG-5k (75 µl, 0.6 % w/v) and N6-PEG-2k (75 µl, 0.4 % w/v) solutions by separate incubation with shaking for 30 min to formulate sMP/antibody/mixed-PEG complex (LAmP-s). As a control, sMP/antiferritin/BSA complex (LAB-s) was prepared similarly to that of the LAP-s complex, except for employing BSA instead of N6-PEG-5k polymer.

The immune response of the test samples was measured by turbidimetric monitoring on a PL-2500 spectrophotometer (Shimadzu, Japan). Briefly, 20 µl of the test sample suspension (sMP concentration = 0.1 % w/v) was added into a mixture of a given amount of human ferritin solution (1 µg/ml) with buffer A or with 100 % fetal bovine serum (FBS) to a total final volume of 500 µl, followed by turbidimetric monitoring at a wavelength of 550 nm for 5 min at room temperature. The initial slope of the turbidimetric progress curve was identified as the immune response here.

Antiferritin Immobilization

The binding of antibody onto sMPs, which is similar to that of protein onto a solid surface, is influenced by various factors, such as antibody concentration, adsorption time, surface characteristics, and so on. The binding time is a key parameter, since antibody may physically adsorb onto the particles within a short time, as means the antibody is unstably immobilized and may easily desorb from the particles during a diagnostic treatment. Conversely, an excessively long binding time may lead to the denaturation of antibody or change its orientation on the surface to prevent the antibody-antigen reaction.

Although the antiferritin was chemically (covalently) immobilized onto the sMPs in this study, physical (passive) adsorption was also considered along with chemical binding, since the passive adsorption of proteins on hydrophobic sorbents, such as polystyrene sMPs, usually occurs very rapidly and irreversibly

Downloaded by DUKE UNIV on June 23, 2012 | http://pubs.acs.org
Publication Date (Web): November 18, 2010 | doi: 10.1021/bk-2010-1054.ch013

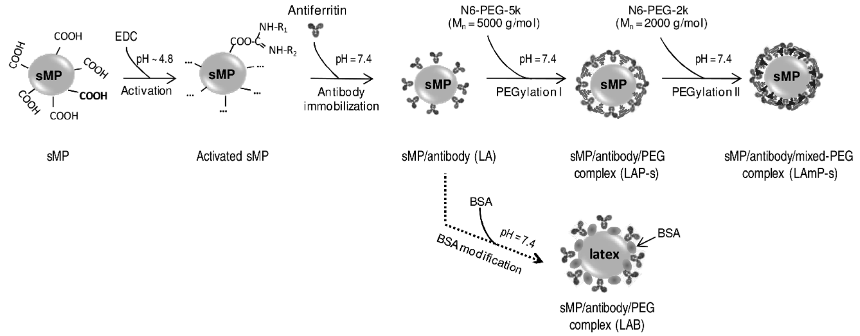
Antiferritin
N6-PEG-5k
(M_n = 5000 g/mol)
N6-PEG-2k
(M_n = 2000 g/mol)
COOH
EDC
pH ~ 4.8
Activation
NH-R₁
NH-R₂
pH = 7.4
Antibody immobilization
pH = 7.4
PEGylation I
pH = 7.4
PEGylation II
sMP
Activated sMP
sMP/antibody (LA)
sMP/antibody/PEG complex (LAP-s)
sMP/antibody/mixed-PEG complex (LAmP-s)
BSA
pH = 7.4
BSA modification
latex
sMP/antibody/PEG complex (LAB)

Figure 1. Schematic representation of the formulation of LAP-s, LAmP-s, and the control of LAB-s complexes.

(*18–20*). It has been demonstrated that physical adsorption occurs significantly in the chemical binding of anti-C reactive protein (a-CRP) antibody to polystyrene sMPs using the same EDC method (*18*). In comparison with the chemically immobilized antibody, the physically adsorbed antibody was more randomly orientated and possibly desorbed from the sorbent to disfavor antibody-antigen recognition (*18*). Hence, it was necessary to ascertain the amount of the physically adsorbed antiferritin.

Immobilization Time

To optimize the reaction time of antiferritin to the activated sMPs, the antiferritin concentration (0.516 mg/ml, s = 0.45 mg/m^2) and other factors were fixed in this experiment. The binding time was estimated in term of the immune response of sMP, onto which antiferritin was immobilized using different reaction time from 15 to 90 min. PEGylation with N6-PEG-5k of 0.1 % w/v in solution was also carried out, since sMP/antiferritin complex (LA) without N6-PEG gave a low response. The LAP-0.45 complex with the reaction time of antiferritin was 15 min, yielded a slightly low immune response compared to the others. The response became almost constant when the immobilization was allowed to continue for more than 30 min, indicating that a period of more than 30 min was required for a complete immobilization of antiferritin. Actually, the amount of immobilized antibody with the reaction time of 15 min (87 %), which was quantified by the copper reduction/bicinchoninic acid reaction (Micro BCA method), was slightly lower than those with a long reaction time (95 %). Since there was no significant difference in both the immune response yield and the antiferritin load for the LAP-0.45 complex with the reaction time longer than 30 min, a 1-h reaction time of antiferritin was employed in the subsequent experiments.

Downloaded by DUKE UNIV on June 23, 2012 | http://pubs.acs.org
Publication Date (Web): November 18, 2010 | doi: 10.1021/bk-2010-1054.ch013

Downloaded by DUKE UNIV on June 23, 2012 | http://pubs.acs.org
Publication Date (Web): November 18, 2010 | doi: 10.1021/bk-2010-1054.ch013

Binding Efficiency

To construct an acceptable and applicable antiferritin-immunolatex, valid antibody load is necessary, since a high antibody load generally corresponds to a high response yield of the immunolatex. To remove purification procedure for a simple praperation, binding efficiency of antiferritin was estimated.

The amount of antiferritin adsorbed onto the sMP and dissolved in the supernatant were separately measured by the Micro BCA method, using freshly prepared LA complex suspension with various original antiferritin concentration in solution (≤ 80 μg/ml). The obtained surface antiferritin concentration of the particles was almost the same with the corresponding original antifferitin concnentration in solution, except of the one corresponding to 80 μg/ml, as was slightly lower than 80 μg/ml along with a measurable amount of free antiferritin in the supernatant. This result clearly suggests that the added antiferritin almost completely bound onto the particles within experimental error.

Chemical Binding and Physical Adsorption

To identify the amount of physically adsorbed antiferritin within the total immobilized antibody, similar quantification was carried out after 24-h incubation with slow shaking at room temperature of a freshly prepared LA complex in 0.1 % w/v of Tween 20 solution. It has been reported that physically adsorbed antibody might be removed from the chemically bonded one under this condition (*21–23*). As a result, physically adsorbed antiferritin (in the supernatant) increased slightly with increasing total antiferritin load (i.e., the antibody load of the LA complex before surfactant addition). This implies that a small amount of physically adsorbed antiferritin existed, especially at a high antiferritin load (at most 10 %).

PEGylation

After the antiferritin was covalently immobilized onto the sMPs through the reaction of its amino groups with the activated carboxyl groups (active ester) of the particles, α-methoxy-poly(ethylene glycol)-pentaethylenehexamine (N6-PEG), which possesses six amino groups at one end, was similarly linked to the particles. Compared to mono-functional amino groups, this positively charged six-amino-group structure may be more electrically attracted to the negatively charged surface of sMPs at pH 7.4. This may accelerate the approach and the reaction of N6-PEG with the active ester on the sMP surface. Moreover, the excess amino groups in N6-PEG may also electrically interact with the carboxyl groups, due to the possible hydration of the active ester on the surface. This is crucial for the construction of a densely packed PEG-chain layer, because the active ester is susceptible to hydrolysis in a aqueous solution to lose its reactivity (*24*).

Downloaded by DUKE UNIV on June 23, 2012 | http://pubs.acs.org
Publication Date (Web): November 18, 2010 | doi: 10.1021/bk-2010-1054.ch013

Optimization of N6-PEG-5k Concentration

The proper N6-PEG-5k concentration should meet two requirements. One is the capability to completely cover the residual particle surface after antibody immobilization in order to avoid any interfacial nonspecific recognition. The other is to create a favorable environment for antibody-antigen agglutination. To obtain a suitable PEGylation condition for LAP-0.45 complex preparation, the electrophoretic mobility (μ_e) of PEGylated sMPs, without antibody on the surface (LP complex), was evaluated simply in order to understand the PEGylation effect. In addition, the immune response of the LAP-0.45 complex was estimated as a function of the N6-PEG-5k concentration in the solution.

The preparation of the LP complex was carried out by mixing N6-PEG-5k of various concentrations with activated sMPs for 30 min. The μ_e value of thus obtained LP complex increased and reached almost zero with increasing N6-PEG-5k concentration in the solution up to 0.01 % w/v. (see Figure 2a) This phenomenon reflected the conjugation of neutral and hydrophilic PEG polymer onto sMPs to generate a N6-PEG-5k polymer layer around the particles (*11b*, *12b*). The proper concentration of N6-PEG-5k in the solution, should be higher than 0.01 % w/v to completely cover the surface of each sMP.

The immune response of the LAP-0.45 complex as a function of the N6-PEG-5k concentration in the solution, gave a profile similar to that of the μ_e value, i.e., the response increased with increasing N6-PEG-5k concentration in the solution from 0.01 to 0.04 % w/v before it became constant. (Figure 2b) In other words, the N6-PEG-5k concentration in the solution should be higher than 0.04 % w/v to obtain a high and constant immune response yield, even though the sMP surface seemed fully covered as a result of the treatment with 0.01 % w/v of N6-PEG-5k. Based on these results, 0.1 % w/v was selected as the suitable N6-PEG-5k concentration in the solution for preparing a desirable LAP-s complex in the subsequent experiments.

As mentioned above, the N6-PEG-5k polymer may chemically (covalent bond) and/or physically (electrical attraction) modify the sMPs, since the oligoamine segment of the N6-PEG-5k polymer is positively charged at pH 7.4. Actually, it was found that electrically PEGylated sMPs (n-LP complex), which was prepared by simply mixing the sMPs (without activation) with the N6-PEG-5k polymer for 30 min, showed a μ_e profile similar to that of covalently PEGylated sMPs (LP complex), regardless of the N6-PEG-5k concentration in the solution. (Figure 2a) Thus, covalent PEGylation *via* an active ester and the N6-PEG-5k might not be required for the modification. To identify the kind of the PEGylation (covalent or electric linkage), the dispersion stability of the LP and n-LPcomplexes (N6-PEG-5k = 0.1 % w/v), and the sMPs were investigated at a high salt concentration (2 M NaCl). Figure 2c shows the time course of the particle sizes within 30 min after salt addition on a Malvern Zetasizer Nano ZS instrument. The size of the sMP itself, regardless of the activation process, significantly increased after salt addition, apparently indicating that the sMPs were unstable without PEG-modification and rapidly aggregated in the 2-M NaCl solution. It is because the salt ions thinned the electrical double layer of the sMP and weakened the electrical inter-particle repulsion, thus promoting their

Downloaded by DUKE UNIV on June 23, 2012 | http://pubs.acs.org
Publication Date (Web): November 18, 2010 | doi: 10.1021/bk-2010-1054.ch013

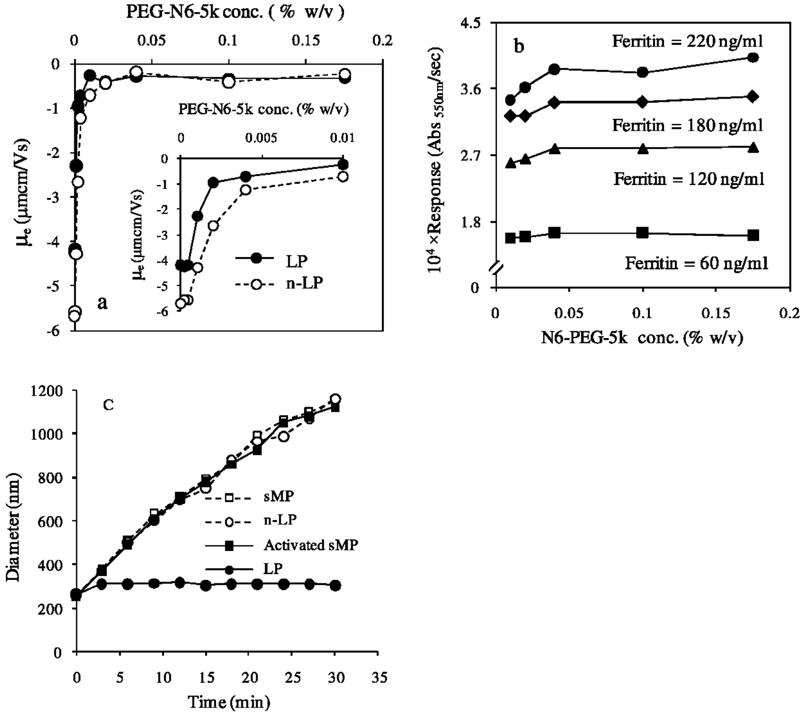

Figure 2. (a) Variations in the μ_e value of the LP complex and the n-LP complex with increasing N6-PEG-5k concentration in the solution. (b) Immunoreactivity of the LAP-0.45 complex corresponding to various ferritin amounts as a function of the N6-PEG-5k concentration in the solution. (c) Time-dependent variation in the size of sMP, activated sMP, LP, and n-LP complexes in 2-M NaCl solution.

aggregation. The n-LP complex aggregated in exactly the same way as the sMP without PEG, and the LP complex almost retained its size even after one day at 4 °C. It is obvious that the electrical interaction between the sMP and the N6-PEG-5k polymer is not sufficiently strong to stably disperse the sMPs at high salt concentrations, since the added salt ions displaced the electrically coupled N6-PEG-5k molecules and released them from the n-LP complex (electrostatic shielding effect), whereas salt had no effect on the covalently coupled N6-PEG-5k of the LP complex. Hence, the N6-PEG-5k polymer was actually covalently linked onto the sMPs, as is crucial for the preparation of a stable complex.

Optimization of the N6-PEG-5k/N6-PEG-2k Ratio (5k/2k)

The proper ratio of long-chain PEG (N6-PEG-5k) to short-chain PEG (N6-PEG-2k), 5k/2k, was determined by immune response measurements at a ferritin concentration of 100 ng/ml. Figure 3a (●) shows the immune response yield of the LAmP-0.45 complex, which was prepared by the successive PEGylation of the LA complex with the N6-PEG-5k (0.6 % w/v) and the N6-PEG-2k (from 0

Downloaded by DUKE UNIV on June 23, 2012 | http://pubs.acs.org
Publication Date (Web): November 18, 2010 | doi: 10.1021/bk-2010-1054.ch013

to 0.6 % w/v) polymer, respectively. The final concentration of the N6-PEG-5k was 0.1 % w/v, and the N6-PEG-2k ranged from 0 to 0.1 % w/v. No meaningful variations in size and μ_e was obtained between the LAP-0.45 and the LAmP-0.45 complexes (data not shown). Interestingly, the immune response of the LAmP-0.45 complex increased after the addition of the N6-PEG-2k, especially when its concentration in solution was 0.07 % w/v (5k/2k = 1: 0.67). In contrast, the response of the LAP-0.45 complex did not increase at all, even consecutively treated with the N6-PEG-5k of 0.1 % w/v in the solution (total polymer conc. = 0.2 % w/v, Figure 3a (○); 5k/5k = 1: 1); i.e., the polymer concentration was equivalent to 5k/2k = 1: 1. These inconsistent immune response yields clearly indicate that the improved performance of the LAmP-0.45 complex was not due to increased polymer concentration in the system, but probably due to increased chain density of the PEG-chain layer around the sMPs.

The LAmP-0.45 complex (5k/2k = 1: 0.67) was more reactive than the LAP-0.45 complex in buffer A (see Figure 3b), regardless of the ferritin concentration examined in this study (10 – 100 ng/ml). Similar results were also obtained in 100 % FBS solution, although the absolute values decreased compared to those in buffer A. Because FBS solution contains various contaminants, which may interfere with the antiferritin-ferritin interaction to reduce the response. All the results represented in Figure 3 agree well with previous reports, that increasing the chain density of the PEG-chain layer around the sMPs efficiently improved the antiferritin-ferritin interaction.

Surface Modification with BSA

So far, most of the immunolatexes have been prepared using BSA blocking treatment after antibody sensitization. Although various BSA concentrations have been used in different systems, explanation was seldom given on how to select a reasonable BSA concentration. It is imperative to choose a proper BSA concentration for an acceptable control of sMP/antibody/BSA (LAB-s) complex in this study.

Optimization of BSA Concentration

The proper concentration of BSA was determined by two methods, i.e., according to the variations in the μ_e value and according to the immune response yield of the LAB-s complex with increasing BSA concentration. For example, the LAB-0.45 complex was prepared with BSA concentration ranging from 6.7×10^{-3} to 3.3 % w/v in the solution. Its μ_e value changed from – 3.8 to – 1.9 with increasing BSA concentration, but notable variations from – 3.8 to – 2.7 occurred below BSA = 2.7×10^{-2} % w/v (see Figure 4), indicating that the negatively charged activated sMP was effectively covered by BSA (> 2.7×10^{-2} % w/v). On the other hand, the immune response yield of the LAB-0.45 complex significantly increased to the maximum at BSA = 1.3×10^{-2} % w/v, and progressively decreased with increasing BSA concentration. In the low concentration-region of BSA (< 2.7×10^{-2} % w/v), the changes in both the μ_e value and the immune response yield

Downloaded by DUKE UNIV on June 23, 2012 | http://pubs.acs.org
Publication Date (Web): November 18, 2010 | doi: 10.1021/bk-2010-1054.ch013

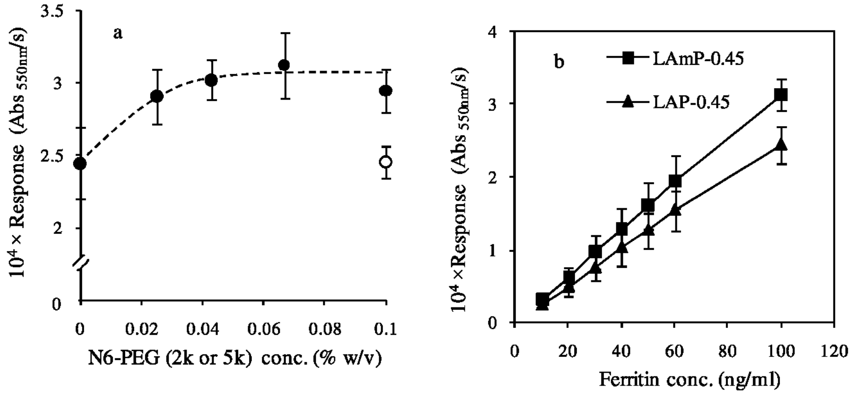

Figure 3. (a) N6-PEG-2K-dependent immune response yield of the LAmP-0.45 complex (N6-PEG-5k = 0.1 % w/v) measured at 100 ng/ml ferritin. ○ denotes the immune response yield of the LAP-0.45 complex (5k/5k = 1: 1, N6-PEG-5k = 0.2 % w/v) for comparison. (b) Immune response yields of the LAmP-0.45 (5k/2k = 1: 0.67) and LAP-0.45 complexes in buffer A.

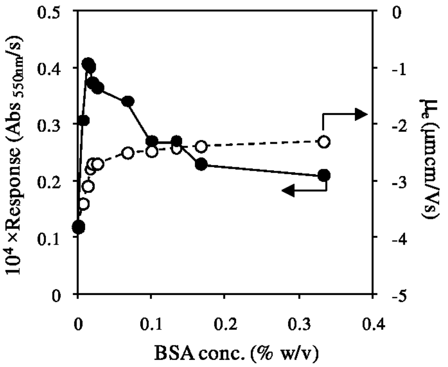

Figure 4. Immune response yield and μ_e value of the LAB-0.45 complex as a function of BSA concentration in the solution.

of the LAB-0.45 complex was concordant, suggesting that the BSA-addition might weaken the electrical repulsion between the ferritin (isoelectric point < 6) and the sMPs to promote their proximity, and then facilitate the ferritin-antiferritin recognition. But too much BSA may have a tendency to occupy the epitopes of antiferritin and interfere with the ferritin-antiferritin recognition, leading to decreased immunoreactivity of the LAB-0.45 complex. Consequently, it is plausible to assume that there is a critical BSA concentration, 1.3×10^{-2} % w/v, for preparing a high-performance LAB-0.45 complex.

It should be noted that no this kind of phenomena was observed for the LAP-0.45 complex. This implies another merit of the PEGylation technique that the N6-PEG-5k has no affinity to the pre-located antiferritin on the sMP surface.

Downloaded by DUKE UNIV on June 23, 2012 | http://pubs.acs.org
Publication Date (Web): November 18, 2010 | doi: 10.1021/bk-2010-1054.ch013

Table 1. Size, polydispersity index (PDI) and electrophoretic mobility (μ_e) values of the versatile sMP complex

sMP complex	Diameter (nm)	PDI	μ_e (μmcm/Vs)
LAmP-0.45	268 ± 2	< 0.1	- 0.23 ± 0.17
LAmP-1.0	269 ± 1	< 0.1	- 0.31 ± 0.09
LAmP-1.5	275 ± 6	< 0.1	- 0.39 ± 0.03
LAmP-2.0	359 ± 41	0.26 ± 0.07	- 0.52 ± 0.04
LAB-0.45	264 ± 4	< 0.1	- 3.12 ± 0.09
LAB-1.0	272 ± 4	< 0.1	- 2.36 ± 0.08
LAB-1.5	273 ± 6	< 0.1	- 1.60 ± 0.12
LAB-2.0	284 ± 6	< 0.1	- 1.37 ± 0.06

Comparison of LAmP-s and LAB-s Complex

The LAmP-s complex (s ranged from 0.45 to 2.0) were prepared using the 5k/2k ratio of 1: 0.67, the proper ratio of the LAmP-0.45 complex. It is worth mentioning that the LAmP-s complex was evidenced to be more reactive than the LAP-s complex (data not shown).

As described above, selection of a proper BSA concentration is critical for preparing an acceptable LAB-s complex. Hence, altered BSA concentration (0.012, 0.01 and 0.008 % w/v in solution), which was obtained similarly as above mentioned, were separately employed to formulate the LAB-1.0, LAB-1.5 and LAB-2.0 complexes, respectively.

Size and Polydispersity Index (PDI)

The size of the LAmP-s complex was almost constant with the polydispersity index (PDI) < 0.1, except for the LAmP-2.0 complex. (Table 1) Considering the average size of a sMP particle (251 ± 3 nm in buffer A) and that of an antiferritin molecule (13 ± 3 nm), these results suggest that the LAmP-0.45, LAmP-1.0 and LAmP-1.5 were monodispersed immunolatex particles. In comparison, the LAmP-2.0 complex became large with PDI > 0.1, which indicates that it was heterogeneous. On the other hand, the LAB-s complex showed results very similar to those for the LAmP-s complex in spite of the LAB-2.0 complex, which was slightly larger than the other LAB-s complexes but with PDI < 0.1.

To explain these discrepancies in size and PDI between s = 2.0 and other s values, the colloidal stability of the complex at s = 2.0 (after 1 day and 3 days at 4 °C) was monitored in terms of size distribution, using the complex at s = 1.5 as a control. Compared to the invariable size distribution of the LAB-1.5 and LAmP-1.5 complexes, that of the complex at s = 2.0 became broad after 3 days, because some large particles appeared in the system with time, leading to an increase in average size to about 9, 47 and 37 nm for the LAB-2.0, LAmP-2.0 and LAP-2.0 complexes, respectively. These remarkably dissimilar size and size distribution among the forms of the complex at s = 2.0, undoubtedly indicate the aggregation of the particles as a result of their colloidal instability. This phenomenon might thus be attributed to the relatively excessive antiferritin coverage onto the particles, i.e., the antiferritin occupied the space required for PEG-chain linkage or BSA adsorption to stabilize the LA complex.

Interestingly, the LAB-2.0 complex seems slightly more stable than the LAP-2.0 and LAmP-2.0 complexes, in that it had a relative small size and a low PDI value. It is possibly due to the epitope-coverage of the pre-localized antiferritin by nonspecifically adsorbed BSA molecules in excess, but not by the PEGylation as mentioned above. This passive deposition of BSA molecules may play a central role in suspending the complex to some extent.

Downloaded by DUKE UNIV on June 23, 2012 | http://pubs.acs.org
Publication Date (Web): November 18, 2010 | doi: 10.1021/bk-2010-1054.ch013

μ_e *Values versus pH*

To explain the colloidal stability of the LAmP-s and LAB-s complexes, and distinguish the effects of PEGylation from those of BSA surface treatment, pH-dependent electrophoretic mobility (μ_e) measurements were carried out. As a control, the same experiment was also performed to the polystyrene sMPs and the analogues of the LAB-0.45, LAB-1.0 and LAB-1.5 complexes, called “LAB-0-1”, “LAB-0-2” and “LAB-0-3” complex, respectively, which were prepared without antiferritin but the same BSA treament as the LAB-0.45, LAB-1.0 and LAB-1.5 complexes, respectively.

The polystyrene sMP gave a large negative μ_e value across the entire pH range, suggesting the presence of many negative charges on its surface. (see Figure 5a) It coincides with the surface carboxyl groups of the sMPs. The BSA surface treatment significantly diminished the μ_e value of the sMPs because of BSA covering. The higher the BSA concentration used, the lower the absolute μ_e value, shown as the variation in the μ_e value of the LAB-0-1, LAB-0-2 and LAB-0-3 complexes. The covering of both antiferritin and BSA onto the particles further underlined this phenomenon, owing to the compensation of the surface charges of the sMPs by the net charge of these proteins (*18*, *23*). In consideration of the isoelectric point (iep) of BSA (~5) (*25*, *26*) and the antiferritin (6 – 7), the gradually decreasing μ_e of the LAB-s complex with increasing s values excellently supports the up-ward tendency of antiferritin coverage in the same order. The negative μ_e value of the LAB-s complex obviously implies that it was dispersed by interparticle electrostatic repulsion. The LAmP-s complex possessed zero-closed mobility at any pH, regardless of the antiferritin load, confirming that it was dispersed by steric exclusion of the neutral and hydrophilic PEG chains, which compactly covered the residual bare surface of the particles after the sensitization. (see Figure 5b)

Nonspecific Adsorption of BSA-FITC

The LAB-1.0 and LAmP-1.0 complexes (sMP conc. = 0.1 % w/v, 0.2 ml) were separately mixed with the buffer A solution of BSA-FITC (0.2 ml, 10 μg/ml). After 1-h mild vibration at 25 °C under cover, a separation procedure (15000 rpm, 20 min, 25 °C) was carried out to these mixtures, followed by

Downloaded by DUKE UNIV on June 23, 2012 | http://pubs.acs.org
Publication Date (Web): November 18, 2010 | doi: 10.1021/bk-2010-1054.ch013

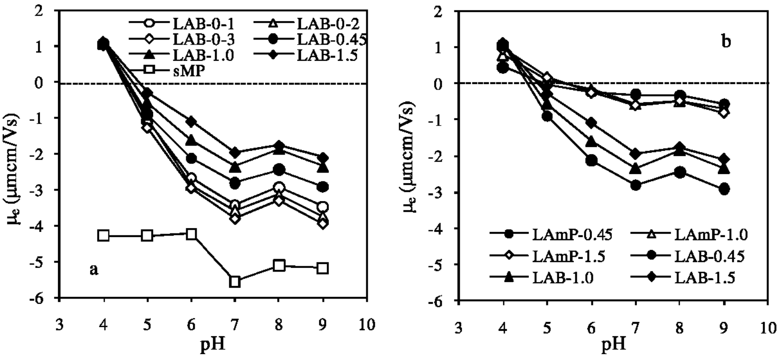

Figure 5. Effect of pH on the electrophoretic mobility (μ_e) of the sMP and various forms of LAB-s complex with or without antiferritin (a), and of the LAmP-s and LAB-s complexes (b).

fluorescence measurements ($\lambda_{ex.}$ = 492 nm, 25 °C) of the supernatant (0.35 ml) to identify its fluorescence intensity at 520 nm ($Int._{520}$). The amount of BSA-FITC nonspecifically adsorbed onto the complex, was then derived from the difference in the $Int._{520}$ of the supernatant of the test samples and control (buffer A solution of BSA (0.012 % w/v) or of mixed N6-PEG polymers (5k/2k = 1: 0.67)). This experiment was also performed at various NaCl concentrations (0.05, 0.15, and 0.5 M) to show the effect of salt on the nonsphecific adsorption of BSA-FITC.

Although the number of nonspecifically adsorbed BSA-FITC molecules gradually increased with salt concententration in both case of the LAB-1.0 and LAmP-1.0 complexes, the deposition level of BSA-FITC for the LAmP-1.0 complex was remarkably lower than that for the LAB-1.0 complex, especially at NaCl = 0 M (5 and 135 molecules per particle, respectively), clearly confirming that the PEGylation efficiently inhited the nonspecific adsorption compared to the BSA blocking treatment (see Figure 6). This salt-boosted BSA-FITC adsorption is consistent with the literature (*27*, *28*), i.e., salt weakened the electric repulsion between the BSA-FITC molecules and the identically charged LAB-s complex to promot the attachment. Analogically, it is plausible that nonspecific adsorption may significantly be triggered to the LAB-s complex in biofluid, such as serum.

Immune Response Yield

The LAmP-s complex (see Figures 7a and 7c) strongly responded to the ferritin antigen in both buffer A and 100 % FBS, although it was more sensitive in buffer A, possibly due to the nonspecific adsorption of the contaminants from the FBS. The response of the LAmP-s complex notably depended on the s value. According to the predictive definition given in the previous paper (*7*), the detection limits of the LAmP-0.45, LAmP-1.0 and LAmP-1.5 complexes were equal to 40, 10 and 10 ng/ml of ferritin in buffer A, and to 100, 20 and 20 ng/ml of ferritin in FBS, respectively. Increased antibody load improved the sensitivity of the LAmP-s complex.

Downloaded by DUKE UNIV on June 23, 2012 | http://pubs.acs.org
Publication Date (Web): November 18, 2010 | doi: 10.1021/bk-2010-1054.ch013

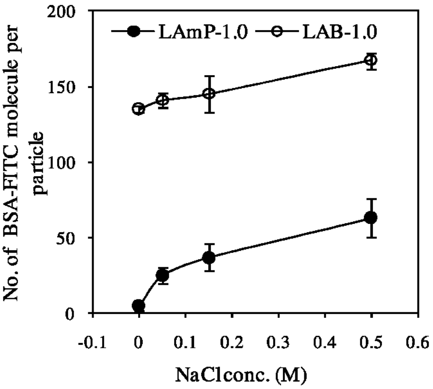

Figure 6. NaCl-dependency of the number of nonspecifically adsorbed BSA-FITC molecules per particle of LAB-1.0 and LAmP-1.0.

The immune response of the LAB-s complex (see Figure 7b) also increased with the antiferritin load in buffer A, but the absolute value was lower than that of the LAmP-s complex, particularly in the case of s = 0.45. The detection limits of the LAB-1.0 and LAB-1.5 complexes in buffer A (ca. 40 ng/ml) were 4 times higher than those of the corresponding LAmP-s complex. The LAB-0.45 complex did not show this value, since no response proportional to the antigen concentration was available within the experimental range. A similar phenomenon also occurred in the measurements using 100% FBS, leading to the absence of a detection limit for all three LAB-s complexes (Figure 7d). The low functionality and the extremely high detection limit of the LAB-s complex, evidently demonstrates that the LAmP-s complex is a more sensitive and efficient form of immunolatex.

In buffer A, the LAB-s complex gave a low immune response yield because of the electric repulsion between the same negatively charged ferritin and the particles, which disfavored the approach of the ferritin to the particle to react with antiferritin. Whereas this kind of interference did not exist in the case of the LAmP-s complex, because of its hydrophilic, flexible and almost net-neutral PEG surface layer. In FBS, salt accelerated nonspecific adsorption of the protein contaminants of FBS to the LAB-s complex, silimar as the BSA-FITC adsorption under various salt concentrations described above. These contaminants might completely cover the epitopes of the antiferritin to inhibit antiferritin-ferritin recognition. As a result, the response of the LAB-s complex in FBS was turned off.

Colloidal Stability

Long-time colloidal stability is one of the primary requirements for the practical utilization of immunolatex particles considering its diagnosis mechanism involved. Estimation of the colloidal stability of the LAmP-s complex (containing 0.1 % w/v of NaN_3 at 4 °C) in terms of the time-dependent size and reactivity for one month in buffer A, was performed to show its potential in clinical diagnosis.

Downloaded by DUKE UNIV on June 23, 2012 | http://pubs.acs.org
Publication Date (Web): November 18, 2010 | doi: 10.1021/bk-2010-1054.ch013

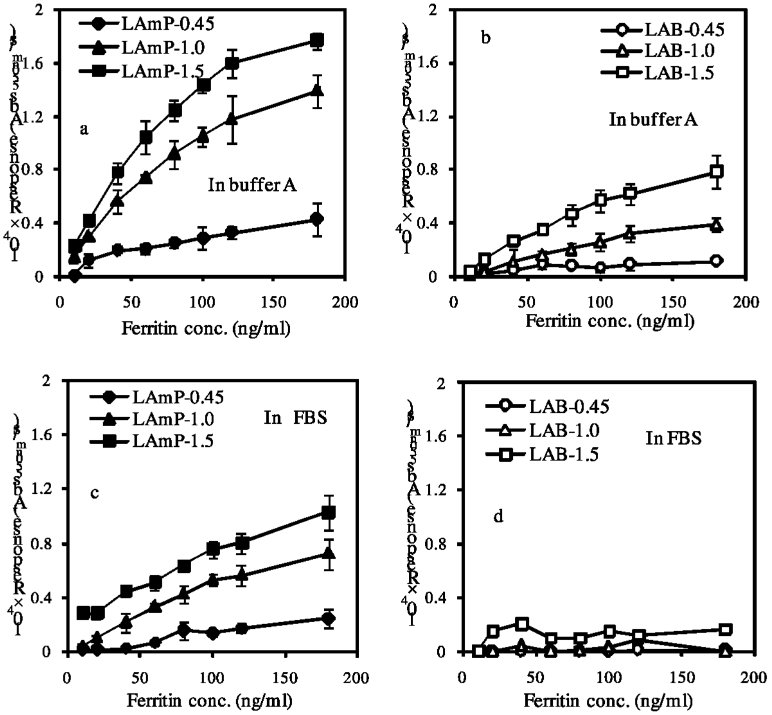

Figure 7. Immune response yield of the LAmP-s complex (a and c) and the LAB-s complex (b and d) in buffer A (a and b) and in fetal bovine serum (c and d).

A freshly prepared ferritin solution (1 μg/ml) was used each time for the reactivity measurements.

No significant variation in these two parameters was observed for the LAmP-s complex, although the LAmP-1.5 showed a slight decreasing tendency in its reactivity with time. This long-term colloidal stability and reactivity retaining of the LAmP-s complex, particularly at s < 1.5, evidently indicates that the PEGylation technique may not only colloidally stabilize the LA complex, but also favor the maintenance of the configuration of the attached antibody for a long period. The aforesaid interference of possible desorption of the physically adsorbed antiferritin was clearly negligible as expected, at least for the complex at s < 1.5. Moreover, the LAmP-s complex was so stable that only a subtle variation in its size was observed even after keep for one week in 2.0 M NaCl at 4 °C. (data not shown) But the LAB-s complex aggregated at 0.15 M NaCl, due to the screening effect of salt on the coagulation of the LAB-s complex, especially that with a high antiferritin load.

Conclusion

To obtain a stable, mono-dispersed and highly functionalized sMP/ antiferritin/PEG complex, various preparation conditions were evaluated in detail. As a result, the LAmP-s complex (5k/2k = 1: 0.67) of about 270 nm (μ_e = – 0.4

μmcm/Vs; PDI < 0.1) was constructed under optimum conditions. Its preparation required no purification and took only about 2 h, which is advantageous for practical utilization. The LAmP-1.0 complex was concluded to be the most suitable or applicable one, because of its high immune response yield per localized antiferritin and a significantly low detection limit in comparison with the LAB-s complex, in both buffer A and 100 % FBS. Also, it posesses a high colloidal stability for a long period. All of these advantages of the LAmP-1.0 complex were attributed to the PEGylation of both long-chain and short-chain N6-PEG polymer, which not only stabilized the complex and maintained the antiferritin configuration on the surface, but also markedly depressed the disturbance caused by various nonspecific interfacial interactions. The LAmP-1.0 complex has the potential for practical utilization as the basis of a novel serological diagnosis system.

Downloaded by DUKE UNIV on June 23, 2012 | http://pubs.acs.org
Publication Date (Web): November 18, 2010 | doi: 10.1021/bk-2010-1054.ch013

Acknowledgments

This research was supported by Biokit S. A. (Barcelona, Spain), a Grant-in-Aid for Scientific Research (A) (No. 18200033) and a Grant-in-Aid for Scientific Research on Innovative Areas, No. 20106011 (Soft Interface), from the Ministry of Education, Culture, Sports, Science and Technology (MEXT) of Japan. The authors would like to express their gratitude to Dr. Miquel Sales (Biokit S. A.) for supplying various laboratory materials and for his helpful discussions.

References

1. Polpanich, D.; Tangboribooonrat, P.; Elaissari, A.; Udomsangpetch, R. *Anal. Chem.* **2007**, *79*, 4690–4695.
2. Chen, J.; Jin, M.; Yu, Z.; Dan, H.; Zhang, A.; Song, Y.; Chen, H. *J. Vet. Diagn. Invest.* **2007**, *19*, 155–160.
3. Bhaskar, S.; Banavaliker, J. N.; Hanif, M. *FEMS Immunol. Med. Microbiol.* **2003**, *39*, 235–239.
4. Senthilkumar, T.; Subathra, M.; Phil, M.; Ramadass, P.; Ramaswamy, V. *Ind. J. Med. Microbiol.* **2008**, *26*, 45–49.
5. Hamano, A.; Umeda, M.; Ueno, Y.; Tanaka, S.; Mimuro, J.; Sakata, Y. *Clin. Chem.* **2005**, *51*, 183–188.
6. Benecky, M.; Post, D. R.; Schmitt, S. M.; Kochar, M. S. *Clin. Chem.* **1997**, *43*, 1764–1770.
7. Nagasaki, Y.; Kobayashi, H.; Katsytana, Y.; Jomura, T.; Sakura, T. *J. Colloid Interface Sci.* **2007**, *309*, 524–530.
8. Yoshimoto, K.; Matsumoto, S.; Asakawa, R.; Uchida, K.; Ishii, T.; Nagasaki, Y. *Chem. Lett.* **2007**, *36*, 1444–1445.
9. Takae, S.; Akiyama, Y.; Yamasaki, Y.; Nagasaki, Y.; Kataoka, K. *Bioconjugate Chem.* **2007**, *18*, 1241–1245.
10. Huang, N. P.; Voros, J.; De Paul, S. M.; Textor, M.; Spencer, N. D. *Langmuir* **2002**, *18*, 220–230.

11. (a) Malmsten, M.; Emoto, K.; Van Alstine, J. M. *J. Colloid Interface Sci.* **1998**, *202*, 507−517. (b) Malmsten, M.; Van Alstine, J. M. *J. Colloid Interface Sci.* **1996**, *177*, 502−512.
12. (a) Otsuka, H.; Nagasaki, Y.; Kataoka, K. *Langmuir* **2004**, *20*, 11285−11287. (b) Otsuka, H.; Nagasaki, Y.; Kataoka, K. *Biomacromolecules* **2000**, *1*, 39−48. (c) Yoshimoto, K.; Hirase, T.; Madsen, J.; Armes S. P.; Nagasaki Y. *Macromol. Rapid Commun.* **2009**, in press.
13. (a) Uchida, K.; Otsuka, H.; Kaneko, M.; Kataoka, K.; Nagasaki, Y. *Anal. Chem.* **2005**, *77*, 1075−1080. (b) Uchida, K.; Hoshino, Y.; Tamura, A.; Yoshimoto, K.; Kojima, S.; Yamashita, K.; Yamanaka, I.; Otsuka, H.; Kataoka, K.; Nagasaki, Y. *Biointerphases* **2007**, *2*, 126−130.
14. Yoshimoto, K.; Hirase, T.; Nemoto, S.; Hatta, T.; Nagasaki, Y. *Langmuir* **2008**, *24*, 9623–9629.
15. Satomi, T.; Nagasaki, Y.; Kobayashi, H.; Otsuka, H.; Kataoka, K. *Langmuir* **2007**, *23*, 6698–6703.
16. Nagasaki, Y.; Yoshinaga, K.; Kurokawa, K.; Iijima, M. *Colloid Polym. Sci.* **2007**, *285*, 563–567.
17. Yuan, X.; Iijima, M.; Oishi, M.; Nagasaki, Y. *Langmuir* **2008**, *24*, 6903–6909.
18. Ortega-Vinuesa, J. L.; Bastos-Gonzalez, D.; Hidalgo-Alvarez, R. J. *J. Colloid Interface Sci.* **1995**, *176*, 240–247.
19. Serra, J.; Puig, J.; Martin, A.; galisteo, F.; Galvez, M.; Alvarez-Hidalgo, R. *Colloid Polym. Sci.* **1992**, *270*, 574–583.
20. Van Dulm, P.; Norde, W. *J. Colloid Interface Sci.* **1983**, *91*, 248–254.
21. Musyanovych, A.; Adler, H. J. P. *Langmuir* **2005**, *21*, 2209–2217.
22. Rapoza, R. J.; Horbett, T. A. *J. Colloid Interface Sci.* **1990**, *136*, 480–493.
23. Ortega-Vinuesa, J. L.; Hidalgo-Alvarez, R.; de las Nieves, F. J.; Davey, C. L.; Newman, D. J.; Price, C. P. *J. Colloid Interface Sci.* **1998**, *204*, 300–311.
24. Staros, J. V.; Wright, R. W.; Swingle, D. M. *Anal. Biochem.* **1986**, *156*, 220–222.
25. Molina-Bolivar, J. A.; Ortega-Vinuesa, J. L. *Langmuir* **1999**, *15*, 2644–2653.
26. Zhang, S.; Sun, Y. *Biotechnol. Bioeng.* **2001**, *75*, 710–717.
27. Tamai, H.; Hasegawa, M.; Suzawa, T. *Colloids Surf.* **1990**, *51*, 271–280.
28. Tamai, H.; Fujii, A.; Suzawa, T. *J. Colloid Interface Sci.* **1987**, *1*, 176–181.

Downloaded by DUKE UNIV on June 23, 2012 | http://pubs.acs.org
Publication Date (Web): November 18, 2010 | doi: 10.1021/bk-2010-1054.ch013

Downloaded by 89.163.34.136 on June 23, 2012 | http://pubs.acs.org
Publication Date (Web): November 18, 2010 | doi: 10.1021/bk-2010-1054.ix002

Subject Index

A

Absorbable polyurethanes, 137, 140
  characterization
    molecular weight, 150
    tensile strength, 150
    in vitro hydrolytic degradation studies, 151
  hydrolytic degradation
    BB002 vs. BB004, 154*f*
    PCL-530 vs. PEG 4600 polyol, 155*f*
  structure, 151*f*
  synthesis, 149
    polyols and chain extender, 151*f*
  tensile properties, 153*t*
AFAM. *See* Atomic force acoustic microscopy
Albumin, 9*f*
ALD. *See* Area selective atomic layer deposition
Alginate-based hydrogels and hepatocytes, 7, 8*f*, 9*f*
Alkanethiols
  Au and SAM formation, 69
  SAM laser patterning, 93*f*
  tapping mode AFM nanolithography, 87
Amidation of hematin
  and MPEGNH_2, 230*f*
  stability, 230*f*
Antiferritin
  immobilization, 245
  immunolatex, 243
  mixed-PEG polymers, 243
  polystyrene submicroparticles, 243
Antiferritin-immunolatex complex, 243, 252, 254*f*
  formulation, 246*f*
  immune response, 256*f*
Area selective atomic layer deposition, 82
Aspirin releasing macromers and oligomers
  and NO, 201*f*
Atomic force acoustic microscopy, 166

B

BF_2dbmOMe dye and PLGA nanofibers, 36*f*
Biomimetic catalysts
  biosensing application, 221, 231
  polymer syntheses, 221
  porphyrin, 231
  vinyl monomers, polymerization, 225*f*
Biomolecules, immobilization, 73*f*
Bis [(2-thioxo-1, 3-oxathiolan-5-yl) methyl] decanedioate, 178
Bis [(2-thioxo-1, 3-oxathiolan-5-yl)methyl] 2,2′-oxydiacetate, 179
Boron dye-PLGA blends
  and nanofibers
    degradation, 33, 36, 39
    fabrication, 33, 35, 37
    optical characterization, 38
Bovine serum albumin, 250
  and LAP-0.45 complex, 251*f*
BSA. *See* Bovine serum albumin

C

Caprolactone, 200*f*, 201*f*
Carbodiimide, 192*f*
Carbohydrate-cyclopentadiene and SAM, 96*f*
κ-Carrageenan
  full-IPN, 128
  glycidyl trimethyl ammonium chloride, 128
  modification, 128
  PAA IPN hydrogel, 125, 128, 132*f*
    and $AgNO_3$, 133*f*, 133*t*
    drug incorporation, 129
    drug release, 129
  and Quat 188, 128, 129*f*
  semi-IPN, 128, 130
Catalysts
  hematin, 226
  metalloporphyrin, 224
  peroxidases, 226
  polymerization, 226
CDI. *See* Carbodiimide
Chemo-biologically synthesized substrates
  and hepatocytes culture, 23
Chitosan
  stainless steel, coatings, 159
    304 stainless steel, 165*f*, 166*f*, 167*f*
    atomic force acoustic microscopy, 163
    electrochemical deposition, 161, 164*f*, 165*f*
    Fourier transform infrared spectroscopy, 162, 165*f*
    microcarrier, 15*f*

Downloaded by 89.163.34.136 on June 23, 2012 | http://pubs.acs.org
Publication Date (Web): November 18, 2010 | doi: 10.1021/bk-2010-1054.ix002

- microscratch testing, 163, 167*f*
- Raman spectroscopy, 162, 166*f*
- scaffolds, 11
- scratch test, 168*f*
- substrate, 164*f*
- tribotesting, 163
- UV exposed, 165*f*, 166*f*, 167*f*
- XRD, 162

Chitosan/galactosylated hyaluronic acid scaffolds, 12*f*
CL. *See* Caprolactone
Conducting polymers, 232*f*
Cyclic dithiocarbonate, 173
  - and diglycidyl sebacate, 181*f*
  - synthesis, 176*s*

Cyclo(Lac-Asp), 192*f*
Cyclo(Lac-Lys), 192*f*

D

D-chloroform, 181*f*
DCM. *See* Dichloromethane
Dendrimer grafted substrates and hepatocytes culture, 20
DGA. *See* Diglycolic acid
Dichloromethane, 189
Difluoroboron dibenzoylmethane polylactides, 35*f*
Diglycidyl sebacate and cyclic dithiocarbonate, 181*f*, 182*f*
Diglycolic acid, 202*f*
Dip pen nanolithography, 85, 86*f*
Direct laser patterning, 91
DLP. *See* Direct laser patterning
DNA
  - biosensors and streptavidin, 73*f*
  - conformational studies and porphyrins, 236

DPN. *See* Dip pen nanolithography

E

E-cadherin, 9*f*
Electron beam lithography, 78
EUVL. *See* Extreme ultraviolet lithography
Extreme ultraviolet lithography, 78

F

Fibrin-based hydrogels, 8
Fourier transform infrared spectroscopy, 162
FTIR. *See* Fourier transform infrared spectroscopy
Full-IPN of κ-carrageenan and PAA, 128

G

GA. *See* Glycolic acid
Galactosylated polymer substrates and hepatocytes culture, 17
Gelation systems for nerve repair
  - applications, 52
    - central nerve regeneration, 53
    - drug delivery, 54
    - peripheral nerve regeneration, 53
  - chemically crosslinkable systems, 45
  - physical gels, 48

Glycidyl trimethyl ammonium chloride, 128
  - κ-carrageenan
    - modification, 129*f*, 130, 132*f*
    - PAA IPN modification, 132*f*, 133*f*

Glycolic acid, 200*f*, 201*f*, 202*f*
Growth factor presenting substrates and hepatocytes culture, 20

H

HA. *See* Hydroxyapatite
Hematin
  - amidation, 230*f*
  - and PEG, 229*f*
  - and polymerization, 227*f*, 229*f*
    - catalysts, 226
  - structures, 225*f*
  - vs. peroxidases, 226

Heme b, 225*f*
Hemin chloride, 225*f*
Heparin-based hydrogels, 8
Hepatic cords, 3*f*
Hepatic lobule, 3*f*
Hepatic sinusoid, 3*f*
Hepatocytes
  - aggregates, 19*f*, 21*f*
  - albumin, 9*f*
  - alginate microspheres, 8*f*
  - CK18, 9*f*
  - co-culture, 5
  - cultured on aligned PLLA nanofibers, 21*f*
  - cultured on 3-D sponges, 10
    - cells cultured, 16*t*

Downloaded by 89.163.34.136 on June 23, 2012 | http://pubs.acs.org
Publication Date (Web): November 18, 2010 | doi: 10.1021/bk-2010-1054.ix002

- chitosan-based scaffolds, 11
- liver-derived biomatrix-based scaffolds, 13
- microcarrier-based scaffolds, 13
- PLGA-based scaffolds, 10
- vegetable-based scaffolds, 14
- 2-D culture, 3
  - co-culture, 5
  - polymers derivatives, 4
- 3-D spheroid culture
  - chemo-biologically synthesized substrates, 23
  - dendrimer grafted substrates, 20
  - galactosylated polymer substrates, 17
  - growth factor presenting substrates, 20
  - inverse colloidal crystal substrates, 19
  - nanofibrous substrates, 21
  - static conditions, 15
  - substrates, 22*t*
  - synthetic polymer substrates, 18
- E-cadherin, 9*f*
- encapsulation in 3-D hydrogels, 6
  - alginate-based hydrogels, 7
  - cells cultured, 10*t*
  - fibrin-based hydrogels, 8
  - heparin-based hydrogels, 8
  - poly(ethylene glycol)-based hydrogels, 9
  - temperature sensitive hydrogels, 9
- PET/PLGA/PVLA scaffold, 19*f*
- polymeric scaffold materials, 1
- and polystyrene surface, 3*f*
- *in vitro* culture, 1

Highly oriented pyrolytic graphite, 75*f*
HOPG. *See* Highly oriented pyrolytic graphite
Hyaluronic acid-based scaffolds, 12
Hydrogels, 3-D
- hepatocytes encapsulation, 6
  - alginate-based hydrogels, 7
  - cells cultured, 10*t*
  - fibrin-based hydrogels, 8
  - heparin-based hydrogels, 8
  - poly(ethylene glycol)-based hydrogels, 9
  - temperature sensitive hydrogels, 9

Hydrolytically degradable aromatic isocyanates, 141*f*, 142
- BB002, 142, 142*f*
- BB003, 142*f*, 145
- BB004, 142*f*, 147
- prior art and our state-of-the-art, comparison, 141*t*
- synthesis, 142

Hydroxyapatite
- biosensor, 115*f*, 116*f*, 118*f*
- SPR biosensor, 117*f*

Hydroxyapatite sensor and SPRi, novel system, 113

I

ICC. *See* Inverse colloidal crystal substrates
Immune response
- LAB-s complex, 256*f*
- LAmP-s complex, 256*f*

Immunolatex complex, 243, 252, 254*f*
- formulation, 246*f*
- immune response, 256*f*

Interpenetrating network hydrogel
- κ-carrageenan and poly(acrylic acid)
  - drug incorporation, 129
  - drug release, 129
  - synthesis, 128
  - wound dressing patch, 125

Inverse colloidal crystal substrates and hepatocytes culture, 19
In vitro culture of hepatocytes, 1
Iodide dye and PLGA nanofibers, 36*f*
Ion beam lithography, 78
IPN. *See* Interpenetrating network hydrogel
Isocyanates, 139*f*

L

LA. *See* Lactic acid
LAB-1.0 complex and BSA-FITC, 255*f*
LAB-s. *See* Immunolatex complex
Lactic acid, 200*f*, 201*f*
Lactose modified microcarrier, 15*f*
LAmP. *See* Antiferritin-immunolatex complex
LAmP-1.0 and BSA-FITC, 255*f*
LAP-0.45 complex
- and BSA, 251*f*
- immunoreactivity, 249*f*
- N6-PEG-2K-dependent immune response, 251*f*

LAP-s, formulation, 246*f*
LBM-based scaffolds. *See* Liver-derived biomatrix-based scaffolds
Liver
- cells and urea synthesis rate, 20*f*
- tissue structure, 2, 3*f*

Liver-derived biomatrix-based scaffolds, 13
Luminescent boron dye-PLGA blends, 33

Downloaded by 89.163.34.136 on June 23, 2012 | http://pubs.acs.org
Publication Date (Web): November 18, 2010 | doi: 10.1021/bk-2010-1054.ix002

M

- MA. *See* Malonic acid
- Malonic acid, 202*f*
- MD. *See* Morpholine-2,5-dione
- MDA. *See* 11-Mercaptodecanoic
- Medical applications
  - absorbable polyurethanes, 140
  - polymerizing biomaterials, 173
- 11-Mercaptodecanoic, 93*f*
- 16-Mercaptohexadecanoic acid, 86*f*
- Metalloporphyrin, 221, 224
- Methoxypolyethylene glycol amine, 230*f*
- α-Methoxy-poly(ethylene glycol)-pentaethylenehexamine, 247
- MHA. *See* 16-Mercaptohexadecanoic acid
- Microcarrier-based scaffolds, 13
  - chitosan microcarrier, 15*f*
  - lactose modified microcarrier, 15*f*
- Microscratch testing and chitosan films, 163
- Morpholine-2,5-dione
  - historical perspective, 186
  - product, 192*f*
  - solid phase organic synthesis, 189, 190*s*, 191*t*
  - structure, 187*f*
  - substituted, 188*f*
  - synthesis, 185, 189
- MPEGNH$_2$. *See* Methoxypolyethylene glycol amine
- Multicomponent / mixed SAM
  - electrochemical modification of adsorbates, 75
  - host-guest self assembled monolayers, 75
  - post adsorption phase separation, 74
  - spontaneous phase separation, 74

N

- Nanofibers
  - degradation, 33, 39
  - fabrication, 33, 35, 37
  - scaffold
    - and phosphate buffered saline, 39*t*
    - PLGA loaded with BF$_2$dbm(I)OH dye, 37*f*
- Nanofibrous substrates and hepatocytes culture, 21
- Nanoimprint lithography, 89
- Naproxen releasing macromers and oligomers and NO, 200*f*
- Nerve cell-material interactions, 49
  - ECM proteins and neurotrophic factors, 51
  - mechanical cues, 50
  - neural stem cell encapsulation, 52
- Nerve regeneration and polymer gel systems, 43
- Nerve repair
  - and polymer gel systems, 43
    - applications, 52
    - chemically crosslinkable systems, 45
    - physical gels, 48
- NIL. *See* Nanoimprint lithography
- Nitric oxide, 198
  - aspirin releasing macromers and oligomers, 201*f*, 202*f*
  - and drug releasing macromers, oligomers, 197, 200*f*, 201
  - and drug releasing pendant groups, 203
    - polyesters, 205*f*
    - polyurethanes, 204*f*
  - and naproxen releasing hydrolytically degradable diol monomer, 204*f*
  - and naproxen releasing macromers and oligomers, 200*f*, 202*f*
  - releasing macromers, synthesis, 205
  - sensors, 234
  - and synthetic porphyrins, 236*f*
- NMR. *See* Nuclear magnetic resonance
- NO. *See* Nitric oxide
- N6-PEG. *See* α-Methoxy-poly(ethylene glycol)-pentaethylenehexamine
- N6-PEG-5k, 248, 249*f*
- N6-PEG-2K-dependent immune response and LAP-0.45 complex, 251*f*
- N6-PEG-5k/N6-PEG-2k, 249
- Nuclear magnetic resonance, 178

O

- Optical characterization, boron dye-PLGA blends, 38

P

- PAA. *See* Polyacrylic acid
- Patterning, 76
  - techniques
    - electron beam and ion beam lithography, 78
    - photolithography, 78
    - X-ray and extreme ultraviolet lithography, 78
- Patterning of SAM

Downloaded by 89.163.34.136 on June 23, 2012 | http://pubs.acs.org
Publication Date (Web): November 18, 2010 | doi: 10.1021/bk-2010-1054.ix002

  - applications
    - biology and biomedicine, 94
    - nanoscience, 93
  - soft lithography, 79
    - area selective atomic layer deposition, 82
    - microcontact insertion printing, 83
    - microcontact printing, 80
    - microdisplacement printing, 82
    - microfluidic patterning, 82, 84*f*
    - multilayer transfer printing, 84
    - nanotransfer printing, 81, 83*f*
  - SPM / AFM based techniques
    - alkanethiols, 87
    - dip pen nanolithography, 85
    - nanografting, 85
    - nanoshaving, 86
    - tapping mode AFM nanolithography, 87
  - techniques
    - atomic beam lithography, 88
    - block copolymers, 90
    - electron - beam lithography, 87
    - electron beam chemical nanolithography, 91
    - formation of gradients, 88
    - ink-jet printing, 88
    - lithography assisted chemical patterning, 90
    - molecular ruler method, 90
    - nanoimprint lithography, 89
    - orthogonal self assembly, 89
    - photolithography, 87
    - scanning tunneling microscope, 89
    - topographically directed assembly, 88
    - X-ray lithography, 87
- PBS. *See* Phosphate buffered saline
- PCLEEP. *See* Poly(ε-caprolactone-co-ethyl ethylene phosphate)
- PDP. *See* Polydepsipeptides
- PEDOT. *See* Poly(ethylene dioxythiophene)
- PEG. *See* Polyethylene glycol
- PEG 200 dithiocarbonate, 180
- PEG 500 dithiocarbonate, 180
- PEGylation, 247
- Pentaethylenehexamine-ended poly(ethylene glycol), 243
- 2,4-Pentanedione, 229*f*
- Peroxidases, 226
- Phosphate buffered saline
  - and nanoscale scaffolds, 39*t*
  - and PLGA/dye nanofiber scaffold, 40*f*
- Photolithography, 78
- PIPAAm. *See* Poly(N-isopropylacrylamide)
- PLGA. *See* Poly(lactic-co-glycolic acid)
- Polyacrylic acid, 125
  - κ-carrageenan IPN, 130, 131*f*
- Polyaniline
  - formation, 233*f*
  - PEG-hematin catalysis, 233*f*
  - structure, 232*f*
- Poly(ε-caprolactone-co-ethyl ethylene phosphate), 21*f*
- Polycarbonates, 119*f*
- Polydepsipeptides
  - preparation, 185
  - structure, 187*f*
  - synthetic and natural materials, hybrids, 185
- Polyesters, 205*f*
- Poly(ethylene dioxythiophene), 232*f*
- Polyethylene glycol
  - cyclic dithiocarbonates, 177*f*
  - diglycidyl ether, 175*s*
  - dithiocarbonate, 175*s*, 176*f*
  - and hematin catalysis
    - polyaniline formation, 233*f*
    - pyrrole EDOT copolymers, 235*f*
    - sodium styrene sulfonate, polymerization, 229*f*
  - hydrogels, 9
- Polyethyleneglycol diglycidyl ether, 181*f*
- Poly(α-hydroxy acid), 187*f*
- Poly(lactic-co-glycolic acid), 35*f*
  - based scaffolds, 10
  - drug depots, 177*f*
  - dye blends, 38*f*
  - dye nanofiber scaffolds
    - degradation, 39
    - optical characterization, 38
    - PBS solution, 39*t*, 40*f*
    - and phosphate buffered saline, 40*f*
    - room temperature phosphorescence, 40*f*, 41*t*
  - nanofibers
    - and BF$_2$dbmOMe dye, 36*f*
    - and iodide dye, 36*f*
- Polymer gel systems and nerve repair and regeneration, 43
- Polymeric scaffold materials and hepatocytes culture, 1
- Polymeric SPRi sensors, 117
- Polymerization
  - catalysts, 226
  - hematin, 226, 229*f*
  - medical applications, 173
  - peroxidases, 226
  - phenols, 227*f*
  - sodium styrene sulfonate, 229*f*
  - vinyl monomers, 229*f*

Downloaded by 89.163.34.136 on June 23, 2012 | http://pubs.acs.org
Publication Date (Web): November 18, 2010 | doi: 10.1021/bk-2010-1054.ix002

Polymers
  conducting, 232*f*
  derivatives, 4
  natural, 4
  synthetic, 4
Poly(N-isopropylacrylamide), 5*f*
Poly(pyrrole), 232*f*
Polystyrene
  submicroparticles and antiferritin/mixed-PEG polymers, 243
  surface and hepatocytes culture, 3*f*
Polyurethanes, 137
  commercial medical grade, 139*t*
  NO and drug releasing pendant groups, 204*f*
  physical properties
    BB002, PCL and 1,4-butanediol, 152*t*
    BB002, PCL and PEG, 153*t*
    BB004, PCL and 1,4-butanediol, 152*t*
  synthesis, 138*f*
Porphyrin
  applications
    biosensing, 231, 234
    toxic wastes, removal, 232
  biomimetic catalysts, 231
  DNA conformational studies, 236
  ring, structure, 223*f*
  superoxide anion radical, electrochemical sensing, 237
  synthetic, 236*f*
  synthetic analogues, 227*f*
PU. *See* Polyurethanes
Purpurogallin, 230*f*, 232*f*
Pyrogallol, oxidative transformation, 230*f*, 232*f*
Pyrrole EDOT copolymers, 235*f*

Q

Quat 188. *See* Glycidyl trimethyl ammonium chloride

R

Raman spectroscopy, 162
Room temperature phosphorescence, PLGA/dye nanofiber scaffold, 40*f*, 41*t*
RTP. *See* Room temperature phosphorescence

S

SA. *See* Succinic acid
SAM. *See* Self assembled monolayers
Scanning tunneling microscope, 89
Scratch test, 167
Self assembled monolayers, 68
  applications
    biology and biochemistry, 72
    nanostructures, 72
    thin metal films, 71
  carbohydrate-cyclopentadiene, 96*f*
  characterization, 76, 77*f*
  formation, 68*f*, 70
    alkanethiolate on Au, 69
  laser patterning
    alkanethiol, 93*f*
    chemically specific, 92
    direct laser patterning, 91
    single pulse laser interference lithography, 92
    surface gradient formation, 92
  multicomponent / mixed, 74
  patterning, 79, 81*f*
  surface patterning, 65
Self assembly, 66
Semi-IPN
  κ-carrageenan and PAA, 130
  synthesis, 128
Single pulse laser interference lithography, 92
SMP. *See* Submicroparticle complex
Sodium styrene sulfonate polymerization, 229*f*
Solid phase organic synthesis, morpholine diones, 190*s*, 191*t*
Spermidine, 176*f*, 177*f*
Sponges, 3-D
  hepatocytes culture, 10
    cells cultured, 16*t*
    chitosan-based scaffolds, 11
    hyaluronic acid-based scaffolds, 12
    liver-derived biomatrix-based scaffolds, 13
    microcarrier-based scaffolds, 13
    PLGA-based scaffolds, 10
    synthetic polymer-based scaffolds, 13
    vegetable-based scaffolds, 14
SPOS. *See* Solid phase organic synthesis
SPR. *See* Surface plasmon resonance imaging
SPRi. *See* Surface plasmon resonance imaging
Stainless steel
  ball friction tests, 168*f*
  and chitosan coatings, 159, 164*f*

Downloaded by 89.163.34.136 on June 23, 2012 | http://pubs.acs.org
Publication Date (Web): November 18, 2010 | doi: 10.1021/bk-2010-1054.ix002

304 Stainless steel and chitosan coating, 165*f*, 166*f*, 167*f*
STM. *See* Scanning tunneling microscope
Streptavidin
  and DNA biosensors, 73*f*
  immobilization, 73*f*
Submicroparticle complex
  electrophoretic mobility, 252*t*, 254*f*
  polydispersity index, 252*t*
Succinic acid, 202*f*
Surface plasmon resonance
  biosensors, 119*f*
  biosensor and hydroxyapatite, 117*f*
  curve, 111*f*
  hydroxyapatite biosensor, 115*f*
  imaging, 112
  iodinated analogue sensor platform, 120*f*
  Kretschmann configurations, 111*f*
  measurements, 109
  Otto configurations, 111*f*
  system and novel hydroxyapatite sensor, 113
  tyrosine-derived polycarbonate, 120*f*
Surface sensor platforms, 113
Surface-biomolecule interactions, 109
Synthetic polymer
  based scaffolds, 13
  substrates and hepatocytes culture, 18
Synthetic porphyrins
  NO detection, 236*f*
  superoxide anion radical, detection, 236*f*

T

Techniques of patterning, 78
Temperature sensitive hydrogels, 9
Tetrathiafulvalene, 75*f*
Toxic wastes removal and porphyrin, 232
Tribotest, 163, 169
TTF. *See* Tetrathiafulvalene

U

UDT. *See* 1-Undecanethiol
1-Undecanethiol, 93*f*
Urea synthesis rate of liver cells, 20*f*

V

Vegetable-based scaffolds, 14
Vinyl monomers
  biomimetic polymerization, 225*f*
  polymerization, 229*f*

W

Wound dressing patch, 125

X

X-ray diffraction, 162, 164
X-ray lithography, 78
XRD. *See* X-ray diffraction
XRL. *See* X-ray lithography